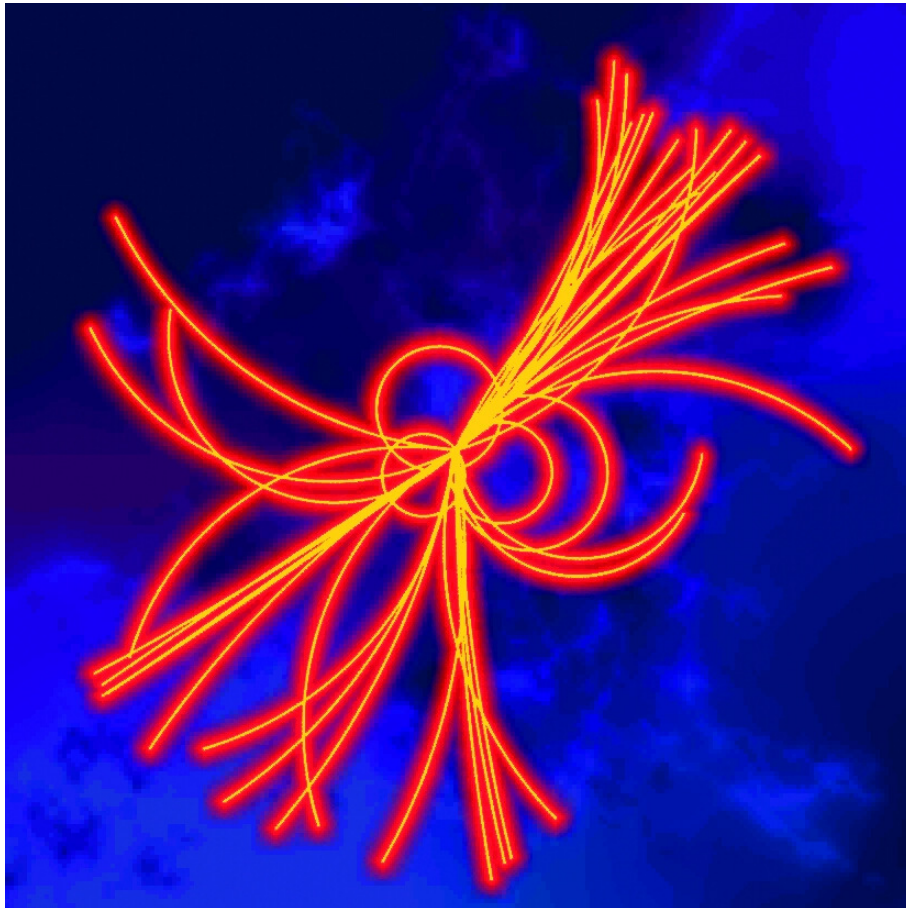


Lectures  
in  
**Particle physics**

latest revision 2016

Leif Jönsson

leif.jonsson@hep.lu.se



## **Preface and Acknowledgements**

These lecture notes were written as I started to lecture the course in Particle Physics at the Physics Department in Lund in 2005. They have been extended and improved over the years. The overall purpose is to give a general understanding of what particle physics is all about. I have tried to avoid giving statements like 'this can easily be shown' but instead carefully derived all relations used. However, it is not the proof itself that is the most important to remember but to understand the physics behind the relations. Some physical phenomena can be more easily deduced mathematically than they can be understood in a simple sense,

Initially I make a thorough review of those parts in relativity and quantum mechanics that are essential for the understanding of particle physics phenomena. In some places I have complemented the formalistic descriptions with more intuitive ones. These are found in the Appendices. After a briefing on quantum numbers and conservation laws, I discuss the forces of nature. Especially the interpretation of interactions by Feynman diagrams is carefully treated. This is followed by a discussion on how the different forces of nature are theoretically described. Next, the most important experimental discoveries are reviewed. The still open questions in particle physics and cosmology are discussed, and possible extensions of the present theory, 'the Standard Model', are presented. An overview of the development in accelerator technology and experimental methods are given. At the end there is a short chapter on the development of the universe from a particle physics point of view.

I am indebted to Hannes Jung for many contributions during the preparatory phase of these lecture notes. In the continuous process of upgrading and improving the content I have profited very much from discussions and suggestions by Cecilia Jarlskog, Magnus Hansson, Albert Knutsson and Sakar Osman. All mistakes are entirely my responsibility.

The author

# Contents

<b>1</b>	<b>Introduction</b>	<b>7</b>
1.1	Units in High Energy Physics . . . . .	10
1.2	Resolving Fundamental Particles . . . . .	11
1.3	Relativity . . . . .	12
1.3.1	Lorentz Transformation . . . . .	12
1.3.2	Velocity Addition . . . . .	14
1.3.3	Momentum and Mass . . . . .	15
1.3.4	Energy . . . . .	17
1.3.5	More Relations . . . . .	19
1.3.6	Example of Time Dilation: The Muon Decay . . . . .	20
1.3.7	Four-Vectors . . . . .	20
1.3.8	Invariant mass . . . . .	26
1.3.9	Reference systems . . . . .	26
<b>2</b>	<b>Quantum Mechanics</b>	<b>28</b>
2.1	The Photoelectric Effect . . . . .	28
2.2	The Uncertainty Principle . . . . .	29
2.3	The Schrödinger Equation . . . . .	31
2.4	The Double Slit Experiment (Interference Effects) . . . . .	32
2.5	Spin . . . . .	34
2.6	Symmetries and Conservation Laws . . . . .	35
2.6.1	Leptons and Lepton Number . . . . .	36
2.6.2	Baryons and Baryon Number . . . . .	37

2.6.3	Helicity . . . . .	38
2.6.4	Charge conjugation . . . . .	38
2.6.5	Time reversal . . . . .	39
2.6.6	Parity . . . . .	39
2.6.7	CP-violation . . . . .	41
2.7	Gauge symmetries, gauge invariance and gauge fields . . . . .	43
2.7.1	Symmetry breaking . . . . .	44
2.8	The Klein-Gordon Equation . . . . .	45
2.8.1	The Continuity Equation . . . . .	46
2.9	The Dirac Equation . . . . .	47
2.10	Antiparticles: The Hole Theory and Feynmans Interpretation . . . . .	49
2.11	Strangeness . . . . .	51
2.12	Isospin (Isotopic spin) . . . . .	56
<b>3</b>	<b>The Forces of Nature</b>	<b>59</b>
3.1	Vacuum and Virtual Particles . . . . .	61
3.2	Electromagnetic Interaction and QED . . . . .	61
3.2.1	Feynman Diagrams . . . . .	62
3.2.2	Electromagnetic Scattering Processes . . . . .	62
3.2.3	Calculation of scattering amplitudes . . . . .	65
3.2.4	Differential Cross Section . . . . .	67
3.2.5	Higher Order Contributions to $ee$ Scattering . . . . .	70
3.2.6	Regularization and Renormalization . . . . .	70
3.2.7	Summary of Amplitude Calculations . . . . .	73
3.2.8	Pair Production and Annihilation . . . . .	73
3.2.9	Compton Scattering . . . . .	76
3.3	Weak Interaction . . . . .	77
3.3.1	Some Other Examples of Weak Decays . . . . .	80
3.3.2	Properties of the Weak Force Mediators . . . . .	82
3.3.3	The Electroweak Theory of Weinberg and Salam . . . . .	84
3.3.4	The Higgs Mechanism . . . . .	86

3.3.5	Electroweak Interaction With Quarks . . . . .	91
3.3.6	Quark Mixing . . . . .	94
3.3.7	The Prediction of the Charm Quark . . . . .	96
3.4	Strong Interactions . . . . .	100
3.4.1	More Feynman Diagrams . . . . .	103
3.4.2	Asymptotic Freedom and Confinement . . . . .	104
3.4.3	Unification of the Forces . . . . .	106
3.4.4	Hadronization . . . . .	107
3.4.5	Jets . . . . .	109
3.4.6	Testing QCD . . . . .	110
<b>4</b>	<b>Experimental Discoveries of Fundamental Importance</b>	<b>117</b>
4.1	Particles and General Properties . . . . .	117
4.1.1	Resonance Particles . . . . .	117
4.1.2	Life times, decay rate, decay width and branching ratio . . . . .	117
4.1.3	Significance . . . . .	118
4.2	Fundamental Discoveries of Particles . . . . .	119
4.2.1	The Experimental Discovery of the Electron . . . . .	119
4.2.2	The Experimental Discovery of the Proton . . . . .	121
4.2.3	The Experimental Discovery of the Positron . . . . .	122
4.2.4	The Experimental Discovery of the Neutron . . . . .	122
4.2.5	The Experimental Discovery of the Muon . . . . .	124
4.2.6	The Experimental Discovery of the Pion . . . . .	125
4.2.7	The Experimental Discovery of the Electron Neutrino . . . . .	126
4.2.8	The Experimental Discovery of the Muon Neutrino . . . . .	127
4.2.9	The neutrino mass . . . . .	128
4.2.10	The Experimental Discovery of Charm . . . . .	130
4.2.11	Charmed Particles . . . . .	134
4.2.12	The Discovery of the Tau-lepton . . . . .	135
4.2.13	The Experimental Observation of the Tau Neutrino . . . . .	136
4.2.14	The Discovery of the <i>b</i> -quark . . . . .	137
4.2.15	The Discovery of the <i>t</i> -quark . . . . .	139
4.2.16	The Cabibbo-Kobayashi-Maskawa Martix and CP-violation . . . . .	142
4.2.17	The Discovery of Higgs . . . . .	144
4.3	Are There More Families? . . . . .	149

<b>5</b>	<b>Nucleon shape and structure</b>	<b>151</b>
5.1	Elastic scattering of electrons . . . . .	152
5.1.1	Determination of the nucleon size . . . . .	156
5.2	Deep inelastic scattering . . . . .	158
5.2.1	Measurement of the nucleon structure . . . . .	158
5.3	Experimental evidence for confinement and asymptotic freedom . . . . .	165
5.4	The Behaviour of the Structure Function . . . . .	167
5.5	Scaling . . . . .	168
5.6	Scaling Violation . . . . .	170
5.7	Comparison of Neutral and Charged Current Processes . . . . .	172
<b>6</b>	<b>Extensions of the Standard Model</b>	<b>175</b>
6.1	Grand Unified Theories (GUT) . . . . .	175
6.2	Supersymmetry (SUSY) . . . . .	177
6.3	String Theories . . . . .	181
<b>7</b>	<b>Experimental Methods</b>	<b>185</b>
7.1	Accelerators . . . . .	185
7.1.1	Linear Accelerators . . . . .	185
7.1.2	Circular Accelerators . . . . .	187
7.2	Colliders . . . . .	188
7.2.1	Circular Colliders . . . . .	188
7.2.2	Linear Colliders . . . . .	190
7.3	Collision Rate and Luminosity . . . . .	190
7.4	Secondary Beams . . . . .	192
7.5	Detectors . . . . .	194
7.5.1	Scintillation Counters . . . . .	194
7.5.2	Tracking Chambers . . . . .	195
7.5.3	Calorimeters . . . . .	202
7.6	Particle Identification . . . . .	205
7.6.1	Time of Flight . . . . .	205
7.6.2	Ionization Measurement . . . . .	206
7.6.3	Cherenkov Radiation . . . . .	207

<b>8</b>	<b>Cosmology</b>	<b>210</b>
8.1	Formation of Galaxies . . . . .	213
8.2	The Creation of a Star . . . . .	213
8.3	The Death of a Star . . . . .	214
<b>9</b>	<b>Appendix A</b>	<b>215</b>
<b>10</b>	<b>Appendix B</b>	<b>217</b>
<b>11</b>	<b>Appendix C</b>	<b>219</b>

# Chapter 1

## Introduction

The aim of particle physics is to find the basic building blocks of matter and to understand how they are bound together by the forces of nature. This would help us to understand how the Universe was created. The definition of the basic building blocks, or elementary particles, is that they have no inner structure; they are *pointlike particles*.

At the end of the 19th century it was generally believed that matter was built out of a few fundamental types of atoms. However, in the beginning of 1900 over 90 different varieties of atoms were known, which was an uncomfortably large number for considering the atom to be fundamental. Already in the late 1890's, the English physicist J.J. Thompson found that by applying an electric field between two electrodes, contained in a cathod ray tube, electrons were emitted when the cathod was heated. This was the first indication that the atoms are not indivisible and led Thompson to propose what was called the 'plum pudding' model, in which the electrons are evenly distributed in a soup of positive charge. Around the same time the German physicist W. Röntgen found that a new form of penetrating radiation was emitted if a beam of electrons was brought to hit a piece of matter. The radiation, which was called X-rays, was proven to be electromagnetic radiation but with a wavelength much shorter than visible light. In France H. Becquerel together with P. and M. Curie observed that a radiation with properties similar to X-rays were emitted spontaneously from a piece of Uranium. In the beginning of the 20th century the cloud chamber, or expansion chamber, was developed (see Section 4.2.5). The cloud chamber enabled more accurate studies of this radiation and revealed that there were three different types of radiation;  $\alpha$ -particles,  $\beta$ -radiation and  $\gamma$ -radiation. The  $\alpha$ -particles turned out to be identical to  $He^4$  nuclei, the  $\gamma$ -radiation is electromagnetic radiation with even shorter wavelengths than X-rays and  $\beta$ -radiation is simply electrons. The discovery of radioactivity opened up the possibility to perform more systematic studies of matter. Thus, in 1911 E. Rutherford set up an experiment in Manchester, where  $\alpha$ -particles from a radioactive source were allowed to hit a thin gold foil and the deflection of the  $\alpha$ -particles was observed. From these results he concluded that the positive charge of the atom had to be concentrated to a small volume ( $10^{-15}$  meter) in the centre of the atom, *the atomic nucleus*, and that the electrons were orbiting around this nucleus, defining the size of the atom to  $10^{-10}$  meter. This can be regarded as the start of modern particle physics. The discovery of Rutherford led to the atomic model of the Danish physicist Niels Bohr, who worked as an assistant to Rutherford at that time. From this model it became clear that the nucleus of the atom must contain positively



charged particles, protons. In 1932 James Chadwick, a student of Rutherford, discovered a new particle with no charge and with a mass close to the proton mass, the neutron. The neutron provided the explanation to why, for example, helium is four times as heavy as hydrogen and not just twice as heavy, as could be assumed if the nucleus contained only protons. Up to the point where the particle accelerators were developed the research was performed using cosmic rays and radioactive elements as particle sources. A historical review of the most important discoveries from that time is:

1895 W. Röntgen: The discovery of *X-rays*

1897 J.J. Thomson: The discovery of the *electron*

1900 H. Becquerel, P. and M Curie: Evidence for  $\alpha$ ,  $\beta$  and  $\gamma$  radioactivity

1905 A. Einstein: The *photon* was identified as the quantum of the electromagnetic field

1911 E. Rutherford: The atomic *nucleus* was established from the scattering of  $\alpha$ -particles against a thin gold foil

1919 As a consequence of the Bohr atomic model it was realized by Rutherford that the nucleus must contain particles with positive charge, *protons*

1932 C.D. Anderson: Discovery of the *positron* from the study of cosmic rays in a cloud chamber

1932 J. Chadwick: The *neutron* was discovered in nuclear reactions where light nuclei were bombarded with  $\alpha$ -particles e.g.  $\alpha + Be^9 \rightarrow C^{12} + n$

1936 C.D. Anderson, S.H. Neddermeyer, J.C. Street, E.C. Stevenson: Discovery of the *muon* from cosmic rays showers using a cloud chamber;

1947 C. Powell: Discovery of the *pion* in studies of cosmic rays using photographic emulsions.

In the beginning of the 1930's J.D. Cockcroft and T.S. Walton developed the first particle accelerator, at the Cavendish laboratory in England, by using high-voltage rectifier units. This was the start of modern accelerators, which was followed by a number of new innovations to achieve increasingly higher energies, higher beam currents (number of particles per beam) and better focusing of the beams, all driven by the desire to make new physics discoveries. As new accelerators were built a large number of 'elementary' particles were found and eventually they became more than 100 like the elements of the periodic table. With the increasing number of new particles it became unlikely that they are 'elementary' and the situation called for an underlying structure. This led to the introduction of the *quarks* in the early 1960's.

According to our present understanding, the fundamental building blocks of nature can be subdivided into two types of particles; the *quarks* and the *leptons*, which with a common name are called *fermions*, having half-integer spin. These particles are bound together by the forces of nature. We have four fundamental forces, which are *gravitation*, *electromagnetism*, the *weak force* and the *strong force*. According to modern theories a force is mediated between the interacting particles via the exchange of force-mediating particles, which belong to a type of particles called *bosons*, having integer spin. This is summarized in Table 1.1 The bosons responsible for the electromagnetic force, the *photon* ( $\gamma$ ), the weak force, the  $W^+$ ,  $W^-$  and  $Z^0$ -bosons, and the strong force, the *gluons*, have been confirmed experimentally, so there are good grounds to believe that also the gravitational force is mediated by a boson, called the *graviton*, although it hasn't been found yet. The strength of gravity is so feeble that it can be neglected in problems on the microcosmic scale at present day's energies. However, there are indications that the four forces we identify on the energy scale we have access to presently are just different manifestations of the same force such that if we go to very high energies (the Planck scale  $10^{19}$  GeV) the

fermions half-integer spin		bosons integer spin	
leptons	quarks	$\gamma, W^+, W^-, Z^0, \text{gluons}$	

Table 1.1: Fermions and bosons

strength of all forces will be the same. This means that it should be possible to find a common theoretical framework to describe all four forces.

The present status on building blocks is that six different *flavours* of quarks and leptons are known, which can be organized in three families as shown in Tables 1.2 and 1.3:

Quarks			Charge
u (up)	c (charm)	t (top)	+2/3
d (down)	s (strange)	b (bottom)	-1/3

Table 1.2: quark flavours and their charge

Leptons			Charge
e (electron)	$\mu$ (muon)	$\tau$ (tau)	-1
$\nu_e$ (electron neutrino)	$\nu_\mu$ (muon neutrino)	$\nu_\tau$ (tau neutrino)	0

Table 1.3: Lepton flavours and their charge

Each quark and lepton has its *antiparticle*. An antiparticle has the same mass as the particle but it has the opposite electric charge. The quantum field theory, which describes the interaction of fermions through the exchange of force mediating bosons, is called the *Standard Model* (SM).

Particles which are built out of quarks are called *hadrons*. There are two types of hadrons, *baryons*, consisting of three quarks and *mesons*, consisting of a quark and an antiquark. Thus, since quarks have half integer spins, the baryons, consequently, have half-integer spin and mesons integer spin.

A summary of the force mediators and some of their properties is given in Table 1.4.

The numbers specified as the relative strengths of the forces should not be taken too literally since such information can not be given unambiguously. A measure of the strength can be given by how strongly the force mediators couple to other particles i.e. how high the probability is that an interaction, governed by a specific force, takes place. This is equivalent to compare the lifetimes of various particles that decay via different force mediators. It is worthwhile to point out that a strong coupling leads to short lifetimes whereas weak couplings result in long lifetimes. The strength of the couplings are expressed in terms of *coupling constants*. However, as we will see later, the coupling strength of a force is not constant, as is indicated by the word 'coupling constant', but it varies with the distance over which the interaction takes place. These are the reasons for regarding the relative strength of the forces just as an overall indication.

	Gravity	Weak force	Electromagnetic force	Strong force
Mediator	graviton (G)	weak vector bosons ( $W^+, W^-, Z^0$ )	photon ( $\gamma$ )	gluons (g)
Mass	0	$W^\pm \sim 80 \text{ GeV}$ $Z^0 \sim 90 \text{ GeV}$	0	0
Range	$\infty$	$\sim 10^{-18} \text{ m}$	$\infty$	$\sim 10^{-15} \text{ m}$
Fermions affected	all with mass	all	electrically charged ( <i>quarks, e, <math>\mu, \tau</math></i> )	colour charged ( <i>quarks</i> )
Relative strength	$\sim 10^{-39}$	$\sim 10^{-6}$	$\sim 10^{-2}$	1

Table 1.4: The properties of the force mediators

## 1.1 Units in High Energy Physics

Due to the fact that elementary particles are so small, conventional mechanical units are not practical to use. Instead the basic unit is *electron volt (eV)*, which is a measure of energy. An *electron volt* is the amount of kinetic energy gained by a single unbound electron when it passes through an electrostatic potential difference of one volt, in vacuum. The various energy units used in high energy physics are shown in Table 1.5.

Units	1 eV (electron volt)	
	1 keV (kilo electron volt)	$10^3 \text{ eV}$
	1 MeV (mega electron volt)	$10^6 \text{ eV}$
	1 GeV (giga electron volt)	$10^9 \text{ eV}$
	1 TeV (terra electron volt)	$10^{12} \text{ eV}$

Table 1.5: Energy units used in high energy physics

$E^2 = (mc^2)^2 + (pc)^2$  relates mass, momentum and energy such that momentum is measured in  $MeV/c$  and mass in  $MeV/c^2$ , for example. Energy is also related to wavelength according to  $E = \hbar/\lambda$ , where  $\hbar = h/2\pi$  is Planck's constant =  $6.588 \cdot 10^{-25} GeV \cdot s$ . However, it is convenient to use *natural units*, where  $\hbar = c = 1$ , which implies that mass and momentum have the dimension of energy, e.g. the mass of the electron  $m_e \approx 0.5 MeV$  and the mass of the proton  $m_p \approx 1 GeV$ . In order to get a feeling for what this means in units we are more used to from classical mechanics,  $1MeV = 1.782 \cdot 10^{-27}g$ . Since  $E = \hbar/\lambda$  we get, by setting  $\hbar = 1$ , that energy gets the dimension  $length^{-1}$  or length gets the dimension  $energy^{-1}$ . Further, setting  $c = x/t = 1$  means that length and time have the same unit. The unit of time is thus the time it takes to travel one unit of length. However, since length has the dimension  $energy^{-1}$ , time also gets this dimension. In order to get the dimensions right in an absolute calculation the values of  $\hbar$  and  $c$  have to be introduced. We need a conversion factor between length and energy:

$$(\hbar \cdot c) [MeV \cdot s \cdot cm/s] = 197.5 [MeV fm].$$

The probability for an interaction between two particles to occur is expressed as a *cross section*, which has the dimension of area. The various units for cross section is shown in Table 1.6

Cross section	barn		$10^{-24} \text{ cm}^2$
	mb	$10^{-3} \text{ b}$ (millibarn)	$10^{-27} \text{ cm}^2$
	$\mu\text{b}$	$10^{-6} \text{ b}$ (microbarn)	$10^{-30} \text{ cm}^2$
	nb	$10^{-9} \text{ b}$ (nanobarn)	$10^{-33} \text{ cm}^2$
	pb	$10^{-12} \text{ b}$ (picobarn)	$10^{-36} \text{ cm}^2$
	fb	$10^{-15} \text{ b}$ (femtobarn)	$10^{-39} \text{ cm}^2$

Table 1.6: Units used for cross sections

In natural units, cross section  $\sim (\text{length})^2 \sim 1/[\text{GeV}]^2$ . The conversion factor between cross section and energy squared is:

$$(\hbar \cdot c)^2 [\text{GeV}^2 \cdot \text{s}^2 \cdot \frac{\text{cm}^2}{\text{s}^2}] = 0.389 [\text{GeV}^2 \cdot \text{mb}]$$

A comparison between units used in high energy physics with SI-units for different parameters are given in Table 1.7.

Quantity	High energy units	SI-units
length	$1 \text{ fm}$	$10^{-15} \text{ m}$
energy	$1 \text{ GeV} = 10^9 \text{ eV}$	$1.602 \cdot 10^{-10} \text{ J}$
mass, $E/c^2$	$1 \text{ GeV}/c^2$	$1.78 \cdot 10^{-27} \text{ kg}$
Planck's constant, $\hbar = h/2\pi$	$6.588 \cdot 10^{-25} \text{ GeVs}$	$1.055 \cdot 10^{-34} \text{ Js}$
velocity of light, $c$		$2.998 \cdot 10^8 \text{ ms}^{-1}$
$\hbar c$	$0.1975 \text{ GeVfm}$	$3.162 \cdot 10^{-26} \text{ Jm}$

Table 1.7: Comparison between high energy physics units and SI-units

## 1.2 Resolving Fundamental Particles

Consider the relation between the energy ( $E$ ) and the frequency ( $\nu$ ) respective the wavelength ( $\lambda$ ) of light.

$$E = \hbar \cdot \nu = \hbar/\lambda$$

where  $\lambda$  is measured in *fermi* (1 fermi = 1 fm =  $10^{-15}$  m). In order to resolve an object the wavelength of the light must be of the same order as the size of the object:  $\lambda \sim \Delta x$ . Since energy is in units of MeV and length is given in units of fermi, we need the conversion factor  $\hbar \cdot c$  to calculate the energy needed to resolve an object of a certain extension.

$$\text{The size of an atom is around } 10^{-10} \text{ m} \Rightarrow E = \frac{197.5 \cdot 10^{-15}}{10^{-10}} \approx 200 \cdot 10^{-5} \text{ MeV} = 2 \text{ keV}$$

$$\text{The size of a proton is about } 10^{-15} \text{ m} \Rightarrow E = \frac{197.5 \cdot 10^{-15}}{10^{-15}} \approx 200 \text{ MeV}$$

$$\text{The size of the quarks are } < 10^{-18} \text{ m} \Rightarrow E > \frac{197.5 \cdot 10^{-15}}{10^{-18}} \approx 200 \text{ GeV}$$

To resolve smaller and smaller objects we need higher and higher energy, and therefore larger and larger accelerators.

## 1.3 Relativity

The physics of macroscopic objects in our everyday life is governed by classical mechanics. However, as the objects start moving very fast the laws of classical mechanics have to be modified by special relativity. For objects being very small i.e. of the size of an atom or smaller, classical mechanics has to be replaced by quantum mechanics. In cases where the objects are both small and fast, the theory has to provide a relativistic description of quantum phenomena, which needs a *quantum field theory*.

### 1) The classical picture:

Velocity can be described by a vector in 3-dimensional space through its direction and magnitude. The addition of two vectors  $\vec{v} = (v_x, v_z, v_y)$  and  $\vec{v}' = (v'_x, v'_y, v'_z)$  is given by:

$$\vec{v} = \vec{v} + \vec{v}'$$

$$\Rightarrow \text{if } |\vec{v}| \sim c \text{ and } |\vec{v}'| \sim c \Rightarrow |\vec{v}| + |\vec{v}'| \sim 2c > c$$

i.e. violation of the fact that  $c$  is the maximum possible speed. Why can't nothing go faster than the speed of light? It is due to the mutual interactions between electricity and magnetism in light i.e. the nature of light as an electromagnetic wave motion. A tentative explanation is given in Appendix A.

### 2) Special relativity:

The basic postulates of the special theory of relativity are:

- a) All reference systems are equivalent with respect to the laws of nature (the laws of nature are all the same independent of reference system i.e. they are invariant).
- b) The speed of light in vacuum is the same in all reference systems.

### 1.3.1 Lorentz Transformation

Choose two reference systems  $S$  and  $S'$  such that  $S'$  moves with respect to  $S$  along the  $x$ -direction, with a velocity  $v$  as illustrated in Figure 1.1. At the time  $t = 0$  the two systems coincide and in this moment the two clocks, measuring the time in  $S$  and  $S'$ , respectively, are set to zero.

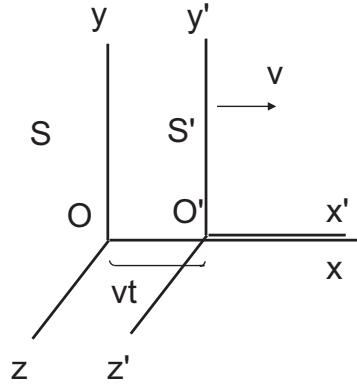


Figure 1.1: The reference systems  $S$  and  $S'$  moving with velocity  $v$  with respect to each other.

Classically, the relation between the coordinates is thus:

$$x' = x - vt \quad y' = y \quad z' = z$$

For  $x' = 0$  we have  $x = vt$ . Relativistically, the transformation is given by:

$$x' = \gamma(x - vt) \tag{1.1}$$

where the factor  $\gamma = \gamma(v)$ , the so called Lorentz factor, has to be determined. In the same way we get:

$$x = \gamma'(x' + vt') \tag{1.2}$$

with  $\gamma' = \gamma(-v)$ , since  $S$  is moving with respect to  $S'$  with the velocity  $-v$ . But from symmetry reasons  $\gamma(-v) = \gamma(v)$ , since reversing the direction of the coordinates ( $x \rightarrow -x$  and  $x' \rightarrow -x'$ ) means that  $v$  changes sign but does not affect  $\gamma$ .

The value of  $\gamma = \gamma'$  is now given by the fact that the speed of light has the same value  $c$  in both systems. Consider a light flash that is emitted at  $t = 0$  in the  $x$ -direction from the common origin  $O = O'$ . In the system  $S$  the light has after some time  $t$  reached the point  $ct$ , whereas, for the same event, in system  $S'$  one would measure a time  $t'$  and the corresponding distance  $ct'$  with respect to  $O'$ . Insertion in (1.1) and (1.2) gives:

$$ct' = \gamma(c - v)t \quad \text{and} \quad ct = \gamma(c + v)t' \tag{1.3}$$

Multiply the two  $\Rightarrow \quad c^2 tt' = \gamma^2 (c + v)(c - v) tt'$

$$\Rightarrow \quad \gamma^2 = \frac{c^2}{c^2 - v^2} = \frac{1}{1 - v^2/c^2}$$

$$\Rightarrow \quad \gamma = \frac{1}{\sqrt{1 - v^2/c^2}}$$

This can be generalized and shown to hold for two systems moving in all three coordinates with respect to each other.

If we insert  $x' = \gamma(x - vt)$  in (1.2) we get:

$$\begin{aligned} \Rightarrow x &= \gamma'[\gamma(x - vt) + vt'] \\ \Rightarrow x &= \gamma^2 x - \gamma^2 vt + \gamma vt' \quad \text{since } \gamma = \gamma' \end{aligned}$$

$$\Rightarrow \gamma vt' = \gamma^2 vt + x(1 - \gamma^2)$$

$$\Rightarrow t' = \gamma t + \frac{x(1 - \gamma^2)}{\gamma v}$$

$$\begin{aligned} \Rightarrow t' &= \gamma \left[ t + \frac{x}{v} \left( \frac{1 - \gamma^2}{\gamma^2} \right) \right] \\ &= \gamma \left[ t + \frac{x}{v} (1/\gamma^2 - 1) \right] \end{aligned}$$

$$\text{But: } \gamma = \frac{1}{\sqrt{1 - v^2/c^2}}$$

$$\Rightarrow \gamma^2 = \frac{1}{1 - v^2/c^2}$$

$$\Rightarrow 1/\gamma^2 = 1 - v^2/c^2$$

If inserted this gives:

$$\begin{aligned} t' &= \gamma \left[ t + \frac{x}{v} \left( 1 - \frac{v^2}{c^2} - 1 \right) \right] \\ \Rightarrow t' &= \gamma \left( t - \frac{v}{c^2} x \right) \end{aligned}$$

In the same way,  $t = \gamma(t' + \frac{v}{c^2}x')$

Summary for the *Lorentz transformations*:

$\bar{x}'_{\perp} = \bar{x}_{\perp}$	$\bar{x}_{\perp} = \bar{x}'_{\perp}$
$\bar{x}'_{\parallel} = \gamma(\bar{x}_{\parallel} - vt)$	$\bar{x}_{\parallel} = \gamma(\bar{x}'_{\parallel} + vt')$
$t' = \gamma(t - v/c^2 \cdot \bar{x}_{\parallel})$	$t = \gamma(t' + v/c^2 \cdot \bar{x}'_{\parallel})$
$\gamma = \frac{1}{\sqrt{1 - v^2/c^2}}$	

where  $\perp$  and  $\parallel$  are the transverse and longitudinal components with respect to the velocity  $v$ .

### 1.3.2 Velocity Addition

Consider a particle moving along the  $x$ -axis with speed  $u'$  in the system  $S'$ . What is the speed  $u$  in the system  $S$ ?

If the system  $S'$  moves with a velocity  $v$  with respect to the system  $S$ , the particle will travel a distance:  $\Delta x = \gamma(\Delta x' + v\Delta t')$

in the time interval :  $\Delta t = \gamma(\Delta t' + \frac{v}{c^2}\Delta x')$

as measured in the system  $S$ .

$$\Rightarrow \frac{\Delta x}{\Delta t} = \frac{\Delta x' + v\Delta t'}{\Delta t' + (v/c^2)\Delta x'} = \frac{(\Delta x'/\Delta t') + v}{1 + (v/c^2)(\Delta x'/\Delta t')}$$

but  $\Delta x/\Delta t = u$  and  $\Delta x'/\Delta t' = u'$

$$\Rightarrow \boxed{u = \frac{u' + v}{1 + (u'v/c^2)}}$$

If  $u'$  or  $v$  are small,  $\frac{u'v}{c^2} \rightarrow 0$  and we get  $u = u' + v$ , which is the classical solution. If  $u \rightarrow c$  then  $u' \rightarrow c$  since  $c$  is equal in all systems.

### 1.3.3 Momentum and Mass

For a particle moving with a velocity  $\bar{v}$ , the momentum  $\bar{p}$  is defined as:

$$\boxed{\bar{p} = m(v)\bar{v}} \quad (1.4)$$

with  $m(v)$  (or  $m_v$ ) being the *relativistic mass*. We denote the *rest mass* of a free particle  $m(0)$  (or  $m_o$ ).

Consider two particles  $A$  and  $B$  with the same rest mass  $m_o$ , which move towards each other with the velocities  $\bar{v}_o$  and  $-\bar{v}_o$ , and collide inelastically such that they would stick together after the collision. This situation is illustrated in Figure 1.2. This means that the pair will be at rest in its common reference system  $S_o$ . Conservation of momentum then means that the total momentum before the collisions also must be zero.

We now introduce two coordinate systems  $S$  and  $S'$ , which move along the  $x_o$ -axis relative to each other with a velocity  $w$ , such that particle  $B$  before the collision travels along the  $y$ -axis (in system  $S$ ) and particle  $A$  along the  $y'$ -axis (in system  $S'$ ), as shown in Figure 1.2 (upper). If particle  $B$  has a velocity  $u$  in the  $y$ -direction (measured in  $S$ ), then particle  $A$  must have a velocity  $-u$  in the  $y'$ -direction (measured in  $S'$ ).

Let us investigate the collisions in the reference system  $S$ , as illustrated in Figure 1.2 (lower). Since the composite system is at rest in  $S_o$ , it consequently must move in the system  $S$  along the  $x$ -direction. The momentum of the particle pair in the  $y$ -direction is, however, still zero and thus the total momentum before the collisions must also be zero. Thus, the velocities of  $A$  and  $B$  as measured in the reference system  $S$  are:

$$\bar{v}_A = \bar{v} = (v_x, v_y) = (w, -u\sqrt{1 - w^2/c^2}) \quad \text{and} \quad \bar{v}_B = \bar{u} = (u_x, u_y) = (0, u)$$

The expression for  $v_y$  comes from the fact that  $dx' = 0$  as  $A$  moves along the  $y'$ -axis and thus the Lorentz transformation of the time can be written:



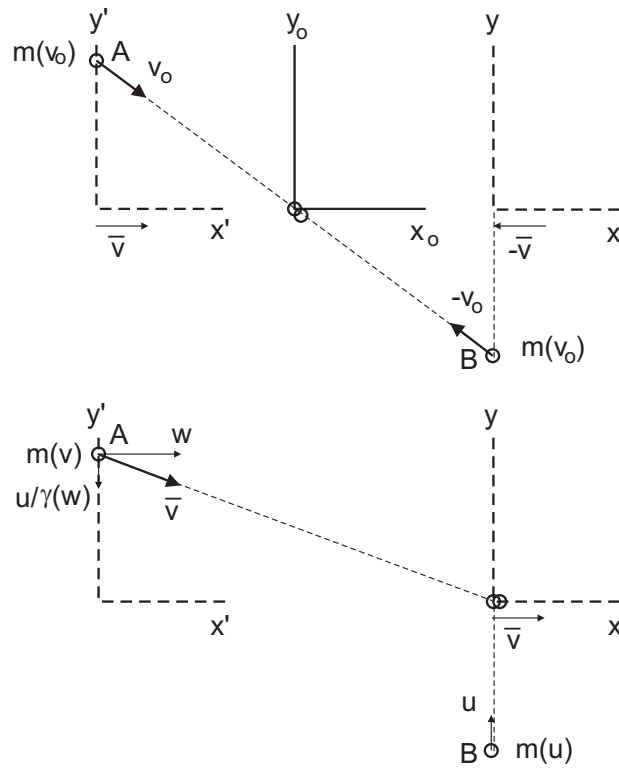


Figure 1.2: Collisions between particles A and B as seen from their common rest frame (upper Figure), and from the reference system in which particle B has no velocity in the  $x$ -direction (lower Figure).

$$dt = \gamma(w)(dt' + w/c^2 dx') = \frac{dt'}{\sqrt{1-w^2/c^2}} \quad \text{since} \quad dx' = 0.$$

Then  $v_y$  as measured in the reference system  $S$  becomes:

$$\Rightarrow v_y = dy'/dt = \frac{dy'}{dt'} \frac{dt'}{dt} = -u\sqrt{1-w^2/c^2} \quad \text{since} \quad \frac{dy'}{dt'} = -u \quad \text{and} \quad \frac{dt'}{dt} = \sqrt{1-w^2/c^2}$$

For the total momentum to be zero we have:

$$m_u \cdot u + m_v \cdot v_y = m_u \cdot u - m_v \cdot u\sqrt{1-w^2/c^2} = 0$$

$$\text{or} \quad m_u = m_v \sqrt{1-w^2/c^2}$$

$$\text{where} \quad v^2 = v_x^2 + v_y^2 = w^2 + u^2(1-w^2/c^2)$$

In the limit  $u \rightarrow 0$  we have  $v \rightarrow w$ . Thus,  $m_v \rightarrow m_w$  and  $m(u) \rightarrow m(0)$ .

$$\Rightarrow m_o = m_w \sqrt{1-w^2/c^2}$$

$$\text{i.e.} \quad \boxed{m_w = \frac{m_o}{\sqrt{1-w^2/c^2}}}$$

For a particle with the rest mass  $m_o$ , moving at a speed  $\bar{v}$ , the momentum  $\bar{p}$  is defined as:

$$\boxed{\bar{p} = m_v \cdot \bar{v} = \frac{m_o \bar{v}}{\sqrt{1-v^2/c^2}} = \frac{m_o \bar{v}}{\sqrt{1-\beta^2}}} \quad \text{where} \quad \boxed{\beta = \bar{v}/c}$$

The relativistic mass,  $m_v = m(v)$ , thus grows with the velocity as:

$$m_v = \frac{m_o}{\sqrt{1-v^2/c^2}} = \gamma(v) \cdot m_o$$

### 1.3.4 Energy

$$\text{Starting from the force equation:} \quad \bar{F} = m \cdot a = m \frac{dv}{dt} = \frac{d\bar{p}}{dt} = \frac{d}{dt} \left( \frac{m_o \bar{v}}{\sqrt{1-v^2/c^2}} \right)$$

one can obtain *work* and *kinetic energy* just as in classical mechanics.

$$\text{Multiply by } \bar{v}: \quad \bar{F} \cdot \bar{v} = \bar{F} \cdot \frac{\Delta \bar{x}}{\Delta t} = \frac{d\bar{p}}{dt} \cdot \bar{v} = \frac{d}{dt} \left( \frac{1}{2} m \bar{v}^2 \right) = dT/dt$$

However, *work* is  $F \Delta \bar{x}$ , and *kinetic energy* is  $\frac{1}{2} m v^2$ . Since  $\frac{d}{dt} \left( \frac{1}{2} m v^2 \right) = \frac{1}{2} m \cdot 2v \frac{dv}{dt} = \frac{d(mv)}{dt} \cdot v = \frac{dp}{dt} \cdot v$ , we have that the work per time unit is equal to the time derivative of the kinetic energy.

The relativistic expression for the change in kinetic energy,  $dT$ , is given by:

$$\frac{dT}{dt} = \frac{dp}{dt} \cdot v$$

$$\Rightarrow dT = \bar{v} \cdot d\bar{p} = d(\bar{v} \cdot \bar{p}) - \bar{p} \cdot d\bar{v} = d\left(\frac{m_o v^2}{\sqrt{1-v^2/c^2}}\right) - \frac{m_o v \cdot dv}{\sqrt{1-v^2/c^2}}$$

$$\text{where} \quad -\frac{m_o v \cdot dv}{\sqrt{1-v^2/c^2}} = m_o c^2 \cdot d(\sqrt{1-v^2/c^2}) = d\left(\frac{m_o c^2 (1-v^2/c^2)}{\sqrt{1-v^2/c^2}}\right) = d\left(\frac{m_o (c^2 - v^2)}{\sqrt{1-v^2/c^2}}\right)$$

$$\text{since} \quad \Rightarrow \quad m_o c^2 d(\sqrt{1-v^2/c^2}) = m_o c^2 \cdot 2 \left(-\frac{v \cdot dv}{c^2}\right) \frac{1}{2} (1-v^2/c^2)^{-1/2} = -\frac{m_o v \cdot dv}{\sqrt{1-v^2/c^2}}$$

$$\Rightarrow dT = d\left(\frac{m_o \cdot v^2}{\sqrt{1-v^2/c^2}}\right) + d\left(\frac{m_o(c^2-v^2)}{\sqrt{1-v^2/c^2}}\right) = d\left(\frac{m_o c^2}{\sqrt{1-v^2/c^2}}\right)$$

However, we have  $T = 0$  for  $v = 0$  which gives:

$$T = \frac{m_o c^2}{\sqrt{1-v^2/c^2}} - m_o c^2 = m_v c^2 - m_o c^2$$

Since the kinetic energy only depends on  $v$  it should approach the non-relativistic expression for small  $v$ , which can be checked by an expansion:

$$\gamma(v) = \frac{1}{\sqrt{1-v^2/c^2}} = 1 + \frac{1}{2} \cdot \frac{v^2}{c^2} + \dots$$

$$\Rightarrow T = m_o c^2 \left( \frac{1}{\sqrt{1-v^2/c^2}} - 1 \right) = m_o c^2 (\gamma - 1) = \frac{1}{2} m_o v^2 + \dots$$

The *rest energy*,  $E_o$ , is related to the rest mass through:

$$\boxed{E_o = m_o c^2} \quad (1.5)$$

which relates energy and mass through the velocity of light,  $c$ . Thus,  $c^2$  is just a conversion factor to go from energy to mass and vice versa, in the same way as we need a conversion factor to transform temperatures measured in degrees Celsius to Fahrenheit. In order to get a tentative understanding of Einstein's very simple formula, please see Appendix B.

The relativistic energy is:

$$E = E_o + T = m_o c^2 + m_v c^2 - m_o c^2 = m_v c^2.$$

Thus, energy and mass is related through the square of the light velocity,  $c^2$ . This means that  $c^2$  act as a conversion factor to go from energy to mass and vice versa, in the same way as we need a conversion factor to transform temperature in degrees Celsius to degrees Fahrenheit.

Thus, energy and mass are related. The equivalence between energy and mass means that if the rest mass could be made disappear it should be converted to energy of some kind. A normal piece of matter does not undergo such processes but in particle physics it may happen that for example an electron and its antiparticle, the positron, annihilate to emit a photon. Like all kinds of electromagnetic radiation it will travel with the speed of light and have zero rest mass.

The general expression for energy is:

$$\boxed{E = m_v c^2 = \frac{m_o c^2}{\sqrt{1-v^2/c^2}}} \quad \text{which means that } v = c \text{ only if } m_o = 0.$$

The momentum relation:  $\bar{p} = m_v \bar{v} = \frac{E}{c^2} \bar{v}$  (since  $m_v = E/c^2$ )

must be valid for every kind of energy travelling at speed  $\bar{v}$ . Especially for an electromagnetic wave (or photon) at speed  $v = c$  we get:

$$p = \frac{E}{c} \quad \text{or} \quad \boxed{E = pc}$$

So, if the photon has zero mass and it travels with the speed of light, how can we then differ between a  $2eV$  photon and one at  $3eV$ ? The answer is given by the Plank's formula,  $E = \hbar\nu$ , which relates energy to frequency. A  $2eV$  photon is *red* whereas a  $3eV$  photon is *blue*.

Generally energy can also be expressed as a function of momentum:

$$E^2 = \frac{m_o^2 c^4}{1-v^2/c^2} = m_o^2 c^2 \left( \frac{c^2 - v^2 + v^2}{1-v^2/c^2} \right) = m_o^2 c^2 \left( \frac{c^2 - v^2}{1-v^2/c^2} + \frac{v^2}{1-v^2/c^2} \right) = m_o^2 c^2 \left( c^2 + \frac{v^2}{1-v^2/c^2} \right)$$

$$\Rightarrow E^2 = c^2 (m_o^2 c^2 + p^2) = m_o^2 c^4 + p^2 c^2 \quad \boxed{E = c \sqrt{m_o^2 c^2 + p^2}}$$

If we set  $c = 1$  we can write  $\boxed{E^2 - p^2 = m_o^2}$

For  $p \ll m_o c$  we can expand:

$$E = m_o c^2 \left( 1 + \frac{p^2}{2m_o^2 c^2} - \dots \right) = m_o c^2 + \frac{p^2}{2m_o} - \dots$$

which is of the form  $E = E_o + T$  with  $T = \frac{p^2}{2m_o}$ .

This illustrates the connection to the non-relativistic expression.

### 1.3.5 More Relations

Using  $p = m_o v = m_o \gamma v$  we obtain:

$$p^2 = m_o^2 \gamma^2 v^2 \Rightarrow \frac{p^2}{\gamma^2} = m_o^2 v^2$$

$$\Rightarrow m_o^2 = \frac{p^2}{v^2} \cdot \frac{1}{\gamma^2} = \frac{p^2}{v^2} (1 - \beta^2)$$

Using the relation:  $m_o^2 c^4 = E^2 - p^2 c^2$

$$\Rightarrow m_o^2 = \frac{E^2 - p^2 c^2}{c^4} \quad \text{but as was shown above} \quad m_o^2 = \frac{p^2}{v^2} (1 - \beta^2)$$

$$\Rightarrow p^2 (1 - \beta^2) = E^2 v^2 / c^4 - p^2 v^2 / c^2$$

$$\Rightarrow p^2 (1 - v^2 / c^2) = E^2 v^2 / c^4 - p^2 v^2 / c^2$$

$$\Rightarrow p^2 = E^2 v^2 / c^4$$

Multiply by  $c^2 \Rightarrow p^2 c^2 = E^2 v^2 / c^2$

$$\Rightarrow \boxed{\frac{pc}{E} = \frac{v}{c} = \beta}$$

$$\boxed{\gamma = \frac{1}{\sqrt{1-\beta^2}} = \frac{1}{\sqrt{1-p^2 c^2 / E^2}} = \frac{E}{\sqrt{E^2 - p^2 c^2}} = \frac{E}{m_o c^2}}$$

### 1.3.6 Example of Time Dilation: The Muon Decay

Muons are unstable particles heavier than electrons (positrons). A negatively (positively) charged muon decays into an electron (a positron), an anti-electron neutrino (electron neutrino) and a muon neutrino (an anti-muon neutrino) according to:



Muon decays will be described in more detail when we discuss the weak interaction (Section 3.3).

The lifetime and mass in the muon rest frame are, respectively:

$$\tau_o \sim 2.2 \mu s; \quad m_\mu = 0.106 \text{ GeV}$$

If we accelerate a muon beam to  $E_\mu = 100 \text{ GeV}$ , what is then the mean lifetime of the muon in the laboratory system? From Section 1.3.1 we have seen that:

$$\tau_{lab} = \gamma(\tau_o - \frac{v}{c^2}x)$$

where  $\tau_0$  is the life time in the muon rest frame.

But  $x = 0$  and  $v = 0$  in the muon rest frame  $\Rightarrow \tau_{lab} = \gamma \cdot \tau_o$

$$\tau_{lab}/\tau_o = \gamma = E/m_o c^2 = 100 \text{ GeV} / 0.106 \text{ GeV} \sim 1000$$

$$\Rightarrow \tau_{lab} = 2.2 \text{ ms}$$

### 1.3.7 Four-Vectors

Physical quantities that have a direction and magnitude can be represented by vectors. Such quantities are for example displacements, velocities, momenta and forces. In ordinary 3-dimensional space, a vector has three components  $(x, y, z)$  and if we choose to place the origin of our reference system at the base of the vector, the length is  $\sqrt{x^2 + y^2 + z^2}$ . In a non-relativistic world a vector looks the same whether you observe it sitting at rest or from a moving car. This is called *invariance* under translation. That this is true will be shown below.

In Section 1.3.1 we discussed Lorentz transformations in a special case where a reference system  $S'$  is moving along the  $x$ -axis of the reference system  $S$ , with a velocity  $v$ . We found that the location of a point  $P$  and the measurement of time in the systems  $S$  and  $S'$  are related through:

$$x' = \frac{x - vt}{1 - v^2/c^2} \tag{1.6}$$

$$y' = y \tag{1.7}$$

$$z' = z \tag{1.8}$$

$$t' = \frac{t - \frac{v}{c^2} \cdot x}{1 - v^2/c^2} \tag{1.9}$$

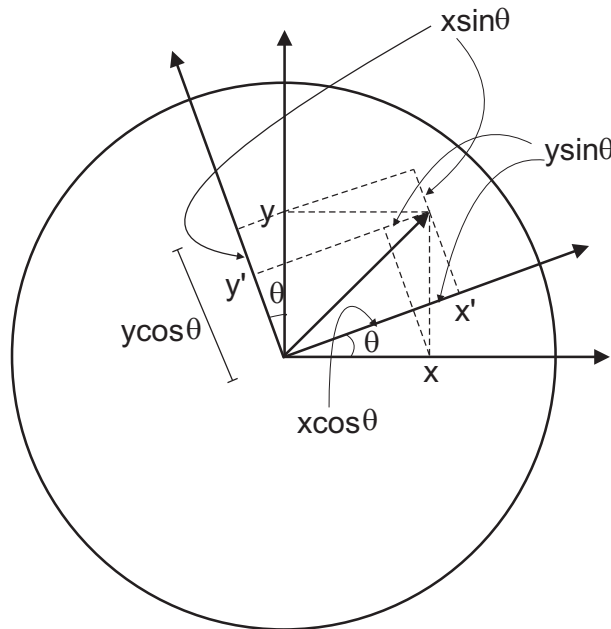
In a non-relativistic description  $v \ll c$  and thus we have from the relations above that  $x' \approx x - vt$  and  $t' \approx t$  i.e. the measurement of time is equal in the two systems to a very good approximation. The length of the vector in system  $S$  is  $x - 0$ . After some time  $t' = t$  the origin of system  $S'$  is at the location  $x' = vt$  and the point  $P$  is at  $x' = x + vt$  and thus the length of the vector is  $x + vt - vt = x$ , i.e. the length of the vector is invariant under translation in a non-relativistic system.

If we now consider a rotation of the two systems in the case where they have a common origin, we find that the vector components will be mixed and if we, for simplicity, limit ourselves to two dimensions, the coordinates of rotated system  $(x', y', z')$  can be expressed in terms of the coordinates of the original system  $(x, y, z)$  as:

$$x' = x \cos \theta + y \sin \theta$$

$$y' = y \cos \theta - x \sin \theta$$

where  $\theta$  is the angle of rotation. This is illustrated in Figure 4.9



$$x' = x \cos \theta + y \sin \theta$$

$$y' = y \cos \theta - x \sin \theta$$

Figure 1.3: *The relation between the coordinates of two rotated coordinate systems.*

However, the length of the vector remains the same since:

$$\begin{aligned} x'^2 + y'^2 &= (x \cos \theta + y \sin \theta)^2 + (y \cos \theta - x \sin \theta)^2 \\ &= x^2 \cos^2 \theta + 2xy \cos \theta \sin \theta + y^2 \sin^2 \theta + y^2 \cos^2 \theta - 2xy \cos \theta \sin \theta + x^2 \sin^2 \theta \\ &= x^2 (\cos^2 \theta + \sin^2 \theta) + y^2 (\sin^2 \theta + \cos^2 \theta) \\ &= x^2 + y^2 \end{aligned}$$

It is interesting to notice that in the same way as  $x'$  and  $y'$  coordinates are a mixture of the  $x$  and  $y$  coordinates for rotated reference systems, we may, from the equations 1.6 and 1.9, regard

$x'$  and  $t'$  as a mixture of  $x$  and  $t$  and thus it corresponds to a rotation in space and time. This indicates that space and time can no longer be treated independently but are components of a single four-dimensional structure. This was first realized by the German physicist Hermann Minkowski, why the four-dimensional space also is called Minkowski space.

In a non-relativistic description, the use of ordinary space instead of space-time is appropriate, because time is treated as universal and constant independent of the motion of an observer. In a relativistic context time is not independent of the object's velocity relative to the observer and thus, time cannot be separated from the three dimensions of space.

A displacement in space-time is not called 'distance' but *interval*, since it corresponds to a distance in a different geometry than the ordinary space. An interval is defined by the quantity  $\sqrt{c^2t^2 - x^2 - y^2 - z^2}$ , and can be represented by a *four-vector*. We notice that  $ct$  is the distance light is travelling in the time  $t$ . The difference between a distance in ordinary space and an interval in space-time is that, if we consider a point in space-time at time  $t = 0$ , we notice that interval squared is negative i.e. the interval is given by an imaginary number, whereas a distance in ordinary space can only be positive. When an interval is imaginary we say that the two points defining the interval makes up a *space-like* interval, whereas if the two points are at the same place but only differ in time, the the square of time is positive and it is called a *time-like* interval. We will meet time- and space-like particle interactions in Sections (3.1) and (3.2), when we discuss virtual particles and Feynman diagrams.

The path of a particle travelling through space and time is called a *world line*. Such world lines can be represented in a two-dimensional space-time diagram, where the vertical axis represents time ( $ct$ ) and the horizontal space ( $x$ ). In order to simplify things we use the same units for time and distance as was discussed in Section 1.1. Thus, either the length unit is  $3 \cdot 10^8$  meter i.e. the distance light travels in one second (light-second), or the time-unit  $1/3 \cdot 10^{-8}$  seconds, which is the time it takes for light to travel one meter. With the units chosen in this way the world line for a photon, which travels with the speed of light, will have a slope of  $45^\circ$ . This world line would sweep a cone in four dimensions and is therefore called a *light cone*. Each point on the light cone have an interval with respect to the origin (the place of an observer), which is zero since  $ct^2 - x^2 = 0$ . Figure 1.4 shows a two-dimensional light-cone diagram with a world line in red.

Thus. space-time from the observers point of view (the origin) can be separated into three regions. In one region we have space-like intervals and in the other two time-like intervals, of which one represents the past and one the future.

Let us investigate if the space-time four-vector is invariant under Lorentz transformations. Using equations (1.6) - (1.9) we get for a four-vector in system  $S'$ , by setting  $c = 1$ :

$$\begin{aligned}
 t'^2 - x'^2 - y'^2 - z'^2 &= \frac{(t - vx)^2}{1 - v^2} - \frac{(x - vt)^2}{1 - v^2} - y^2 - z^2 \\
 &= \frac{t^2 - 2tvx + v^2t^2}{1 - v^2} - \frac{x^2 + 2xvt - v^2t^2}{1 - v^2} - y^2 - z^2 \\
 &= \frac{t^2 - v^2t^2 - x^2 + v^2x^2}{1 - v^2} - y^2 - z^2
 \end{aligned} \tag{1.10}$$

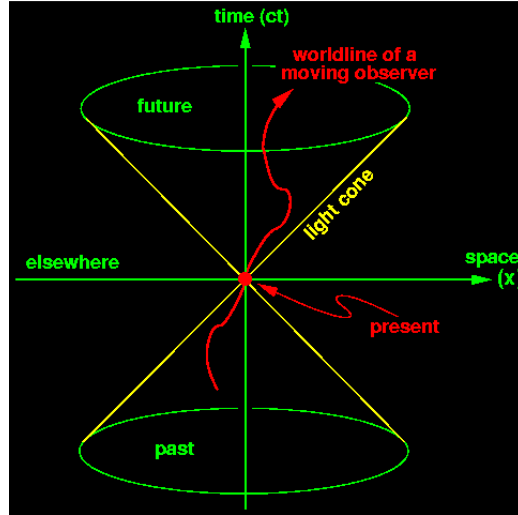


Figure 1.4: A two-dimensional light-cone diagram with the vertical axis representing time and the horizontal space. Also the trajectory of a particle moving through space-time is shown.

$$\begin{aligned}
 &= \frac{t^2(1-v^2) - x^2(1-v^2)}{1-v^2} - y^2 - z^2 \\
 &= t^2 - x^2 - y^2 - z^2
 \end{aligned}$$

Thus, we have proven that a four-vector in space time is invariant under Lorentz transformations, i.e. the four-vector is the same before and after the transformation.

The notation we use for a general four-vector is often  $a_\mu$ , where  $\mu$  stands for the four possible directions  $(t, x, y, z)$ , is:

$$a_\mu = (a_0, a_1, a_2, a_3) = (a_0, \bar{a}),$$

where  $\bar{a} = (a_1, a_2, a_3)$  is a vector in three dimensions. However, since we are running out of indices we will in later discussions drop the  $\mu$  and denote four-vectors by  $a$  and three-vectors by  $\bar{a}$ .

The value of an arbitrary four-vector  $a_\mu$  is given by the length squared of the interval:

$$a_\mu^2 = a_o^2 - (a_1^2 + a_2^2 + a_3^2) = (a_o^2 - \bar{a}^2)$$

$a_\mu^2$  transforms like a *scalar* in Lorentz space, which means:

$$a_\mu^2 = a_\mu \cdot a_\mu.$$

This quantity is *invariant* under Lorentz transformations and will thus be the same in all coordinate systems.

If we want to add four-vectors we just add the four components, exactly the same way as in the case of adding the three components in normal vector addition. This means that any conservation law that is valid for four-vectors are also valid for each component.

The scalar product of the two four-vectors  $a_\mu$  and  $b_\mu$  is:

$$a_\mu \cdot b_\mu = a_o \cdot b_o - (a_1 b_1 + a_2 b_2 + a_3 b_3) = a_o \cdot b_o - \bar{a} \cdot \bar{b}$$

$$\Rightarrow (a_\mu + b_\mu)^2 = a_\mu^2 + b_\mu^2 + 2a_\mu \cdot b_\mu$$



Space-time coordinates can consequently be written:

$$r_\mu = (r_0, \bar{r}) = (ct, \bar{r}),$$

where  $r_0 = ct$  is the time component and  $\bar{r} = (x, y, z)$  is the space component.

Are there other four-vectors, similar to that describing space-time, that are invariant under Lorentz transformations? It turns out that energy and momentum can be combined in a four vector. With  $c = 1$  we have seen that energy is equal to mass (equation 1.5) and the momentum is mass times velocity (equation 1.4). This is true for both non-relativistic and relativistic systems, only the definition of mass is different. In the relativistic case, again setting  $c = 1$ , mass is defined as:

$$m = \frac{m_0}{\sqrt{1-v^2}}, \quad \text{where } m_0 \text{ is the rest mass.}$$

thus, the equations for energy and momentum are:

$$E = m = \frac{m_0}{\sqrt{1-v^2}} \quad (1.11)$$

$$p = mv = \frac{m_0 \cdot v}{\sqrt{1-v^2}} \quad (1.12)$$

Since velocity can be represented by a vector, also momentum is a vector quantity. The relation between energy and momentum is:

$$E^2 - p^2 = m_0^2$$

What is the energy and momentum measured in the reference system  $S'$ , moving along the  $x$ -axis with velocity  $v$  with respect to the system  $S$ ? In order to find out we have to perform Lorentz transformations of the relations for energy and momentum, given in equations (1.11) and (1.12). Let us study an object, which is moving with velocity  $u$  in the system  $S$ , but we want to measure it sitting in the system  $S'$ . This velocity we call  $u'$  and this is what we need to calculate. Using equations (1.6) and (1.9) we have:

$$u' = \frac{x'}{t'} = \frac{x - vt}{t - vx}$$

divide by  $t$  and use that  $u = x/t$

$$\begin{aligned} \Rightarrow u' &= \frac{u - v}{1 - uv} \\ \Rightarrow 1 - u' &= 1 - \frac{(u - v)^2}{(1 - uv)^2} = 1 - \frac{u^2 - 2uv + v^2}{1 - 2uv + u^2v^2} \\ &= \frac{1 - 2uv + u^2v^2 - u^2 + 2uv - v^2}{1 - 2uv + u^2v^2} = \frac{(1 - v^2)(1 - u^2)}{(1 - uv)^2} \\ \Rightarrow \frac{1}{\sqrt{1 - u'^2}} &= \frac{(1 - uv)}{\sqrt{1 - v^2}\sqrt{1 - u^2}} \end{aligned} \quad (1.13)$$

Inserting equation (1.13) into (1.11) we get:

$$E' = \frac{m_0}{\sqrt{1 - u'^2}} = \frac{m_0 - m_0uv}{\sqrt{1 - v^2}\sqrt{1 - u^2}} = \left( \frac{m_0 - m_0uv}{\sqrt{1 - u^2}} \right) \cdot \frac{1}{\sqrt{1 - v^2}}$$

$$\begin{aligned}
&= \left( \frac{m_0}{\sqrt{1-u^2}} - \frac{m_0 u}{\sqrt{1-u^2}} \cdot v \right) \frac{1}{\sqrt{1-v^2}} \\
\Rightarrow E' &= \frac{E - p \cdot v}{\sqrt{1-v^2}} \quad \text{Cf. } t' = \frac{t - vx}{\sqrt{1-v^2}}
\end{aligned}$$

Similarly we get by inserting equation (1.13) into (1.12):

$$\begin{aligned}
p'_x &= \frac{m_0 u'}{\sqrt{1-u'^2}} = E' u' \quad \text{since } E' = \frac{m_0}{\sqrt{1-u'^2}} \\
\Rightarrow p'_x &= \frac{m_0(1-uv)}{\sqrt{1-v^2}\sqrt{1-u^2}} \cdot \frac{u-v}{1-uv} \\
&= \frac{m_0 u - m_0 v}{\sqrt{1-v^2}\sqrt{1-u^2}} = \left( \frac{m_0 u}{\sqrt{1-u^2}} - \frac{m_0 v}{\sqrt{1-u^2}} \right) \cdot \frac{1}{\sqrt{1-v^2}} \\
\Rightarrow p'_x &= \frac{p_x - vE}{\sqrt{1-v^2}} \quad \text{Cf. } x' = \frac{x - vt}{\sqrt{1-v^2}}
\end{aligned}$$

i.e. energy transforms the same way as time, and momentum the same way as space.

$$\begin{aligned}
p'_x &= \frac{p_x - vE}{\sqrt{1-v^2}} \\
p'_y &= p_y \\
p'_z &= p_z \\
E' &= \frac{E - p \cdot v}{\sqrt{1-v^2}}
\end{aligned}$$

Thus, the definition of a four-vector in energy-momentum space is:

$$p_\mu = (p_0, \vec{p}) = (E, \vec{p})$$

Conservation of three-vector momenta means that the sum of momenta of colliding particles will be constant. However, we have found that in a relativistic world, we have to extend this description by adding a fourth component, the energy, to arrive at a valid four-vector relationship in the geometry of space and time.

Thus, the conservation of energy is the fourth requirement that has to be valid in addition to the conservation of momentum. This means conservation of four-momenta:

$$\sum_i p_{\mu i} = \sum_j p_{\mu j}$$

where  $i = 1, 2, 3, \dots$  are the incoming particles and  $j = 1, 2, 3, \dots$  are the outgoing, and  $\mu = (E, p_x, p_y, p_z)$ .

What is the square of the length of the four-vector of a single particle? This is equal to  $E^2 - p_x^2 - p_y^2 - p_z^2 = E^2 - \vec{p}^2$ . According to what we have discussed above this quantity had to be the same in all coordinate systems and especially it has to be unchanged as we go to the rest frame of the particle. In this reference frame the particle is not moving and has only energy, which is equivalent to rest mass. Thus,  $E^2 - \vec{p}^2 = m_0^2$ .

The motion of a particle in Lorentz space is represented by a space-time curve (a world line) given by a differential transformation of a four-vector.

$$dx_\mu = (cdt, d\bar{x}) = (cdt, \bar{v}dt),$$

where  $x_\mu$  and  $\bar{x}$  represent the four-vector and space components, respectively

The time derivative

$$u_\mu = \frac{dx_\mu}{dt} = (c, \frac{d\bar{x}}{dt}) = (c, \bar{v})$$

is also a four-vector since  $dx_\mu$  is one.

### 1.3.8 Invariant mass

In the previous section we have seen that the four-momentum of a particle is equal to its rest mass. This means that the rest mass is given by the relativistic length of the four-vector and this length is preserved under Lorentz transformations. Therefore the rest mass is also called the invariant mass.

The invariant mass of a system of particles is given by:

$$m^2 = (\sum E_i)^2 - (\sum \bar{p}_i)^2 = \sum p_{\mu i}^2 \quad \text{i.e. the sum of the four-vectors for all the particles in the system.}$$

If we specifically look at a decay of a particle A into two particles B and C, then the invariant mass of particle A can be calculated from the four-vectors of particles B and C in the following way:

$$m_A^2 = (p_{\mu B} + p_{\mu C})^2 = p_{\mu B}^2 + p_{\mu C}^2 + 2p_{\mu B} \cdot p_{\mu C} = m_B^2 + m_C^2 + 2(E_B E_C - \bar{p}_B \bar{p}_C)$$

### 1.3.9 Reference systems

The *centre-of-mass* or *CM* system is the system in which the momentum sum of all particles in the initial as well as in the final states is zero. This has to be true since momentum has to be conserved in any reaction between particles.

The *laboratory* frame is the system in which the detector is at rest. The *laboratory* system and the *centre-of-mass* system coincide if we have colliding particles and antiparticles with equal energies.

**Example 1)** Calculate the *centre-of-mass energy*,  $\sqrt{s}$ , for a muon-proton scattering process

where  $E_\mu = 100 \text{ GeV}$ , and the proton is at rest

$$\mu \xrightarrow[p_{\mu}(E_{\mu}, \bar{p}_{\mu})]{E \gg m_{\mu}} \begin{matrix} p_p(E_p, \bar{p}_p) \\ \bullet \\ p \end{matrix}$$

(Note that  $\mu$  is now the notation for the muon)

$$p_\mu = (E_\mu, \bar{p}_\mu)$$

$$E_\mu^2 - \bar{p}_\mu^2 = m_\mu^2 \Rightarrow E_\mu \approx |\bar{p}_\mu| \text{ since } m_\mu = 0.1 \text{ GeV} \ll E_\mu$$

$$p_p = (m_p, 0) \quad (E_p = m_p \text{ since the proton is at rest.})$$

The centre-of-mass energy squared is:

$$\begin{aligned} s &= (p_\mu + p_p)^2 = p_\mu^2 + p_p^2 + 2p_\mu p_p = \\ &= m_\mu^2 + m_p^2 + 2p_\mu p_p = \\ &= m_\mu^2 + m_p^2 + 2(E_\mu E_p - \bar{p}_\mu \bar{p}_p) \approx \\ &\approx m_\mu^2 + m_p^2 + 2E_\mu m_p \text{ since } E_p = m_p \text{ and } |\bar{p}_p| = 0 \end{aligned}$$

But  $E_\mu \gg m_\mu$  and  $m_p$

$$\Rightarrow s \approx 2E_\mu m_p$$

$$\Rightarrow s \approx 200 \text{ GeV}^2 \Rightarrow \sqrt{s} \approx 14 \text{ GeV}$$

**Example 2)** What energy is needed to get the same centre-of-mass energy if the muon and the proton are colliding?



As in Example 1):

$$s = (p_\mu + p_p)^2 = m_\mu^2 + m_p^2 + 2(E_\mu E_p - \bar{p}_\mu \bar{p}_p)$$

Assume that  $m_\mu$  and  $m_p$  are small compared to their momenta  $\Rightarrow E_\mu \approx |\bar{p}_\mu|$  and  $E_p \approx |\bar{p}_p|$ .

$\bar{p}_\mu \cdot \bar{p}_p = |\bar{p}_\mu| |\bar{p}_p| \cos\theta$ ; where  $\cos\theta = -1$  since the directions of motion for the muon and the proton are opposite.

$$\Rightarrow s \approx 2(E_\mu E_p - |\bar{p}_\mu| |\bar{p}_p| \cos\theta) \approx 2(E_\mu E_p + |\bar{p}_\mu| |\bar{p}_p|) \approx 4E_\mu E_p$$

$$4E_\mu E_p = 200 \text{ GeV}^2$$

$$\Rightarrow E_\mu E_p = 50 \text{ GeV}^2$$

$$\text{If } E_\mu = E_p \Rightarrow E = \sqrt{50} \approx 7 \text{ GeV}$$

Compare to Example 1) where  $E_\mu = 100 \text{ GeV}$

**Example 3)** Calculate the center of mass energy for  $e^+e^-$  scattering if  $E_{e^-} = E_{e^+} = 100 \text{ GeV}$ .

$$|\bar{p}_{e^-}| = |-\bar{p}_{e^+}| \approx E_{e^\pm}$$

$$s = (p_{e^-} + p_{e^+})^2 = p_{e^-}^2 + p_{e^+}^2 + 2p_{e^-} p_{e^+} =$$

$$2m_e^2 + 2(E_{e^-} E_{e^+} - p_{e^-} p_{e^+}) = 2m_e^2 + 2(E_{e^-} E_{e^+} + E_{e^-} E_{e^+}) \approx 4E_{e^\pm}^2$$

$$s = 4 \cdot 100^2 = 40000 \text{ GeV}^2$$

$$\sqrt{s} = 200 \text{ GeV}$$

# Chapter 2

## Quantum Mechanics

### 2.1 The Photoelectric Effect

The German physicist Max Planck proposed in the year 1900 that light can be emitted or absorbed by matter only in multiples of a minimum energy quantum, which is given by:

$$E_\gamma = h\nu; \quad (\text{Planck's formula}) \quad (2.1)$$

where  $\nu$  is the frequency of the light wave and  $h$  is called the *Planck constant*, which has a value of  $6.63 \cdot 10^{-34} J \cdot s$

Since the frequency,  $\nu$ , the wavelength,  $\lambda$  and the speed of light,  $c$ , are related through:  $\nu \cdot \lambda = c$ , Planck's formula can also be written:

$$E_\gamma = hc/\lambda \quad (2.2)$$

This is regarded as the foundation of quantum mechanics. Planck introduced the notation of quantized electromagnetic radiation in order to explain the spectrum of blackbody radiation but he did not fully realize the consequences of his proposal. This was recognized by Albert Einstein who in 1905 proposed that a beam of light is not a wave propagating through space but rather a stream of discrete wave packets (photons). From this assumption he was able to give an explanation to the photoelectric effect.

In order to release an electron from the surface of a metal foil a minimum energy of the photon is needed ( $\geq$  the binding energy of the electron). Once this requirement is fulfilled the number of released electrons only depends on the intensity of the photons and not on their energy.

Intensity  $\sim$  number of quanta

The fact that light behaves like a wave motion in some applications but as particles in others, which is also true for what we normally call elementary particles, is called the wave-particle duality.

## 2.2 The Uncertainty Principle

The uncertainty principle comes from the fact that any observation (measurement) is an interaction with the observer and thus will cause a disturbance to the system. This will prevent a perfect measurement. According to quantum mechanics (the theory of particles) there is always some uncertainty in the specification of positions and velocities. The best we can do is to give a certain probability that a particle will have a position near some coordinate  $x$ . We can give a *probability density*  $\rho_1(x)$ , such that  $\rho_1(x)\Delta x$  is the probability that the particle will be found between  $x$  and  $x + \Delta x$ . This can be described by a distribution with a width  $\Delta x$ . In the same way we must specify the velocity of the particle by means of the probability density  $\rho_2(v)$ , with  $\rho_2(v)\Delta v$  being the probability that the velocity will be in the range  $v$  and  $v + \Delta v$ . The corresponding distribution has a width of  $\Delta v$ .

One of the fundamental results of quantum mechanics is that the two functions  $\rho_1(x)$  and  $\rho_2(v)$  can not be chosen independently and can not both be made arbitrarily narrow. Nature demands that the product of the two widths would be at least as big as  $\hbar/m$ , where  $\hbar = h/2\pi$  and  $m$  is the mass of the particle. This is the *Heisenberg uncertainty principle*:

$$\Delta v \cdot \Delta x \geq \hbar/m$$
$$\Rightarrow \boxed{\Delta p \cdot \Delta x \geq \hbar}$$

Thus, when we try to measure the position of a particle more accurately, the measurement of its momentum becomes less exact and vice versa.

A similar limitation occurs if one tries to measure the energy of a quantum system at a certain time. An instantaneous measurement requires a high frequency probe, which according to Planck's relation is equivalent to a high energy probe. This gives a large disturbance to the system such that the energy can not be determined accurately. Conversely a low energy probe, which allows for a precise determination of the energy, is of low frequency and therefore the time can not be specified very well.

$$\Rightarrow \boxed{\Delta E \cdot \Delta t \geq \hbar} \quad (2.3)$$

This situation can be illustrated by an attempt to localize the position of an electron orbiting around a nucleus by scattering a photon off it, as illustrated in Figure 2.1. The wavelength ( $\lambda$ ) of the photon is related to its momentum ( $p$ ) through  $\lambda = \frac{h}{p}$ .

Since the wavelength is inversely proportional to the momentum one needs the highest possible momentum in order to determine the position as accurately as possible. However, in using a high momentum photon the electron will be greatly disturbed such that the knowledge of its momentum will be very uncertain.

On the other hand, an electron travelling through space without being disturbed has a definite momentum ( $\Delta p = 0$ ), given by  $p = \hbar/\lambda$ . However, since it corresponds to a wave extending infinitely through space it is impossible to specify its location.

Figure 2.2 shows the waves of an electron in different situations. An electron bound to an atom is localised by the size of the atom ( $\Delta x$ ), which corresponds to an uncertainty in its momentum,

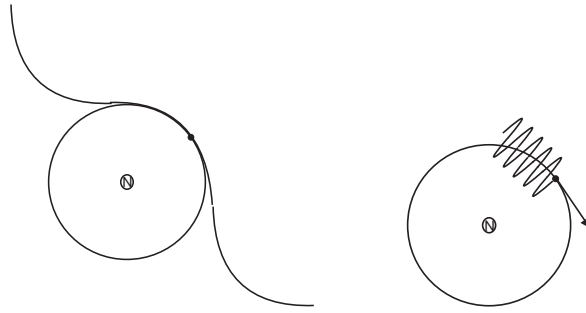


Figure 2.1: *The ability to localize the position of an electron, orbiting around a nucleus, using photons of different wave lengths.*

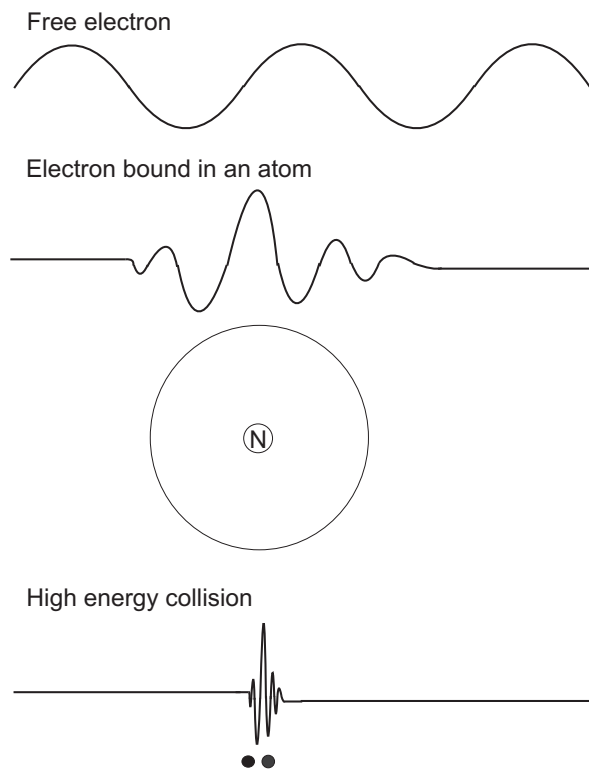


Figure 2.2: *The particle's wavefunction reflecting its localization.*

$\Delta p$ , given by the uncertainty principle. The spread in the wavelength of the wavefunction then becomes  $\Delta \lambda = \frac{h}{\Delta p}$ . This gives a localised wave packet reflecting the approximate localisation of the electron. In high energy collisions the electron is very accurately localised and it becomes sensible to regard the electron as a particle.

## 2.3 The Schrödinger Equation

The principle foundation of *non-relativistic quantum theory* is the Schrödinger equation. As well as light in some cases can be described as a wave motion and in other as a stream of particles, the German physicist Erwin Schrödinger formulated a matter wave function as the accurate representation of the behaviour of a matter particle. Schrödinger's equation describes a particle by its wavefunction ( $\psi$ ) showing how the particle wavefunction evolves in space and time under certain circumstances. The consequence of this description is that collisions between particles no longer have to be viewed as collisions between billiard balls but rather as an interference of wavefunctions. The Schrödinger equation can not really be derived but is rather an *axiom* of the theory.

Quantum mechanics relies upon the correspondance principle, introduced by Niels Bohr in 1920. It states that the behaviour of systems described by the theory of quantum mechanics should reproduce the classical physics results in regions where classical physics is valid.

The parameters, describing a physical system, in classical physics are scalars i.e. numerical quantites used to specify position, momentum, energy etc. For example the linear momentum of an object is just the product of its mass and velocity. However, in a quantum mechanical description it is not possible to use scalars, since due to the Heisenberg uncertainty principle exact values of properties can not be given. Thus, the classical variables have to be replaced by the corresponding quantum mechanical operators, which convert scalars into vectors.

In non-relativistic classical mechanics the linear momentum of a free particle is given by:

$$p = m \cdot v \text{ and the kinetic energy by } E = \frac{1}{2}m \cdot v^2$$

$$\Rightarrow E = \frac{p^2}{2m} \text{ (classical energy-momentum relation)}$$

In quantum mechanics energy and momentum are replaced by the following operators acting on the wave function describing a particle in space and time,  $\Psi(\vec{x}, t)$ , where  $\vec{x}$  represents a vector in  $x$ ,  $y$  and  $z$  coordinates:

$$E \rightarrow i\hbar \frac{\partial}{\partial t} \quad (\text{the energy operator})$$

$$\vec{p} \rightarrow -i\hbar \vec{\nabla} \quad (\text{the momentum operator})$$

$$\text{where } \vec{\nabla} = \left( \frac{\partial}{\partial x}, \frac{\partial}{\partial y}, \frac{\partial}{\partial z} \right).$$

$\Rightarrow$  Schrödinger equation for a free particle:

$$i\hbar \frac{\partial}{\partial t} \Psi(\vec{x}, t) = \frac{(-i\hbar \vec{\nabla})^2}{2m} \Psi(\vec{x}, t)$$

and for a bound state:

$$i\hbar \frac{\partial}{\partial t} \Psi(\vec{x}, t) = \frac{(-i\hbar \vec{\nabla})^2}{2m} \Psi(\vec{x}, t) + V \Psi(\vec{x}, t)$$

where  $H = -\frac{\hbar^2}{2m} \vec{\nabla}^2 + V$  is the so called *Hamilton operator*, representing the total energy of a particle with mass  $m$  in the potential  $V$ .



The Schrödinger equation is of first order in time and second order in space. This is unsatisfactory when dealing with high energy particles, where the description must be relativistically invariant, with space and time coordinates occurring to the same order.

The Schrödinger equation describes non relativistic bound states like:

- Bohr's atomic model
- The energy levels of atoms
- Bound states of heavy quarks

How do we know whether a bound state is relativistic or not? A rule of thumb is that if the binding energy is small compared to the rest energies of the constituents, then the system is non-relativistic. For example the binding energy of hydrogen is 13.6 eV, whereas the rest energy of an electron is 511 eV, which consequently is a non-relativistic system. On the other hand the binding energies of quarks in a nucleon are of the order of a few hundred MeV, which is essentially the same as the effective rest energy of the light quarks ( $u, d, s$ ), but substantially less than those of the heavy quarks ( $c, b, t$ ). Thus, in the latter case we are dealing with relativistic systems.

## 2.4 The Double Slit Experiment (Interference Effects)

Problems in particle physics often concern interactions between particles, where we need to calculate the *density flux*,  $j$ , of a beam of particles. Consider the case of the double slit experiment (a more intuitive description can be found in Appendix C), where each slit can be regarded as a source of particles, as illustrated in Figure 2.3, with the particles being described by the wave functions  $\Psi_1$  and  $\Psi_2$ .

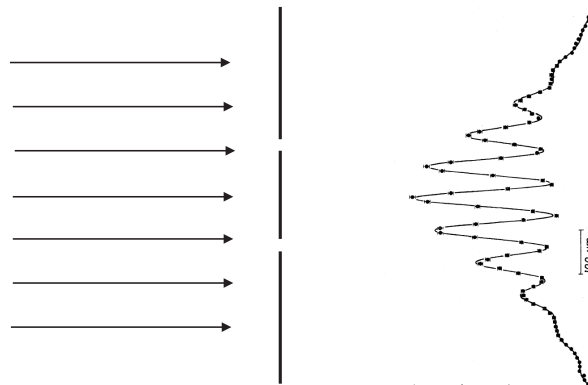


Figure 2.3: *Interference pattern caused by a parallel flow of particles passing through two nearby slits.*

The probability to find a particle anywhere is the square of the wave function:

$$|\Psi|^2 = |\Psi_1 + \Psi_2|^2 = |\Psi_1|^2 + |\Psi_2|^2 + \Psi_1\Psi_2^* + \Psi_1^*\Psi_2$$

where  $|\Psi|^2 = \Psi\Psi^*$  and  $\Psi^*$  is the complex conjugate of  $\Psi$ .

$\Rightarrow$  The interference can be constructive or destructive depending on the sign of  $\Psi_1^*\Psi_2$  etc.

Define the *probability density* as  $\rho = |\Psi|^2$

and  $|\Psi|^2 d^3x$  as the probability to find a particle in the volume  $d^3x$ .

Let us now convince ourselves that  $|\Psi|^2$  is a probability density. Then it should obey the *continuity equation*, which describes conservation of probability, i.e. the rate with which the number of particles decreases in a given volume is equivalent to the total flux of particles out of that volume.

$$\Rightarrow -\frac{\partial}{\partial t} \int_V \rho dV = \int_S \vec{j} \cdot \vec{n} dS = \int_V \nabla \cdot \vec{j} dV$$

where  $j$  is the particle density flux and  $\vec{n}$  is a unit vector normal to the surface element  $dS$  and  $S$  is the surface enclosing the volume  $V$ . The last equality is the Gauss theorem. The probability density and the flux density are thus related through:

$$\Rightarrow \frac{\partial \rho}{\partial t} + \nabla \cdot \vec{j} = 0 \quad (\text{continuity equation})$$

Use the Schrödinger equation for a free particle to determine the flux.

$$\begin{aligned} i\hbar \frac{\partial}{\partial t} \Psi(\vec{x}, t) &= \frac{(-i\hbar \nabla)^2}{2m} \Psi(\vec{x}, t) \\ \Rightarrow i \frac{\partial}{\partial t} \Psi + \frac{\nabla^2}{2m} \Psi &= 0; \quad \text{if } \hbar = 1 \end{aligned} \quad (2.4)$$

The complex conjugate equation:

$$-i \frac{\partial}{\partial t} \Psi^* + \frac{\nabla^2}{2m} \Psi^* = 0 \quad (2.5)$$

Multiply (2.4) with  $-i\Psi^*$

$$\Rightarrow (-i\Psi^*) \left( i \frac{\partial}{\partial t} \Psi + \frac{\nabla^2}{2m} \Psi \right) = 0 \quad (2.6)$$

Multiply (2.5) with  $-i\Psi$

$$\Rightarrow (-i\Psi) \left( -i \frac{\partial}{\partial t} \Psi^* + \frac{\nabla^2}{2m} \Psi^* \right) = 0 \quad (2.7)$$

Subtract (2.6) from (2.7)

$$\begin{aligned} \Rightarrow \Psi^* \frac{\partial}{\partial t} \Psi + \Psi \frac{\partial}{\partial t} \Psi^* + \frac{-i}{2m} (\Psi^* \nabla^2 \Psi - \Psi \nabla^2 \Psi^*) &= 0 \\ \Rightarrow \boxed{\frac{\partial}{\partial t} (\Psi^* \Psi) - \frac{i}{2m} (\Psi^* \nabla^2 \Psi - \Psi \nabla^2 \Psi^*)} &= 0 \end{aligned} \quad (2.8)$$

since

$$\frac{\partial}{\partial t}(\Psi^*\Psi) = \Psi \frac{\partial}{\partial t}\Psi^* + \Psi^* \frac{\partial}{\partial t}\Psi \quad (2.9)$$

Compare this relation to the continuity equation:  $\frac{\partial \rho}{\partial t} + \nabla \cdot \vec{j} = 0$

$$\vec{j} = \frac{i}{2m}(\Psi^*\nabla\Psi - \Psi\nabla\Psi^*). \quad (2.10)$$

$$\begin{aligned} \text{Since } \nabla \cdot \vec{j} &= \nabla(\Psi^*\nabla\Psi - \Psi\nabla\Psi^*) = \\ &= \nabla\Psi^*\nabla\Psi + \Psi^*\nabla^2\Psi - \nabla\Psi\nabla\Psi^* - \Psi\nabla^2\Psi^* = \\ &= \Psi^*\nabla^2\Psi - \Psi\nabla^2\Psi^*, \end{aligned}$$

$$\text{we have } \frac{\partial}{\partial t}(\Psi^*\Psi) \equiv \frac{\partial \rho}{\partial t} \quad \text{and} \quad -\frac{i}{2m}(\Psi^*\nabla^2\Psi - \Psi\nabla^2\Psi^*) \equiv \nabla \cdot \vec{j}$$

**Example 1)**  $\Psi = N \cdot e^{i(\bar{p}x - Et)}$  which describes a free particle of energy  $E$  and momentum  $\bar{p}$ , with  $N$  being a normalization coefficient.

$$\rho = \Psi^*\Psi = N \cdot e^{-i(\bar{p}x - Et)} \cdot N \cdot e^{i(\bar{p}x - Et)} = |N|^2$$

$$\nabla \cdot \vec{j} = -\frac{i}{2m}(\Psi^*\nabla^2\Psi - \Psi\nabla^2\Psi^*)$$

$$\begin{aligned} \text{Insert into (2.10) gives: } \vec{j} &= -\frac{i}{2m}(N \cdot e^{-i(\bar{p}x - Et)} \cdot iN\bar{p}e^{i(\bar{p}x - Et)} - N \cdot e^{i(\bar{p}x - Et)} \cdot (-i)N\bar{p}e^{-i(\bar{p}x - Et)}) \\ &= -\frac{i}{2m}(i|N|^2\bar{p} + i|N|^2\bar{p}) = \frac{2\bar{p}|N|^2}{2m} = \frac{\bar{p}}{m}|N|^2 \end{aligned}$$

## 2.5 Spin

The measurement of atomic spectra around 1925 revealed structures with double lines where only a single line was expected according to Bohr's atomic model. The explanation proposed was that this effect is caused by the fact that the electron rotates around its own axis, a property called *spin*. According to Bohr the electron also orbits around the nucleus and thereby it gives rise to a magnetic field in the same way as a loop of electric current does. Equivalently the spin of the electron around its own axis can be regarded as a small loop of current, which creates a small magnetic field. The two magnetic fields can either be aligned or be opposite to each other, which corresponds to different directions of the electron spin. The energy of the two possible states differ slightly and give rise to a splitting of the spectral lines associated with the Bohr orbit.

The description of spin as a rotating ball is attractive since it gives us an intuitive feeling which helps understanding the phenomena observed. Although the point of the rotation axis will not

move, all other points on the surface of the ball will rotate. Now, the electron is as far as we know a pointlike particle and therefore it is hard to define the rotation of an electron in a classical way. It must, however, be kept in mind that this is just a model and that spin in reality is a quantum concept, that can be used to specify the state of an electron, like the quanta of intrinsic angular momentum and electric charge.

Elementary particles appear in two types; *fermions*, which have half integer spin ( $\frac{1}{2}\hbar, \frac{3}{2}\hbar, \dots$ ) and obey Fermi-Dirac statistics, and *bosons*, with integer spin ( $0, \hbar, 2\hbar, \dots$ ), obeying Bose-Einstein statistics. The statistics, which the different particle types are said to obey determines how the wave function,  $\psi$ , describing a system of identical particles behaves under the interchange of any two particles. The probability  $|\psi|^2$  will not be affected by the interchange since all particles are identical. The so called *spin statistics theorem* says:

a system under exchange of identical bosons  $\psi$  is symmetric

a system under exchange of identical fermions  $\psi$  is antisymmetric

What implications does this have? Assume that we have two fermions in the same quantum state. If we interchange these particles the wave function, describing the two-particle state, would obviously not change. But according to the rule of spin statistics the wave function of fermions must change under an exchange. Consequently it is not allowed for two fermions to exist in the same quantum state. This is called the *Pauli exclusion principle*.

On the other hand there are no such restrictions to bosons, where an arbitrary number can be in the same quantum state. Compare to photons in a laser.

## 2.6 Symmetries and Conservation Laws

Symmetries play an important role in particle physics. There is a relation between symmetries and conservation laws as for example in classical physics:

- Invariance under change of time  $\Rightarrow$  conservation of energy
- Invariance under translation in space  $\Rightarrow$  conservation of momentum
- Invariance under rotation  $\Rightarrow$  conservation of angular momentum

In particle physics there are many examples of symmetries and their associated conservation laws. Maybe even more important are cases where symmetries are broken, since these are necessary to, for example, explain why particles have masses (the Higgs mechanism, see section 3.3.4) and why universe consists of matter and not equal amounts of matter and antimatter, as it is believed was the case right after the Big Bang.

Some basic conserved quantities are:

- *energy*: the energy of the initial state must be equal to that of the final state  
 $\Rightarrow p \rightarrow n + e^+ + \nu_e$  can not occur spontaneously since  $m_p(938) < m_n(939)$
- *momentum*: the momentum of the initial state must be equal to that of the final state

- *electric charge*: the electric charge of the initial state must be equal to that of the final state

Beside these, there are also other quantities that has been found to be conserved as will be described in the following sections.

## 2.6.1 Leptons and Lepton Number

The known leptons and some of their properties are listed in Table 2.1.

Charged leptons				Neutrinos			
name	symbol	electric charge	mass (MeV/c <sup>2</sup> )	name	symbol	electric charge	mass (MeV/c <sup>2</sup> )
Electron	$e^-$	-1	0.511	Electron neutrino	$\nu_e$	0	< 0.000022
Positron	$e^+$	+1	0.511	Electron antineutrino	$\bar{\nu}_e$	0	
Muon	$\mu^-$	-1	105.7	Muon neutrino	$\nu_\mu$	0	< 0.17
	$\mu^+$	+1	105.7	Muon antineutrino	$\bar{\nu}_\mu$	0	
Tau lepton	$\tau^-$	-1	1777	Tau neutrino	$\nu_\tau$	0	< 15.5
	$\tau^+$	+1	1777	Tau antineutrino	$\bar{\nu}_\tau$	0	

Table 2.1: The various leptons and some properties

*Lepton number conservation* means that the number of leptons minus the number of antileptons must be the same in the initial and final state.

Consider the decay:

$$\mu^- \rightarrow e^- + \gamma \quad (2.11)$$

this reaction is allowed by energy, momentum and charge conservation and appears to fulfill lepton number conservation but it could not be observed experimentally. The solution to this problem was to assume that there were separate lepton number conservation rules for electrons and muons. A consequence of this is that there must exist one neutrino belonging to the electron ( $\nu_e$ ) and one belonging to the muon ( $\nu_\mu$ ). However, due to the possible neutrino oscillations, lepton number conservation might be broken in some cases as for example:

$$\mu^- \rightarrow e^- + \bar{\nu}_e + \nu_\mu \xrightarrow{osc.} e^- + \bar{\nu}_e + \nu_e$$

but this effect is so small that it will be disregarded in the following.

$$\begin{aligned} L_e &= 1 \text{ for } e^- \text{ and } \nu_e \\ &= -1 \text{ for } e^+ \text{ and } \bar{\nu}_e \\ &= 0 \text{ for all other particles} \end{aligned}$$

$$\begin{aligned} L_\mu &= 1 \text{ for } \mu^- \text{ and } \nu_\mu \\ &= -1 \text{ for } \mu^+ \text{ and } \bar{\nu}_\mu \\ &= 0 \text{ for all other particles} \end{aligned}$$

and in the same way the  $\tau$ -lepton must have its own neutrino.

$$\begin{aligned}
 L_\tau &= 1 \text{ for } \tau^- \text{ and } \nu_\tau \\
 &= -1 \text{ for } \tau^+ \text{ and } \bar{\nu}_\tau \\
 &= 0 \text{ for all other particles}
 \end{aligned}$$

If we now take a look at what this definition of lepton numbers means in the case of the decay 2.11, we find:

$$\begin{array}{cccc}
 & \mu^- & \rightarrow & e^- & + & \gamma \\
 L_\mu & 1 & & 0 & & 0 \\
 L_e & 0 & & 1 & & 0
 \end{array}$$

Thus, lepton number conservation is broken twice in this reaction.

Another example is the normal muon decay:

$$\begin{array}{cccccc}
 & \mu^- & \rightarrow & e^- & + & \bar{\nu}_e & + & \nu_\mu \\
 L_\mu & 1 & & 0 & & 0 & & 1 \\
 L_e & 0 & & 1 & & -1 & & 0
 \end{array}$$

for which the lepton number is conserved.

## 2.6.2 Baryons and Baryon Number

*Baryons* are particles, which contain three quarks, ( $qqq$ ), whereas the *antibaryons* contain three antiquarks, ( $\bar{q}\bar{q}\bar{q}$ ). The most prominent baryons are the *proton* and the *neutron*.

$B = 1$  for baryons and  $-1$  for antibaryons

$\Rightarrow B = 1/3$  for quarks and  $-1/3$  for antiquarks

Example: investigate whether the decay of a proton into a neutral  $\pi$ -meson (pion),  $\pi^0$ , and a positron is allowed. The *mesons* are particles which consist of a bound quark and an antiquark, ( $q\bar{q}$ ), and consequently have baryon number equal to  $(+1/3) + (-1/3) = 0$ .

$$\begin{array}{cccc}
 & p & \rightarrow & \pi^0 & + & e^+ \\
 B & 1 & & 0 & & 0 \\
 L_e & 0 & & 0 & & -1
 \end{array}$$

this reaction fulfills the conservation of energy and charge but is not allowed by baryon and lepton number conservation.

### 2.6.3 Helicity

The *helicity* (or handedness) of a relativistic particle defines whether the spin is oriented parallel or antiparallel with respect to the direction of motion (the momentum vector). If the spin is parallel to the momentum vector the rotation of the particle corresponds to that of a right-handed screw, whereas if the spin is antiparallel to the momentum vector its rotation corresponds to a left-handed screw. Thus, the particles are said to be right-handed or left-handed. This is illustrated in Figure 2.4

For massless particles the helicity is a well defined quantity since the particles travel with the speed of light. However, for massive particles the helicity can change depending on the velocity of our reference system compared to the velocity of the particle which is observed. The helicity of a particle observed from a system which moves in the same direction as the particle but with a velocity which is smaller than that of the particle is opposite to that observed from a system which moves faster than the particle. Thus, massive particles can be either right-handed or left-handed. Antiparticles have the opposite helicity compared to particles.

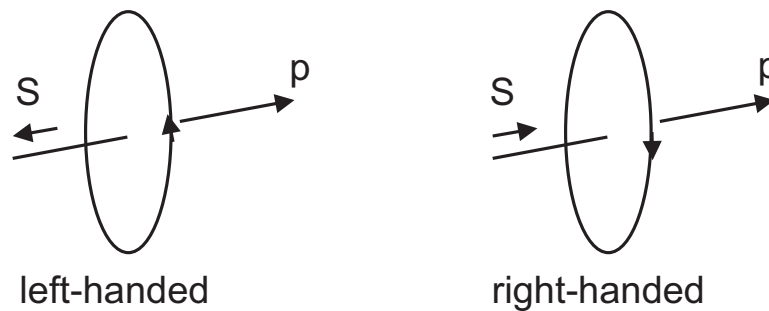


Figure 2.4: *Definition of helicities.*

From studies of  $\beta$ -decays it was found that the emitted electrons were predominantly left-handed if they were relativistic i.e. their velocity was close to that of light. This indicates that *massless particles should be left-handed*. This was also confirmed by measurements of the helicity of neutrino particles, which we know are almost massless. Thus, *antineutrinos are right-handed*.

### 2.6.4 Charge conjugation

Charge conjugation,  $C$ , is a discrete symmetry that reverses the sign of the electric charge, colour charge and magnetic moment of a particle. Applying charge conjugation twice restores the original particle state i.e.  $C^2 = 1$ , with the eigenvalues  $C = \pm 1$ .

Electromagnetism is invariant under charge conjugation since Maxwell's equations are valid for both positive and negative charges. However, the electromagnetic field changes sign under charge conjugation, which means that the photon, which is the force mediator of the electromagnetic field, has  $C_\gamma = -1$ .

## 2.6.5 Time reversal

Time reversal,  $T$ , is another discrete symmetry operator, which causes the particles to go backward in time, like running a movie backwards. According to Feynman's interpretation a particle that travels backward in time is equal to an antiparticle traveling forward in time (see section 2.10). Applying time reversal twice brings us back to the original state i.e.  $T^2 = 1$  with the possible eigenvalues  $T = \pm 1$ .

## 2.6.6 Parity

Parity is a property which is related to the symmetry of the wave function representing a system of fundamental particles. A parity transformation replaces such a system with a type of mirror image, i.e. the spatial coordinates describing the system are inverted through the point at the origin. If a system remains identical after such a transformation, the parity is said to be *even*, whereas if the formulation after the transformation is the negative of the original, the parity is *odd*. For physical observables which depend on the square of the wave function, the parity is unchanged. A complex system has an overall parity that is the product of the parities of its components.

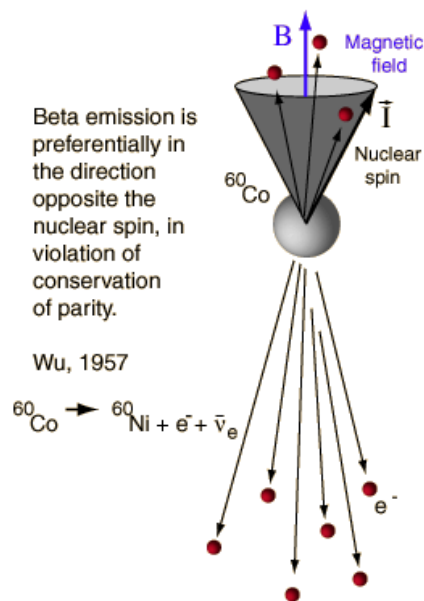


Figure 2.5: *The experiment by C.S.Wu, in which parity violation was proven by studying the  $\beta$ -decay of  $^{60}\text{Co}$  atoms.*

Up to 1956 it was assumed that the mirror image of any physics process would also be a possible physics process. This was called *parity conservation*, which means *even parity*. Although this is always true for strong and electromagnetic interactions, it is not always the case for weak interactions (see Chapter 3). This was found in an experiment by the American physicist C.S. Wu, who studied the  $\beta$ -decay ( $n \rightarrow p + e^- + \bar{\nu}_e$ ) of  $^{60}\text{Co}$ . If the  $^{60}\text{Co}$  atoms were cooled down



to 0.01 K the spin of the atoms could be aligned by applying a strong a magnetic field and it was found that the electrons were emitted predominantly in the direction opposite to the nuclear spin, as illustrated in Figure 2.5.

A simple illustration of this process is shown in Figure 2.6, where the emitted electron is represented by a momentum *vector*, which is defined through a direction and a magnitude. The spin is a measure of the angular (orbital) momentum of the nucleus and is defined as a vector product,  $\vec{L} = \vec{r} \times \vec{p}$ . This is called an *axial vector* or a *pseudovector*.

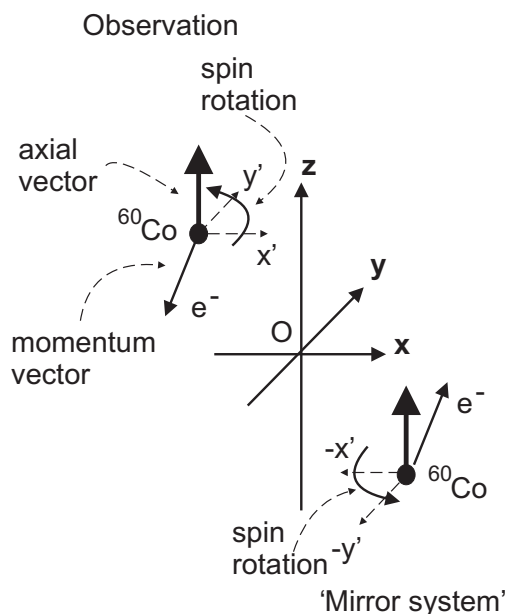


Figure 2.6: Interpretation of the experimental results of the Wu-experiment.

We now reconstruct the 'mirror system' by performing a reflection through the origin of a coordinate system (equivalent to changing signs of all the coordinate axes), which we can choose such that its z-axis is parallel to the nuclear spin direction. It is clear that the momentum *vector* will change direction when it is reflected in the origin so that the electrons will be emitted in the opposite direction in the 'mirror system' compared to the original system. Since the direction of the spin is given by the vector product  $x' \times y'$  in the original system and  $(-x') \times (-y')$  in the 'mirror system', we notice that the direction of the spin will remain the same in both systems. This means that an equal number of electrons should be emitted parallel and antiparallel to the spin if parity is conserved. This is in contradiction with the observation. Thus, we have the experimental evidence that *parity* is violated i.e. parity is *odd*. This kind of parity is called *extrinsic parity*, which is defined as  $P = (-1)^L$ , where L is the orbital momentum.

Every particle has also been assigned an *intrinsic parity* and the total parity is the product of the intrinsic parities of the particles and the extrinsic parity of the system. By convention spin 1/2 fermions (quarks and charged leptons) have been given an intrinsic parity of +1, whereas the corresponding antiparticles have been assigned an intrinsic parity of -1. It doesn't make much sense to assign the neutrino particles an intrinsic parity since the neutrinos can only interact weakly and as we have seen parity can be broken in weak interactions. Nucleons are defined to

have intrinsic parity +1, given by  $P_q P_{\bar{q}} P_q = +1$ . The parity of a meson, consisting of a quark and an antiquark, can be written:

$$P = P_q P_{\bar{q}} (-1)^L \quad \Rightarrow \quad P = -(-1)^L = (-1)^{L+1}$$

Mesons with zero spin will in their lowest energy state have orbital momentum zero and thus get parity  $(-1)^{0+1} = -1$ , i.e. they have negative parity. This is normally denoted  $J^P = 0^-$ , where  $J$  is the total orbital momentum and '-' gives the parity. The definition of the total orbital momentum is  $J = L + S$ , with  $L$  and  $S$  being integer numbers such that  $|L - S| \leq J \leq L + S$ . We can identify mesons with different parities:

	$L$	$S$	$J^P$
Pseudoscalar meson (e.g. $\pi, \eta$ )	0	0	$0^-$
Scalar meson (e.g. $K_0^*$ )	1	1	$0^+$
Vector meson (e.g. $\rho, \omega$ )	0	1	$1^-$
Axial vector meson (e.g. $\rho'$ )	1	0	$1^+$

## 2.6.7 CP-violation

As discussed in section 2.6.6 it was believed until 1956 that parity conservation was one of the fundamental conservation laws of nature, like energy- and momentum conservation. As it turned out not to be true it was assumed that in principle the broken symmetry of any quantum mechanical system could be restored by applying another operation given by a different conservation law. Thus, it was proposed that the product of parity transformation and charge conjugation would restore the order such that the CP-conservation would be an exact symmetry.

Charge conjugation transforms matter particles into antimatter particles and implies that every charged particle has an oppositely charged antiparticle. The antiparticle of an electrically neutral particle may or may not be identical to the particle. Thus, the neutral  $\pi$ -meson is its own antiparticle (the quark content is the same), whereas the neutron is not.

CP-conservation can be illustrated through a simple example, shown in Figure 2.7, where we consider a massless neutrino particle (which is almost true). As we have discussed in section 2.6.3 the helicity (handedness) of (massless) neutrino particles is a well defined quantity, with a neutrino particle being left-handed in all reference systems i.e. its spin is directed opposite to its direction of motion. The antineutrino is, on the other hand, always right-handed i.e. the direction of its spin is the same as the direction of motion.

A parity transformation would convert a left-handed neutrino into a right-handed neutrino, which is non-existing. On the other hand, charge conjugation would transform a left-handed neutrino to a left-handed antineutrino, which is also not existing. With the combined CP operation, however, a left-handed neutrino would turn into a right-handed antineutrino, which is completely allowed. These operations are illustrated in Figure 2.7.

If matter and antimatter are treated in the same way by nature, it would be CP-symmetric. Breaking of the CP-symmetry could have cosmological consequences such that it could give an

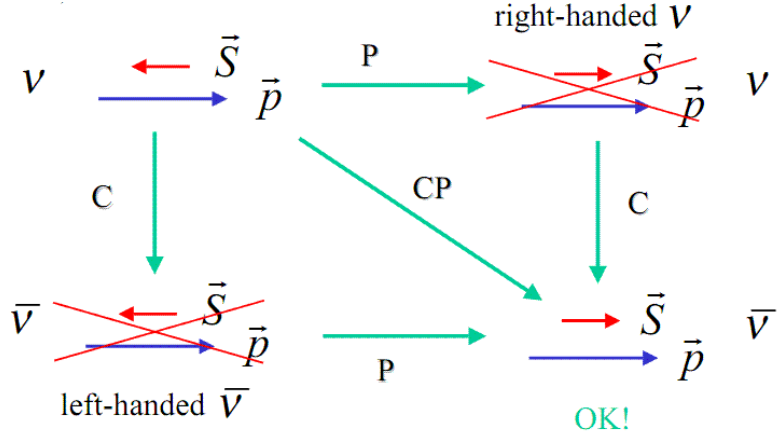


Figure 2.7: The operations of charge conjugation and parity transformation applied to a (massless) neutrino particle.

explanation to the evolution of the Universe. We know that the Universe, that we can observe, consists of particles, like protons, neutron and electrons, and not antiparticles. On the other hand, we also believe that an equal amount of particles and antiparticles was created in Big Bang. So, what has happened after Big Bang that left us with only particles and no antiparticles? CP-violation could possibly provide an explanation to this mystery.

We know that K-mesons are unstable particles and that they do not exist in our common day life. However, K-mesons can be created in high energy collisions at accelerators. For example it is copiously produced in the following strong interaction processes:  $\pi^- + p \rightarrow \Lambda + K^0$  and  $\pi^+ + p \rightarrow K^+ + \bar{K}^0 + p$ . However, the decay of K-mesons is governed by the weak interaction.

In terms of flavour there are two eigenstates of neutral K-mesons  $|K^0 \rangle = |d\bar{s} \rangle$  and  $|\bar{K}^0 \rangle = |\bar{d}s \rangle$ . However, experimental measurements of the neutral K-meson decays showed that there were two, so called weak eigenstates (or CP-eigenstates) with highly different lifetimes. This is due to a strange feature of the neutral K-mesons. They can not exist as pure  $K^0$  or  $\bar{K}^0$  but they continuously transform into each other resulting in one short-lived and one long-lived combination, which in case of no CP-violation, can be written;  $K_S = \frac{1}{\sqrt{2}}(|K^0 \rangle - |\bar{K}^0 \rangle)$  and  $K_L = \frac{1}{\sqrt{2}}(|K^0 \rangle + |\bar{K}^0 \rangle)$ , respectively. If CP is conserved the decay of the short lived version proceeds into two pions,  $K_S \rightarrow \pi^+\pi^-$ , whereas the long lived version decays into three pions,  $K_L \rightarrow \pi^+\pi^-\pi^0$ . The kaon masses are approximately 498 MeV and the pion masses are approximately 139 MeV so the energy available for the two-pion decay is  $m_K - 2m_\pi = 220$  MeV and for the three pion decay  $m_K - 3m_\pi = 80$  MeV. Therefore  $K_S$  decays more rapidly than  $K_L$ .

In case of CP-violation these expressions for  $K_S$  and  $K_L$  have to be modified to  $|K_S \rangle = \frac{1}{\sqrt{1+\epsilon^2}}(|K_S \rangle + \epsilon|\bar{K}^0 \rangle)$  and  $|\bar{K}^0 \rangle = \frac{1}{\sqrt{1+\epsilon^2}}(|K_L \rangle + \epsilon|K_S \rangle)$ , where  $\epsilon$  is a quantity which quantifies the degree of CP-violation. An alternative way to describe these mixed states is to consider the  $K^0$ -meson (and  $\bar{K}^0$ ) containing one short lived component and one long-lived.

Thus the  $K^0$ -mesons oscillates between matter and antimatter states, which has also been experimentally confirmed. Such oscillations can be understood when we have introduced quarks

and antiquarks in terms of Feynman diagrams (see Section 3.3.1). Similar oscillations have also been observed in neutral mesons containing b-quarks,  $B^0$ - and  $\bar{B}^0$ -mesons (see Section 4.2.15). In the case of CP-symmetry a  $K_S$  should always decay into two pions and a  $K_L$  always into three pions. Due to the largely different lifetimes a beam of neutral kaons observed at a long distance from its production point will almost only contain  $K_L$ 's since essentially all the  $K_S$ 's have decayed. This means that we should expect to only observe decays into three pions if CP-symmetry is valid. However, in 1964 the American physicists James Cronin and Val Fitch presented experimental evidence for CP-violation in the weak decay of neutral  $K$ -mesons. They found that a small fraction (1 in about 500) of the remaining long lived neutral kaons decayed into two pions. This was a clear violation of the expected symmetry between matter and anti-matter and thus CP was violated.

There are two types of CP-violations. Indirect CP-violation is when a small fraction of  $K_L$ 's oscillate into  $K_S$ 's, which subsequently decay into two pions. This form of CP-violation is said to be indirect, since the violation occurs from the way kaons mix with each other and not the way the kaons decay. This is what Cronin and Fitch observed. A direct CP-violation means that for example  $K_L$  decays directly into two pions. Despite many experimental searches, no manifestation of direct CP violation was found until the 1990s

## 2.7 Gauge symmetries, gauge invariance and gauge fields

The concept of *gauge* essentially means scale, reference system or coordinate system. A transformation from one reference system to another is called *gauge transformation*. If there is no change in the measurable quantities in going from one system to another, it is called *gauge invariance*. In order to understand what this means, let us consider some simple examples.

If you were asked what the gravitational potential is at a certain point in space, you wouldn't be able to give a correct answer unless you know the reference system. The gravitational potential is different if you refer to the sea level or to the tip of a high mountain. So a change of reference frame or gauge leads to different answers. However, if you were asked what the difference between the gravitational potential of two arbitrary points in space is, this will be independent of the reference system (gauge).

Gauge invariance means that what you measure is independent of the frame of reference in which you perform the measurement. *Gauge theories* is another term for field theories. They describe the various forces of nature as vector fields and the interaction between particles as an exchange of field quanta, also called *gauge bosons*, acting as mediators of the forces. Any kind of invariance under a field transformation is considered a symmetry, also called *gauge symmetry*.

Charged particles interact through the electromagnetic field via the exchange of photons. The emission or absorption of a photon, by a charged particle, does not change the electric charge of the particle, since the photon itself doesn't carry electric charge. The effect of the electromagnetic field on the wave function of a quantum mechanical particle,  $\Psi(\vec{x}, t)$ , is a change in phase. The wave functions  $\Psi(\vec{x}, t)$  and  $e^{i\phi}\Psi(\vec{x}, t)$ , with an arbitrarily chosen phase  $\phi$ , correspond to the

same particle state. The emission or absorption of a photon, by a charged particle, would thus result in a transformation of the phase angle. The gauge invariance of quantum electrodynamics (QED) is mathematically described by the symmetry group  $U(1)$ , which has one gauge field, the electromagnetic field, with the photon as the gauge boson.

The weak interaction changes the flavour of the quarks or transfer leptons into neutrinos and vice versa, by emitting or absorbing a charged weak boson ( $W^\pm$ ; see section 3.3). Such transitions are described by the symmetry group  $SU(2)$ , since there are two flavours of quarks, one up-type (charge =  $+2/3$ ) and one down-type (charge =  $-1/3$ ) and two 'flavours of leptons', charged leptons and neutrinos.

The strong force, on the other hand, changes the colour charge of the quarks, by emitting or absorbing a gluon, and the interaction is described by the symmetry group  $SU(3)$ , since there are 3 colours.

Gauge invariance means that these transformations, phase transformation in the case of the electromagnetic interaction, flavour transformation in the case of the weak interaction and colour transformation in the case of the strong interaction, must be independent of the frame of reference in which they take place.

### 2.7.1 Symmetry breaking

In order to illustrate spontaneous symmetry breaking, consider a container filled with water. Seen from a specific water molecule the surrounding looks the same independent of in which direction you look and so you would say that this is a symmetric system. If we now cool the water to  $0^\circ$  centigrade or below we might get ice, snow, frost or rime, depending on the circumstances. This can be regarded as some kind of spontaneous symmetry breaking since a symmetric system of water has transformed into states that are not complete symmetric.

Thus, spontaneous symmetry breaking causes a system in a symmetrical state to end up in an asymmetric state. Another example is the following; if we place a small marble ball in a round vase with a round base, it will roll to the bottom of the vase where its potential energy is the smallest. From the marble ball's point of view it is sitting in a rotational symmetric system, since the walls of the vase look the same in all directions and if you give it a push it will always roll back to the same position. If you, however, use a champagne bottle with a bulge in the middle of its bottom, you may be able to place the marble ball on the top of the bulge, such that the system will be rotational symmetric with regard to the marble ball, but the potential energy will not be at its lowest value. In case of a tiny disturbance the marble ball will roll down the bulge into the valley in the base of the bottle. Here the potential is the smallest but the symmetry is broken. Whereas in the case with the vase there is only one state of minimal energy (the position at the bottom of the vase), for a champagne bottle the energy is at its minimum all around the valley in the base of the bottle.

An example of such symmetry breaking in particle physics is given by the mechanism, which provides masses to the particles, the so called Higgs mechanism. The Higgs potential has such a shape, which makes the potential energy  $V(\Phi)$  of the Higgs field  $\Phi$  having its lowest value separate from  $\Phi = 0$ . The particles receive masses through interaction with the Higgs field as will be described in Section 3.3.4.

## 2.8 The Klein-Gordon Equation

In order to describe relativistic systems it is necessary to start from the relativistic relation between energy and momentum. In non-relativistic quantum mechanics, particles are described by the Schrödinger equation, but since it violates Lorentz invariance it can not be used for particles moving relativistically. In relativistic quantum mechanics, particles of spin 0 are described by the Klein-Gordon equation, formulated by the German physicists Oscar Klein and Walter Gordon, and particles with spin 1/2 by the Dirac equation, developed by the British physicist Paul Dirac.

Start from the relativistic energy-momentum conservation and replace energy and momentum with the same operators as introduced for the Schrödinger equation:

$$E^2 = \bar{p}^2 + m^2 \quad (2.12)$$

$$E \rightarrow i\hbar \frac{\partial}{\partial t}$$

$$\Rightarrow E^2 \rightarrow i^2 \frac{\partial^2}{\partial t^2} = -\frac{\partial^2}{\partial t^2}; \quad \hbar = 1$$

$$\bar{p} \rightarrow -i\hbar \nabla$$

$$\Rightarrow \bar{p}^2 \rightarrow i^2 \nabla^2 = -\nabla^2; \quad \hbar = 1$$

Inserting in (2.12) gives the Klein-Gordon equation

$$\boxed{-\frac{\partial^2}{\partial t^2} \Psi(x, t) = -\nabla^2 \Psi(x, t) + m^2 \Psi(x, t)} \quad (2.13)$$

The plane wave solutions to the Klein-Gordon equation, describing a free particle, are:

$$\begin{aligned} \Psi(\bar{x}, t) &= N \cdot e^{i(\bar{p}\bar{x} - Et)} \\ \Rightarrow \frac{\partial}{\partial t} \Psi &= -iEN \cdot e^{i(\bar{p}\bar{x} - Et)} \\ \Rightarrow \frac{\partial^2}{\partial t^2} \Psi &= \frac{\partial}{\partial t} \left( \frac{\partial}{\partial t} \Psi \right) = \frac{\partial}{\partial t} (-iEN \cdot e^{i(\bar{p}\bar{x} - Et)}) = \\ &= i^2 E^2 N \cdot e^{i(\bar{p}\bar{x} - Et)} = -E^2 N \cdot e^{i(\bar{p}\bar{x} - Et)} = \\ &= -E^2 \cdot \Psi \end{aligned}$$

$$\begin{aligned} \nabla \Psi &= i\bar{p}N \cdot e^{i(\bar{p}\bar{x} - Et)} \\ \nabla^2 \Psi &= \frac{\partial}{\partial x} \left( \frac{\partial}{\partial x} \Psi \right) = \\ &= \nabla (i\bar{p}N \cdot e^{i(\bar{p}\bar{x} - Et)}) = \\ &= -\bar{p}^2 N \cdot e^{i(\bar{p}\bar{x} - Et)} = -\bar{p}^2 \cdot \Psi \end{aligned}$$

Insert into (2.13) gives:

$$\begin{aligned} -(-E^2\Psi) &= -(-\vec{p}^2\Psi) + m^2\Psi \\ \Rightarrow E^2 &= \vec{p}^2 + m^2 \\ \Rightarrow E &= \pm\sqrt{\vec{p}^2 + m^2} \end{aligned}$$

$\Rightarrow$  gives positive and negative energies as a direct consequence of momentum conservation

$$\Psi_+ = N \cdot e^{i(\vec{p}\vec{x} - Et)} \rightarrow i\frac{\partial}{\partial t}\Psi_+ = i(-iE)\Psi_+ = E\Psi_+ \rightarrow \text{positive energies}$$

$$\Psi_- = N \cdot e^{i(\vec{p}\vec{x} + Et)} \rightarrow i\frac{\partial}{\partial t}\Psi_- = i(iE)\Psi_- = -E\Psi_- \rightarrow \text{negative energies}$$

## 2.8.1 The Continuity Equation

We have the Klein-Gordon equation:

$$-\frac{\partial^2}{\partial t^2}\Psi + \nabla^2\Psi = m^2\Psi$$

Multiply by  $-i\Psi^*$

$$-(-i\Psi^*)\frac{\partial^2}{\partial t^2}\Psi + (-i\Psi^*)\nabla^2\Psi = m^2(-i\Psi^*)\Psi \quad (2.14)$$

Multiply the complex conjugate equation with  $-i\Psi$

$$-(-i\Psi)\frac{\partial^2}{\partial t^2}\Psi^* + (-i\Psi)\nabla^2\Psi^* = m^2(-i\Psi)\Psi^* \quad (2.15)$$

Subtract 2.14 from 2.15

$$i(\Psi^*\frac{\partial^2}{\partial t^2}\Psi - \Psi\frac{\partial^2}{\partial t^2}\Psi^*) - i(\Psi^*\nabla^2\Psi - \Psi\nabla^2\Psi^*) = -im^2(\Psi^*\Psi - \Psi\Psi^*) \quad (2.16)$$

Study:

$$\begin{aligned} &\frac{\partial}{\partial t}(\Psi^*\frac{\partial}{\partial t}\Psi - \Psi\frac{\partial}{\partial t}\Psi^*) = \\ &= \frac{\partial}{\partial t}\Psi^*\frac{\partial}{\partial t}\Psi + \Psi^*\frac{\partial^2}{\partial t^2}\Psi - \frac{\partial}{\partial t}\Psi\frac{\partial}{\partial t}\Psi^* - \Psi\frac{\partial^2}{\partial t^2}\Psi^* \\ &= \Psi^*\frac{\partial^2}{\partial t^2}\Psi - \Psi\frac{\partial^2}{\partial t^2}\Psi^* = \text{1st term in equation 2.16} \end{aligned}$$

Study:

$$\nabla(\Psi^*\nabla\Psi - \Psi\nabla\Psi^*) =$$

$$= \nabla\Psi^*\nabla\Psi + \Psi^*\nabla^2\Psi - \nabla\Psi\nabla\Psi^* - \Psi\nabla^2\Psi^* = \Psi^*\nabla^2\Psi - \Psi\nabla^2\Psi^*$$

= 2nd term in the equation above since:  $(\nabla\Psi^*\nabla\Psi - \nabla\Psi\nabla\Psi^* = 0)$

$$\Rightarrow \frac{\partial}{\partial t}[i(\Psi^* \frac{\partial}{\partial t} \Psi - \Psi \frac{\partial}{\partial t} \Psi^*)] + \nabla[-i(\Psi^*\nabla\Psi - \Psi\nabla\Psi^*)] = 0$$

Compare to the continuity equation:  $\frac{\partial}{\partial t}\rho + \nabla\bar{j} = 0.$

Calculate the probability density,  $\rho$ , and the density flux,  $j$  for a free particle described by

$$\Psi = N \cdot e^{i(\bar{p}x - Et)}$$

$$\Psi = N \cdot e^{i(\bar{p}x - Et)} \Rightarrow \frac{\partial\Psi}{\partial t} = (-iE) \cdot \Psi \quad \text{and} \quad \nabla\Psi = (ip) \cdot \Psi$$

$$\Psi^* = N \cdot e^{-i(\bar{p}x - Et)} \Rightarrow \frac{\partial\Psi^*}{\partial t} = (iE) \cdot \Psi^* \quad \text{and} \quad \nabla\Psi^* = -(ip) \cdot \Psi^*$$

From above we obtain  $j$  and  $\rho$ :

$$\begin{aligned} \bar{j} &= -i(N \cdot e^{-i(\bar{p}x - Et)} \cdot (ip)N \cdot e^{i(\bar{p}x - Et)} - N \cdot e^{i(\bar{p}x - Et)} \cdot (-ip)N \cdot e^{-i(\bar{p}x - Et)}) = \\ &= -i(i\bar{p}N^2 - (-i\bar{p})N^2) = -i(i\bar{p}N^2 + i\bar{p}N^2) = 2\bar{p}N^2 \end{aligned}$$

$$\begin{aligned} \rho &= i(N \cdot e^{-i(\bar{p}x - Et)} \cdot (-iE)N \cdot e^{i(\bar{p}x - Et)} - N \cdot e^{i(\bar{p}x - Et)}(iE)N \cdot e^{-i(\bar{p}x - Et)}) = \\ &= i(-iEN^2 - iEN^2) = 2EN^2 \end{aligned}$$

For  $E < 0$  we get  $\rho < 0$  i.e. a probability  $< 0$ , which is unphysical. Hence, we need a new interpretation of  $\rho$ .

## 2.9 The Dirac Equation

To overcome the problems with  $\rho < 0$  and negative  $E$ -solutions Dirac formulated a wave equation for a free particle of mass  $m$ , linear in the  $E$  and  $p$  operators, which is first order in both derivatives.

$$E\Psi = \bar{\alpha}p\Psi + \beta m\Psi$$

$$E \rightarrow i\hbar \frac{\partial}{\partial t}$$

$$\bar{p} \rightarrow -i\hbar\nabla$$

$$\boxed{i \frac{\partial}{\partial t} \Psi = -i(\alpha_1 \frac{\partial}{\partial x_1} \Psi + \alpha_2 \frac{\partial}{\partial x_2} \Psi + \alpha_3 \frac{\partial}{\partial x_3} \Psi) + \beta m \Psi} \quad \hbar = 1 \quad (2.17)$$

The four coefficients  $\alpha_i$  and  $\beta$  are determined by the requirement that a free particle must satisfy the energy-momentum conservation  $E^2 = \bar{p}^2 + m^2$ .



Differentiate 2.17:

$$i \frac{\partial^2}{\partial t^2} \Psi = -i(\alpha_1 \frac{\partial^2}{\partial x_1 \partial t} \Psi + \alpha_2 \frac{\partial^2}{\partial x_2 \partial t} \Psi + \alpha_3 \frac{\partial^2}{\partial x_3 \partial t} \Psi) + \beta m \frac{\partial}{\partial t} \Psi; \quad (2.18)$$

but  $\frac{\partial^2}{\partial x_1 \partial t} \Psi = \frac{\partial}{\partial x_1} \cdot \frac{\partial}{\partial t} \Psi$

Multiply 2.17 by  $-i$

$$\Rightarrow \frac{\partial}{\partial t} \Psi = -(\alpha_1 \frac{\partial}{\partial x_1} \Psi + \alpha_2 \frac{\partial}{\partial x_2} \Psi + \alpha_3 \frac{\partial}{\partial x_3} \Psi) - i\beta m \Psi \quad (2.19)$$

$$\Rightarrow \frac{\partial^2}{\partial t^2} \Psi = -(\alpha_1 \frac{\partial^2}{\partial x_1 \partial t} \Psi + \alpha_2 \frac{\partial^2}{\partial x_2 \partial t} \Psi + \alpha_3 \frac{\partial^2}{\partial x_3 \partial t} \Psi) - i\beta m \frac{\partial}{\partial t} \Psi \quad (2.20)$$

Study:

$$\begin{aligned} \alpha_1 \cdot \frac{\partial}{\partial x_1} \cdot \frac{\partial}{\partial t} \Psi &= \alpha_1 \frac{\partial}{\partial x_1} [-(\alpha_1 \frac{\partial}{\partial x_1} \Psi + \alpha_2 \frac{\partial}{\partial x_2} \Psi + \alpha_3 \frac{\partial}{\partial x_3} \Psi) - i\beta m \Psi] = \\ &= -(\alpha_1^2 \frac{\partial^2}{\partial x_1^2} \Psi + \alpha_1 \alpha_2 \frac{\partial^2}{\partial x_1 \partial x_2} \Psi + \alpha_1 \alpha_3 \frac{\partial^2}{\partial x_1 \partial x_3} \Psi) - i\alpha_1 \beta m \frac{\partial}{\partial x_1} \Psi \end{aligned}$$

In the same way:

$$\alpha_2 \cdot \frac{\partial}{\partial x_2} \cdot \frac{\partial}{\partial t} \Psi = -(\alpha_2 \alpha_1 \frac{\partial^2}{\partial x_1 \partial x_2} \Psi + \alpha_2^2 \frac{\partial^2}{\partial x_2^2} \Psi + \alpha_2 \alpha_3 \frac{\partial^2}{\partial x_2 \partial x_3} \Psi) - i\alpha_2 \beta m \frac{\partial}{\partial x_2} \Psi$$

and:

$$\alpha_3 \cdot \frac{\partial}{\partial x_3} \cdot \frac{\partial}{\partial t} \Psi = -(\alpha_3 \alpha_1 \frac{\partial^2}{\partial x_1 \partial x_3} \Psi + \alpha_3 \alpha_2 \frac{\partial^2}{\partial x_2 \partial x_3} \Psi + \alpha_3^2 \frac{\partial^2}{\partial x_3^2} \Psi) - i\alpha_3 \beta m \frac{\partial}{\partial x_3} \Psi$$

and:

$$\begin{aligned} -i\beta m \frac{\partial}{\partial t} \Psi &= -i\beta m \{ [-(\alpha_1 \frac{\partial}{\partial x_1} \Psi + \alpha_2 \frac{\partial}{\partial x_2} \Psi + \alpha_3 \frac{\partial}{\partial x_3} \Psi)] - i\beta m \Psi \} = \\ &= i\beta m (\alpha_1 \frac{\partial}{\partial x_1} \Psi + \alpha_2 \frac{\partial}{\partial x_2} \Psi + \alpha_3 \frac{\partial}{\partial x_3} \Psi) - \beta^2 m^2 \Psi \end{aligned}$$

Insert in 2.20

$$\Rightarrow \frac{\partial^2}{\partial t^2} \Psi = \sum_{j=1}^3 \alpha_j^2 \frac{\partial^2}{\partial x_j^2} \Psi + \frac{1}{2} \sum_{j \neq k} (\alpha_j \alpha_k + \alpha_k \alpha_j) \frac{\partial^2}{\partial x_j \partial x_k} \Psi + i \cdot m \sum_{j=1}^3 (\alpha_j \beta + \beta \alpha_j) \frac{\partial}{\partial x_j} \Psi - \beta^2 m^2 \Psi$$

For  $\Psi \sim e^{i(\overline{p}\overline{x} - Et)}$

$$\Rightarrow \frac{d^2}{dt^2} \Psi = -E^2 \cdot e^{i(\overline{p}\overline{x} - Et)}$$

$$\Rightarrow \frac{d^2}{dx^2} \Psi = -p^2 \cdot e^{i(\overline{p}\overline{x} - Et)}$$

$$\Rightarrow \boxed{E^2 = \vec{p}^2 + m^2}$$

This is a valid equality if and only if:

$$\boxed{\begin{aligned} \alpha_1^2 = \alpha_2^2 = \alpha_3^2 = \beta^2 = 1 \\ \alpha_j \alpha_k + \alpha_k \alpha_j = 0 \quad \text{for } j \neq k \\ \alpha_j \beta + \beta \alpha_j = 0 \end{aligned}}$$

Dirac realized that this could not be fulfilled by giving  $\alpha_i$  and  $\beta$  just *numbers* but they had to be specified as  $4 \times 4$  *matrices* with complex elements.

$\alpha_i$  is thus identified with:

$$\alpha_i = \begin{pmatrix} 0 & \sigma_i \\ \sigma_i & 0 \end{pmatrix}$$

and  $\beta$  with:

$$\beta = \begin{pmatrix} I & 0 \\ 0 & -I \end{pmatrix}$$

where  $I$  is a  $2 \times 2$  unit matrix and  $\sigma$  are the  $2 \times 2$  Pauli spin matrices:

$$\sigma_1 = \begin{pmatrix} 0 & 1 \\ 1 & 0 \end{pmatrix}$$

$$\sigma_2 = \begin{pmatrix} 0 & -i \\ i & 0 \end{pmatrix}$$

$$\sigma_3 = \begin{pmatrix} 1 & 0 \\ 0 & -1 \end{pmatrix}$$

## 2.10 Antiparticles: The Hole Theory and Feynmans Interpretation

The fact that the Klein-Gordon equation, for each quantum state of positive energy,  $E$ , also predicts a corresponding state with negative energy,  $-E$ , indeed created a problem. Dirac proposed a solution to this problem by defining 'vacuum' as a state were all negative energy states are occupied, but none of the positive energy states. Thus vacuum in this picture is an infinite sea of particles with negative energy,  $E < 0$ . If we now introduce a particle into vacuum it can obviously not enter any of the negative states, since these are all occupied, but it has to fill one of the positive energy states. Furthermore, if the particle loses energy by emitting photons it may drop to a lower lying positive energy state but not to a negative energy state. On the other hand, a particle in a negative energy state may be excited to a positive energy state leaving behind a *hole* in the sea, as illustrated in Figure 2.8. The *hole* left over can in this picture be interpreted as an antiparticle. The net effect of the excitation is pair production  $e^-(E') + e^+(E)$  with the condition:

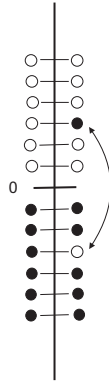


Figure 2.8: *Illustration of the Dirac 'hole theory'.*

$$E + E' \geq 2m_e$$

in the case of electrons.

This picture works well for *fermions* since the Pauli exclusion principle forbids two particles to be in exactly the same quantum state. However, this restriction is not valid for bosons, for which arbitrarily many particles can be in the same state, and therefore a different interpretation is called for.

By introducing electric charge into the continuity equation, such that we instead of particle flow discuss charge flow, then  $\rho$  would represent *charge density* instead of probability density and  $j$  would represent *charge density flux* instead of probability density flux. This opens up for an interpretation, introduced by the American physicist Richard Feynman, and illustrated in Figure 2.9, which means that the  $(E, \vec{p})$  solution is identical to the  $(-E, -\vec{p})$  solution for a particle with opposite charge (antiparticle). In other words, a *negative-energy particle solution* going backwards in time is identical to a *positive-energy antiparticle solution* going forward in time. This interpretation is valid for both fermions and bosons. Such a representation is used in so called *Feynman diagrams* in order to illustrate scattering processes and they constitute a valuable tool to calculate the probability for the process to happen. A short introduction to Feynman diagrams will be given in chapter 3.

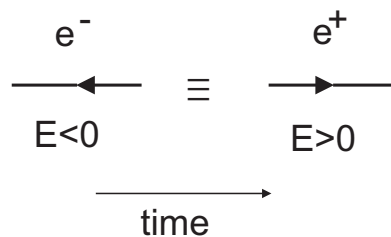


Figure 2.9: *Feynman's interpretation that particles and antiparticles are related to the direction of time.*

## 2.11 Strangeness

As mentioned in the introduction only a handful of 'elementary' particles were known up to the era of particle accelerators. Matter could be explained as being built out of protons, neutrons and electrons, and the photon was just light of shorter wavelength. The discovery of the positron proved that there is antimatter but it did not confuse the overall picture. However, when the muon was observed and identified as a heavier version of the electron, the physicists were puzzled and it caused somebody to ask 'Who ordered that?'

Although the quarks were not introduced until 1963 it might be interesting to follow how physics developed over the coming years and how new observations can be understood in terms of quarks and leptons.

Until 1947 all observed particles could be explained by the building blocks shown in Table 2.2. Note that the neutrino particle had been predicted by Pauli in 1930, in order to explain the missing energy in  $\beta$ -decays, but it was not verified experimentally until 1956:

	charge	spin
$\nu$	0	1/2
$e \mu$	-1	1/2
$u$	2/3	1/2
$d$	-1/3	1/2

Table 2.2: Quarks and leptons needed to explain all known particles in 1947

On the quark level the proton would be described as being built out of a  $uud$ -state and the neutron would be a  $udd$ -state. The lightest charged mesons are the pi-mesons, where the  $\pi^+$  is a  $u\bar{d}$ -state and the  $\pi^-$  is a  $\bar{u}d$ .

In 1947 so called 'V'-particles were observed from cosmic ray events detected in a cloud chamber. They were called 'V'-particles since they left 'V'-shaped tracks in the detector. The particles had a 'strange' behaviour in the sense that they were frequently produced, which is consistent with production through strong interaction ( $\tau \sim 10^{-23}s$ ), but they had a long decay time ( $\tau \sim 10^{-10}s$ ).

In 1953 the 'V'-particles were observed also in a bubble chamber experiment, from which pictures of one event, taken from two cameras placed in different positions, are shown in Figure 2.10. A bubble chamber works according to a similar principle as the cloud chamber but instead of having a supersaturated vapour, one uses a superheated transparent liquid, usually liquid hydrogen. As a track passes through the liquid the pressure is decreased by the movement of a piston and the liquid starts boiling along the particle trajectory and small bubbles are created. The density of bubbles is proportional to the ionisation power of the particle. A photograph is taken as the bubbles have grown large enough to be visible on a film and after that the piston increase the pressure again to stop the boiling process.

The experiment used a beam of pions which interact with the protons in the liquid hydrogen and gives rise to a reaction creating two V-particles:  $\pi^- + p \rightarrow V + V$ . An example of such

a decay is shown in Figure 2.10, where the  $\pi^-$  meson is coming in from below in the pictures and interacts with a proton in the liquid hydrogen. The two pictures on the left show the two different views of the same event including background tracks and on the right the same event is shown again, now with the background tracks removed.

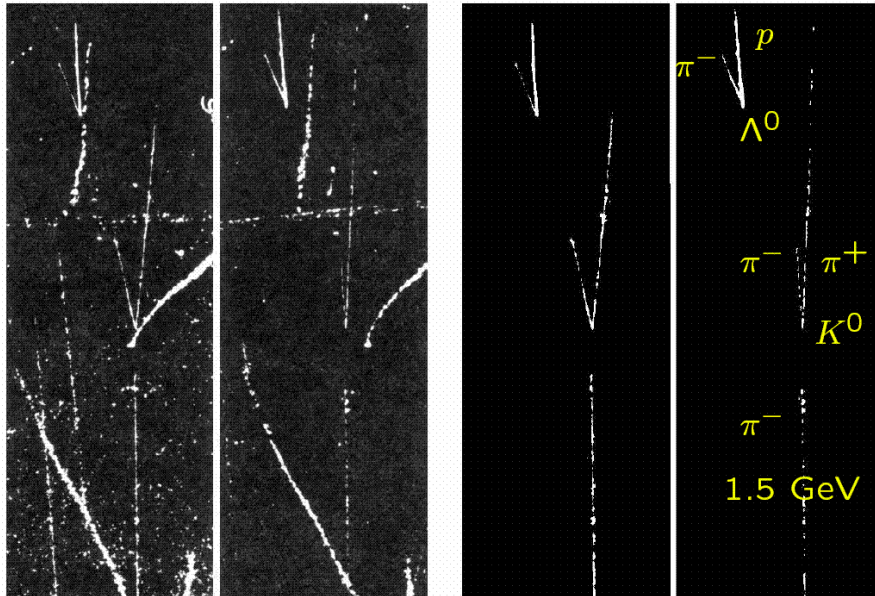
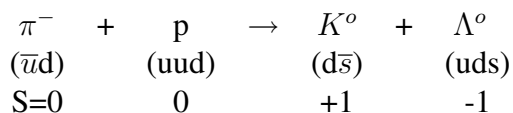


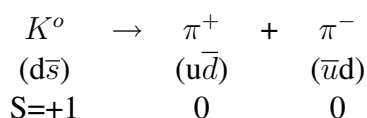
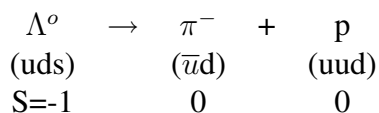
Figure 2.10: Bubble chamber pictures showing different views of a collision between an incoming  $\pi^-$ -meson and a proton creating 'V'-particles. To the right background tracks have been removed. The 'V' particles were later identified as decays of a  $K^0$  and a  $\Lambda^0$ -particle.

From analysing the recorded pictures in detail this reaction could be identified as:  $\pi^- + p \rightarrow K^0 + \Lambda^0$  where  $K^0 \rightarrow \pi^+ + \pi^-$  and  $\Lambda^0 \rightarrow \pi^- + p$ .

The behaviour of the reaction could be explained if a new quantum number, called *strangeness* ( $S$ ), was introduced.  $K^0$  was assigned  $S = 1$  and  $\Lambda^0$   $S = -1$ . On the quark level a new kind of quark, the *strange* quark ( $s$ ), had to be introduced, such that a  $K^0$ -meson consists of a  $d\bar{s}$  state and the  $\Lambda^0$ -baryon of a  $uds$ -state. Thus, the  $s$ -quark has a charge of  $-1/3$  and strangeness  $-1$ . The convention is that the *flavourness* has the same sign as the quark charge. Strangeness is conserved in strong and electromagnetic interactions but broken in weak interaction.



Strangeness conserved in the production mechanism (strong interaction)



Strangeness not conserved in the decays (weak interaction)

We now have to add the  $s$ -quark to the family of fundamental particles in order to explain the existence of  $K$ -mesons which and so the quarks and leptons extends as shown in Table 2.3:

flavour	charge	spin
$\nu$	0	1/2
$e \ \mu$	-1	1/2
$u$	2/3	1/2
$d \ s$	-1/3	1/2

Table 2.3: Quarks and leptons needed to explain all known particles after the discovery of 'V'-particles

According to the quark model all hadrons are made up from various combinations of quarks (and antiquarks). By combining the  $u(\bar{u})$ ,  $d(\bar{d})$  and  $s(\bar{s})$  quarks in  $q\bar{q}$  pairs or 3-quark systems all *hadrons* that had been found experimentally up to then could be constructed. Particles which consist of a quark and an antiquark are called *mesons* whereas particles built out of three quarks are called *baryons*. The particles could be arranged in so called multiplets, containing particles with similar properties. From some empty spaces in such multiplets new particles could be predicted and observed in experiments. In Figures 2.11 and 2.12 the multiplets of mesons with spin 0 and 1, respectively, are shown.

### Mesons, spin 0

	-1	0	+1	Charge
+1		$K^0$ ( $d\bar{s}$ )	$K^+$ ( $u\bar{s}$ )	
0	$\pi^-$ ( $d\bar{u}$ )	$\pi^0, \eta, \eta'$ ( $u\bar{u}$ )( $d\bar{d}$ )( $s\bar{s}$ )	$\pi^+$ ( $u\bar{d}$ )	
-1	$K^-$ ( $s\bar{u}$ )	$\bar{K}^0$ ( $s\bar{d}$ )		
Strangeness				

Figure 2.11: The multiplet for spin 0 mesons.

The particle states with charge zero and strangeness zero do not appear as pure quark-antiquark states but as mixed states of which one linear combination corresponds to a singlet state and the others to octet states, as specified in Table 2.4. Note that the quark content of the singlet states are completely symmetric with respect to the quark content.

### Mesons, spin 1

	-1	0	+1	Charge
+1		$K^{*0}$ $(d\bar{s})$	$K^{*+}$ $(u\bar{s})$	
0	$\rho^-$ $(d\bar{u})$	$\rho^0, \omega, \phi$ $(u\bar{u})(d\bar{d})(s\bar{s})$	$\rho^+$ $(u\bar{d})$	
-1	$K^{*-}$ $(s\bar{u})$	$\bar{K}^{*0}$ $(s\bar{d})$		

Strangeness

Figure 2.12: The multiplet for spin 1 mesons.

<i>Meson</i>		<i>quark combination</i>	
spin 0	spin 1		
$\pi^0$	$\rho^0$	$\frac{1}{\sqrt{2}}(d\bar{d} - u\bar{u})$	octet state
$\eta_8 \equiv \eta$	$\omega$	$\frac{1}{\sqrt{6}}(d\bar{d} + u\bar{u} - 2s\bar{s})$	-"-
$\eta_o \equiv \eta'$	$\phi$	$\frac{1}{\sqrt{3}}(d\bar{d} + u\bar{u} + s\bar{s})$	singlet state

Table 2.4: Quark - antiquark combinations for different mesons

The multiplets for baryons with spin 1/2 and 3/2 are seen in Figures 2.13 and 2.14, respectively.

### Baryons, spin 1/2

	-1	0	+1	Charge
0		$n$ ( $udd$ )	$p$ ( $uud$ )	
-1	$\Sigma^-$ ( $dds$ )	$\Lambda^0, \Sigma^0$ ( $uds$ )	$\Sigma^+$ ( $uus$ )	
-2	$\Xi^-$ ( $dss$ )	$\Xi^0$ ( $uss$ )		
Strangeness				

Figure 2.13: Multiplet for spin 1/2 baryons

### Baryons, spin 3/2

	-1	0	+1	+2	Charge
0	$\Delta^-$ ( $ddd$ )	$\Delta^0$ ( $udd$ )	$\Delta^+$ ( $uud$ )	$\Delta^{++}$ ( $uuu$ )	
-1	$\Sigma^{*-}$ ( $dds$ )	$\Sigma^{*0}$ ( $uds$ )	$\Sigma^{*+}$ ( $uus$ )		
-2	$\Xi^{*-}$ ( $dss$ )	$\Xi^{*0}$ ( $uss$ )			
-3	$\Omega^-$ ( $sss$ )				
Strangeness					

Figure 2.14: Multiplet for spin 3/2 baryons

States like  $\Delta^{++}$  and  $\Omega^-$  do not obey the Pauli exclusion principle. The solution is to introduce a new quantum number called *colour*. Colour will be discussed in more detail later.



	Spin			Isotopic spin		
	Quantum numbers		State vectors	Quantum numbers		State vectors
Doublet	$s = 1/2$	$s_z = -1/2$ $s_z = +1/2$	$ \downarrow\rangle$ $ \uparrow\rangle$	$I = 1/2$	$I_3 = -1/2$ $I_3 = +1/2$	$ d\rangle$ $ u\rangle$
Singlet	$s = 0$	$s_z = 0$	$\frac{1}{\sqrt{2}} \uparrow\downarrow - \downarrow\uparrow\rangle$	$I = 0$	$I_3 = 0$	$\frac{1}{\sqrt{2}} ud - du\rangle$
Triplet	$s = 1$	$s_z = -1$ $s_z = 0$ $s_z = +1$	$ \downarrow\downarrow\rangle$ $\frac{1}{\sqrt{2}} \uparrow\downarrow + \downarrow\uparrow\rangle$ $ \uparrow\uparrow\rangle$	$I = 1$	$I_3 = -1$ $I_3 = 0$ $I_3 = +1$	$ dd\rangle$ $\frac{1}{\sqrt{2}} ud + du\rangle$ $ uu\rangle$

Table 2.5: The various spin and isospin orientations

## 2.12 Isospin (Isotopic spin)

We can notice that there are many more hadrons than leptons and if we compare the hadrons within a multiplet we find, from experimental observations, that those with the same strangeness number have very similar properties. A closer look at the multiplets reveals that the exchange of u- and d-quarks or the antiquarks takes us from one hadron state to another. If we take the proton and the neutron as an example we see that although they have different electric charge they have the same spin, baryon number +1 and their masses differ only slightly. Both the proton and the neutron interact via strong interaction in the same way and this led Heisenberg in 1932 to the conclusion that the strong force does not make any difference between protons and neutrons i.e. it is not sensitive to electric charge. So, as far as the strong force is concerned there is only one nucleon and one pion etc.

At the quark level this means that it is not possible to tell the difference between a u- and d-quark except by their electric charge or equivalently, only in electromagnetic interaction a difference is noticed between a proton and a neutron. If we compare to atomic physics we know that a spin-up ( $\uparrow$ ) electron can not be distinguished from a spin-down ( $\downarrow$ ) unless a magnetic field is applied. This causes the spin of the electrons to take two different orientations corresponding to two distinct states of the atom, separated in energy (fine structure). The various orientations of spin and isospin are shown in Table 2.5. Just as the orientation of normal spin can only be observed under the influence of a magnetic field, the orientation of the isospin can only be determined in an abstract isospin space through the presence of an electromagnetic field. The different orientations of isotopic spin correspond to different mass states i.e. different hadrons, related to the small mass difference between the u- and d-quarks. Isotopic spin-up corresponds to a u-quark whereas isotopic spin-down corresponds to a d-quark and it is not possible to distinguish the two without the presence of an electromagnetic field. Thus, the u- and d-quarks have isospin  $I = 1/2$  with the third components  $I_3 = +1/2$  (u-quark) and  $I_3 = -1/2$  (d-quark).

For a doublet of particles, like the proton and neutron, the isospins of the quarks add up in a linear combination giving a total isospin of  $I = 1/2$ , where  $I_3 = +1/2$  represents the proton and  $I_3 = -1/2$  the neutron. A triplet of particles, like the pions, has isospin  $I = 1$ , with  $I_3 = +1$  representing  $\pi^+$ ,  $I_3 = 0$  representing  $\pi^0$  and  $I_3 = -1$  representing  $\pi^-$ . In the decuplet we have four states of  $\Delta$ -particles giving an isospin of  $I = 3/2$ , with  $I_3 = +3/2$  representing  $\Delta^{++}$ ,  $I_3 = +1/2$  representing  $\Delta^+$ ,  $I_3 = -1/2$  representing  $\Delta^0$  and  $I_3 = -3/2$  representing  $\Delta^-$ .

The isospin  $I$  of a family of particles, affected in the same way by the strong force, is related to the number of states in the family, according to: number of states =  $2I + 1$

$$\begin{aligned} 2 \text{ states} &\Rightarrow 2I + 1 \Rightarrow I = 1/2 \\ 3 \text{ states} &\Rightarrow 2I + 1 \Rightarrow I = 1 \\ 4 \text{ states} &\Rightarrow 2I + 1 \Rightarrow I = 3/2 \end{aligned}$$

The splitting of these isospin states into their three components is illustrated in Figure 2.15.

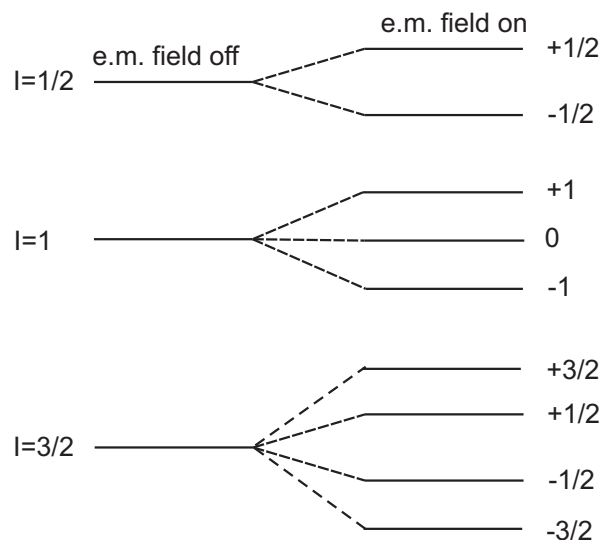


Figure 2.15: *Splitting of the isospin into third components under the influence of an electromagnetic field.*

Instead of using electric charge in the representation of the multiplets we can replace it with isospin. We have seen that the third component of the isospin is  $I_3 = -1/2$  for the d-quark, whereas it for the u-quark is  $I_3 = +1/2$ . The isospin for a singlet state is  $I_3 = 0$ , which corresponds to the s-quark. If we construct the basic quark and antiquark multiplets in the isospin-strangeness space, they would look like as shown in Figure 2.16 (upper part). By combining the quark and antiquark triplets in various ways we can reconstruct the hadron multiplets. One example is shown in Figure 2.16 (lower part).

The composition of the possible 3 quark combinations is a bit more complicated than that for the mesons, but can be obtained using the same techniques. You may notice that the position of

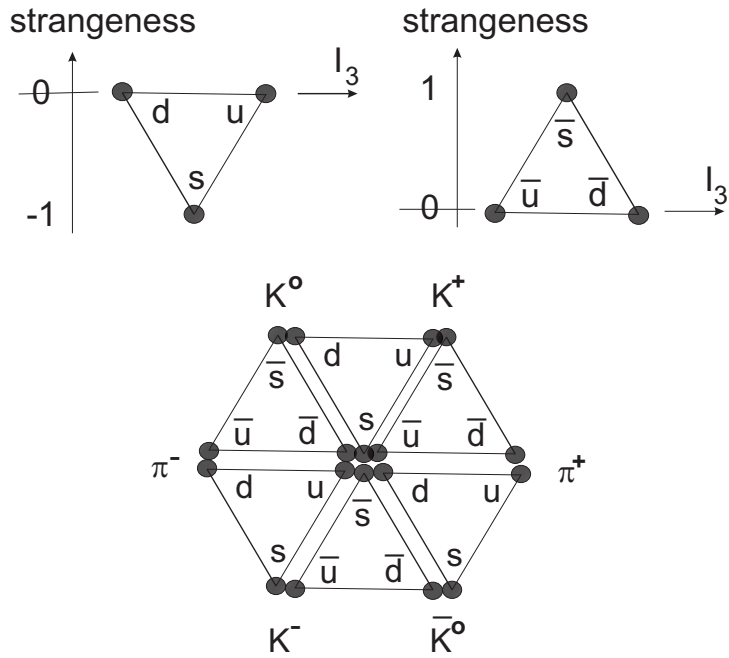


Figure 2.16: Allocation of quarks and antiquarks according to their isospin third components and strangeness, and how they can be combined to give octets of particles.

### Mesons, spin 0

	-1	-1/2	0	1/2	+1	$I_3$
+1		$K^0$ ( $d\bar{s}$ )		$K^+$ ( $u\bar{s}$ )		
0	$\pi^-$ ( $d\bar{u}$ )		$\pi^0, \eta, \eta'$ ( $u\bar{u}$ )( $d\bar{d}$ )( $s\bar{s}$ )		$\pi^+$ ( $u\bar{d}$ )	
-1		$K^-$ ( $s\bar{u}$ )		$\bar{K}^0$ ( $s\bar{d}$ )		
Strangeness						

Figure 2.17: Multiplet for spin 0 mesons plotted as isospin versus strangeness

the hadrons are symmetric around  $I_3 = 0$  and that a hadron transforms into its isospin partner by exchanging a  $u$  ( $\bar{u}$ )-quark with a  $d$  ( $\bar{d}$ )-quark and vice versa. Thus we have *isospin symmetry*. Since the strong force is blind with respect to the quark flavours i.e. it can not tell the difference between  $u$  and  $d$ -quarks for example, it means that isospin is conserved in strong interaction. As an example the complete multiplet for mesons of spin zero is shown in Figure 2.17.

# Chapter 3

## The Forces of Nature

In the investigation of the forces of nature we want to establish the sources of the forces and the intrinsic strength of the interaction to which they give rise. Further, we are interested in the space-time properties of the force; how it propagates through space and how it affects the motion of particles under its influence. Finally, we must consider both the macroscopic (or classical) description of the force (where appropriate) and the microscopic (or quantum-mechanical) picture (where possible).

We experience two fundamental forces on the macroscopic scale in our daily life; the *gravitational force* that keeps our solar system together and ensure that we stay on earth, and the *electromagnetic force* which acts between objects carrying electric charge. Both act over long distances and the force is proportional to the inverse square of the distance between the objects. The well-known formula which describes the gravitational attraction of two objects with the masses  $m_1$  and  $m_2$ , separated by a distance  $r$  can be written:

$$F = G \cdot \frac{m_1 m_2}{r^2} \quad ,$$

where  $G$  is a constant of proportionality, the *gravitational constant*.

Electromagnetic interactions are interactions between light and matter or between electric field and charge. Already in 1865 the Scottish physicist James Clerk Maxwell managed to unify the concepts of electricity and magnetism into one theory of electromagnetism. The force is mediated by the electromagnetic field. For two static objects with electric charges  $e_1$  and  $e_2$  at a distance  $r$ , the force is:

$$F = k \cdot \frac{e_1 e_2}{r^2} \quad ,$$

where  $k$  is again a proportionality constant. The difference to gravitation is that the electromagnetic force can not only be attractive but also be repulsive. With the advent of quantum mechanics in the first decades of the 20th century it was realized that the electromagnetic field, including light, is quantized and that the electromagnetic force is mediated by the exchange of a stream of particles, *photons*. In a similar way the gravitational force is believed to be mediated by particles called *gravitons*, but since gravitation is of the order of  $10^{37}$  times weaker than the electromagnetic force, the gravitons have not yet been observed.

In addition to these long range forces there are also two forces that only act over short distances; the *strong force* that holds a nucleus together and the *weak force* that is responsible for radioactive

decays. A natural route to follow for a description of these forces was to search for a mechanism like the one, which so successfully describes the electromagnetic force.

The simplest manifestation of the weak force is the well-known  $\beta$ -decay where a neutron decays into a proton, an electron and an antineutrino. The Italian physicist Enrico Fermi described this decay by assuming that, at a single point in space-time, the quantum-mechanical wave function of the neutron is transformed into that of the proton and that the wavefunction of the incoming neutrino, which is equivalent to an outgoing antineutrino, is transformed into that of an electron. Although this theory of point-like interactions was successful at the time, it turned out that it was not sufficient to describe data at higher energies. To solve this problem and to put the description of weak interaction on a common ground to the successful theory of electromagnetism, a field theory with a particle exchange mechanism had to be introduced. However, in contrast to the electromagnetic force, which has a long range and which is mediated by the massless photon it was assumed that the weak force has to be mediated by massive particles to accommodate the short range of the force. In a generalization of quantum electrodynamics the American physicists Sheldon Glashow and Steven Weinberg, and the Pakistani physicist Abdus Salam succeeded in formulating the electroweak theory, which is a common theory for electromagnetic and weak interactions. In addition to the photon as force mediator, this theory also contains the weak force mediators,  $W^+$ ,  $W^-$  and  $Z^0$ , which contrary to the photon also can interact with each other. The strength of the weak force is of the order of  $10^6$  times weaker than that of the strong force. This has been estimated by comparing the decay times of the processes  $\Delta^-(ddd) \rightarrow n(udd) + \pi^-(\bar{u}d)$  and  $\Sigma^-(dds) \rightarrow n(udd) + \pi(\bar{u}d)$ . Since strangeness is broken in the  $\Sigma^-$ -decay it has to proceed via the weak interaction and thus the lifetime is several orders of magnitude longer than the  $\Delta^-$ -decay which follows the strong interaction. The probability for a decay is related to how strongly the force mediator couples to the quarks, which in turn is related to the decay time. The ratio of the decay times is therefore a measure of the relative strength of the weak force compared to the strong.

In 1935 the Japanese physicist Hideki Yukawa proposed that the strong force is mediated by a new particle in analogy with the electromagnetic and weak forces. Knowing the approximate range of the strong force  $10^{-15}$  meter (the size of the nucleon), the mass of the particle could be estimated to  $100\text{-}200 \text{ MeV}/c^2$ . This particle was called the pion ( $\pi$ ). A couple of years after the prediction of the pion a particle in this mass range was discovered in cosmic ray experiments, but later it was understood that this particle has too weak an interaction compared to what is needed for strong interaction. Instead it turned out that the observed particle is a heavier version of the electron, the muon ( $\mu$ ). The pion was not discovered until 1947. Eventually it turned out that the pion, like a large number of other *hadrons* discovered in the 1950's, was not an elementary particle but they were composite particles, built out of quarks and antiquarks. In a more careful study of the strong force it was shown that it has properties, which are different from those of the electromagnetic and weak forces. The specific behaviour of the strong force could be related to the properties of the massless force mediator, the *gluon*, which also explains the short range of the strong force.

It is believed that the four fundamental forces of nature as we experience them in our daily life are just different appearances of the same force, such that if we go to high enough energy ( $10^{19}$  GeV) the forces should be of the same strength. It should thus be possible to formulate a theory which describes the interactions of all the forces.

In the following sections we will discuss in more detail the electromagnetic, weak and strong forces. First, however, we must introduce the concept of *virtual particles*.

### 3.1 Vacuum and Virtual Particles

*Vacuum* is normally regarded as empty space. This is, however, not quite so from a quantum mechanics point of view, where vacuum can be assumed to be full of activity. According to the Heisenberg uncertainty principle,  $\Delta E \cdot \Delta t \geq \hbar$ , non-zero energy may be created from vacuum over short periods of time. This means that particles continuously can appear and disappear as long as it happens within a time that is given by the uncertainty principle. Such *quantum fluctuations* can not be observed due to the uncertainty in energy, and since the particles produced can not be measured directly they are called *virtual particles*. The quantum fluctuation itself is not allowed according to the laws of physics (energy and momentum conservation) and consequently the virtual particles do also not obey the conservation laws.

A real particle satisfies the relation  $p^2 = E^2/c^2 - \vec{p}^2 = m_o^2 c^2$ , where  $p$  and  $\vec{p}$  are the four- and three-momenta, respectively, and  $m_o$  is the mass of the particle at rest. However, for a virtual particle  $p^2 = E^2/c^2 - \vec{p}^2$  can take any value, which means that the mass (four-momentum) of a virtual particle is not necessarily the same as the mass (four-momentum) of the corresponding real particle.

According to *field theories* the various interactions proceed via the exchange of force mediating particles or field particles. Each real particle is surrounded by a cloud of all kinds of field particles that couple to that specific particle. For example charged leptons are surrounded by a cloud of photons and weak force mediators, whereas neutrino particles are only surrounding itself with weak force mediators. Quarks are accompanied by a cloud of gluons as well as photons and weak force mediators. Normally a field particles is reabsorbed by the same particle but in case another particle is close enough to absorb it, we have an interaction. This must then happen within the time that the field particle exists, which is given by the uncertainty principle, and thus it can not be directly observed.

### 3.2 Electromagnetic Interaction and QED

The electromagnetic force, which acts between particles carrying electric charge, is quite well understood. Since the force has an infinite range it also has an influence on macroscopic phenomena. The force between two particles with unlike charges is attractive whereas the force between particles carrying like charges is repulsive. The strength is given by Coulomb's law:

$$F = k \cdot \frac{q_1 \cdot q_2}{r^2}$$

where  $q_1$  and  $q_2$  are the charges of the particles and  $r$  is the distance between them.

A consistent quantum theory, Quantum Electrodynamics (QED), for electromagnetic interactions was formulated in the mid 1960's by Richard Feynman. According to this theory the interaction between electrically charged particles occurs via the electromagnetic field as an exchange of the field quanta, the *photons*, between the interacting particles. This description implies that the interaction is not instantaneous, since it takes some time for the field quantum (in this case the photon) to propagate from the emitting particle to the particle that absorbs it. In this respect it is in contradiction to Newton's description, which postulates that the interaction between two distant objects is instantaneous. Charged particles can emit and absorb photons.

### 3.2.1 Feynman Diagrams

Feynman invented a very useful diagrammatical formulation to illustrate the interactions. To each particle he introduced a propagator describing the free propagation of the particle. The theory then defines the interaction *vertices*, which are combined with *propagators* to build a specific diagram. Feynman also introduced the rule that a particle going backwards in time corresponds to an antiparticle going forward in time (see Section 2.10). Considering electromagnetic interactions and assuming time to proceed from left to right, the representation of the three particles (electron, positron and photon) are shown in Figure 3.1.




Image	Description	Particle Represented
	straight line, arrow to the right	electron
	straight line, arrow to the left	positron
	wavy line	photon

Figure 3.1: *Symbols used in Feynman diagrams.*

Any line for a propagating charged particle and any line for a propagating photon can be combined and they are tied together in a vertex, giving the possibilities shown in Figure 3.2.

### 3.2.2 Electromagnetic Scattering Processes

The simplest diagram for the interaction between two electrons is given in Figure 3.3.

Such a process can be subdivided into the following two steps as illustrated in Figure 3.4. The one electron emitting a photon in the first step and the other absorbing it in the second step. The photon, representing the field quantum of the electromagnetic field, carries momentum. Since it takes some time for the photon to propagate from the emitting electron to the absorbing one, it means that while the first electron will feel a loss of momentum in the instant of emission, the

	An electron emits a photon
	An electron absorbs a photon
	A positron emits a photon
	A positron absorbs a photon
	A photon produces an electron and a positron (an electron-positron pair)
	An electron and a positron meet and annihilate (disappear), producing a photon

Figure 3.2: Description in terms of Feynman diagrams of various interactions between electrons and photons.

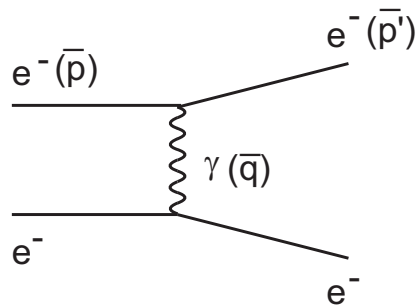


Figure 3.3: Feynman diagram describing an interaction between two electrons via the exchange of a virtual photon.

second one will feel nothing. For a very short time the momentum of the two electron system is not conserved. However, as soon as the second electron has absorbed the photon the momentum conservation is restored. If we take the momentum of the photon into account, the momentum of each step is always conserved. Thus, for the first step we have:

$$\vec{p}_1 - \vec{q} = \vec{p}_1',$$

and for the second:

$$\vec{p}_2 + \vec{q} = \vec{p}_2',$$



and for the whole process, momentum conservation gives:

$$\vec{p}_1 + \vec{p}_2 = (\vec{p}_1 - \vec{q}) + (\vec{p}_2 + \vec{q}) = \vec{p}'_1 + \vec{p}'_2$$

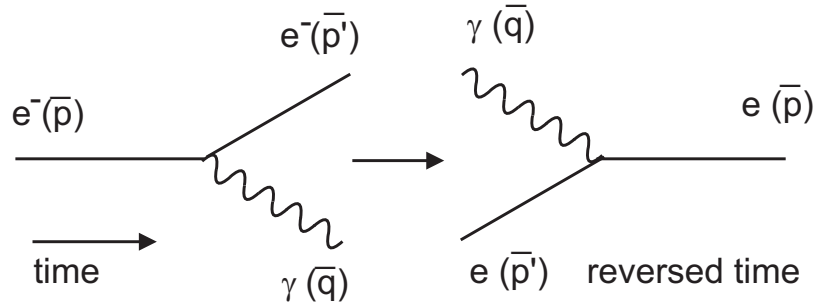


Figure 3.4: Feynman diagram describing the emission and absorption of a photon by an electron.

Let us consider the first step of the process and investigate whether energy is conserved. We denote the energy of the incoming electron  $E$  and the outgoing  $E'$ , such that  $E' + E_\gamma = E$  if energy conservation holds.

$$E' = \sqrt{\vec{p}'^2 + m_e^2} = \sqrt{|\vec{p} - \vec{q}|^2 + m_e^2}$$

$$\text{If the photon is real } E_\gamma = \sqrt{|\vec{q}|^2}$$

$$\Rightarrow E' + E_\gamma = \sqrt{|\vec{p} - \vec{q}|^2 + m_e^2} + |\vec{q}|$$

$$= \sqrt{|\vec{p}|^2 + |\vec{q}|^2 - 2\vec{p}\vec{q} + m_e^2} + |\vec{q}|$$

$$\neq \sqrt{|\vec{p}|^2 + m_e^2} = E$$

$\Rightarrow$  Energy conservation is violated in the first step and the process should not be able to happen. However, if the violation of the energy and momentum conservation occurs within a time interval shorter than given by the Heisenberg uncertainty principle,  $\Delta E \Delta t \sim \hbar$ , it is allowed. It should be realized that if the energy is not conserved then the relation  $E^2 = \vec{p}^2 + m^2$  tells us that the mass of the photon might not be zero. Such photons are called *virtual photons* and may have a non-zero mass due to the fluctuation of energy in a very short time. If the photon is absorbed by the other electron within the time  $\Delta t$  the process will occur. If not, the photon will be reabsorbed by the same electron. This explains how an electron propagating through space can be surrounded by a cloud of photons. Photons are constantly emitted and reabsorbed by the electron within the time given by Heisenberg's uncertainty principle.

Some other examples of diagrams with virtual photons are shown in Figure 3.5.

One necessary condition for a process, which involves the exchange of a force quantum, to happen is that the energy of the initial and final states are the same (energy conservation).

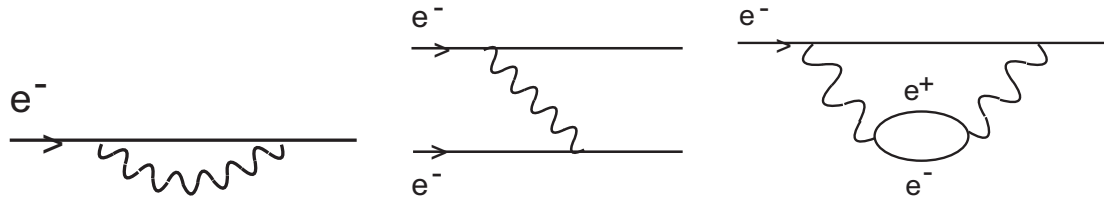


Figure 3.5: Some Feynman diagrams with virtual photons.

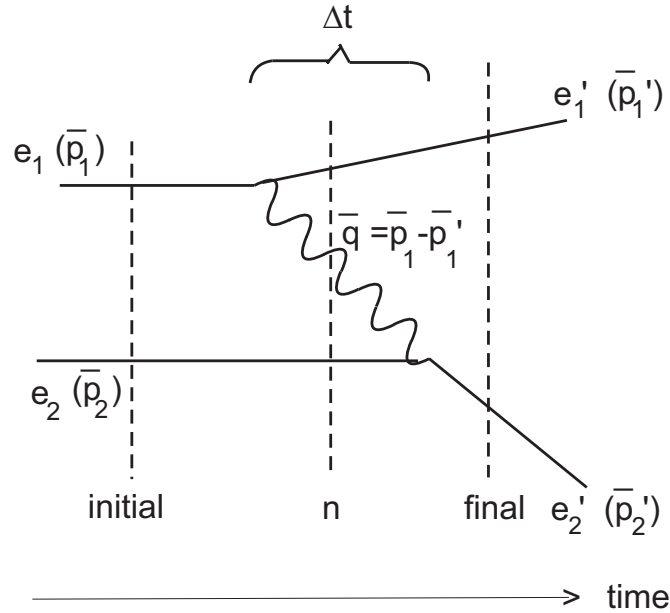


Figure 3.6: Feynman diagram describing electron-electron scattering (referred to as diagram X later on).

### 3.2.3 Calculation of scattering amplitudes

Consider the electron-electron scattering process as given in Figure 3.6.

$$\vec{p}_1 = \vec{p}'_1 + \vec{q} \Rightarrow \vec{q} = \vec{p}_1 - \vec{p}'_1$$

$$\vec{p}_2 + \vec{q} = \vec{p}'_2 \Rightarrow \vec{q} = \vec{p}'_2 - \vec{p}_2$$

The electron  $e_1$  emits a virtual photon, which after some time,  $\Delta t$ , is absorbed by the electron  $e_2$ .

$$\Rightarrow \Delta t \sim \frac{\hbar}{\Delta E} = \frac{\hbar}{E_n - E_i} ; \quad \text{according to the Heisenberg uncertainty principle.}$$

where the index  $i$  represents the initial state and  $n$  the intermediate state.

Vertices are generally speaking points in space-time where particles are created or annihilated. In the case of electromagnetic interactions there is only one basic vertex, which couples a photon to a charged particle. The photon is the force mediator of the electromagnetic field, the strength of which is related to the force between two charged particles, as given by Coulomb's law.  $F = k \cdot \frac{q_1 q_2}{r^2}$ , where  $k = \frac{1}{4\pi\epsilon_0}$  is the Coulomb's constant and  $\epsilon_0$  is the vacuum permittivity.

A *coupling constant* is a quantity which represents the strength of the interaction between a particle and the force mediator at a specific vertex. For the electromagnetic force the coupling strength must thus be proportional to the electric charge of the particle. The fine structure constant, which specifies the strength of the electromagnetic field and is related to the elementary charge,  $e$ , is defined as:

$$\alpha = \frac{2\pi k e^2}{hc} = \frac{2\pi e^2}{4\pi\epsilon_0 hc} = \frac{2\pi e^2}{E_\gamma \cdot \lambda_\gamma}, \quad \text{since } E_\gamma = \frac{hc}{\lambda_\gamma}$$

The units are chosen such that  $\alpha$  becomes dimensionless.

In other units the fundamental unit of charge can be given as  $g_e = \sqrt{4\pi\alpha}$ , which means that the coupling strength is given by  $\alpha = \frac{g_e^2}{4\pi}$ . Thus,  $g_e$  is a dimensionless measure of the charge of the electron.

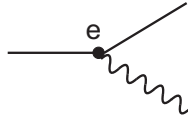


Figure 3.7: *Strength of an electron-photon vertex.*

In quantum mechanics the motion of a particle can be described by a wavefunction and the probability to observe the particle in a given state is given by the wavefunction squared. The photon is a quantum of the electromagnetic field and the number of photons surrounding an electrically charged particle is given by the strength of this field, which is proportional to the charge of the particle.

A certain process is described by how the wavefunction is changing with time. The probability that the process occurs is thus given by the square of the wavefunction describing that process. In order to describe the process illustrated in Figure 3.6, we have to consider how the wavefunction changes from representing a single electron to an electron which emits a photon which is then absorbed by another electron. The probability that the electron emits a photon is related to the strength of the electromagnetic coupling  $\alpha$  i.e.  $e \sim \sqrt{\alpha}$ . In the following we will use the notation  $-e$  for the charge of the electron. The probability (or more correctly, the amplitude) that a photon is emitted by an electron is thus proportional to  $-e$ . Further, the probability (or amplitude) that a photon, which has been emitted by one electron, will be absorbed by another one within the time  $\Delta t$  is related to  $\Delta t \cdot (-e)$ .

The scattering amplitude for the process, shown in Figure 3.6, which we may call process X, is then:

$$A_X = (-e) \cdot \Delta t \cdot (-e) = \frac{e^2 \hbar}{\Delta E} = \frac{e^2 \hbar}{(E_n - E_i)}$$

The process shown in Figure 3.8, called process Y, gives the same final state.

$$\begin{aligned} \bar{p}_1 + \bar{q}' &= \bar{p}'_1 \Rightarrow \bar{q}' = \bar{p}'_1 - \bar{p}_1 \\ \bar{p}_2 &= \bar{p}'_2 + \bar{q}' \Rightarrow \bar{q}' = \bar{p}_2 - \bar{p}'_2 \\ \Rightarrow \bar{q}' &= (\bar{p}_2 - \bar{p}'_2) = (\bar{p}'_1 - \bar{p}_1) = -(\bar{p}_1 - \bar{p}'_1) = -\bar{q} \end{aligned}$$

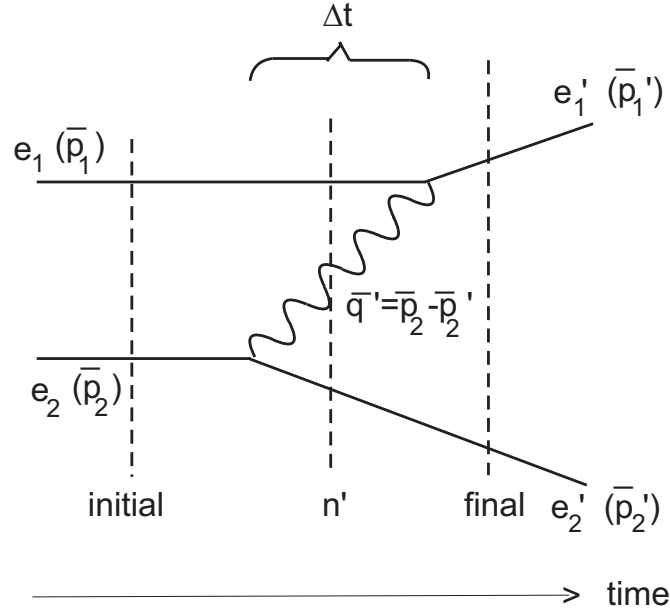


Figure 3.8: Feynman diagram describing electron-electron scattering (referred to as diagram Y later on).

The amplitude is:

$$A_Y = (-e) \cdot \frac{\hbar}{(E'_n - E_i)} \cdot (-e)$$

With  $\bar{q}' = -\bar{q}$  we have  $E_\gamma = |\bar{q}| = |\bar{q}'| = E'_\gamma$

$$\text{Diagram X: } E_i = E_1 + E_2; \quad E_n = E_\gamma + E'_1 + E_2 \Rightarrow E_n - E_i = \boxed{E_\gamma + E'_1 - E_1}$$

$$\text{Diagram Y: } E_i = E_1 + E_2; \quad E'_n = E'_2 + E_\gamma + E_1 \Rightarrow E'_n - E_i = E'_2 + E_\gamma - E_2 = \boxed{E_1 + E_\gamma - E'_1},$$

where we have used energy conservation:  $E_1 + E_2 = E'_1 + E'_2 \Rightarrow E'_2 - E_2 = E_1 - E'_1$

Since we can not distinguish the two diagrams X and Y we have to add the amplitudes and square in order to obtain the probability (cross section) for the process to happen.

### 3.2.4 Differential Cross Section

Consider a parallel beam of particles incident on a thin slice of material containing N scattering centres per volume unit, as illustrated in Figure 3.9.

The flux of particles (particles per unit area and unit time) can be written  $\Phi = n_o \cdot v$  where  $n_o$  is the density of particles in the incoming beam (number of particles per unit volume) and  $v$  their velocity with respect to the target. If we have a detector sitting at a *polar angle*  $\theta$ , covering a *solid angle*  $d\Omega$  ( $d\Omega = ds/r^2$ , where  $ds$  is the area of the detector and  $r$  the distance to the detector from the target), the number of particles per unit time observed in the detector would be:

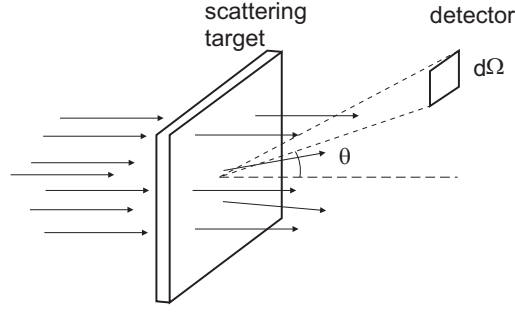


Figure 3.9: Scattering of a flux of particles impinging on a target foil.

$$dn = \sigma(\theta)d\Omega \cdot \Phi \cdot N = d\sigma \cdot \Phi \cdot N ,$$

since  $\sigma(\theta) = \frac{d\sigma}{d\Omega}$ . This describes the probability that a particle is scattered an angle  $\theta$ , within the solid angle  $d\Omega$ . The *differential cross section* is then

$$\frac{d\sigma}{d\Omega} = \frac{1}{\Phi \cdot N} \cdot \frac{dn}{d\Omega} ,$$

which is the number of scattered particles per unit time and solid angle divided by the number of incoming particles per unit time and area. The *total cross section* is defined as the differential cross section integrated over the total solid angle (except including particle going straight ahead):

$$\sigma = \int \frac{d\sigma}{d\Omega} d\Omega$$

In quantum mechanics, the differential cross section for electron-electron scattering is the sum of the amplitudes  $A_X$  and  $A_Y$  squared.

$$\begin{aligned} \frac{d\sigma}{d\Omega} &\sim |A_X + A_Y|^2 = \left| \frac{e^2}{E_n - E_i} + \frac{e^2}{E'_n - E_i} \right|^2 \approx e^4 \left( \frac{1}{E_n - E_i} + \frac{1}{E'_n - E_i} \right)^2 = \\ &= e^4 \left( \frac{1}{E_\gamma + E'_1 - E_1} + \frac{1}{E_1 + E_\gamma - E'_1} \right)^2 = \\ &= e^4 \left( \frac{E_1 + E_\gamma - E'_1 + E_\gamma + E'_1 - E_1}{(E_\gamma + E'_1 - E_1)(E_1 + E_\gamma - E'_1)} \right)^2 = \\ &= e^4 \left( \frac{2E_\gamma}{(E_\gamma - (E_1 - E'_1))(E_\gamma + (E_1 - E'_1))} \right)^2 = \\ &= e^4 \left( \frac{2E_\gamma}{E_\gamma^2 - (E_1 - E'_1)^2} \right)^2 \end{aligned}$$

The factor  $2E_\gamma$  does not appear if we do an exact calculation.

We introduce  $E_\gamma^2 = |\vec{q}|^2 + m_\gamma^2$ , where  $m_\gamma = 0$  is the rest mass of the photon, and  $\epsilon = E_1 - E'_1$  (the energy the photon would have had if energy was conserved, which is true for the whole scattering process).

$$\Rightarrow \frac{d\sigma}{d\Omega} \sim e^4 \left( \frac{2E_\gamma}{|\vec{q}|^2 - \epsilon^2 + m_\gamma^2} \right)^2 \sim e^4 \left( \frac{1}{|\vec{q}|^2 - \epsilon^2 + m_\gamma^2} \right)^2 .$$

But  $q^2 = \epsilon^2 - |\bar{q}|^2$ , where  $q$  is the four-momentum transferred by the exchanged photon as calculated from the conservation of energy and momentum given by:

$$q = p'_1 - p_1 \quad \text{with} \quad p_1'^2 = E_1'^2 - |\bar{p}'_1|^2 \quad \text{and} \quad p_1^2 = E_1^2 - |\bar{p}_1|^2$$

$$\Rightarrow \frac{d\sigma}{d\Omega} \sim e^4 \left( \frac{1}{m_e^2 - q^2} \right)^2 .$$

This is the general expression which can be used also for massive exchange particles if the photon mass is replaced by the rest mass of the exchange particle which is responsible for that specific interaction. For a photon we get:

$$\frac{d\sigma}{d\Omega} \sim e^4 \left( \frac{1}{-q^2} \right)^2 \quad (m_\gamma = 0) .$$

In the center-of-mass system:

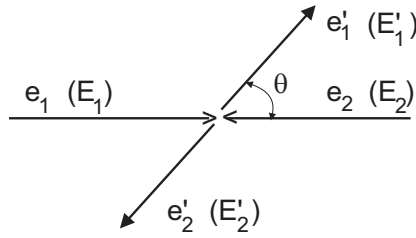


Figure 3.10: Scattering of two equally energetic electrons in their centre-of-mass system, which in this case is the same as the laboratory system.

$$E_1 = E_2 = E_1' = E_2' \quad |\bar{p}_1| = |\bar{p}_2| = |\bar{p}'_1| = |\bar{p}'_2| ,$$

as clear from Figure 3.10. The 4-momentum squared transferred by the virtual photon is:

$$q^2 = (p_1 - p'_1)^2 = p_1^2 + p_1'^2 - 2p_1 p_1' =$$

$$= m_e^2 + m_e^2 - 2(E_1 E_1' - |\bar{p}_1| |\bar{p}'_1| \cos \theta) .$$

But we assume  $E_1 = E_2 \gg m_e$ , and thus we have:

$$E = E_1 = E_1' \approx |\bar{p}_1| = |\bar{p}'_1|$$

$$\Rightarrow q^2 = -2E^2(1 - \cos \theta) = -2E^2 \cdot 2 \sin^2 \frac{\theta}{2} = -4E^2 \sin^2 \frac{\theta}{2} , \quad \text{since} \quad \sin^2 \frac{\theta}{2} = (1 - \cos \theta)/2$$

$$\Rightarrow \frac{d\sigma}{d\Omega} \sim \frac{e^4}{E^4 \sin^4 \frac{\theta}{2}} \sim \frac{\alpha^2}{E^2 \sin^4 \theta} .$$

This is the classical Rutherford formula for scattering in a potential  $V = 1/r$ .

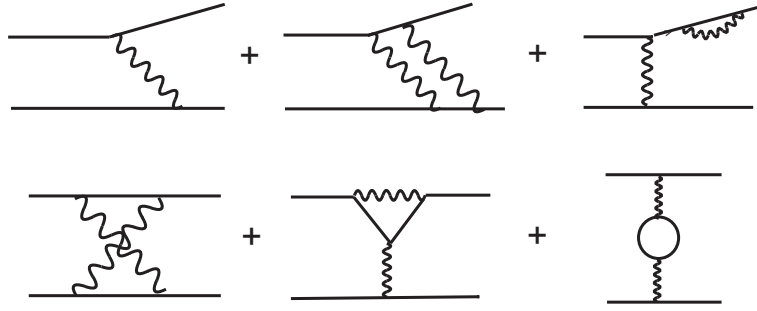


Figure 3.11: Feynman diagrams describing scattering between two electrons at different orders in the electromagnetic coupling constant (number of scattering vertices).

### 3.2.5 Higher Order Contributions to $ee$ Scattering

In these calculations we have only considered the contribution from the diagram of lowest order in the electromagnetic coupling constant ( $\alpha$ ), where we have only one photon exchange. The problem that we encounter is that we can add more diagrams by just adding more internal lines such that the total number of possible diagrams giving the same final state becomes infinite. Some examples of higher order electron-electron scattering diagrams are given in Figure 3.11.

However, we have already pointed out that the strength of the interactions between two electrons is proportional to the electric charge. A dimensionless measure of the interactions strength is given by the electromagnetic coupling strength (or fine structure constant),  $\alpha = \frac{e^2}{4\pi\epsilon_0\hbar c}$ . Each vertex adds a factor  $\alpha$ , but since  $\alpha$  is small ( $\sim 1/137$ ), diagrams of higher orders in  $\alpha$  (more vertices) will give smaller contributions than a lower order  $\alpha$  diagram (fewer vertices), and consequently the cross section can be written as a converging series expansion in terms of  $\alpha$ .

$$\sigma = O(\alpha) + O(\alpha^2) + O(\alpha^3) + \dots$$

### 3.2.6 Regularization and Renormalization

Experimentally the cross section (scattering amplitude) of a process with specific initial and final state can be measured but the experimental information does not explain how the initial state turned into the final state. As we have mentioned in section 3.2.5, discussing  $ee$ -scattering we can imagine an infinite number of diagrams that describes a process with specific initial and final states by just adding more virtual particles to the intermediate state. Internal propagators can be added and combined in an infinite number of ways. This is not only true for  $ee$ -interactions but for all electromagnetic, weak and strong interactions. The most basic diagram is the one with the least number of coupling vertices between the virtual force mediator (propagator) and the incoming and outgoing particles, respectively. More complicated diagrams are of higher orders in the coupling constant.

Although the energies and momenta of the initial and final state particles are well defined this is not so for the virtual particles of the intermediate state (internal propagators). Even if energy

and momentum conservation is satisfied for the whole process, the virtual particles may violate basic kinematic rules, which are valid for real particles. For example  $m^2 = E^2 - p^2$  must not necessarily be the invariant mass of the particles involved in the intermediate state because virtual particles can have any energy and momentum, such that a virtual photon can have a mass different from zero. In this case the particle is said to be *off-shell*.

Thus, in order to calculate the scattering amplitude (cross section) of a specific process we have, according to the summation rule of Feynman, to sum up the contributions from all possible diagrams that takes us from the initial state to the final state. This will lead to an infinite power series in the coupling strength. However, this is not all, we also have to integrate over all momenta of the virtual particles. Especially diagrams containing loops of particles cause a problem. Loops arise when for example a photon creates a virtual electron-positron pair which subsequently annihilates. These loop particles have no unique energy and momentum but a change of the energy and momentum of one particle has to be balanced by the energy and momentum of the other particle in the loop. Such calculations are not only a mathematical challenge but also lead to infinities that are unphysical. The integration over momenta frequently diverges at large loop momenta (ultraviolet divergencies). Since particles in the theory are treated as massless the loops also lead to infrared divergencies, coming from the zero-momentum limit of the loop integrals. Such divergences can, however, be controlled by mathematical methods called *regularization* and *renormalization*. In the following we will discuss how this is implemented in QED but the same general arguments are also valid for QCD

## Regularization

The challenge of regularization is to explicitly calculate the divergent integral:

$$I = \int_0^\infty d^4k F(k),$$

where  $k$  is the four-momentum. This has to be done in such a way that the final result does not depend on the regularization scheme chosen. There are a number of regularization schemes on the market but we will discuss only the one called 'Momentum Cutoff', just to give an example. In this method the integral is not performed to infinity but to a very large momentum,  $\Lambda$ , which then gives:

$$I \rightarrow I_\Lambda = \int_0^\Lambda d^4k F(k),$$

where  $I_\Lambda$  is certainly convergent and approaches  $I$  as  $\Lambda$  approaches infinity. If we perform the integral  $I_\Lambda$  the result can be parameterized in the following way:

$$I_\Lambda = A(\Lambda) + B + C(1/\Lambda),$$

where in the limit  $\Lambda \rightarrow \infty$ ,  $A$  is divergent,  $C$  vanishes and  $B$  is independent of  $\Lambda$  and thus remains finite. So, the problem is now to find a way to get rid of the divergent piece. In order to get rid of the divergent part the regularization step has to be followed by a renormalization step.



## Renormalization

As we have demonstrated in the previous sections the calculation of scattering amplitudes includes contribution from the coupling strength (in principle the charge) at the various vertices and the four-momentum (mass) of the propagator. Thus, the integral we have considered can be written as a function of mass,  $m$ , coupling strength,  $\alpha$  and the momentum cutoff,  $\Lambda$ :

$$I \rightarrow I(m, \alpha, \Lambda).$$

In the theory the coupling strength is, however, given by the *bare charge* and the propagator four-momentum includes the *bare mass*, which can never be measured. These differ from the *physical masses* and *physical charges*, as observed from experimental measurements, by the fact that every particle is surrounded by a cloud of virtual particles. The relation between the physical (*renormalized*) and bare parameters includes the contributions from higher order diagrams and can be written:

$$\begin{aligned} m &\rightarrow m(\Lambda) \equiv m_o + \delta m(\Lambda) \\ \alpha &\rightarrow \alpha(\Lambda) \equiv \alpha_o + \delta \alpha(\Lambda) \\ I(m, \alpha, \Lambda) &\rightarrow I(m(\Lambda), \alpha(\Lambda)), \end{aligned}$$

where  $m_o$  and  $\alpha_o$  are the bare mass and bare coupling, respectively, whereas  $\delta m(\Lambda)$  and  $\delta \alpha(\Lambda)$  are the contributions from higher order diagrams.

What we have achieved with this operation is to absorb all of the divergent behaviour into the physical parameters,  $m(\Lambda)$  and  $\alpha(\Lambda)$ , such that  $I$  is no longer explicitly divergent but merely depend on physical quantities, which, however, will diverge as  $\Lambda$  approaches infinity. The next step is to specify the renormalization conditions:

$$\begin{aligned} m(\Lambda) &\rightarrow m_R \\ \alpha(\Lambda) &\rightarrow \alpha_R \end{aligned}$$

where  $R$  stands for *renormalized* in the physical limit. Then the final result is simply  $I(m_R, \alpha_R)$ , with  $m_R$  and  $\alpha_R$  being the quantities we *measure* for the electron mass and coupling, respectively. This result has a finite value.

Now, it has to be kept in mind that each regularization scheme gives finite parts that differ such that the details of the regularization scheme have to be specified as the final answer is given. This is called the *subtraction scheme*. Thus, as the final renormalization answer is quoted also the subtraction scheme used to renormalize the observable quantities has to be given.

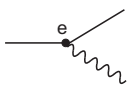
Two of the mostly used subtraction schemes are the minimal subtraction ( $MS$ ), where only the divergent part of the amplitude is subtracted and the modified minimal subtraction ( $\overline{MS}$ ), in which certain additional finite terms are subtracted from the  $MS$ -scheme.

It might be hard to accept that the values of the bare mass and bare charge of an electron are infinite. The explanation stems from the fact that many of the *intrinsic properties* of an electron are tied to the electromagnetic field that it carries around with it. The energy carried by a single electron, the self energy, is not only the bare value but also includes the energy contained in its electromagnetic field. As we have discussed in section 3.1 electrons can emit spontaneously virtual photons through quantum fluctuations, which can subsequently split up into an electron-positron pair. In this way the electron is always accompanied by a cloud of virtual photons

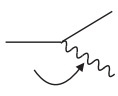
and virtual electron-positron pairs through its interaction with the electromagnetic field. This cloud screens the bare charge so the measured charge is reduced and dependent on the distance (energy) at which the measurement is performed (see also section 3.4.2). An evidence that this is the case is that in our everyday world  $\alpha = \frac{1}{137}$ , whereas its value decreases at higher energies as measured by accelerator experiments. So the deeper we penetrate the cloud of virtual particles the larger the charge and mass of the electron gets.

In order to make contact with reality, the formulae should be rewritten in terms of measurable, *renormalized* quantities. Thus, the charge of the electron, for example, should be defined in terms of a quantity measured at a specific kinematic *renormalization point* or *subtraction point*, which normally has a characteristic energy, called the *renormalization scale* or simply the *energy scale*, but it also depends on the subtraction scheme.

### 3.2.7 Summary of Amplitude Calculations

- Each vertex  gives a factor  $(-e)$  or equivalently a factor  $\sqrt{\alpha}$

- Four-momentum is conserved

- Internal lines  give a factor  $\frac{1}{-P^2+M^2}$

where  $P$  is the four-momentum of the exchanged particle and  $M$  is the rest mass of the propagator.

$$Probability = |Amplitude|^2$$

The total amplitude for scattering between two electrons (or any other process) is the sum of the amplitudes for all contributing diagrams.

### 3.2.8 Pair Production and Annihilation

In a time-like exchange, annihilation and pair production are described by the Feynman diagrams in Figure 3.12.

The above diagrams can be modified such that instead of creating a photon by electron-positron annihilation, a photon can be annihilated by the electron-positron pair, within the time given by the Heisenberg uncertainty principle, and we are left with vacuum. Similarly an electron-positron pair can be created out of vacuum together with a photon. The Feynman diagrams corresponding to these situations are given in Figure 3.13.

These processes can not occur by themselves since energy and momentum are not conserved, but they can be part of processes with two vertices like the ones in Figure 3.14.

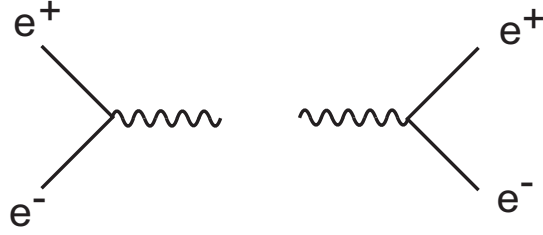


Figure 3.12: Feynman diagrams describing annihilation of an electron with a positron (left), and pair production (right), respectively.

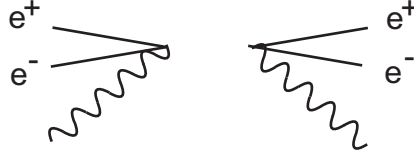


Figure 3.13: Feynman diagrams describing the annihilation of an electron, a positron and a photon resulting in vacuum (left) and created from vacuum (right), respectively.

In the upper process the  $e^+e^-$ -pair annihilates into a photon, which then creates an  $e^+e^-$ -pair. In the lower process the  $e^+e^-$ -pair is first created out of vacuum together with the photon, which then is annihilated with the  $e^+e^-$ -pair.

$$1) E_n - E_i = E_\gamma - (E_1 + E_2) = E_\gamma - \epsilon$$

$$\epsilon = E_1 + E_2 \quad (\text{the energy the photon would have had if energy was conserved})$$

$$2) E'_n - E_i = E_1 + E_2 + E_\gamma + E'_1 + E'_2 - (E_1 + E_2)$$

but  $E_1 = E_2 = E'_1 = E'_2$ ; in the centre-of-mass system

$$\text{and } \epsilon = E_1 + E_2 = E'_1 + E'_2$$

$$\Rightarrow E'_n - E_i = 2\epsilon + E_\gamma - \epsilon = E_\gamma + \epsilon$$

Again we can not distinguish between the two diagrams. We therefore have to add their amplitudes and square to get the probability for this process to happen.

$$\frac{d\sigma}{d\Omega} \sim \left| \frac{e^2}{E_n - E_i} + \frac{e^2}{E_{n'} - E_i} \right|^2 = e^4 \left| \frac{1}{E_n - E_i} + \frac{1}{E_{n'} - E_i} \right|^2 = e^4 \left| \frac{1}{E_\gamma - \epsilon} + \frac{1}{E_\gamma + \epsilon} \right|^2 = e^4 \left| \frac{E_\gamma + \epsilon + E_\gamma - \epsilon}{(E_\gamma - \epsilon)(E_\gamma + \epsilon)} \right|^2 = e^4 \left| \frac{2E_\gamma}{E_\gamma^2 - \epsilon^2} \right|^2$$

$$\text{but } E_\gamma^2 = |\vec{q}|^2 + m_\gamma^2$$

$$\Rightarrow \frac{d\sigma}{d\Omega} \sim e^4 \left( \frac{1}{(|\vec{q}|^2 - \epsilon^2 + m_\gamma^2)} \right)^2$$

Now  $q^2 = \epsilon^2 - |\vec{q}|^2$  where  $q$  is the four momentum of the photon

$$\text{with } q^2 = p_1^2 + p_2^2, \quad p_1^2 = E_1^2 - |\vec{p}_1|^2, \quad p_2^2 = E_2^2 - |\vec{p}_2|^2$$

$$\Rightarrow \frac{d\sigma}{d\Omega} \sim e^4 \left( \frac{1}{(\epsilon^2 - q^2 - \epsilon^2 + m_\gamma^2)} \right)^2$$

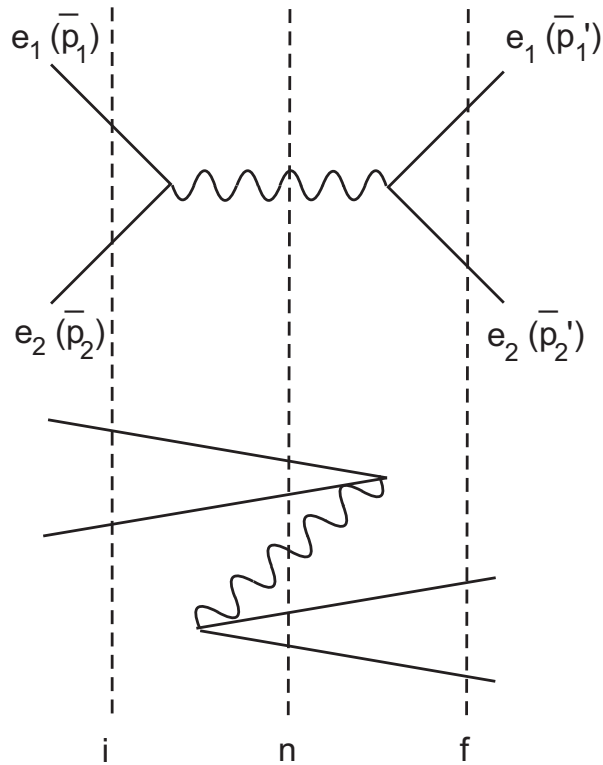


Figure 3.14: *Feynman diagrams describing the annihilation of an electron with a positron followed by pair production.*

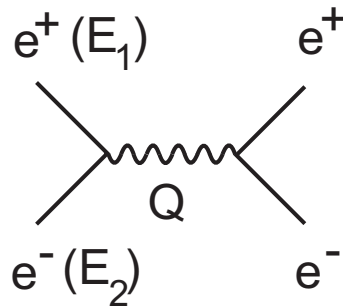


Figure 3.15: *The generic Feynman diagram describing the time-like contribution to the annihilation-pair production process.*

$$\sim e^4 \left( \frac{1}{(m_\gamma^2 - q^2)} \right)^2$$

The sum of the two contributing diagrams are by convention drawn as the generic diagram shown in Figure 3.15.

which is the *time like contribution*, where  $Q$  is the four-momentum of the exchanged particle.

However, we have also additional diagrams to the total  $e^+e^- \rightarrow e^+e^-$  process, which is the *spacelike contribution*, where  $P$  is the four-momentum of the exchanged particle, as shown in Figure 3.16.

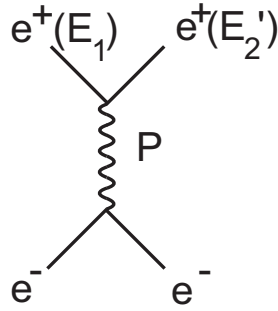


Figure 3.16: *The generic Feynman diagram describing the space-like contribution to the annihilation-pair production process.*

The total cross section then becomes  $\frac{d\sigma}{d\Omega} \sim \left| \frac{e^2}{-Q^2} + \frac{e^2}{-P^2} \right|^2$

### 3.2.9 Compton Scattering

Compton scattering is the scattering of a photon against a charged particle e.g. an electron. The process is illustrated in Figure 3.17.

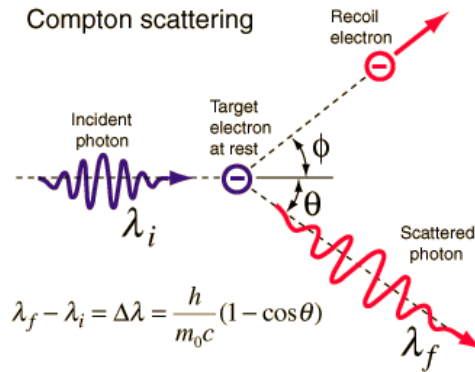


Figure 3.17: *Schematic description of Compton scattering.*

The corresponding Feynman diagrams, for the space-like exchange of a virtual electron, are the given in Figure 3.18.

- 1)  $E_n - E_i = K + Q + K' - (K + P) = Q + (K' - P)$
- 2)  $E_n - E_i = P' + Q + P - (P + K) = Q + (P' - K)$

where  $K$  and  $K'$  are the energies of the incoming and outgoing photon, respectively, and  $P$  and  $P'$  are the energies of the incoming and outgoing electron, respectively.

Similar to the case of electron-electron scattering  $\Rightarrow \frac{d\sigma}{d\Omega} \sim \frac{e^4}{(m_e^2 - Q^2)^2}$ ;  $Q^2 = (K' - P)^2 = (P' - K)^2$

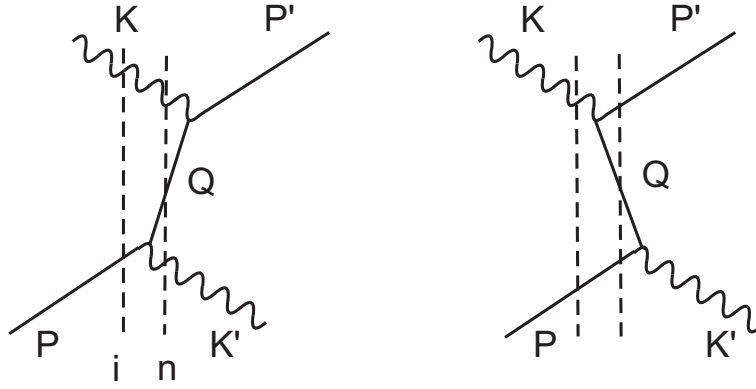


Figure 3.18: Feynman diagrams describing the space-like contributions to Compton scattering.

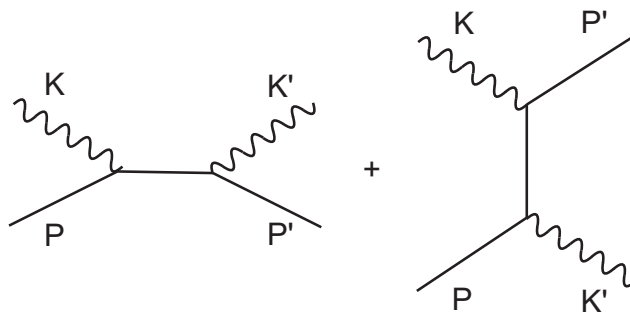


Figure 3.19: The generic Feynman diagrams describing the time-like (left) and space-like (right) contributions to Compton scattering.

As before there is also a time-like contribution to the total cross section, which becomes the sum of the diagrams shown in Figure 3.19.

$$\frac{d\sigma}{d\Omega} \sim \left| \frac{e^2}{m_e^2 - (K+P)^2} + \frac{e^2}{m_e^2 - (K'-P)^2} \right|^2$$

### 3.3 Weak Interaction

As the name indicates, the effects of the weak interactions are very weak and it was also found that its range is very short. Actually Enrico Fermi assumed that the interaction took place in a single point and described the  $\beta$ -decay with the diagram shown in Figure 3.20.

The Fermi theory was successful in describing essentially all experimental data at low energies but it gave unacceptable predictions for high energy weak interactions. For example the theory predicted that the cross section for neutrino-electron scattering should rise linearly with the energy of the incoming neutrino ( $\sigma \sim E_\nu$ ). This was in clear contradiction with observations from cosmic ray experiments.

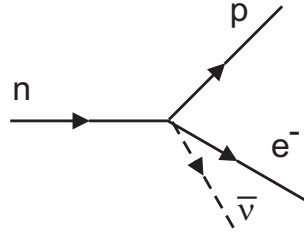


Figure 3.20: Beta decay described as a point interaction by Enrico Fermi.

In order to circumvent this problem and to get a description of the weak interaction similar to that of the electromagnetic force it was necessary to give up the four-fermion point like interaction and replace it with a particle exchange mechanism. The force mediating particle has to be very massive to be compatible with the short range of the force. They have to come in three varieties of two charged mediators, the  $W^+$  and  $W^-$  particles and one neutral, the  $Z^0$  particle. Consider a particle  $A$  at rest emitting a force mediator  $X$ , as illustrated in Figure 3.21.

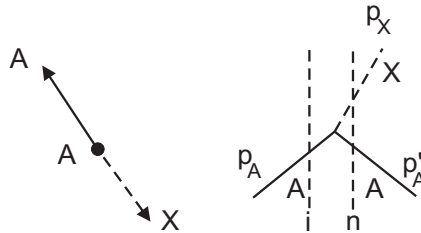


Figure 3.21: A particle 'A' emitting a force mediating particle 'X' in the centre-of-mass system (left), and versus time (right), respectively.

The initial state:  $p_A = (m_A, 0)$

The final state:  $p'_A = (E'_A, \vec{p}'_A)$ ,  $E'^2_A = \vec{p}'^2_A + m^2_A$

$p_X = (E_X, \vec{p}_X)$ ,  $E^2_X = \vec{p}_X^2 + m^2_X$

but  $\vec{p}'_A = -\vec{p}_X$  (momentum conservation)

$\Delta E = E_n - E_i = E'_A + E_X - m_A$

If  $|\vec{p}'_A| = |\vec{p}_X| \rightarrow 0 \Rightarrow E'_A \approx m_A$  and  $E_X \approx m_X$

$\Rightarrow \Delta E \rightarrow m_X$

Heisenberg:  $\Delta t \sim \frac{\hbar}{\Delta E}$

but  $\Delta t = R/c$  where  $R$  is the range of  $X$ .

$$\Rightarrow R \approx \frac{\hbar c}{m_X} \quad (3.1)$$

The coupling of the  $W$  and  $Z$  particles to quarks and leptons would give the amplitude,  $A$ :

$$A = \frac{g_w^2}{-q^2 + M_{W,Z}^2} \quad \text{cf.} \quad A = \frac{e^2}{-q^2} \quad \text{for e.m. interaction.}$$

where  $g_w$  can be regarded as the *weak charge*, defined as  $g_w = \sqrt{4\pi\alpha_w}$ , where  $\alpha_w$  is the weak coupling strength (equivalently to the definition of  $g_e$  as the fundamental unit of electric charge).

At low  $q^2$  ( $q^2 \ll M_{W,Z}^2$ ) the amplitude is independent of  $q^2$  and the Fermi description is valid. The Fermi coupling constant,  $G_F$ , is

$$\frac{G_F}{(\hbar c)^3} = \frac{\sqrt{2}}{8} \left( \frac{g_w}{M_{W,Z} c^2} \right)^2 = 1.166 \cdot 10^{-5} \text{ GeV}^{-2} \quad \text{determined from the rate of } \beta\text{-decays.}$$

At the mass of the  $W$  and  $Z$ , the strength of the weak and electromagnetic forces is the same and consequently the coupling  $g_w$  to leptons and quarks should be the same as that of the photon, i.e.  $g_w = e$ , due to the unification (some numerical factors have been omitted).

$$\Rightarrow M_{W,Z} \sim \frac{e}{\sqrt{G_F}} \sim 80 \text{ GeV}$$

Using Equation 3.1 and the mass of  $m_X = m_W = 80 \text{ GeV}$

$$\Rightarrow R = \frac{200 \text{ MeV} \cdot \text{fm}}{80 \cdot 10^3 \text{ MeV}} \approx 2.5 \cdot 10^{-3} \text{ fm}, \text{ which is a typical range of the weak interaction.}$$

The weak interaction is thus mediated by massive weak vector bosons, the  $W^\pm$  and  $Z^0$  particles, which couple to both quarks and leptons. There is a strong similarity between the Feynman diagrams for electromagnetic interactions mediated by photon exchange and weak interactions mediated by the weak vector bosons. However, by emitting or absorbing a  $W$ -boson a quark with charge  $+2/3$  will be converted into a quark with charge  $-1/3$ , or vice versa. Also the leptons can be converted from a  $-1$  charge state into a zero charge state, or oppositely. Reactions where a  $W^\pm$ -boson is exchanged are called *charged current* processes.

By convention the weak propagators are drawn as broken lines in the Feynman diagrams, as shown for example in the diagrams of Figure 3.22, which illustrates *transitions within the first family* of quarks and leptons.

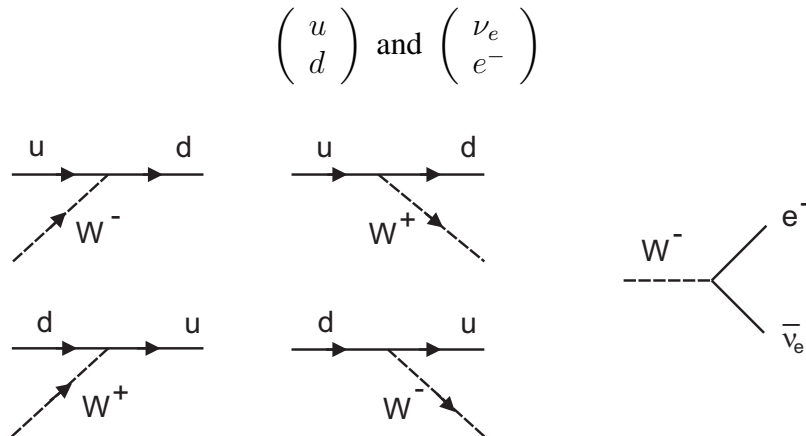


Figure 3.22: *Feynman diagrams describing quark transitions through the emission and absorption of a  $W$ -boson, respectively, as well as the decay of a  $W$ -boson into an electron and neutrino.*

The most well-known weak decay, which illustrates the transitions inside the first family, is the neutron decay ( $\beta$ -decay):  $n \rightarrow p + e^- + \bar{\nu}_e$ .



On the quark level it corresponds to the conversion of a  $d$ -quark into a  $u$ -quark.

$$udd \rightarrow uud + e^- + \bar{\nu}_e$$

The Feynman diagram describing the beta-decay is shown in Figure 3.23.

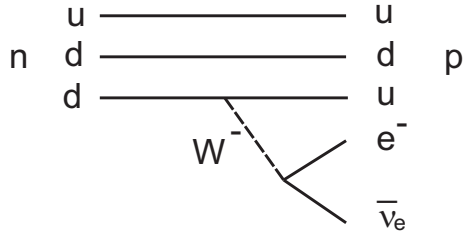


Figure 3.23: Feynman diagram describing the beta decay.

### 3.3.1 Some Other Examples of Weak Decays

$$K^0 \rightarrow \pi^+ + \pi^-$$

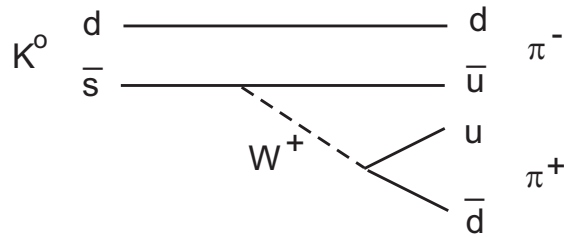


Figure 3.24: Feynman diagram describing a  $K^0$ -decay into  $\pi^+ \pi^-$ .

$$K^0 \rightarrow \bar{K}^0$$

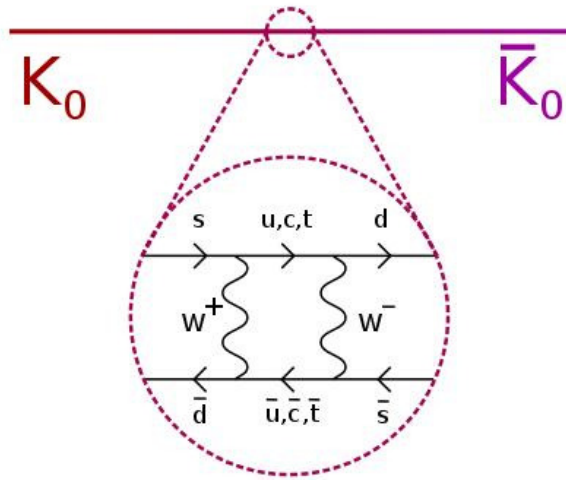


Figure 3.25: Feynman diagram describing  $K^0 - \bar{K}^0$  oscillation.

$$\Lambda^0 \rightarrow p + \pi^-$$

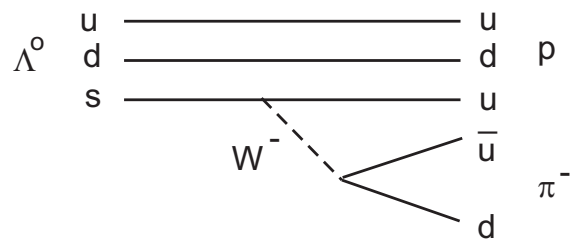


Figure 3.26: Feynman diagram describing the decay of a  $\Lambda^0$  into a proton and a  $\pi^-$ .

$$\mu^- \rightarrow e^- + \bar{\nu}_e + \nu_\mu$$

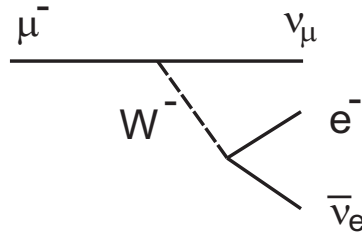


Figure 3.27: Feynman diagram describing a muon decay.

$$\pi^- \rightarrow \mu^- + \bar{\nu}_\mu$$

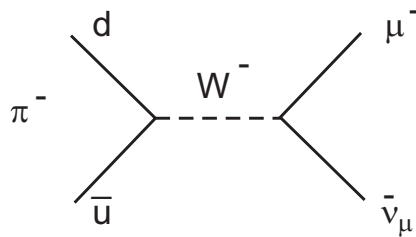


Figure 3.28: Feynman diagram describing a pion decay.

### 3.3.2 Properties of the Weak Force Mediators

The emission or absorption of a W-boson transfers a charged lepton into a neutrino or vice versa depending on the charge of the W-boson. It can also convert an up-type quark into a down-type or the other way around as summarized in Table 3.1.

Weak interactions take place between all quarks and leptons. By convention the weak coupling strength (or the weak charge) of  $W^\pm$  is set to  $\frac{g_w}{\sqrt{2}}$  (for simplicity we use  $g = g_w$  in the following). Similar to QED where the electromagnetic coupling strength  $-e$  gives the probability that an electron will emit a photon, does the weak coupling strength give the probability for a neutrino to emit a  $W^+$ -boson and become an electron, as indicated in Figure 3.29. The weak coupling strength of  $W^+$  and  $W^-$  is the same for all leptons and quarks.

If a neutrino should be able to remain a neutrino in weak interaction and not always be converted into a charged lepton a neutral weak boson would be needed, and the reaction would then accordingly be called *neutral current* interaction. In 1973 such processes were observed in bubble chamber experiments.

$$\nu_\mu + N \rightarrow \nu_\mu + X$$

$$\bar{\nu}_\mu + N \rightarrow \bar{\nu}_\mu + X$$

	absorption	emission
$e^- \rightarrow \nu_e$	$W^+$	$W^-$
$\nu_e \rightarrow e^-$	$W^-$	$W^+$
$u \rightarrow d$	$W^-$	$W^+$
$d \rightarrow u$	$W^+$	$W^-$

Table 3.1: The various weak lepton interactions

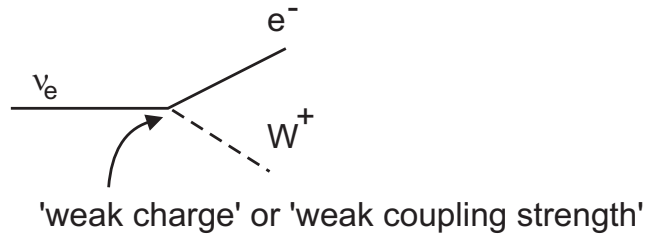


Figure 3.29: The vertex of a neutrino, electron and a W-boson.

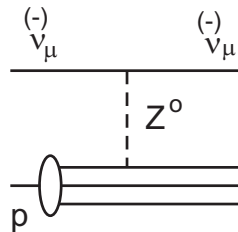


Figure 3.30: Feynman diagram describing the interaction of a neutrino (antineutrino) with a proton via the exchange of a  $Z^0$ -boson (neutral current interaction).

where  $N$  is a nucleon and  $X$  is one or more final state particles. The corresponding Feynman diagram would then look like the one in Figure 3.30.

The relative strength of the  $Z^0$ -coupling compared to the  $W$ -coupling can be estimated by comparing the occurrence of neutral and charged current processes, shown in Figure 3.31. The neutral current reactions turned out to occur on a rate which is in the same order as the charged current processes. This holds for both particles and anti-particles.

In 1983 the weak bosons were directly observed in collisions between protons and antiprotons at CERN. The particle beams had energies of 270 GeV each, which corresponds to a center-of-mass energy of  $\sqrt{s} = 2E = 540 \text{ GeV}$ . It should, however, be kept in mind that the effective collision is between a quark and an antiquark, which only carry a fraction of the proton momentum. Some examples of weak processes, leading to leptonic final states, in  $p\bar{p}$  collisions are shown in Figure 3.32.

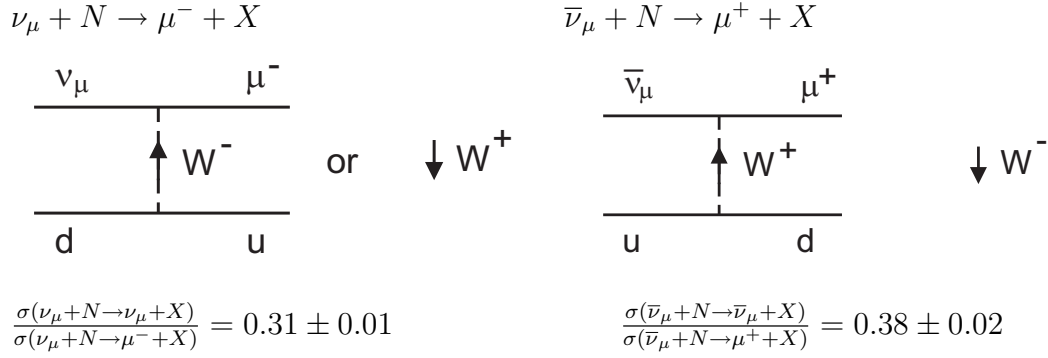


Figure 3.31: Feynman diagrams describing the interaction of a neutrino (left) and antineutrino (right) with quarks of the first generation through the exchange of a  $W$ -boson (charge current processes). Also shown are the ratios of the charge and neutral current interaction cross sections.

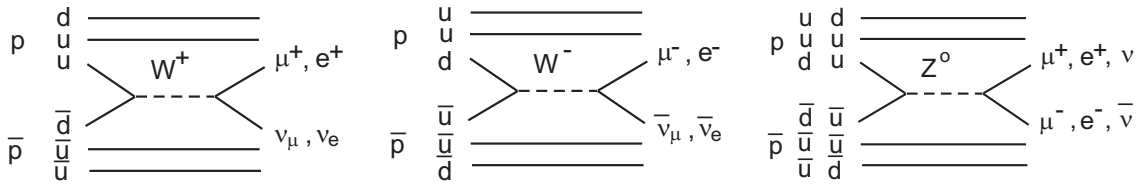


Figure 3.32: Feynman diagrams describing proton-proton interactions giving rise to the leptonic final states through which the existence of the  $W$ - and  $Z$ -bosons were experimentally proven.

### 3.3.3 The Electroweak Theory of Weinberg and Salam

The starting point of the electroweak theory was to introduce three massless particles,  $W^+$ ,  $W^-$  and  $W^0$ . However, the measured probability of neutral current processes did not agree with what was expected from theoretical calculations assuming the neutral partner  $W^0$  to the charged  $W$ -bosons. In order to solve this problem it was assumed that another field, the  $B$ -field, exists with a field particle called  $B$ . All leptons have the same probability to emit or absorb a  $B$ -particle. The couplings to  $W$  and  $B$  are proportional to  $g$  and  $g'$ , respectively.

Thus we have the following field particles:  $W^0$ ,  $W^+$ ,  $W^-$  and  $B$ , with the coupling strengths:

$$W^\pm \text{ to } \nu, e \quad \frac{g}{\sqrt{2}} \quad (3.2)$$

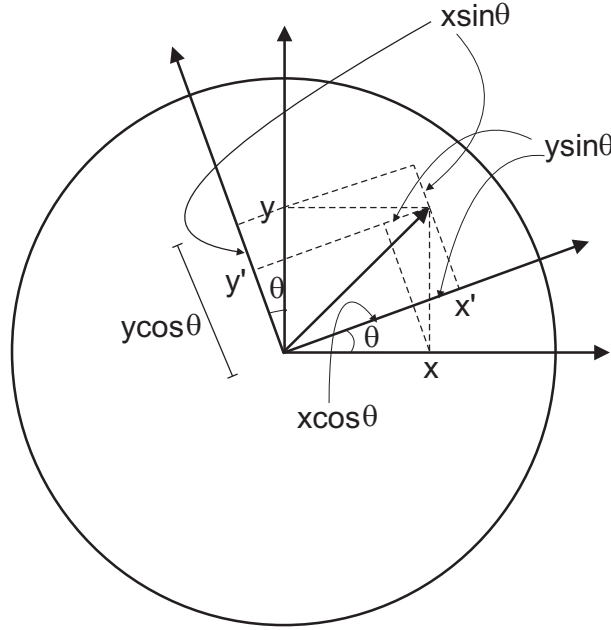
$$W^0 \text{ to } e \quad -\frac{g}{2} \quad (3.3)$$

$$W^0 \text{ to } \nu \quad \frac{g}{2} \quad (3.4)$$

$$B \text{ to } \nu, e \quad -\frac{g'}{2} \quad (3.5)$$

We realized earlier that an electron may emit and reabsorb photons continuously such that the electron at each moment is surrounded by a cloud of photons. In the same way an electron may emit and absorb both  $W^0$  and  $B$  particles, but since it is impossible to separate the two, the

interaction is given as the exchange of a mixture of the  $W^0$  and  $B$  particles. All interactions which involve a  $W^0$  exchange also involve a  $B$  exchange. Let us consider the representation of a vector in two coordinate systems which are rotated with respect to each other, as illustrated in Figure 3.33.



$$x' = x \cos\theta + y \sin\theta$$

$$y' = y \cos\theta - x \sin\theta$$

Figure 3.33: *The relation between the coordinates of two rotated coordinate systems.*

If we identify the  $x$  component with the  $B$ -particle and the  $y$  component with the  $W^0$ -particle, these particles will exist in combinations given by  $x'$  and  $y'$ , respectively. In the Weinberg-Salam theory it is assumed that the  $W^0$  and  $B$  particles are massless but via the so called Higgs-mechanism one combination of  $W^0$  and  $B$  will get mass, corresponding to the  $Z^0$  particle, whereas the other combination will remain massless, identical to the photon.

$$\gamma = \sin\theta_W \cdot W^0 + \cos\theta_W \cdot B \quad (3.6)$$

$$Z^0 = \cos\theta_W \cdot W^0 - \sin\theta_W \cdot B \quad (3.7)$$

The sinus and cosinus of the weak mixing angle (or the Weinberg angle)  $\theta_W$  define the mixing ratio since  $\sin^2\theta_W + \cos^2\theta_W = 1$ .

Using 3.2 - 3.5 gives

$$\nu \text{ to } \gamma \text{ coupling: } \sin\theta_W \cdot \frac{g}{2} + \cos\theta_W \cdot \left(-\frac{g'}{2}\right) = \frac{1}{2}(g \sin\theta_W - g' \cos\theta_W)$$

$$\nu \text{ to } Z^0 \text{ coupling: } \frac{1}{2}(g \cos\theta_W + g' \sin\theta_W)$$

$$e \text{ to } \gamma \text{ coupling: } \frac{1}{2}(-g \sin\theta_W - g' \cos\theta_W)$$

$e$  to  $Z^0$  coupling:  $\frac{1}{2}(-g \cos \theta_W + g' \sin \theta_W)$

1) but a neutrino does not couple to a photon  $\Rightarrow$  the coupling = 0

$$\frac{1}{2}(g \sin \theta_W - g' \cos \theta_W) = 0$$

$$\Rightarrow g \sin \theta_W = g' \cos \theta_W$$

$$\frac{g'}{g} = \frac{\sin \theta_W}{\cos \theta_W} = \tan \theta_W$$

2) The strength of the  $e$  to  $\gamma$  coupling is  $-e$

$$\Rightarrow \frac{1}{2}(-g \sin \theta_W - g' \cos \theta_W) = -e$$

$$\Rightarrow e = \frac{1}{2}(g \sin \theta_W + g' \cos \theta_W)$$

but since  $g \sin \theta_W = g' \cos \theta_W$  we get:

$$e = g \sin \theta_W = g' \cos \theta_W$$

$$\Rightarrow \boxed{g = \frac{e}{\sin \theta_W}} \quad \text{and} \quad \boxed{g' = \frac{e}{\cos \theta_W}}$$

3) Insertion into the expression for the  $\nu$  to  $Z^0$  coupling gives:

$$\frac{1}{2}(g \cos \theta_W + g' \sin \theta_W) = \frac{1}{2}\left(\frac{e}{\sin \theta_W} \cdot \cos \theta_W + \frac{e}{\cos \theta_W} \cdot \sin \theta_W\right) = \frac{e}{2}(\cot \theta_W + \tan \theta_W)$$

4) and for the  $e$  to  $Z^0$  coupling we get:

$$\frac{1}{2}(-g \cos \theta_W + g' \sin \theta_W) = \frac{1}{2}\left(-\frac{e}{\sin \theta_W} \cdot \cos \theta_W + \frac{e}{\cos \theta_W} \cdot \sin \theta_W\right) = \frac{e}{2}(-\cot \theta_W + \tan \theta_W)$$

5) The  $W^\pm$  coupling is  $\frac{g}{\sqrt{2}}$

but since  $g \sin \theta_W = e \Rightarrow \frac{g}{\sqrt{2}} \sin \theta_W = \frac{e}{\sqrt{2}}$  we get for the  $W^\pm$  coupling:

$$\boxed{\frac{g}{\sqrt{2}} = \frac{e}{\sqrt{2} \sin \theta_W}}$$

### 3.3.4 The Higgs Mechanism

The theory is only consistent if the weak bosons are assumed to be massless. However, experimental results show that  $W^\pm$  and  $Z^0$  are massive whereas the photon is massless. In order to solve this problem the Higgs mechanism has been introduced. How can the Higgs mechanism be understood?

Consider a photon that travels in a gas of some density. The speed of this photon is given by  $v = c/n$  where  $c$  is the speed of light in vacuum and  $n$  is the refractive index of the gas. Thus,

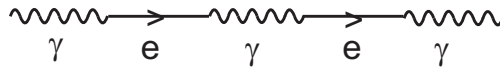


Figure 3.34: *The passage of a photon through a gas and its absorption and re-emission by the electrons of the gas.*

if  $n$  is greater than unity the photon travels slower than in vacuum. This can be understood by the fact that the photons continuously are absorbed and re-emitted by the electrons of the gas, as illustrated in Figure 3.34. This is slowing down the velocity of the photons and gives the impression that they move like particles with mass would do in vacuum.

In order to illustrate how the  $W$  and  $Z$  particles get their masses we may in analogy with the case of the photon assume that vacuum contains some 'weak' medium consisting of spinless neutrino-like particles  $N$ , electronlike particles  $E$ , and their antiparticles  $\bar{N}$  and  $\bar{E}$ . When a  $W^-$  particle moves through this medium it might be absorbed by an  $N$  particle. The  $N$  particle then converts into an electron-like particles  $E$ , which after a while re-emits a  $W^-$  and is re-converted into an  $N$  according to Figure 3.35.

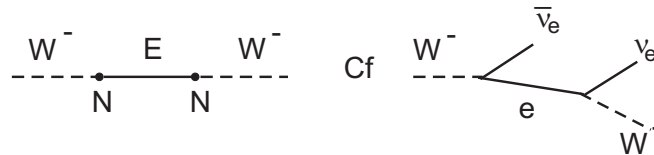


Figure 3.35: *The passage of a  $W^-$ -boson through a weak medium, containing neutrino-like  $N$ -particles. The interaction between these converts the  $N$ -particle into an electron-like  $E$ -particle, which in a subsequent interaction with an  $N$ -particle recreates a  $W$ -boson. A comparison with the normal interaction between a  $W$ -boson and a neutrino particle is shown in the right hand picture.*

The corresponding diagram for a  $W^+$  is shown in Figure 3.36.

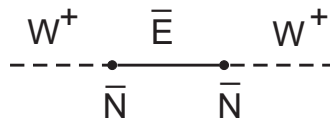


Figure 3.36: *The passage of a  $W^+$ -boson through a weak medium, containing antineutrino-like  $\bar{N}$ -particles. The interaction between these converts the  $\bar{N}$ -particle into an positron-like  $\bar{E}$ -particle, which in a subsequent interaction with an  $\bar{N}$ -particle recreates a  $W^+$ -boson.*

The originally massless  $W^\pm$  particles get their masses through the interaction with the 'weak' medium such that the mass is related to the probability for being absorbed and the number of absorbing particles in the medium. The coupling  $W^\pm$  to  $N$  is  $g_w = \frac{g}{\sqrt{2}}$  (in analogy with the  $W^\pm$  to  $\nu$  coupling) and if we assume that  $\kappa$  is a constant related to the density of  $N$  particles we get:

$$m_{W^\pm}^2 = \kappa \cdot \frac{g^2}{2}$$



Also the  $W^0$  and  $B$  particles may be absorbed by the  $N$  particles, which will remain an  $N$  particle before it re-emits a  $W^0$  or  $B$ , as shown in Figure 3.37. At this point the  $N$  particle will not remember by which kind of particle it was absorbed and the probability for sending out a  $W^0$  or  $B$  is given by the coupling strengths:

$$\begin{array}{ll} BN & (B\nu) : -\frac{g'}{2} \\ W^0N & (W^0\nu) : \frac{g}{2} \end{array}$$

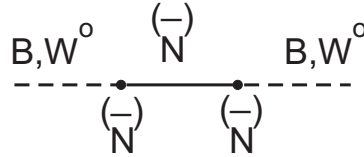


Figure 3.37: The passage of the hypothetical  $B$ - and  $W^0$ -particles through a weak medium interacting with  $N$ - and  $\bar{N}$ -particles.

The emissions are therefore in a mixture, which are related to the coupling strengths according to:

$$\frac{g}{2} \cdot W^0 - \frac{g'}{2} \cdot B ,$$

but  $g \sin \theta_W = g' \cos \theta_W$  .

We have  $g^2 = g^2(\sin^2 \theta_W + \cos^2 \theta_W) = g^2 \sin^2 \theta_W + g^2 \cos^2 \theta_W = g'^2 \cos^2 \theta_W + g^2 \cos^2 \theta_W =$   
 $= \cos^2 \theta_W (g'^2 + g^2)$

$$\Rightarrow g = \sqrt{g^2 + g'^2} \cdot \cos \theta_W$$

In the same way we get:  $g' = \sqrt{g^2 + g'^2} \cdot \sin \theta_W$

$$\begin{aligned} \Rightarrow \frac{g}{2} \cdot W^0 - \frac{g'}{2} \cdot B &= \frac{1}{2} \sqrt{g^2 + g'^2} (\cos \theta_W \cdot W^0 - \sin \theta_W \cdot B) = \\ &= \frac{\sqrt{g^2 + g'^2}}{2} \cdot Z^0 \end{aligned}$$

Thus, independent of whether a  $W^0$  or a  $B$  particle was absorbed the emitted state is a mixed state which corresponds to the  $Z^0$  particle. This is even true if the absorbed is not a pure  $W^0$  or  $B$  but a mixture of them, like the  $Z^0$  particle. So an incoming  $Z^0$  particle will be absorbed by an  $N$  or an  $\bar{N}$  and re-emitted in a similar way as the  $W^\pm$  particles, according to the diagrams of Figure 3.38.

The coupling of the  $Z^0$  particle to the  $N(\bar{N})$  particles is the same as the coupling to  $\nu(\bar{\nu})$ .

With  $Z^0 = W^0 \cos \theta_W - B \sin \theta_W$

and the couplings:

$$\begin{array}{ll} BN & (B\nu) : -\frac{g'}{2} \\ W^0N & (W^0\nu) : \frac{g}{2} , \end{array}$$

the coupling of the  $Z^0$  particle to the  $N(\bar{N})$  particles is given by:

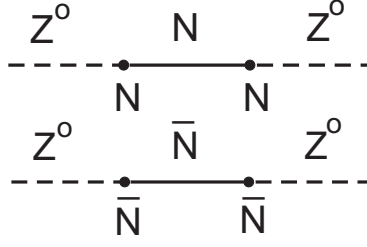


Figure 3.38: The passage of a  $Z^0$ -boson through a weak medium, containing neutrino-like  $N$ - and  $\bar{N}$ -particles. The  $Z$ -boson is absorbed by either an  $N$ - or an  $\bar{N}$ -particle and subsequently re-emitted.

$$\begin{aligned} \frac{g}{2} \cos \theta_W + \frac{g'}{2} \sin \theta_W &= \\ &= \frac{1}{2}(g \cos \theta_W + g' \sin \theta_W), \quad \text{which is the same as the } Z^0 \text{ to } \nu \text{ coupling.} \end{aligned}$$

The mass of the  $Z^0$  particle is related to the probability for absorption in the same way as for the  $W$  particles. However, since the  $Z^0$  particle can also couple to  $\bar{N}$  particles we get an additional factor 2.

$$\begin{aligned} \Rightarrow m_{Z^0}^2 &= \frac{2\kappa}{4}(g \cos \theta_W + g' \sin \theta_W)^2 = \\ &= \frac{\kappa}{2}(g \cos \theta_W + g \frac{\sin \theta_W}{\cos \theta_W} \sin \theta_W)^2, \quad \text{since } g' = g \cdot \frac{\sin \theta_W}{\cos \theta_W} \\ \Rightarrow m_{Z^0}^2 &= \frac{\kappa}{2} \left[ \frac{g}{\cos \theta_W} (\cos^2 \theta_W + \sin^2 \theta_W) \right]^2 \\ \Rightarrow \boxed{m_{Z^0}^2} &= \frac{\kappa}{2} \cdot \frac{g^2}{\cos^2 \theta_W} \end{aligned}$$

$$\text{From above we have } m_W^2 = \kappa \frac{g^2}{2} \Rightarrow \kappa = \frac{2m_W^2}{g^2}$$

$$\Rightarrow m_{Z^0}^2 = \frac{2m_W^2}{2g^2} \cdot \frac{g^2}{\cos^2 \theta_W} = \frac{m_W^2}{\cos^2 \theta_W}$$

$$\Rightarrow \boxed{m_{Z^0} = \frac{m_W}{\cos \theta_W}} \quad (3.8)$$

We have already used the relation between the Fermi coupling and the mass of the  $W$ -particle in order to estimate the mass of the  $W$  particle.

$$m_W \sim \frac{g_w}{\sqrt{G_F}}, \quad g_w = \frac{g}{\sqrt{2}} = \frac{e}{\sqrt{2} \sin \theta_W}$$

If we introduce the numerical constants we get:

$$m_W = \sqrt{\frac{\sqrt{2}e^2(\hbar c)^3}{8G_F \sin^2 \theta_W}} = \frac{37.4}{\sin^2 \theta_W}$$

If we insert the value of  $m_W = 80 \text{ GeV}$ , we get  $\theta_W \approx 28^\circ$

This is consistent with the experimental value  $\theta_W \approx 29^\circ$

$$\sin \theta_W = 0.485$$

$$\cos \theta_W = 0.875$$

$$\tan \theta_W = 0.55$$

If we now introduce the value of  $m_W = 80 \text{ GeV}$  and  $\theta_W = 29^\circ$  into 3.8 we get  $m_{Z^0} = 91 \text{ GeV}$ , which agrees with the experimentally measured value of the  $Z^0$  mass..

The photon can not couple to the  $N(\bar{N})$  particles, consistent with the fact that they don't couple to neutrino particles. It means that the contributions from the  $W^0$  and  $B$  particles in the photon mixture compensate each other completely and the photon will not be absorbed by the  $N$  particles.

$$\text{With } \gamma = W^0 \sin \theta_W + B \cos \theta_W$$

and the couplings:

$$\begin{array}{ll} BN & (B\nu) : -\frac{g'}{2} \\ W^0 N & (W^0\nu) : \frac{g}{2} \end{array} ,$$

the coupling of the  $\gamma$  particle to the  $N(\bar{N})$  particles is given by:

$$\frac{g}{2} \sin \theta_W - \frac{g'}{2} \cos \theta_W = \frac{g}{2} (\sin \theta_W - \frac{\sin \theta_W}{\cos \theta_W} \cos \theta_W) = 0 \quad \text{since} \quad g' = g \frac{\sin \theta_W}{\cos \theta_W}$$

Thus, the photons can move freely through the 'weak' medium with the speed of light which corresponds to zero mass.

However, no  $N$  or  $E$  particles have been observed. The solution to this problem can be found in an analogy with the properties of the photon. In vacuum a photon can have two polarization states which can be represented with two polarization vectors transverse to the direction of motion. If we have a medium containing electrons and protons also longitudinal wave motions are created, caused by the mutual movements of the electrons and protons. These movements corresponds to fluctuations in time of the charge density  $\rho^+ - \rho^-$ , where  $\rho^+$  and  $\rho^-$  are the densities of positive and negative charges, respectively. Variations in the total density of particles,  $\rho^+ + \rho^-$  create pressure waves, also called *phonons*.

If an electron travels through this medium it will cause a disturbance of the the charge structure and create waves in the densities  $\rho^+ - \rho^-$  and  $\rho^+ + \rho^-$ , which propagate through the medium independently of each other and with different velocities.

⇒ The  $\rho^+ - \rho^-$  wave motion corresponds to longitudinal electromagnetic oscillations and can be identified with a longitudinally polarized photon.

⇒ Photons with mass (virtual photons) can be longitudinally polarized.

⇒ The  $\rho^+ + \rho^-$  wave motion can be identified with phonons.

The 'weak' medium contains four components  $N, \bar{N}, E$  and  $\bar{E}$ . The density variation of three of these combinations correspond to longitudinal polarization states of  $W^+, W^-$  and  $Z^0$ . Variations of the fourth combination correspond to variations in the total density of all four components. These create pressure waves in the weak medium, which can be identified with the Higgs particle.

Since  $W^\pm$  and  $Z^0$  are massive particles they can be longitudinally polarized.

The number of degrees of freedom are:

1) In the electroweak theory

Massless $W^+, W^-, W^0, B$ $\otimes$ 2 polarization states	$4 \otimes 2 = 8$
$N, \bar{N}, E, \bar{E}$	4
$\Sigma$	12

2) Experimentally

Massive $W^+, W^-, Z^0$ $\otimes$ 3 polarization states	$3 \otimes 3 = 9$
Massless $\gamma$ , $\otimes$ 2 polarization states	$1 \otimes 2 = 2$
$\Sigma$	11

The remaining degree of freedom corresponds to the Higgs particle.

Also other particles like quarks and leptons get their masses through the Higgs mechanism.

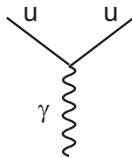
### 3.3.5 Electroweak Interaction With Quarks

$W$ -particles ( $W^+, W^-$  and  $W^0$ ) couple in the same way to left-handed quarks and leptons or their right-handed antiparticles. All couplings of the  $W$ -particles to right-handed particles or left-handed antiparticles are *zero*.

$W^\pm$ to quarks	$=$	$W^\pm$ to leptons	$\frac{g}{\sqrt{2}}$
$W^0$ to $u, c, t$	$=$	$W^0$ to $\nu$ 's	$\frac{g}{2}$
$W^0$ to $d, s, b$	$=$	$W^0$ to $e, \mu, \tau$	$-\frac{g}{2}$
		$B$ to leptons	$-\frac{g'}{2}$
$B$ to quarks			$\frac{g'}{6}$

*Couplings to left-handed particles (right-handed antiparticles)*

$u_L$  to  $\gamma$  coupling

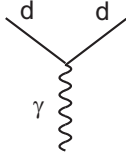


$$\gamma = W^0 \sin \theta_W + B \cos \theta_W \quad \Rightarrow \quad u_L \text{ to } \gamma \text{ coupling: } \frac{g}{2} \sin \theta_W + \frac{g'}{6} \cos \theta_W$$

$$\text{but } g = \frac{e}{\sin \theta_W} \text{ and } g' = \frac{e}{\cos \theta_W}$$

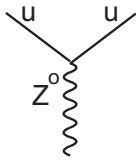
$$\Rightarrow \gamma \text{ to } u_L \text{ coupling: } e\left(\frac{1}{2} + \frac{1}{6}\right) = e \cdot \frac{2}{3}$$

$d_L$  to  $\gamma$  coupling



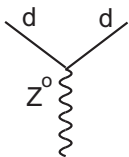
$$\begin{aligned} \gamma &= W^0 \sin \theta_W + B \cos \theta_W \quad \Rightarrow \quad d_L \text{ to } \gamma \text{ coupling: } -\frac{g}{2} \sin \theta_W + \frac{g'}{6} \cos \theta_W \\ &= e\left(-\frac{1}{2} + \frac{1}{6}\right) = e \cdot -\frac{1}{3} \end{aligned}$$

$u_L$  to  $Z^0$  coupling



$$\begin{aligned} Z^0 &= W^0 \cos \theta_W - B \sin \theta_W \quad \Rightarrow \quad u_L \text{ to } Z^0 \text{ coupling: } \frac{g}{2} \cos \theta_W - \frac{g'}{6} \sin \theta_W \\ &= \frac{e}{2} \left( \frac{\cos \theta_W}{\sin \theta_W} - \frac{1}{3} \frac{\sin \theta_W}{\cos \theta_W} \right) = -\frac{e}{2} \left( \frac{1}{3} \tan \theta_W - \cot \theta_W \right) \end{aligned}$$

$d_L$  to  $Z^0$  coupling



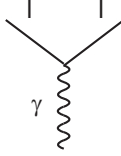
$$\begin{aligned} Z^0 &= W^0 \cos \theta_W - B \sin \theta_W \quad \Rightarrow \quad d_L \text{ to } Z^0 \text{ coupling: } -\frac{g}{2} \cos \theta_W - \frac{g'}{6} \sin \theta_W \\ &= -\frac{e}{2} \left( \frac{\cos \theta_W}{\sin \theta_W} + \frac{1}{3} \frac{\sin \theta_W}{\cos \theta_W} \right) = -\frac{e}{2} \left( \frac{1}{3} \tan \theta_W + \cot \theta_W \right) \end{aligned}$$

*Coupling to right handed particles (left-handed antiparticles)*

No right-handed  $\nu$ 's exist.

$W^\pm, W^0$ to $q_R$	$=$	$W^\pm, W^0$ to $l_R$	$0$
$B$ to $u_R, c_R, t_R$		$B$ to $l_R$	$-g'$
$B$ to $d_R, s_R, b_R$			$\frac{2}{3}g'$
			$-\frac{1}{3}g'$

$l_R$  to  $\gamma$  coupling



$$\gamma = W^0 \sin \theta_W + B \cos \theta_W$$

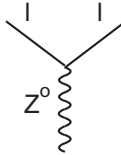
but the  $W^0$  to  $l_R$  coupling is 0.

$$\Rightarrow \gamma = B \cos \theta_W \quad \Rightarrow \quad l_R \text{ to } \gamma \text{ coupling: } -g' \cos \theta_W$$

$$\text{but } g' = \frac{e}{\cos \theta_W}$$

$$\Rightarrow \gamma \text{ to } l_R \text{ coupling: } -e$$

$l_R$  to  $Z^0$  coupling



$$Z^0 = W^0 \cos \theta_W - B \sin \theta_W$$

but as before the  $W^0$  to  $l_R$  coupling is 0.

$$\Rightarrow Z^0 = -B \sin \theta_W \quad \Rightarrow \quad l_R \text{ to } Z^0 \text{ coupling: } g' \sin \theta_W = e \frac{\sin \theta_W}{\cos \theta_W} = e \tan \theta_W$$

$u_R$  to  $\gamma$  coupling

$$\gamma = B \cos \theta_W \quad \Rightarrow \quad u_R \text{ to } \gamma \text{ coupling: } \frac{2}{3}g' \cos \theta_W = \frac{2e \cos \theta_W}{3 \cos \theta_W} = \frac{2e}{3}$$

$u_R$  to  $Z^0$  coupling

$$Z^0 = -B \sin \theta_W \quad \Rightarrow \quad u_R \text{ to } Z^0 \text{ coupling: } -\frac{2}{3}g' \sin \theta_W = -\frac{2e \sin \theta_W}{3 \cos \theta_W} = -\frac{2e}{3} \tan \theta_W$$

$d_R$  to  $\gamma$  coupling

$$\gamma = B \cos \theta_W \quad \Rightarrow \quad d_R \text{ to } \gamma \text{ coupling: } -1/3g' \cos \theta_W = -\frac{1}{3}e \frac{\cos \theta_W}{\cos \theta_W} = -\frac{1}{3}e$$

$d_R$  to  $Z^0$  coupling

$$Z^0 = -B \sin \theta_W \quad \Rightarrow \quad d_R \text{ to } Z^0 \text{ coupling: } -(-\frac{1}{3}g' \sin \theta_W) = \frac{1}{3}e \frac{\sin \theta_W}{\cos \theta_W} = \frac{1}{3}e \tan \theta_W$$

### 3.3.6 Quark Mixing

We have seen that the emission or absorption of a charged W-boson will change the flavour of a quark. For example a  $d$ -quark is converted into a  $u$ -quark in the  $\beta$ -decay. The  $s$ -quark was introduced to explain the observation of so called 'V'-particles in 1953. The particles known at that time could be explained by the families of leptons and quarks, shown in Table 3.2.

flavour	charge	spin
$\nu_e \quad \nu_\mu$	0	1/2
$e \quad \mu$	-1	1/2
$u$	2/3	1/2
$d \quad s$	-1/3	1/2

Table 3.2: *Quarks and leptons needed to explain all known particles after the discovery of 'V'-particles*

The 'V'-particles were later identified as the decays of the  $K^0$  and  $\Lambda^0$  particles in the decay modes:

$$K^0 \rightarrow \pi^+ + \pi^-$$

$$\Lambda^0 \rightarrow \pi^- + p$$

where  $K^0$  contains an  $\bar{s}$ -quark and  $\Lambda^0$  an  $s$ -quark, whereas the final state particles, the proton and the pions, do not carry any strangeness. This means that an  $s(\bar{s})$ -quark has been converted into a  $u(\bar{u})$ -quark by the emission of a  $W^-$  ( $W^+$ ). Thus, transitions are not only possible within a specific quark family but also between the families, as illustrated in Figure 3.39. Instead of introducing new couplings to accommodate such decays, a modification of the quark doublets were made. It was assumed that the charged  $W$ 's couple to a mixture of quark states ('rotated' quark states). Compare with the representation of a vector in two coordinate systems that are rotated with respect to each other, shown in Figure 3.40.

Assume that  $x$  and  $y$  represent the *mass (flavour) eigenstates*  $d$  and  $s$ , respectively, whereas  $x'$  and  $y'$  correspond to *weak (mixed) states*  $d'$  and  $s'$ . Then we get:

$$d' = d \cos \theta_C + s \sin \theta_C$$

$$s' = -d \sin \theta_C + s \cos \theta_C$$

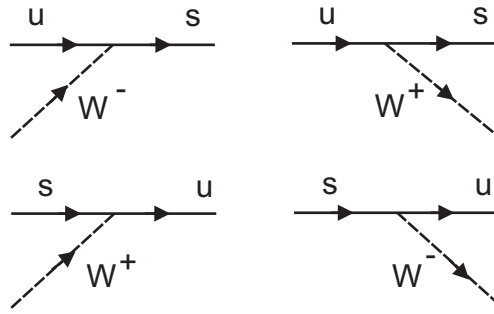
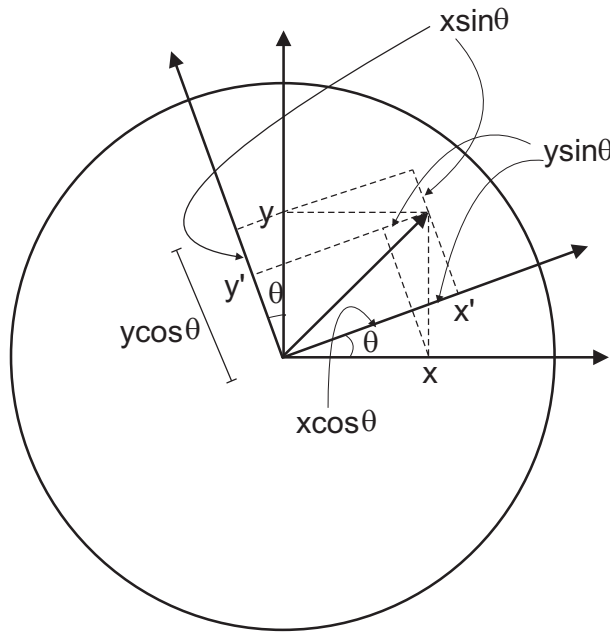


Figure 3.39: Transitions between  $u$ - and  $s$ -quarks through the emission and absorption, respectively, of a  $W$ -boson.



$$x' = x \cos \theta + y \sin \theta$$

$$y' = y \cos \theta - x \sin \theta$$

Figure 3.40: The relation between the coordinates of two rotated coordinate systems.

where  $\theta_C$  is called the quark mixing angle or the Cabibbo angle, named after the Italian physicist Nicola Cabibbo. The mixing angle is not given by the theory but has to be determined by experiments.

The fact that only the charge  $-1/3$  quarks occur in mixed states and not the charge  $+2/3$  quarks is just by convention.

We now have a so called 'Cabibbo favoured' transition, with the coupling strength  $g_W \cos \theta_C$  (where  $g_W = g/\sqrt{2}$ ), and a 'Cabibbo unfavoured' transition, with the coupling strength  $g_W \sin \theta_C$ . This is illustrated in Figure 3.41.



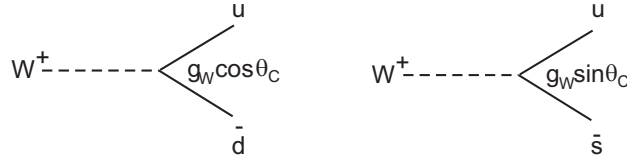


Figure 3.41: *Cabibbo favoured and Cabibbo unfavoured transitions.*

Thus, the transition  $W^+ \rightarrow u\bar{d}'$  can be interpreted as a sum of the transitions  $W^+ \rightarrow u\bar{d}$  and  $W^+ \rightarrow u\bar{s}$ , as shown in Figure 3.42.

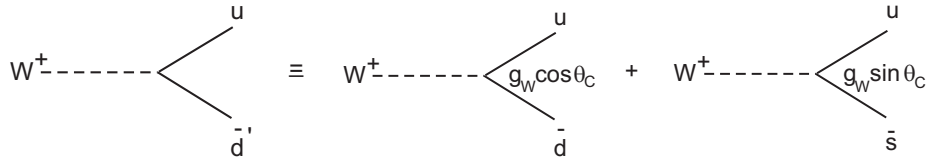


Figure 3.42: *Interpretation of a  $W^+$ -decay into a  $u$ - and a mixed  $\bar{d}'$ -quark in terms of the flavour states  $\bar{d}$  and  $\bar{s}$ .*

In the same way the transition  $W^- \rightarrow \bar{u}d'$  can be interpreted as a sum of the transitions  $W^- \rightarrow \bar{u}d$  and  $W^- \rightarrow \bar{u}s$ . Transitions that change flavour but not charge are not allowed.

The determination of the Cabibbo angle can be done by measuring the ratio between  $\Delta S = 1$  and  $\Delta S = 0$  decays, where  $\Delta S$  is the difference in strangeness of the initial and final state. Two such particle decays that have been used to determine the Cabibbo angle are  $K^+ \rightarrow \mu^+ + \nu$ , which has  $\Delta S = 1$ , and  $\pi^+ \rightarrow \mu^+ + \nu$ , with  $\Delta S = 0$ . Figure 3.43 shows the Feynman diagram for the  $K^+$ -decay into a  $\mu^+$  and a muon-neutrino. The corresponding diagram for  $\pi^+$ -decay is obtained if the  $\bar{s}$ -quark is replaced by a  $\bar{d}$ -quark. What we can observe is the second vertices are identical for the two decays. The first vertex, however, is for the  $K^+$ -decay Cabibbo-unfavoured, whereas it for the  $\pi^+$ -decay is Cabibbo-favoured. Thus, the strength of the first vertices are  $g_W \sin \theta_C$  and  $g_W \cos \theta_C$ , respectively, as seen from Figure 3.41. Now, the decay rate is proportional to the amplitude squared of the decay process. The amplitude is in turn proportional to the strength of the coupling constant, as we have discussed in Section 3.2 and consequently is the decay rate proportional to the square of the coupling constant. As we take the ratio of the  $K^+$  and  $\pi^+$  decays the contribution from the second vertices cancel and we are left with:

$$\frac{\Gamma(K^+ \rightarrow \mu^+ + \nu_\mu)}{\Gamma(\pi^+ \rightarrow \mu^+ + \nu_\mu)} \sim \sin^2 \theta_C / \cos^2 \theta_C$$

The experimental results show that the  $\Delta S = 1$  transition is suppressed by a factor of about 20 compared to the  $\Delta S = 0$  transition. This corresponds to a mixing angle  $\theta_C = 13^\circ$ .

### 3.3.7 The Prediction of the Charm Quark

Although there were no difficulties to produce the decay  $K^+ \rightarrow \mu^+ + \nu_\mu$ , the Feynman diagram of which is shown in Figure 3.43,

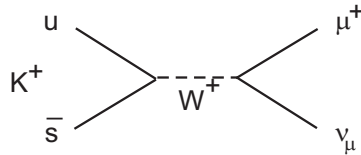


Figure 3.43: Feynman diagram describing the decay of a  $K^+$ -meson into a  $\mu^+$  and a  $\nu_\mu$ .

it took a long time until the decay of a neutral  $K$ -meson into a  $\mu^+\mu^-$  pair was observed. This decay can not proceed via an annihilation diagram given by Figure 3.44.

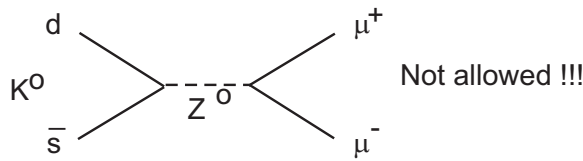


Figure 3.44: Feynman diagram showing the forbidden decay of a  $K^0$ -meson into a muon pair.

The reason is that transitions between d-type quarks or u-type quarks, respectively, through the emission of a  $Z^0$  particle, are not allowed or equivalently the emission of a  $Z^0$  particle can not change the flavour of a quark. However, since in weak interaction we have couplings between both  $ud$  and  $us$ , a  $K^0$ -meson can decay through a box diagram according to the Feynman diagram of Figure 3.45.

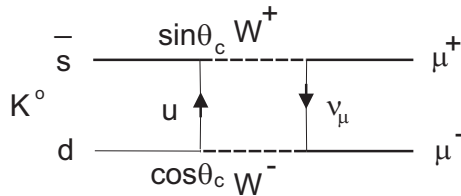


Figure 3.45: Feynman diagram describing the decay of a  $K^0$ -meson into a muon pair via a so called box diagram, in which a virtual  $u$ -quark is exchanged.

The amplitude of this diagram is proportional to  $\sin\theta_C \cos\theta_C$  and should therefore not be strongly suppressed compared to the charged kaon decay, in contradiction with experimental measurements. A solution to this problem was provided by introducing a fourth quark, called the 'charm' quark or the  $c$ -quark, with charge  $+2/3$ . The  $c$ -quark couples to the  $d$ - and  $s$ -quarks with a strength that is proportional to  $\cos\theta$  and  $-\sin\theta$ , respectively, as illustrated in Figure 3.46.

Thus, with the  $c$ -quark the neutral kaon decay should also be possible through the box diagram shown in Figure 3.47.

The amplitude of this diagram is proportional to  $-\sin\theta_C \cos\theta_C$  such that the amplitudes for the two possible decay mechanisms of  $K^0$  would cancel exactly if the masses of the  $u$ - and  $c$ -quarks were the same. This is, however, not the case. The mass of the  $c$ -quark could be constrained by the experimentally measured decay rate of  $K^0 \rightarrow \mu^+\mu^-$ .

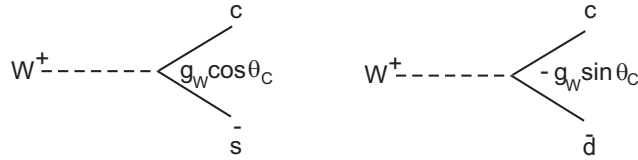


Figure 3.46: Feynman diagram describing the decay of a  $W^+$ -boson into a quark antiquark pair.

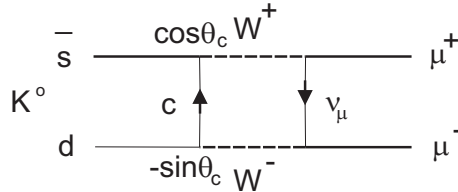


Figure 3.47: Feynman diagram describing the decay of a  $K^0$ -meson into a muon pair via a so called box diagram, in which a virtual  $c$ -quark is exchanged.

With four quarks we now have two complete families of quarks and leptons, specified in Table 3.3.

flavour	charge	spin
$\nu_e \quad \nu_\mu$	0	1/2
$e^- \quad \mu^-$	-1	1/2
$u \quad c$	+2/3	1/2
$d' \quad s'$	-1/3	1/2

or

flavour	charge	spin
$\nu_e \quad \nu_\mu$	0	1/2
$e^- \quad \mu^-$	-1	1/2
$u \quad c$	+2/3	1/2
$d \cdot \cos\theta + s \cdot \sin\theta \quad s \cdot \cos\theta - d \cdot \sin\theta$	-1/3	1/2

Table 3.3: The situations of known quarks and leptons after the discovery of the charm quark.

Although transitions between quarks of different families are allowed, cross transitions between leptons would violate the lepton number conservation.

The relation between the mixed quark states and the flavour (mass) eigenstates is given by the Cabibbo mixing matrix, given in Figure 3.48.

We now have the 'Cabibbo favoured' transitions shown in Figure 3.49, and the 'Cabibbo unfavoured' transitions shown in Figure 3.50.

The introduction of the  $c$ -quark means that the multiplets have to be extended to include another dimension as shown in Figure 3.51.

$$\begin{pmatrix} d' \\ s' \end{pmatrix} = \begin{pmatrix} V_{ud} & V_{us} \\ V_{cd} & V_{cs} \end{pmatrix} \begin{pmatrix} d \\ s \end{pmatrix} = \begin{pmatrix} \cos\theta_c & \sin\theta_c \\ -\sin\theta_c & \cos\theta_c \end{pmatrix} \begin{pmatrix} d \\ s \end{pmatrix}$$

Figure 3.48: The mixed quark states and the flavour states are related via the Cabibbo mixing matrix.

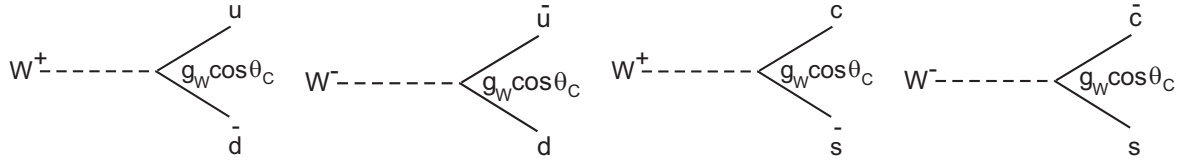


Figure 3.49: Feynman diagram showing Cabibbo favoured W-decays.

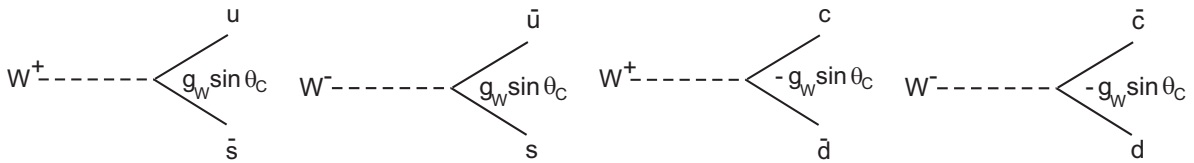


Figure 3.50: Feynman diagram showing Cabibbo unfavoured W-decays.

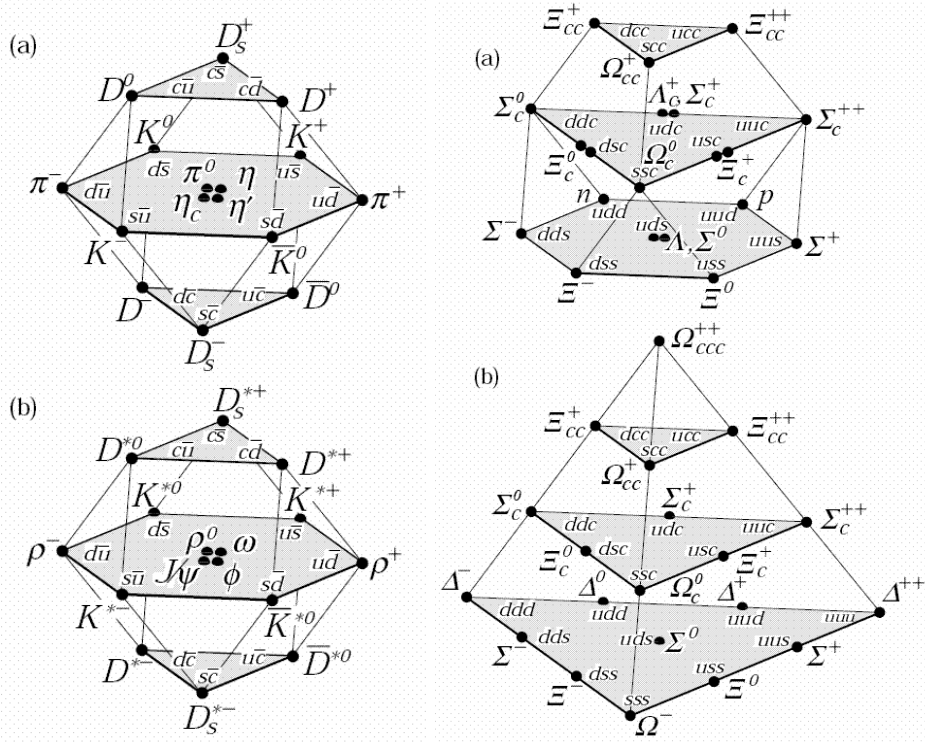


Figure 3.51: Particle multiplets including 'charmed' particles.

### 3.4 Strong Interactions

In finding an explanation to the short range nature of the strong force it was tempting to describe the interaction as an exchange of a massive field boson. From the measured widths of a number of hadronic resonance states it could be calculated that the typical lifetime for the strong decay is  $10^{-23}$  seconds. The typical range of the strong force is  $10^{-15}$  meters i.e. the size of a nucleon. From this it is straight forward to calculate that the exchange particle should have a mass around 100 - 200 MeV and it had to exist in three different charge modes (positive, negative and neutral). In 1947 the  $\pi$ -meson was discovered with apparently the right properties but it was soon realized that the spinless  $\pi$ -meson could not be the particle responsible for the strong force.

With the discovery of a large number of hadrons it became obvious that these particles could not be fundamental but had to be built out of more fundamental constituents. The quark model, which was introduced in 1963, was very successful in explaining all experimentally observed hadrons but in the beginning it was not believed that the quarks were real particles. As it was experimentally verified that the proton has an internal structure, by deep inelastic scattering experiments in 1969 (see Chapter 5), then the constituents of the proton were called *partons*. The partons could later be shown to be identical with the quarks. However, there were two important problems with the quark model. Firstly, no free quarks have ever been observed but they always appear in combinations of three quarks (or three anti-quarks) or as quark-antiquark pairs. Secondly, the quarks didn't seem to obey the Pauli exclusion principle since in some of the baryons, the spin of the three quarks pointed in the same direction ( $\Delta^{++}$ ). The solution to the second problem was to introduce a new quantum number, *colour*, such that the quarks can exist in three different colour states (*red*, *green* and *blue*) and the antiquarks have the corresponding anticolours. Thus, even if all three quarks in a baryon would have the same spin direction they would differ in the colour quantum number. Since no coloured hadrons have been observed the quarks must exist in combinations, which are colourless, or more accurately in colour singlet states.

red + blue + green = color neutral (and similarly for anti-colors)

red + antired, blue + antiblue and green + antigreen = color neutral

However, out of all possible color neutral states there is only one combination of quark-antiquark pairs and one combination of three quarks, which are in a colour singlet state. The colour singlet states are completely symmetric with respect to colour. For a meson ( $q\bar{q}$ ) this colour combination is:

$$1/\sqrt{3}\{|r\bar{r}\rangle + |g\bar{g}\rangle + |b\bar{b}\rangle\}$$

i.e. if one could measure the color of the state one would find equal probability for it being  $|r\bar{r}\rangle$ ,  $|g\bar{g}\rangle$  or  $|b\bar{b}\rangle$ .

The colour combination for a baryon (qqq) is:

$$1/\sqrt{6}\{|rgb\rangle - |rbg\rangle + |brg\rangle - |bgr\rangle + |gbr\rangle - |grb\rangle\}$$

In the same way as the flavour of a quark can be changed by emitting or absorbing a  $W$ -boson, a quark can change its colour by emitting or absorbing a gluon, as illustrated in Figure 3.52. In order to do so the gluon must carry *colour-anticolour*. In a Feynman diagram gluons are normally represented by a curled line, as shown in Figure 3.52. The gluons are massless *vector bosons*, just as the photon, and thus carry a spin of 1.

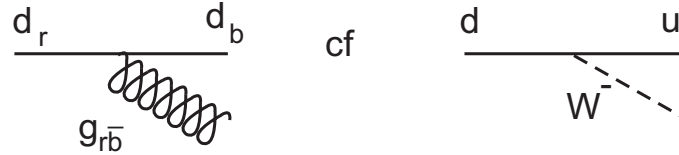


Figure 3.52: Feynman diagram illustrating how the emission of a gluon can change the colour of a quark and compared to how the emission of a  $W$ -boson change the flavour of the quark.

The fact that there are three different colour charges means that the following transitions are possible

$$\begin{array}{lll}
 \text{red} \rightarrow \text{red} & \text{red} \rightarrow \text{green} & \text{red} \rightarrow \text{blue} \\
 \text{green} \rightarrow \text{red} & \text{green} \rightarrow \text{green} & \text{green} \rightarrow \text{blue} \\
 \text{blue} \rightarrow \text{red} & \text{blue} \rightarrow \text{green} & \text{blue} \rightarrow \text{blue}
 \end{array}$$

The corresponding gluon states can be obtained if we organise the colours and anticolours in triplets similar to what we did with the  $u$ ,  $d$  and  $s$ -quarks in chapter 2, in order to construct the hadron multiplets. Thus this would lead to the colour-anticolour states shown in Figure 3.53 .

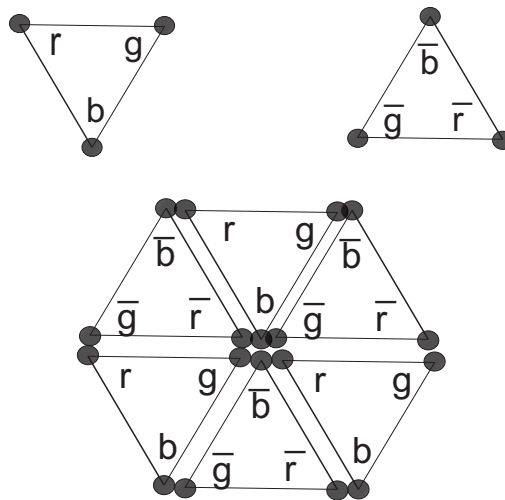


Figure 3.53: The arrangement of the three colour and anticolours in triplets (upper Figure) and how these triplet can be combined to form an octet of mesons (colour-anticolour combinations).

Just as in the case of the hadron multiplets there should be nine possible states i.e in this case nine gluon states. Out of these six change the colour of the quark whereas three do not. A

Triplet	$s = 1$	$s_z = -1$ $s_z = 0$ $s_z = +1$	$ \downarrow\downarrow\rangle$ $\frac{1}{\sqrt{2}} \uparrow\downarrow + \downarrow\uparrow\rangle$ $ \uparrow\uparrow\rangle$
Singlet	$s = 0$	$s_z = 0$	$\frac{1}{\sqrt{2}} \uparrow\downarrow - \downarrow\uparrow\rangle$

Table 3.4: Spin arrangements of a quark-antiquark pair

comparison with how the spin of a quark-antiquark system can combine to give a total spin of one and zero is given in Table 3.4.

Thus, three of the spin combinations are in a triplet state with the total spin,  $s = 1$ , with the three possibilities for the  $z$ -component,  $s_z = -1, 0, 1$ . The spin singlet state has total spin 0, which only gives one possibility for the  $z$ -component,  $s_z = 0$ . This is summarized in Table 3.4. In a similar way as spin up and spin down can be combined to obtain triplet and singlet states, the three colours and anti-colours can be combined such that eight colour combinations are in an *colour octet* state and one in a *colour singlet* state.

The various colour combinations are summarized in Table 3.5. Six of the colour octet states (gluons) lead to a change in colour charge, when emitted or absorbed by a quark or anti-quark, whereas two of the octet states do not cause any change in the colour charge of quarks or anti-quarks,

$ 1\rangle = 1/\sqrt{2}(r\bar{b} + b\bar{r})$ $ 2\rangle = -i/\sqrt{2}(r\bar{b} - b\bar{r})$ $ 3\rangle = 1/\sqrt{2}(r\bar{g} + g\bar{r})$ $ 4\rangle = -i/\sqrt{2}(r\bar{g} - g\bar{r})$ $ 5\rangle = 1/\sqrt{2}(b\bar{g} + g\bar{b})$ $ 6\rangle = -i/\sqrt{2}(b\bar{g} - g\bar{b})$	octet states $\rightarrow$ change in colour
$ 7\rangle = 1/\sqrt{2}(r\bar{r} - g\bar{g})$ $ 8\rangle = 1/\sqrt{6}(r\bar{r} + g\bar{g} - 2b\bar{b})$	octet states $\rightarrow$ no change in colour
$ 9\rangle = \sqrt{1/3}(r\bar{r} + g\bar{g} + b\bar{b})$	singlet state

Table 3.5: Colour combinations of gluons

The ninth linear combination is completely symmetric with respect to colour and is thus in a

the colour singlet state, which means that it doesn't carry any *net* colour and consequently it doesn't couple to the coloured quarks.

Thus, we end up with eight gluons in total.

The scattering of two quarks in strong interaction is described as an exchange of gluons, as shown in Figure 3.54, and the probability that a quark emits or absorbs a gluon is given by the coupling strength of the strong force, which is  $\alpha_S$ . The fundamental unit of colour charge is defined as  $g_S = \sqrt{4\pi\alpha_S}$ , similar to the definition of  $g_e$  for the electromagnetic force and  $g_w$  for the weak force.

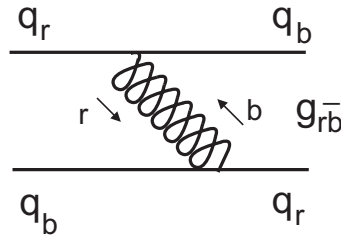


Figure 3.54: Feynman diagram showing the how the quark colours can change through the exchange of a gluon.

Since photons do not carry electric charge they can not interact mutually. On the other hand the gluons carry colour charge and therefore they can couple to each other. This allows for three- and four-gluon vertices, as presented in Figure 3.55.

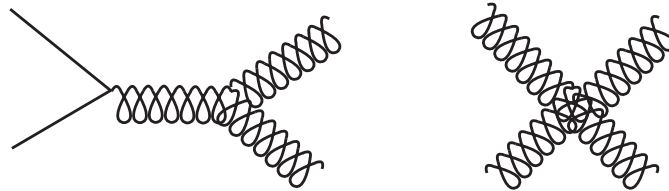


Figure 3.55: Feynman diagrams showing three and four gluon interaction.

Due to the fact that the strong force only act between particles that carry colour charge, the theory describing such interactions has been called *Quantum Chromo Dynamics*.

### 3.4.1 More Feynman Diagrams

Consider the Feynman diagrams of Figures 3.56 and 3.57 as examples of strong interactions processes.



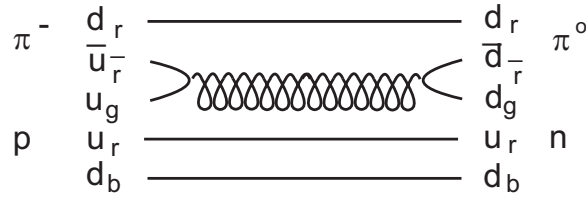


Figure 3.56: Feynman diagram showing the reaction  $\pi^- + p \rightarrow \pi^0 + n$ .

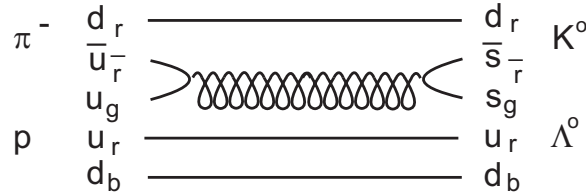


Figure 3.57: Feynman diagram showing the reaction  $\pi^- + p \rightarrow K^0 + \Lambda^0$ .

### 3.4.2 Asymptotic Freedom and Confinement

Results from experiments where an electron was used to probe the inner structure of the proton revealed that the quarks seem to behave like free particles when they are close together. This is called *asymptotic freedom*. On the other hand, at larger distances they are strongly bound to each other, such that they can not escape from the hadrons. This is called *confinement*. The behaviour of the strong force is thus completely opposite to what is the case for the electromagnetic force, which gets weaker the more we separate the electrically charged particles from each other. The explanation to this difference is given by the self-coupling of the gluons.

An electron which travels through space is constantly emitting and absorbing virtual photons, which can fluctuate into electron-positron pairs. These pairs will screen the original charge of the electron such that the effective charge is decreased. As can be seen from Figure 3.58 the orientation of the electric field changes direction as we move away from the original electron. The further we move out the more electron-positron pairs will screen the field generated by the original charge. Consequently the strength of the electromagnetic force increases the more we penetrate the cloud of screening electron-positron pairs. It also means that the coupling strength will increase as we increase the energy of the probe, since we then better penetrate the screening pairs. We may say that the intrinsic strength of the electromagnetic force increases as we penetrate the cloud of screening pairs.

Due to similar quantum fluctuations a quark can emit and absorb gluons, which may fluctuate into quark-antiquark pairs. These will cause a screening of the colour field produced by the original colour charge exactly as the electric charge is screened by electron-positron pairs. Figure 3.59 shows how the direction of the colour field changes as we move away from the original colour charge.

It can, however, also happen that a gluon which is emitted from a quark fluctuates into two gluons, as shown in Figure 3.60. This gives a new situation where the colour charges line up in such a way that the colour field always point in the same direction, thereby giving rise to

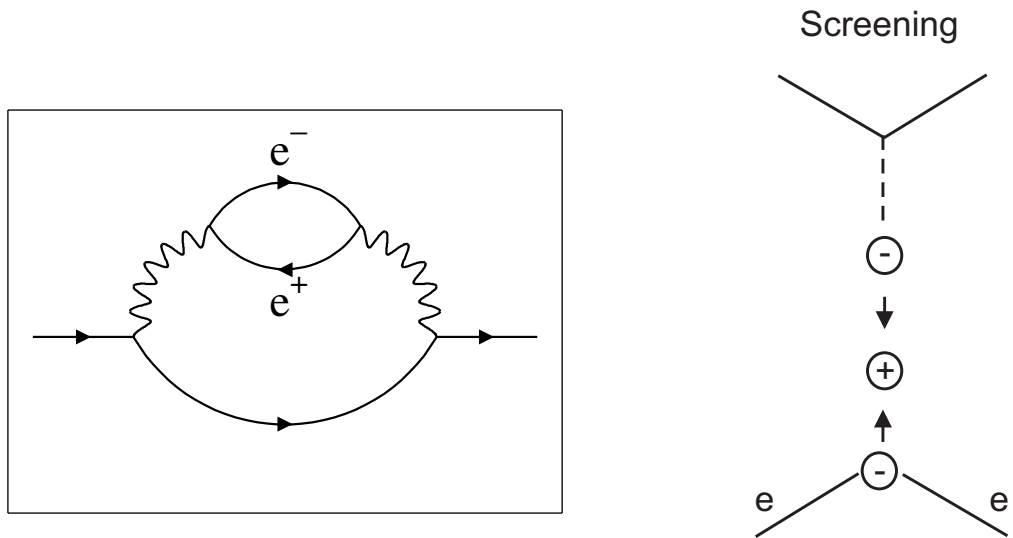


Figure 3.58: Illustration of screening of the electric charge of the electron via the creation of a virtual  $e^+e^-$  pair.

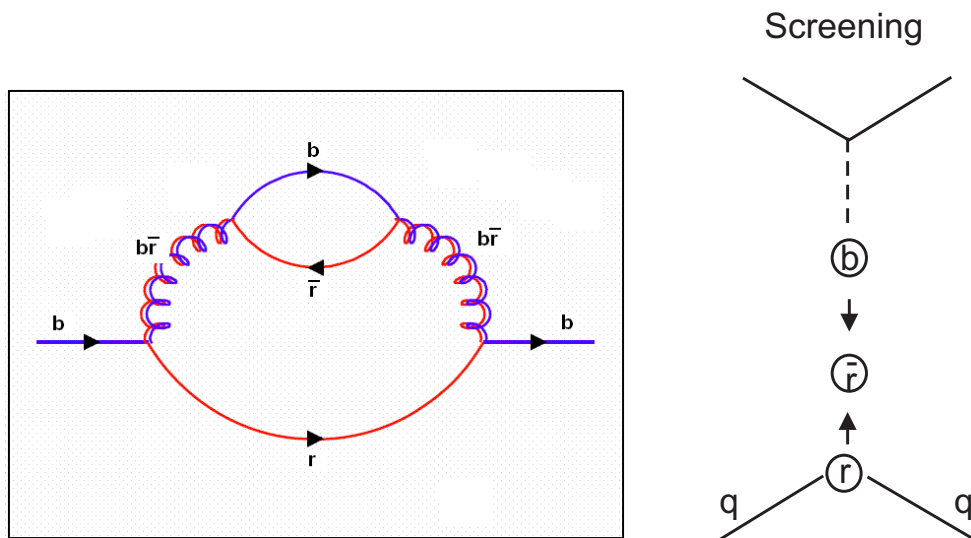


Figure 3.59: Illustration of screening of the colour charge of a quark via the creation of a virtual  $q\bar{q}$  pair.

*antiscreening*. Whereas a gluon can only fluctuate into a quark-antiquark pair with the same colour-anticolour combination as the gluon, it can fluctuate into a pair of gluons with several colour-anticolour combinations. Consequently, the effect of the antiscreening will dominate over screening and the strength of the colour field will increase as we move further away from the original quark. In contrast to electromagnetism the coupling strength of the strong force will decrease as we increase the energy of our probe, due to the fact that the effective colour charge gets smaller the deeper we penetrate the gluon cloud as illustrated in Figure 3.61.

From the discussion above we have learnt that the strength of the electromagnetic coupling

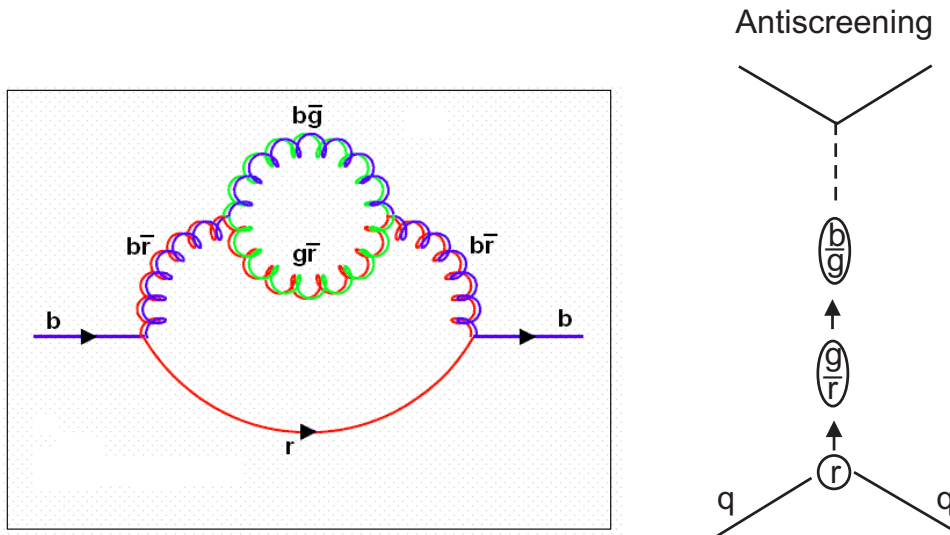


Figure 3.60: Illustration of antiscreening of the colour charge of a quark via the creation of a virtual pair of gluons.

constant increases if we increase the energy of the probe and this can be understood as a consequence of screening. The strength of the strong coupling constant, on the other hand, decreases as we increase the energy of the probe, which explains why the quarks behave like free particles as long as they are close together (asymptotic freedom) and are strongly bound at large distances (confinement). The variation of the coupling strengths with energy is shown in Figure 3.61.

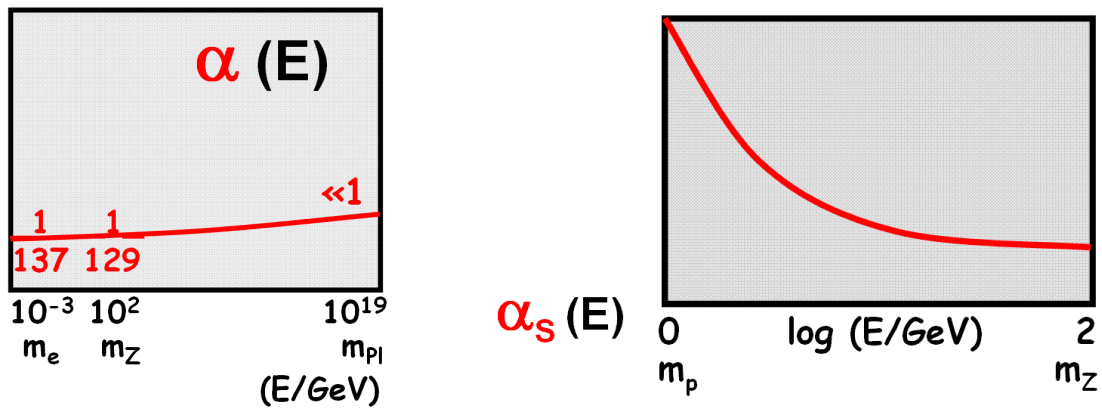


Figure 3.61: The variation with energy of the electromagnetic coupling constant  $\alpha_e$  (left), and of the strong coupling constant  $\alpha_s$ , respectively.

### 3.4.3 Unification of the Forces

The strength of the forces are at normal energies different by several order of magnitude as we have discussed already in the introduction. This is a consequence of the different influences

of the particle clouds generated by quantum fluctuations due to the different forces. However, if it would be possible to probe the strength of the forces that we have discussed so far (i.e. the electromagnetic, weak and strong forces) at an energy at which these clouds of screening particles are penetrated, the strength of all forces should be equal. Calculations have shown that this energy is around  $10^{16}$  GeV, which is thus the energy at which the three forces unify.

### 3.4.4 Hadronization

We now know that the quarks can not escape from the hadrons due to the properties of the strong force and that they always appear in either combinations of three quarks (antiquarks) as baryons (antibaryons) or in quark-antiquark pairs as mesons. What will then happen if we force the quarks to move apart?

Let us start by considering the electromagnetic field between two electrically charged particles. If we move these particles apart the field lines joining the two charges will start spreading out in space in a spherical fashion, as illustrated in Figure 3.62. The density of the field lines becomes smaller as the charges are separated and since the density of the field lines is proportional to the strength of the field, the force becomes weaker. This is consistent with our observations.

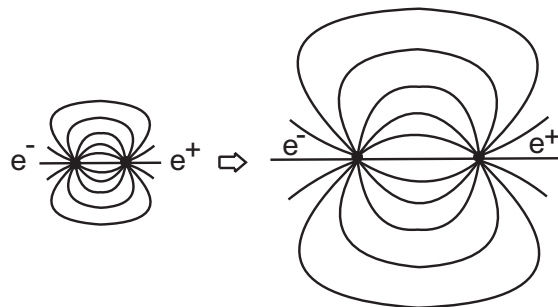


Figure 3.62: *The extension of the field lines between two electrically charged particles and how it changes with the distance between the charges.*

If we now instead separate a quark and an antiquark in a meson, we find that the field lines of the colour field do not spread out in space as was the case for the electromagnetic field. The reason for this is again given by the possibilities for the gluons to couple to each other, which means that we do not only have colour field lines between the quark and antiquark but gluons are also exchanged between the field lines and as a consequence of this they are kept together. This is illustrated in Figure 3.63.

If we compare with the case of the electromagnetic field, which is mediated by the photons, such self-couplings can not occur since a photon can not couple to a photon.

As the quark and antiquark are separated the density of the field lines thus stays constant in a *colour tube* or *colour string*. This means that the force is constant whereas the energy in the colour string increases as the quarks are separated. Mathematically, the colour field is approximated by a massless relativistic one dimensional string. A  $q\bar{q}$ -pair which is created out

of vacuum from a quantum fluctuation process, may tunnel through the barrier presented by the constant field inside the colour tube, with a certain probability. The new  $q\bar{q}$ -pair will be pulled apart by the field of the original quarks and the field which is built up between them will at some point cancel the original field in that region, and cause the tube to split up in two parts of lower energy as shown in Figure 3.63. We are now left with two mesons instead of one. If the initial energy in the string is high the quarks continue to move apart and new hadrons will be created up to a point where the energies in the strings are below the mass of the lightest hadron. These hadrons will mainly be emitted in the direction of the original quark and antiquark in the form of collimated flows of particles, called *hadron jets*. The situation can be compared to pulling a rubber band.

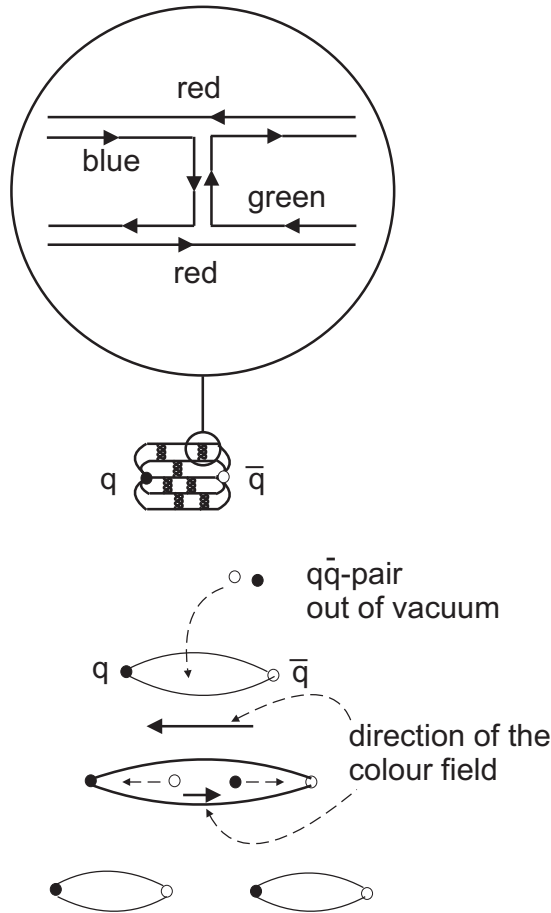


Figure 3.63: *The extension of the colour field between a quark and an anti-quark. The mechanism how the colour field is broken when the quark and anti-quark are separated is also illustrated.*

From experiments we know that not only mesons are created when the colour field breaks up but also baryons. This happens if, instead of a quark-antiquark pair, a pair of quarks ( $qq$ ) and a pair of antiquarks ( $\bar{q}\bar{q}$ ) are created when the string breaks, as illustrated in Figure 3.64. According to this a baryon is always created together with an antibaryon, which is in agreement with the conservation of the baryon number.

A gluon, which is emitted, can according to QCD obviously not escape since it also carries

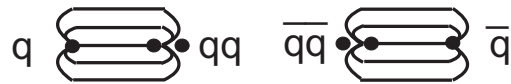


Figure 3.64: The production of a baryon - anti-baryon pair from a split up of the colour field between a quark and an anti-quark.

colour charge. The effect of an emitted gluon is that it will pull the colour string in the direction of its motion such that the string will get a kink. This is illustrated in Figure 3.65. The kink will collect some momentum and increase the probability that the string breaks in this region. In such a case we will get three jets of particles, two from the original quark/antiquark and one from the gluon.

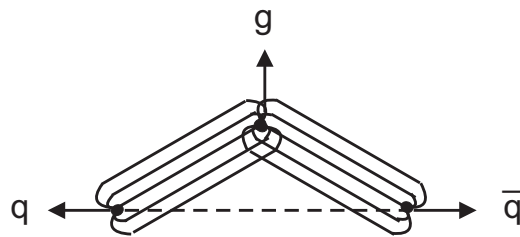


Figure 3.65: The kink of the colour field caused by the emission of a gluon.

### 3.4.5 Jets

Let us continue the comparison with pulling a rubber band. If we put marks along the rubber band and pull it from both ends we will notice that the marks at the ends will move faster than the marks closer to the middle. Obviously most of the energy will be at the ends of the rubber band as it will be also at the ends of the colour string due to the kinetic energy of the initial quark and antiquark. Consequently, the string will primarily break at the ends rather than in the center and most of the hadrons will be produced close to the original quark and antiquark such that we get collimated flows of particles, called *jets*, moving in essentially the same direction as the original quarks (or gluons). This is schematically illustrated in Figure 3.66, which is a Feynman diagram showing an electron positron collision producing a quark and an antiquark, where the quark is emitting a gluon, leading to a three-jet event. Intuitively one would assume that the particles in a jet carry the properties of the quark and that by studying jet production one could learn more about the quarks. However, some hadrons of low momenta will still be produced in the region between the original quarks and for that reason it is not completely unambiguous whether some of the particles should be assigned to one jet or the other. Nevertheless, this is the only way to study the properties of the quarks and the gluons.

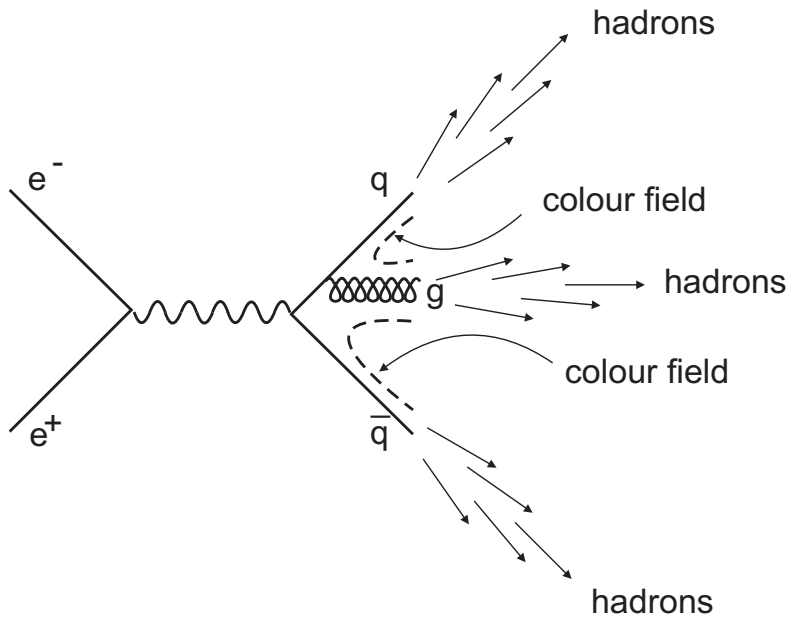


Figure 3.66: *Feynman diagram for an electron positron collision producing a quark, antiquark and gluon final state. The Figure also illustrates how the color field is stretched between the partons (broken lines) and how the collimated flow of hadrons are emitted.*

### 3.4.6 Testing QCD

#### Electron-Positron Scattering

In electron-positron scattering the electron and positron annihilate into a virtual photon (or  $Z^0$ ), which can decay either into a lepton-antilepton pair or into a quark-antiquark pair. According to the discussion above the quarks will hadronize and produce jets of hadrons. As the facilities which collide electrons and positrons (*colliders*) reached higher collision energies, clear evidence for collimated flows of particles (jets) could be observed in the experiments. One such event is shown in Figure 3.67.

Since a quark may emit gluons it should happen that the final state also contained a gluon in addition to the quark and antiquark. This would give rise to events with three jets, which was also observed at DESY. Two examples of three-jet events are shown in Figure 3.68.

#### Test of the String Model

Three-jet events can be used to test whether the theory of independent parton fragmentation or fragmentation according to the colour string model gives the correct description of the hadronization process. The model predicts that the strings connect the quark and antiquark with the gluon as illustrated in Figure 3.69. When the strings break up, jets with high momentum particles will be produced along the directions of the quarks and the gluon. However, the string

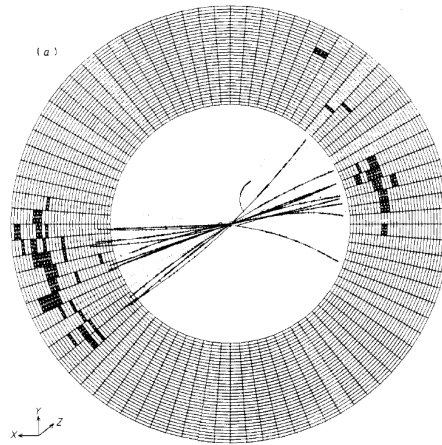


Figure 3.67: A 2-jet event as experimentally measured.

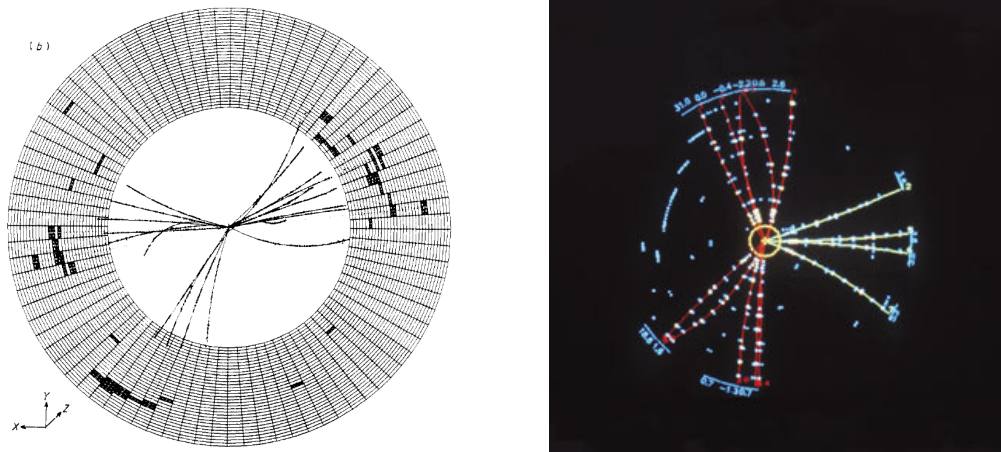


Figure 3.68: Two examples of 3-jet events as experimentally observed.

may also break in a region between the quarks and the gluon where it is not obvious whether the produced particle should be allocated to the quark jet or the gluon jet. These are mainly low momentum particles since the energy carried by the colour string in this region is small. Thus, it is expected to find additional low momentum particles between the quark and gluon jets but not between the quark jets since there is no string connecting the quark and antiquark directly.

This is exactly what was observed by experiments, the results of which is presented in Figure 3.70.



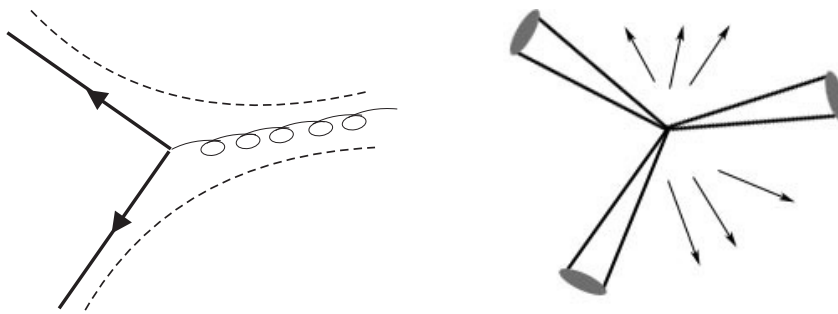


Figure 3.69: *The stretching of the colour strings (broken lines) in a 3-jet event (left), and the expected hadron flow between the three jets (right).*

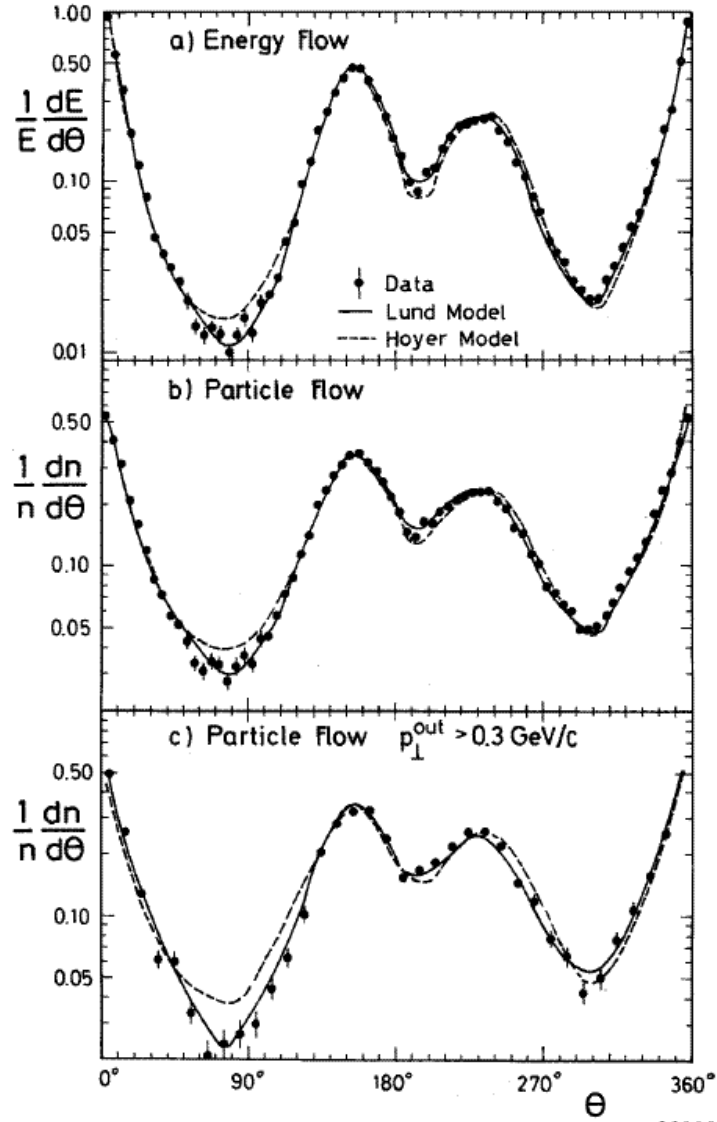


Figure 3.70: The energy flow, particle flow and flow of particles with a transverse momentum of bigger than  $0.3 \text{ GeV}/c$  out of the jet plane as a function of the angle,  $\Theta$ , with respect to the direction of the most energetic jet ( $\Theta=0$ ). The predictions of the independent fragmentation model (broken line) and the string fragmentation model (solid line) are compared with the experimental data points.

If instead of a gluon a photon is emitted, then the colour string will be pulled between the quark and the antiquark, as shown in Figure 3.71. In this case the additional low momentum particles will appear in the region between the quark jets.

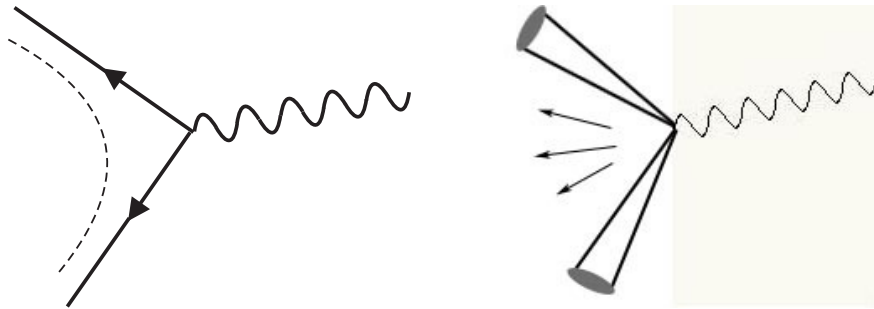


Figure 3.71: *The stretching of the colour string (broken lines) in a quark, anti-quark, gamma event (left), and the expected hadron flow between the two jets (right).*

### The Property of Colour Charge

How can we test experimentally whether colour charge is a relevant property of the quarks? If we consider production of a quark pair from electron-positron collisions, it occurs according to the Feynman diagram of Figure 3.72,

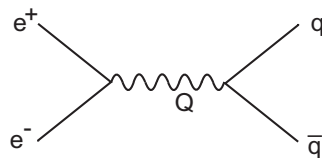


Figure 3.72: *Feynman diagram showing the production of a quark, antiquark pair from an electron, positron collision. The four-momentum ( $Q$ ) of the photon propagator is given.*

with the amplitude  $A_{qq} \sim \frac{ee_q}{Q^2}$ , where  $e$  is the electron charge,  $e_q$  the quark charge and  $Q$  the four momentum of the propagator

This can be compared to the production of a muon pair from  $e^+e^-$ -collisions, the Feynman diagram of which is shown in Figure 3.73,

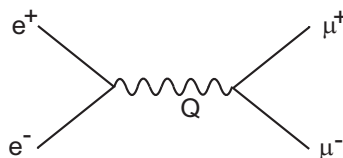


Figure 3.73: *Feynman diagram showing the production of a  $\mu^+\mu^-$ -pair from an electron, positron collision. The four-momentum ( $Q$ ) of the photon propagator is given.*

which has the amplitude  $A_{\mu\mu} \sim \frac{e^2}{Q^2}$ .

If we measure the ratio between the cross sections of these two processes one would thus expect it to be given by the square of the quark charge, since  $A_{qq}^2/A_{\mu\mu}^2 = e_q^2/e^2 = e_q^2$ , and  $e = -1$ . The different quark flavours that can be produced in  $e^+e^-$ -collisions depend on the collision energy and in order to take all cases into account one has to sum over all quark flavours with masses, which allow them to be produced at that specific collider energy. Experimentally we do not observe quarks but since quarks decay into hadrons, we have to look for events with hadrons in the final state i.e. events with a number of tracks  $> 2$ . Thus, we want to measure:

$$R = \frac{\sigma(e^+e^- \rightarrow \text{hadrons})}{\sigma(e^+e^- \rightarrow \mu^+\mu^-)} = \frac{\sum e_q^2}{e^2} = \frac{\sum e_q^2}{1} \quad \text{since } e = -1 ,$$

where we sum over all possible quark flavours. In a detector it is trivial to differentiate between a hadronic final state, which contains many particles, and a leptonic final state, which only has two particles.

We can now calculate the expected ratio for some specific collision energies. If the collision energy is below 3 GeV only pairs of the lightest quarks  $u\bar{u}$ ,  $d\bar{d}$  and  $s\bar{s}$  can be produced. In the region 3 to 9 GeV also  $c\bar{c}$ -pairs can be created and above 9 GeV  $b\bar{b}$ -pairs can be produced in addition. Thus the expected ratio for:

$$\text{three quarks : } R = [(2/3)^2 + (-1/3)^2 + (-1/3)^2] = 2/3$$

$$\text{four quarks: } R = [(2/3)^2 + (-1/3)^2 + (-1/3)^2 + (2/3)^2] = \frac{10}{9}$$

$$\text{five quarks: } R = [(2/3)^2 + (-1/3)^2 + (-1/3)^2 + (2/3)^2 + (-1/3)^2] = \frac{11}{9}$$

Comparisons to experimental data show disagreement with these predictions. However, according to QCD the quarks can appear in three different colours and to account for these additional production modes we have to multiply by a factor 3. Then we get:

$$R = 2 \quad \text{for 3 quarks}$$

$$R = 3\frac{1}{3} \quad \text{for 4 quarks}$$

$$\text{and } R = 3\frac{2}{3} \quad \text{for 5 quarks}$$

The agreement now became considerably better but it was still not as good as expected. You may however, remember, that at energies above  $\sim 3.5$  GeV also a  $\tau$ -lepton pair can be produced. Since the  $\tau$ -lepton is so heavy it can not only decay into lighter leptons but also into hadrons via a weak decay (see Section 4.2.12). This of course adds to the probability that hadronic events are observed and increases the cross section ratio for energies above 3.5 GeV. Taking this into account the agreement between measurements and expectations becomes quite good as can be seen from Figure 3.74.

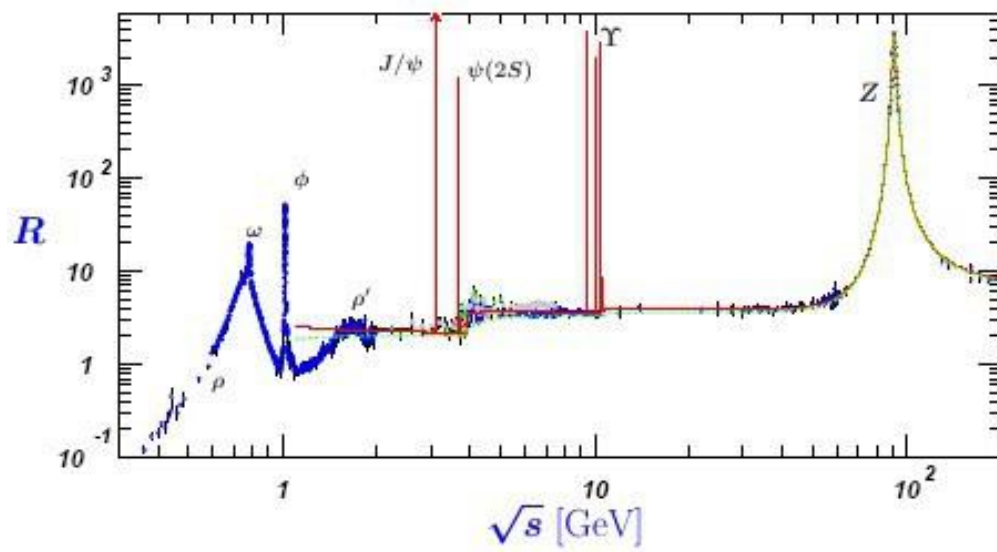


Figure 3.74: Measurements of the ratio  $R = \frac{\sigma(e^+e^- \rightarrow \text{hadrons})}{\sigma(e^+e^- \rightarrow \mu^+\mu^-)}$  as a function of the centre-of-mass energy. The expected ratios with the assumption of three colours are also shown.

# Chapter 4

## Experimental Discoveries of Fundamental Importance

### 4.1 Particles and General Properties

#### 4.1.1 Resonance Particles

The particles which were discovered by the early experiments, are either stable or have lifetimes, which are sufficient for them to leave tracks in a detector. Typical lifetimes of such particles are greater than  $10^{-12}$  seconds. This of course does not exclude that there might exist particles with significantly shorter lifetimes, such that they would decay into more longlived particles so quickly that they would not be detected directly. The only way to prove their existence is through their decay products. Such transient particles are called *resonance particles*.

Two types of experiments can be performed in order to search for resonance particles. One possibility is to calculate the invariant mass (the four-vector sum) of decay particles and investigate if a peak is observed in the invariant mass spectrum. The invariant mass distribution of uncorrelated final state particles will lead to an essentially flat distribution and only for particles originating from a decay, a peak will appear. This method has the disadvantage that normally only one specific decay mode is investigated while other possible decays are neglected. The other method is to measure the cross section of particle interactions as a function of the collisions energy and look for dramatic variations in the cross section. In this view, the presence of resonance particles adds to the cross section of the particles involved in the collision, making the collisions more likely. The reason why this leads to a peak in the cross section and not just to a plateau is that in the vicinity of the resonance peak the interaction of the quarks, building up the resonance particle, plays an important role, whereas at higher energies these quarks can be treated as free particles.

#### 4.1.2 Life times, decay rate, decay width and branching ratio

In spite of the fact that resonance particles have extremely short lifetimes, they are just as real as other particles, that can be directly observed in a detector. Typically, the lifetimes of resonance

particles are  $10^{-23}$  seconds and they can consequently only travel a distance  $10^{-15}$  meter at the speed of light, before they decay. Since most particles we know of are unstable, *life time* is an essential characteristic of such particles. If we consider a large number of identical unstable particles,  $N$ , the number of particles, which have decayed,  $dN$ , after some time,  $dt$ , is:

$$dN = -\Gamma N dt \quad ,$$

where  $\Gamma$  is called the *decay rate*, which thus is the probability per unit time that a given particle will decay. The number of remaining particles after a time  $t$  is:

$$N(t) = N(0)e^{-\Gamma t} \quad .$$

The life time is defined as the time after which the number of decaying particles has decreased by a factor  $1/e$ :

$$\tau = \frac{1}{\Gamma}$$

Most unstable particles may decay in different ways i.e. there are several *decay modes*, and then the total decay rate is the sum of the decay rates of all possible decay channels.

$$\Gamma_{tot} = \sum_{i=1}^n \Gamma_i \quad ,$$

where  $n$  is the number of decay channels. The more decay possibilities the shorter the life time of the particle is.

$$\tau = \frac{1}{\Gamma_{tot}} \quad .$$

The relative probability that a particle decays into a specific final state,  $f$ , is called *branching ratio* or *branching fraction*, and is defined as:

$$B_f = \frac{\Gamma_f}{\Gamma_{tot}} \quad .$$

$\Gamma$  has the dimension of inverse time. However, as was discussed in Section 1.1 inverse time, in natural units, is the same as energy and therefore  $\Gamma$  is also called the *decay width*. Consequently, the actual lifetime of a resonance particle can be extracted in a fairly uncomplicated way by measuring the width of the resonance peak. According to the Heisenberg uncertainty principle  $\Delta t = \hbar/\Delta E$ , where  $\Delta t$  is the time interval over which the particle exists and  $\Delta E$  represents the width of the resonance peak at half the maximum. Thus, a longlived particle will create a narrow resonance peak whereas a shortlived particle will give rise to a broad peak. It should be remembered that the measured lifetime and decay width depend on the Lorentz frame in which they are measured, as was discussed in Section 1.3.6.

### 4.1.3 Significance

When we claim that we have made a significant observation we in general mean that the probability for the selected hypothesis is significantly higher than any other hypothesis. Furthermore, we normally assume that the statistical sample, on which the observation is made, is large enough so that additional observations will not change the conclusion. In particle physics the latter requirement is not always fulfilled. Especially this is so in the search for rare particles, where the claim for an observation in some cases is based on a limited number of events.

Searches for new particle states in particle physics experiment are based on the observation of a class of events fulfilling specific criteria for being signal events, and an estimate of events coming from various background sources. The probability,  $P$ , for an observed excess of events to be the expected particle is given by the Poisson probability:

$$P(N_0, N_B) = \frac{e^{-N_B} \cdot N_B^{N_0}}{N_0!},$$

where  $N_B$  is the number of expected events in case of no signal i.e. the number of background events, and  $N_0$  is the total number of events observed in this mass region i.e. the sum of signal and background events. Assuming that the observed signal has a Gaussian mass distribution with its centre at the mass value  $\mu$  and a width of  $\sigma$ , then the mass region which is used to calculate the significance is usually  $\pm 2\sigma$  around  $\mu$ . The significance of an observed signal is frequently expressed in terms of *standard deviations* ( $\sigma$ ). When  $N_B$  is large the significance of an observation can be well approximated by  $N_S/\sqrt{N_B}$ , where  $N_S = N_0 - N_B$ , and  $\sqrt{N_B}$  is the statistical uncertainty in the measurement. Normally a significance of  $5\sigma$  is required to claim a discovery, which correspond to the probability that the observed signal is due to a statistical fluctuation being smaller than  $2.9 \cdot 10^{-7}$ . As a comparison we can notice that  $2\sigma$  and  $3\sigma$  correspond to 2.8% and 0.14% probability, respectively, that the enhancement would be caused by a statistical fluctuation.

The problem becomes more complicated when the signal is not very outstanding such that the mass and width can not be estimated from a visual inspection, as is the case if the enhancement is spread out over a large mass range due to bad mass resolution of the detector. In such cases the current procedure is to use the so called Sliding-Window method, in which an excess of events is searched for within a narrow mass region, which is moved stepwise over the entire kinematic range. However, some precaution has to be taken in using this method since the value of the significance may depend on the step size by which the Sliding-Window is moved. Thus, for observations of physical signals of unknown location or shape a careful evaluation of the significance is necessary.

## 4.2 Fundamental Discoveries of Particles

### 4.2.1 The Experimental Discovery of the Electron

The British chemist John Dalton confirmed experimentally in 1808, through his studies of gases, the almost two millenia old hypothesis of the atom, proposed by the Greek philosopher Democritus. It was by then believed that the atom was indivisible.

Experiments with electricity were performed long before it was understood that electricity was conveyed by electrons. By applying a voltage between two electrodes it was possible to create an electric arc but nobody could explain how it worked. The British physicist Joseph J. Thomson decided to solve this mystery and started experiments, in the mid 1880:ies, where he investigated electric discharge in gases. Under normal circumstances gas is a poor conductor but at low pressure discharges occur and the gas become conducting. Thomson used a so



called cathode tube, in which the gas was contained at low pressure. When he applied a voltage between the cathode (the negative electrode) and the anode (the positive electrode), he created a discharge and could observe a stream of bright lines emitted from the cathode. At the time these were called *cathode rays* and it was speculated whether they were some kind of waves or a stream of particles. In case of a particle, it should have a well-defined mass.

The basic structure of Thomson's apparatus is shown in Figure 4.2.

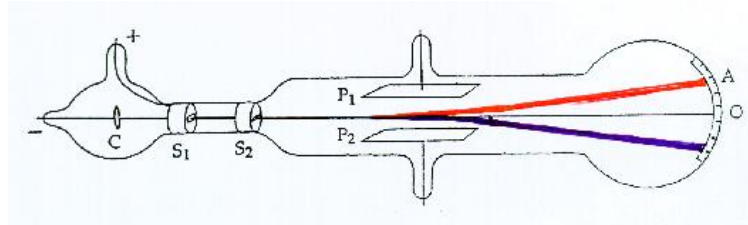


Figure 4.1: A pictorial representation of the cathode tube used by J.J. Thomson, which he used to discover the electron.

The cathode (C) was given a negative potential whereas the anode was kept at ground. The emitted cathode rays travelled through two slits (S1 and S2) collimating them to a narrow beam hitting the end of the tube, which was coated with a fluorescent layer, so that he could observe the impact position of the beam.. Thomson introduced a pair of parallel metal plates (P1 and P2) between which the cathode rays passed. When he applied a voltage over these plates he found that the cathode rays were deflected and depending on which plate was at a positive and negative potential, respectively, the cathode rays bent one way or the other. By mounting the tube between two coils, through which an electric current was sent, a magnetic field was generated and Thomson could conclude that the cathode rays were also influenced by magnetic fields. He was able to determine the velocity of the cathode rays by applying the electric and magnetic fields simultaneously. The force of the electric field on a charge  $q$  is given by  $F_E = E \cdot q$ , where  $E$  is the strength of the electric field, whereas the same charge is influenced by the magnetic field according to  $F_B = B \cdot v \cdot q$ , where  $B$  is the strength of the magnetic field and  $v$  is the velocity of the charge. He adjusted the electric and magnetic fields such that they compensate each other i.e.  $E \cdot q = B \cdot q \cdot v$ , and the beam passed undeflected through the tube. Under these conditions the velocity equals  $v = E/B$ . Now, the magnetic force has to be equal to the centripetal force  $F_{centripetal} = m \cdot v^2/r$ , where  $r$  is the radius of curvature of the charge in the magnetic field. Rearranging the parameters gives  $q/m = v/(B \cdot r)$ , and inserting  $v$  gives  $q/m = E/(B^2 \cdot r)$ . From his measurements he concluded that the cathode rays were particles with a mass of the order of 1000 times smaller than that of the hydrogen atom (we today of course know that the electron is 1836 times lighter than the proton).

By using different materials for his cathode he realized that this particle was a constituent in several kinds of atoms and concluded that it was a universal constituent of matter. He announced the existence of the 'corpuscle', later named *electron*, in 1897.

In order to explain that atoms have no effective electric charge, he proposed that the electrons were swimming in a sea of positive charge, contained in a very small volume, to compensate for the negative charge of the electrons. However, in order to account for the mass, the atom

had to contain thousands of electrons. The atomic model of Thompson was called the 'plum pudding' model.

#### 4.2.2 The Experimental Discovery of the Proton

The British physicist Ernest Rutherford and the British chemist Frederick Soddy proposed in 1903, as a result of their study of radioactive emanation from thorium and radium, that radioactivity occurs as a consequence of transmutation between elements, in which particles are emitted from the nucleus. They concluded that there must be objects smaller than the atom.

In the following years Rutherford investigated the scattering of  $5\text{ MeV}$   $\alpha$ -particles, emitted by a uranium metal, against a target of gold atoms. In order to do so he had to develop a way of detecting individual  $\alpha$ -particles. He found that a screen coated with zink sulfide (ZnS) emitted a light flash as it was hit by an  $\alpha$ -particle. He sent a narrow beam of  $\alpha$ -particles towards a thin gold foil and studied, together with his assistant Hans Geiger, how the  $\alpha$ -particles were scattered through visual examination of how the light flashes on the ZnS screen were distributed.

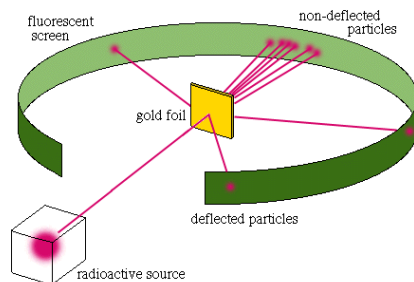
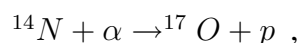


Figure 4.2: An illustration of the experimental set-up of Rutherford, which he used to investigate the scattering of  $\alpha$ -particles by a thin gold foil.

Their first results showed that the  $\alpha$ -particles were only scattered slightly in accordance with Rutherford's expectations. At this time Ernest Marsden joined the project and was given the task to study whether any  $\alpha$ -particles were scattered through large angles. Marsden found that a small fraction, about 1 in 20.000, of the  $\alpha$ -particles indeed were scattered through more than  $90^\circ$ . The unexpectedly large deflection of some of the  $\alpha$ -particles led Rutherford to exclaim: 'It was as incredible as if you fire a 15-inch shell at a piece of tissue paper and it comes back and hit you'. These results were presented in a publication in 1911 where Rutherford also proposed a model for the structure of the atom in which the positive charge and almost the complete mass of the atom is concentrated in a tiny fraction of the atom's total volume, which he called the *nucleus*. By carefully measuring the fraction of  $\alpha$ -particles deflected through large angles he was able to estimate the size of the nucleus as at least 10.000 times smaller than the atomic radius, and he could derive equations for how the scattering occurred.

In 1917 Rutherford observed that  $\alpha$ -particles traveling through air produced radiation, through the reaction:



which had a penetration and a signature in his scintillation counters (see Section 7.5.1) typical for a hydrogen nuclei. Knowing that hydrogen is the lightest element and is a fundamental building block of all nuclei, Rutherford gave the hydrogen nucleus the name *proton*.

### 4.2.3 The Experimental Discovery of the Positron

In 1928 Dirac proposed that electrons existed with both negative and positive charge, as a consequence of the outcome of the Klein-Gordon equation (see Section 2.8).

The following year the Soviet physicist Dmitri Skobeltsyn, in his studies of cosmic radiation with a cloud chamber (see below), observed tracks similar to those left behind by electrons but curving in the opposite direction in a magnetic field. In the same year Chung-Yao Chao, a graduate student at Caltech in USA, used a radioactive source to study scattering of gamma rays in lead and found that his results on the amount of scattering in lead didn't agree with the theoretical predictions. This was later understood as a consequence of the formation of a pair of an electron and a positron. Neither Skobeltsyn nor Chao were able to interpret their observations and the phenomenon was not pursued by them.

In 1932 the American physicist Carl Anderson performed studies of cosmic rays using a cloud chamber. A cloud chamber is a cylinder filled with supersaturated vapour, where the bottom of the cylinder consists of a piston. A picture of the cloud chamber used by Anderson is shown in Figure 4.3 (left). By rapidly pulling the piston back, an adiabatic expansion is achieved, by which the temperature of the vapour is decreased. If a charged particle is traversing the chamber at this moment, it causes condensation of the supersaturated vapour into drops along the path of the ionizing particle. In addition to the cloud chamber a typical experimental set-up included a camera and a Geiger-Mueller (GM) tube, where the GM-tube registered the passage of a particle and triggered the expansion of the cloud chamber and activated the camera. Anderson's chamber was placed vertically inside an electromagnet in order to be able to measure the curvature of charged particles.

Anderson noticed, when inspecting his results, that in cosmic ray showers there were both negatively and positively charged particles as seen from their curvature in the magnetic field. By measuring the density of drops along the track he concluded that the mass of the positively charged particles was about the same as that of the electron. In order to make sure that these particles were not just electrons moving in the opposite direction he inserted a lead plate radially inside the cloud chamber, by which the curvature of the tracks could be measured, before and after the particles traversed the lead plate. In traversing the lead plate the particle will lose momentum and the curvature will change. A photograph of a positron passing the chamber is shown in Figure 4.3 (right).

### 4.2.4 The Experimental Discovery of the Neutron

In 1911 Rutherford discovered that the atom contained a nucleus, which carried almost the whole mass of the atom. However, it was soon realized that the number of protons (= the number of electrons) in the nucleus could not account for the total mass of the atom. For example  ${}^4_2\text{He}$

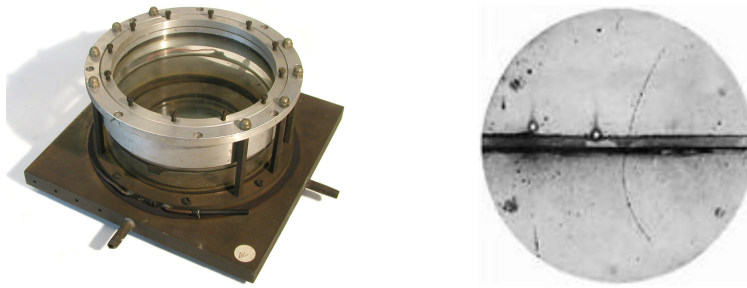


Figure 4.3: A picture of the cloud chamber used by Anderson and Neddermeyer (left) and a picture of a positron track, where the positron has lost some momentum in traversing the lead plate in the middle (right).

consists of 2 protons but have an atomic mass of 4. In order to account for this discrepancy Rutherford proposed that a proton and an electron could form a pair, which essentially had the mass of the proton but its positive charge was cancelled by the electron, and that such pairs were present in the nucleus. He called these particle pairs *neutrons* and instructed his student James Chadwick to find evidence for their existence.

In 1930 the German physicist Walter Bothe and his student Herbert Becker performed experiments where they bombarded a Beryllium target with  $\alpha$ -particles from a polonium source and found that an unusually penetrating radiation was produced. Since the radiation was not influenced by electric fields, it was initially assumed to be gamma radiation, although it was much more penetrating compared to any gamma radiation detected so far. In the following years the French physicists Irène and Frédéric Joliot-Curie studied this radiation as it interacted with paraffin and found that it knocked out high velocity protons from the hydrogen atoms in the paraffin. These protons were detected in a Geiger counter. An illustration of their apparatus is shown in Figure 4.4. The conclusion of Joliot-Curie was that this radiation had to be very high energy photons.

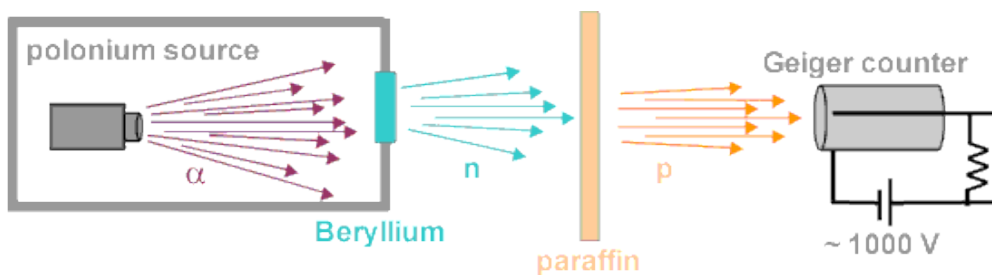
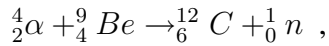


Figure 4.4: The experimental set-up used to study the radiation which later turned out to be neutrons.

This explanation, however, didn't convince Chadwick, who realized that a massless photon would not be able to kick out the heavy proton in the paraffin, and he started to perform similar experiment himself. He was able to determine the velocity of the emitted protons and performed kinematic calculations on the process:



where  $n$  so far stands for the neutral radiation. He, thereby, found that the mass of the of the neutral radiation was almost exactly the same as that of the proton. In 1932 he, accordingly, proposed that the observed neutral radiation consisted of neutrons rather than high energy photons. In 1934 it became clear that the neutron was not a bound state of a proton and an electron but a new fundamental particle.

## 4.2.5 The Experimental Discovery of the Muon

The muon was discovered in 1936 by the American physicists Carl Anderson and Seth Neddermeyer in their studies of cosmic-ray showers, using the same cloud chamber as in the discovery of the positron. They performed measurements both on a 4000 meter high mountain and at sea level. Cosmic muons are created in collisions of cosmic-ray particles, primarily proton emitted by stars, with atoms in the upper atmosphere. Two kinds of particles were identified in the cloud chamber, of which one kind gave rise to secondary showers of electrons, positrons and photons in their interactions with the lead plate, typical for an incoming electron. The other kind of particle easily penetrated the lead plate. It was noticed that the penetrating particles had a curvature in the magnetic field which was less than that expected for an electron but greater than that of a proton. From the way it was bent in the magnetic field it could be concluded that the charge of the particle was negative and assuming that the charge was equal to that of the electron, its mass had to be between that of the electron and the proton. Figure 4.5 shows a cloud chamber picture of a muon track.

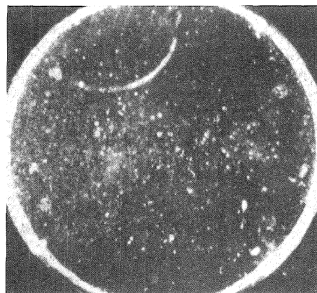


Figure 4.5: A cloud chamber picture of Anderson showing a muon track.

It was excluded that the new particle was just a heavier electron by the non-observation of the decay into the familiar electron and a photon. Also the energy loss of the new particle in the lead plate was less than expected from the predictions of QED. Another peculiarity was that the number of such particles was smaller at sea level than on the tip of the mountain, which led to the conclusion that these particles are not stable, but they decay into more stable particles. Consequently it had to be a completely new particle, which was given the name muon. Shortly after the announcement of Anderson and Neddemeyer, this discovery was confirmed by the American physicists J.C. Street and E.C. Stevenson.

The first assumption was that the new particle was identical to that, proposed by the Japanese physicist Hideki Yukawa, to be the mediator of the strong force, but it turned out that its interaction with matter was much to weak.

Thus, the discovery of the muon was the first indication of further families of quarks and leptons.

## 4.2.6 The Experimental Discovery of the Pion

After the introduction of light quanta (photons) by Einstein in order to explain the photoelectric effect, the description, at that time, of interactions between charged particles had to be modified. The development of Quantum Field Theories (QFT) started in the 1920-ies and this theory describes the interaction of electrically charged particles as an exchange of virtual photons. In 1935 Yukawa proposed that the strong nuclear force is also mediated by a force carrier. In order to explain the short range of the strong force the mediator particle needs to have a mass. This can be estimated from the Heisenberg uncertainty principle, which gives that the range of the force is inversely proportional to the mass of the force carrier.

$$\Delta E \cdot \Delta t \geq \hbar ,$$

where  $\Delta E \approx m c^2$  and  $m$  is the mass. But the range  $R$  is:

$$R = \Delta t \cdot c$$

$$\Rightarrow R \approx (\hbar \cdot c) / m$$

If we assume that the range of the strong force is  $R = 10^{-15}$  meter = 1 fermi then we get:

$$\Rightarrow m_{\pi} \approx (\hbar \cdot c) / R = 197 \text{ MeV}$$

The prediction of Yukawa was thus that the exchange particle should have a mass in the range 100 - 200 MeV. Since the mass of the mediator particle was in the range between the electron and proton mass it was given the name *meson*, meaning 'middle' or 'intermediate'.

As the muon was discovered it was initially called the  $\mu$ -meson, since its mass was in the range predicted by Yukawa. However, later experiments showed that this particle did not interact strongly and could therefore not be a meson but was a lepton.

It would take until 1947 before the first evidence of a meson was given, by the British Physicist Cecil Powel et al., from their studies of atmospheric cosmic rays using photographic emulsions. Until then the technique of photographic emulsions was sparsely used but Powel developed it into a powerful tool in the studies of cosmic rays. Cosmic pions are produced through the interaction of mainly cosmic protons with atoms in the upper atmosphere. However, due to nuclear absorption and decay into muons, only a tiny fraction of the pions reaches the sea level. Thus, the emulsions had to be exposed to the cosmic radiation for long periods of time in sites located at high altitudes. Charged particles interact with the material (silver bromide) in the emulsion, which through the development of the photographic plate appear as black tracks. The subsequent inspection of the emulsions revealed some tracks which indicated a meson decaying into another meson, and they were therefore called 'double meson' tracks. In reality it was a pion decaying into a muon and a neutrino. One of the first pictures of a pion decaying into a muon is shown in Figure 4.6.

The interaction and Coulomb scattering of charged particles in the emulsion depend on their masses, such that a heavier particle gives a thicker track (more grains) and is scattered less than a lighter particle of the same momentum. This was used in the subsequent inspection of the

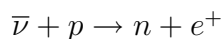


Figure 4.6: A photograph of a pion decay into a muon and a neutrino recorded in a nuclear photographic emulsion.

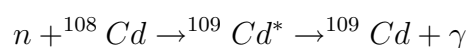
photographic plates and it was found that the distribution of the grain-density was less than that expected from protons. From comparing the the grain density of the recorded tracks with that expected by protons, the mass of the new particle was estimated to lie between 50 and 115  $MeV$ , with large uncertainties. The number of Coulomb scatterings of the new particle was three times higher than that of a proton with the same range in the emulsion. Calculations gave a mass of  $175 \pm 100 MeV$ . Although the mass of the particle could not be determined very accurately it was clear that a new kind of particle had been discovered and it was given the name  $\pi$ -meson or pion.

#### 4.2.7 The Experimental Discovery of the Electron Neutrino

The electron neutrino was introduced by Pauli in 1930 to explain the missing energy in  $\beta$ -decays,  $n \rightarrow p + e^- + \bar{\nu}_e$ . The experimental evidence for the existence of the electron neutrino was given by the American physicists Frederick Reines and Clyde Cowan more than 20 years later. They used the high flux of anti-neutrinos ( $10^{13} s^{-1} cm^{-2}$ ) from beta decays in a reactor to hit a tank of water in which photon detectors where positioned. Some of the anti-neutrinos will interact with the protons in the water and create a neutron and a positron, according to:



The positron will annihilate with an electron in the water and thereby two photons are emitted, which can be detected by the photon detectors. However, this was not an unambiguous proof of the neutrino detection but also the emission of a neutron had to be verified. By mixing cadmium chloride into the water the neutron could be absorbed by the  $^{108}Cd$  atom and produce an excited state of  $^{109}Cd$  which subsequently decays by emitting a photon with a delay of  $5 \mu s$ .



This provided a distinctive signature for the neutrino reaction with three photons in the final state and thus the existence of the neutrino was experimentally proven.

## 4.2.8 The Experimental Discovery of the Muon Neutrino

In 1962 the American Physicists Leon Lederman, Melvin Schwartz, Jack Steinberger et al. performed an experiment at the Brookhaven National Laboratory (BNL) with the aim to demonstrate that there are more than one type of neutrino particles. This experiment was motivated by the non-observation of the decay  $\mu \rightarrow e + \gamma$ , which could only be explained if there was one type of neutrino coupled to the muon and another type coupled to the electron.

The advantage of performing neutrino experiments at particle accelerators, compare with reactors, is that a high flux neutrino 'beam' can be created. The neutrino particles were produced by letting 15 GeV protons, from the Brookhaven accelerator, impinging on a beryllium target and thereby producing a flux of various particles, moving in essentially the same direction as the incoming protons. Over the flight distance up to a shielding wall of iron upstream of the beam, the pions produced decayed according to:

$$\pi^\pm \rightarrow \mu^\pm + \nu/\bar{\nu} ,$$

This wall was thick enough to absorb the strongly interacting particles by nuclear reactions and muons through ionization processes. Some of the neutrinos penetrating the shielding wall occasionally interacted in the detector causing the following reactions:

$$\bar{\nu} + p \rightarrow \mu^+(e^+) + n$$

$$\nu + n \rightarrow \mu^-(e^-) + p$$

The detector consisted of *spark chambers* as tracking detector and the signature of the above reactions was a lepton track with no incoming track connecting to it. A spark chamber consists of a stack of metal plates (in this case aluminum plates), separated by typically 1 cm, contained in a gas filled box. When a charged particle passes the chamber, it ionizes the gas and if a voltage is applied between the plates, at the moment of a particle passage, sparks are developed between the metal plates along the particle trajectory. Scintillation counters (see Section 7.5.1) are placed at the entrance and exit of the chamber to announce the passage of a particle, so that the high voltage is switched on long enough for the sparks to develop. The pattern of sparks is recorded on photographic film by cameras from different directions, in order to get a three-dimensional view of the tracks. These pictures were later on studied and evaluated. Such detectors are no longer in use but are replaced by electronics detectors where the information is stored in computers. In Figure 4.7 the principle of how a spark chamber is working is shown in the lefthand figure and a real track passing a spark chamber in the righthand figure.

In case there is only one kind of neutrino particle, the interactions of the neutrinos, produced in the pion decays, should produce equal amounts of muons and electrons, whereas in the case there would be one muon-neutrino and one electron-neutrino, it was not expected to observe any electrons at all. The signature of a muon in the spark chamber is a straight track, whereas an electron produces a shower of particles, through interactions with the plates in the spark chamber. In their data they identified 34 muon events, out of which 5 were considered to originate from cosmic-ray background. Thus in case  $\nu_\mu = \nu_e$  they would have expected 29 events with electron showers. None was observed and consequently the conclusion was that  $\nu_\mu \neq \nu_e$ .





Figure 4.7: The general build up of a spark chamber (left) and a real track in a spark chamber (right).

### 4.2.9 The neutrino mass

Attempts have been made to determine the mass of the electron neutrino by measuring the energy spectrum of electrons emitted in  $\beta$ -decays, which must fulfill:

$$m_e c^2 < E_e < (m_n - m_p - m_{\nu_e}) c^2$$

For example the decay of tritium,  ${}^3\text{H} \rightarrow {}^3\text{He} + e^- + \bar{\nu}_e$  ( $pnn \rightarrow ppn + e^- + \bar{\nu}_e$ ), has been studied, but so far the results of the measurements have only provided upper limits on the mass. The presently best limit gives  $m_{\nu_e} < 2.2$  eV (Mainz 2005).

If the neutrino particles have masses it is possible for them to undergo *flavour oscillations*, which means that although they are created as a certain flavour eigenstate they might oscillate into a different flavour eigenstate after some time. The explanation is that the neutrino is created as a *flavour eigenstate* but propagate through space as a superposition of *mass eigenstates*. Thus, the flavour eigenstates  $\nu_e$  and  $\nu_\mu$  are expressed as combinations of the mass eigenstates  $\nu_1$  and  $\nu_2$ , which propagate with slightly different frequencies due to their different masses. This leads to a phase shift that depends on the distance the neutrino has travelled such that at some distance the combination of mass eigenstates will no longer correspond to a pure neutrino flavour.

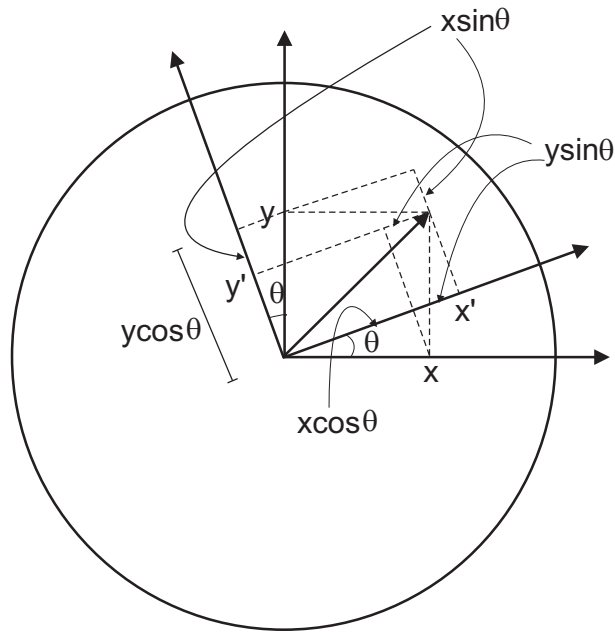
The two neutrino flavour system,  $\nu_e$  and  $\nu_\mu$ , would be connected to the mass eigenstates through the mixing matrix as shown in Figure 4.8.

$$\begin{pmatrix} \nu_\mu \\ \nu_e \end{pmatrix} = \begin{pmatrix} \cos \theta & \sin \theta \\ -\sin \theta & \cos \theta \end{pmatrix} \begin{pmatrix} \nu_1 \\ \nu_2 \end{pmatrix}$$

Figure 4.8: The neutrino flavour eigenstates and the mass eigenstates are related through the Cabibbo mixing matrix.

such that:

$$\begin{aligned} \nu_\mu &= \nu_1 \cos \theta + \nu_2 \sin \theta \\ \nu_e &= -\nu_1 \sin \theta + \nu_2 \cos \theta \end{aligned}$$



$$x' = x \cos\theta + y \sin\theta$$

$$y' = y \cos\theta - x \sin\theta$$

Figure 4.9: *The relation between the coordinates of two rotated coordinate systems.*

where  $\theta$  is the mixing angle. This is equivalent to the relation between the coordinates in two rotated coordinate systems as illustrated in Figure 4.9.

Conversely, the mass eigenstates can be expressed as a combination of the flavour eigenstates,  $\nu_e$  and  $\nu_\mu$ .

Let us assume that we start out with a beam of muon neutrinos, with the flavour eigenstate represented by a plane wave function. However, the flavour eigenstate is a combination of two mass eigenstates,  $\nu_1$  and  $\nu_2$ , also represented by plane wave functions. At  $t = 0$  the wave functions of the mass eigenstates will add up to the full wave function for the pure flavour  $\nu_\mu$  (100% probability to have  $\nu_\mu$ ), since they are in the same phase. On the other hand at  $t = 0$ , the mass eigenstates will cancel for the flavour  $\nu_e$  (0% probability to have  $\nu_e$ ), since they for this flavour eigenstate are in opposite phase. Due to the fact that the mass eigenstates travel at different frequencies, such that the heavier one,  $\nu_1$ , is slower than the lighter one,  $\nu_2$ , we will after some distance no longer have a pure flavour eigenstate but a little less of  $\nu_\mu$  and a non-zero contribution of  $\nu_e$ . It means that the probability to identify the flavour state as a  $\nu_\mu$  is less than 100% and to identify the flavour state as a  $\nu_e$  becomes bigger than 0%. At an even longer distance the mass eigenstate  $\nu_1$  has lagged behind so much with respect to  $\nu_2$  that  $\nu_1$  and  $\nu_2$  are completely out of phase for the flavour eigenstate  $\nu_\mu$  and thus will cancel. However, for the flavour eigenstate  $\nu_e$  the mass eigenstates are in phase and will add up to the full wave function representing this flavour eigenstate. At this point the muon neutrino has oscillated into an electron neutrino. The propagation with time of the probability for the flavour eigenstates  $\nu_\mu$  and  $\nu_e$  are illustrated in Figure 4.10.

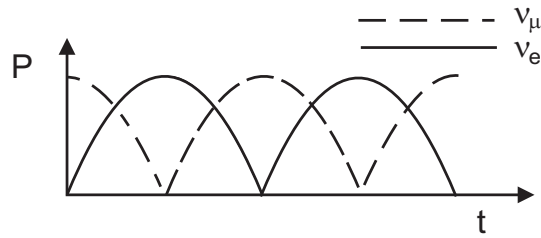
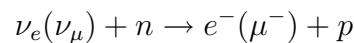


Figure 4.10: *The probability variation with time of the neutrino flavour eigenstates  $\nu_\mu$  and  $\nu_e$ .*

The only way to determine the flavour of a neutrino is through its interaction, where  $\nu_e$  always goes together with an electron and  $\nu_\mu$  goes together with a muon. Thus, through the charged leptons appearing in the reaction the flavour of the neutrino is known.

Although it has not so far been possible to measure the masses of the neutrino particles, we know that they must have a small mass since neutrino oscillations have been observed. The experimental evidence for neutrino oscillations was given in 1978 by the underground neutrino experiment Super-Kamiokande in Japan, which observed the neutrino flux from cosmic particles. Cosmic particles interact with the atmosphere and produce secondary particles (mostly pions and kaons) of which some may decay weakly and give rise to mainly muon neutrinos. These neutrinos normally penetrate the earth, whereas all other particles are absorbed. However, due to the small but finite probability for weak interactions, a few of the neutrinos will occasionally interact with the underground detector. If the detector contains water the neutrino will interact with the nucleons according to:



The leptons will travel with a speed higher than the speed of light in the water and thereby emit so called Cherenkov radiation, which can be detected by photosensitive detectors in the water. From measuring the emission angle of Cherenkov radiation the electrons and muons can be distinguished (see Section 7.6.3).

In the 1970's it was experimentally found that the number of  $\nu_e$  emitted from the sun was only about one third of what was expected. A possible explanation could come from the existence of neutrino oscillations. In 2002 it was found at the Sudbury Neutrino Observatory (SNO), in Ontario, Canada, that some of the electron-neutrinos emitted by nuclear reactions in the core of the Sun changed type as they travelled through the Sun, which is only possible in case the neutrino particles have mass. Thus, this was an independent result that confirmed neutrino oscillations.

The observation of neutrino oscillations and from the discussion above it is clear that the neutrinos must have a small mass. However, so far the experimental technique has not been accurate enough to measure the masses.

#### 4.2.10 The Experimental Discovery of Charm

Although the existence of the  $c$ -quark had been predicted already in 1964, by the American physicists James Bjorken and Sheldon Glashow, using the arguments given in Section 3.3.7, it

was quite a surprise when a narrow resonance with a mass of about 3.1 GeV was observed by two experiments independently in 1974. The remarkable property was that the resonance peak was about thousand times narrower than those of other mesons in the same mass range. Thus, the lifetime of this particle was thousand times longer than expected.

One of the experiments, at the  $e^+e^-$ -collider SPEAR at Stanford, studied  $e^+ + e^- \rightarrow \text{hadrons}$  by performing an energy scan, increasing the center-of-mass energy in small steps. Their detector was a cylindrical general purpose detector, surrounding the collision point. The layout of the detector was typical for detectors at colliders, with layers of different types of detectors to measure the various properties of the particles produced. At the point where the energies of the colliding electron and positron beams add up to the mass of the resonance, the threshold for producing this resonance is reached and a peak in the cross section is observed. The cross section for the resonance particle to decay into hadrons is shown in Figure 4.11a.

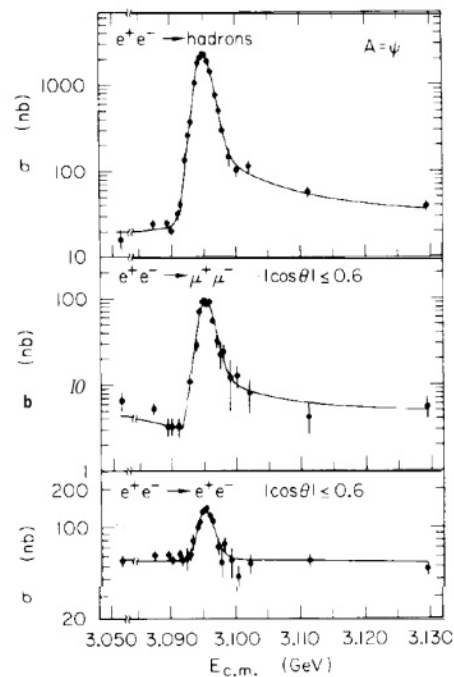


Figure 4.11: Cross section versus energy for a) hadron final states, b)  $\mu^+\mu^-$  final states and  $e^+e^-$  final states.

A sharp rise in the cross section can be observed at the energy of 3.1 GeV, indicating the production of a resonance particle. The mass resolution is determined by the energy spread in the colliding beams and the measured width at half maximum (FWHM: Full Width Half Maximum) of the resonance was determined to be  $\sigma_{FWHM} \leq 1.3 \text{ MeV}$ . The natural width of the resonance is smaller than this spread and a fit to the resonance peak, taking the mass resolution into account, gave a value of the natural width  $\Gamma_\psi \sim 69 \text{ keV}$ , which corresponds to a lifetime of  $7 \cdot 10^{-21} \text{ sec}$ .

The  $e^+ + e^- \rightarrow \text{hadrons}$  process was assumed to proceed through the one photon intermediate state, as shown in Figure 4.12, but what was the decay mechanism? Further, it was hard to

understand how this resonance could have such a long lifetime without involving a new quantum number (compare with the decay of  $V'$ -particles in Section 2.11).

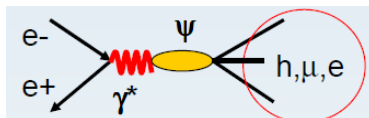


Figure 4.12: Production of the  $J/\Psi$ -particle and its decay into hadrons,  $e^+e^-$ - and  $\mu^+\mu^-$ -pairs

After having observed this peak in the hadron channel the Stanford group also studied the decays into  $\mu^+\mu^-$ - and  $e^+e^-$ -pairs and the production cross sections for the final states are shown in 4.11b and c, respectively. The observed resonance state was named  $\Psi$  by the Stanford group.

The resonance particle was interpreted as a bound state of a charm quark and an anticharm quark ( $c\bar{c}$ ). A particle-antiparticle bound state have the suffix *-onium* in its name such that a bound  $c\bar{c}$  states is called *charmonium*.

In the other experiment, at Brookhaven National Laboratory, a beam of 24 GeV protons was brought to hit a Beryllium target and a search for new particles, which decayed into  $e^+e^-$ - and  $\mu^+\mu^-$ -pairs, was performed using a two arm magnetic spectrometer. The invariant mass spectrum for  $e^+e^-$ - and  $\mu^+\mu^-$ -pairs in the final state was reconstructed. Figure 4.13 shows the mass spectrum for  $e^+e^-$ -pairs at two settings of the spectrometer magnets. In both cases a sharp peak can be observed at a mass of about 3.1 GeV.

The mass resolution is given by the measuring accuracy of the spectrometer and was estimated to  $\sigma_M \sim 20 MeV$ . The Brookhaven group assigned the name  $J$  to the particle state. The process in the fixed target experiment at Brookhaven was essentially  $p + p \rightarrow J + X \rightarrow e^+(\mu^+) + e^-(\mu^-) + X$ , where a quark from one proton annihilate with an antiquark (from the sea) from the other proton and produce a virtual photon, which create a bound  $c\bar{c}$ -state, where the two quarks exchange gluons. After a short period of time, the  $c$  and  $\bar{c}$  quarks annihilate into a virtual photon, which subsequently decays into an  $e^+e^-$ - or  $\mu^+\mu^-$ -pair, as described by the Feynman diagram shown in Figure 4.14.  $X$  represents the addition final state particles produced by the spectator quarks, not shown in the diagram. Eventually the mass of the  $J/\Psi$ -particle was determined to be 3096 MeV.

Normally one would expect the  $J/\Psi$ -resonance, consisting of a bound  $c\bar{c}$ -state, to decay into particles, which contain a charm-quark and an anticharm-quark, respectively. Such particles have a charm quantum number which is different from zero and are called *open charm* states. The lightest particles of this kind are the  $D$ -mesons. The production of the  $J/\Psi$  particle from  $e^+e^-$ -collisions and its subsequent decay into a pair of  $D$ -mesons is illustrated by the Feynman diagram of Figure 4.15.

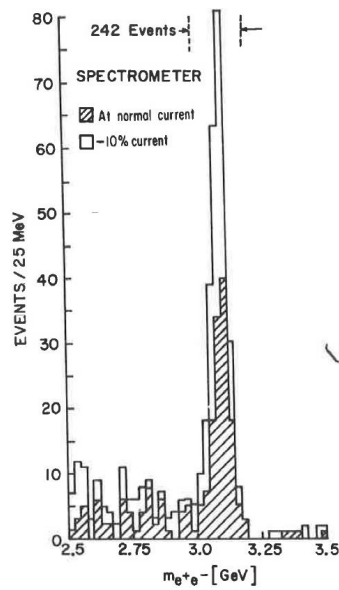


Figure 4.13: Mass spectrum of  $e^+e^-$ -pairs from proton-proton collisions.

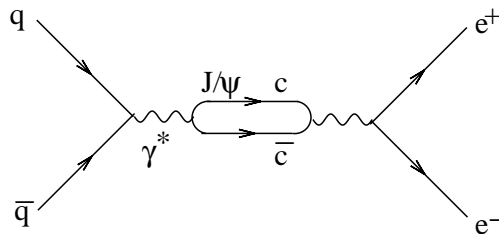


Figure 4.14: Feynman diagram describing the production of an  $e^+e^-$ -final state via the decay of a virtual intermediate  $J/\Psi$ -meson produced in a quark-antiquark interaction (proton-proton collision).

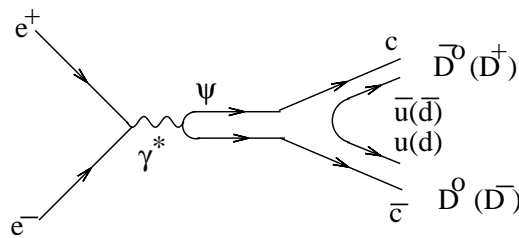


Figure 4.15: Feynman diagram describing the production of a  $\Psi$ -meson from an  $e^+e^-$ -collision, via a virtual intermediate  $\Psi$ -state and its subsequent decay into a pair of  $D$ -mesons.

This decay is however not possible for the  $J/\Psi$  since the mass of the  $D$ -meson is  $1.86 \text{ GeV}$  and therefore it would require a particle with a mass of at least  $3.72 \text{ GeV}$  to produce this decay,

whereas the mass of the  $J/\Psi$  is only  $3.1 \text{ GeV}$ . Instead the  $J/\Psi$  decays predominantly via three gluons into hadrons, as shown in Figure 4.16. This, however, gives a suppression by a factor  $\alpha_s^3$ , which results in the long lifetime.

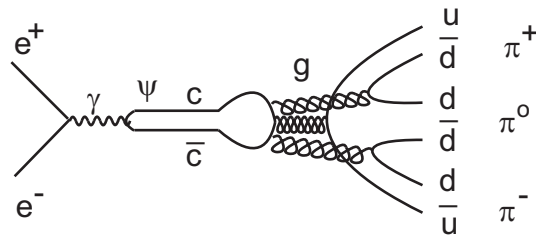


Figure 4.16: Feynman diagram describing the production of a three pion final state from an  $e^+e^-$ -collision, via a virtual intermediate  $J/\Psi$ -state.

### 4.2.11 Charmed Particles

Since the  $J/\Psi$  particle consists of a  $c\bar{c}$  pair, the net charm content (charm quantum number) is zero. There are several additional  $c\bar{c}$  states, which are excited states of the  $J/\Psi$  particle. All these states are so called *charmonium states*. In the subsequent measurements, performed at the SPEAR collider at Stanford and the DORIS collider at DESY, several of these excited  $\Psi$ -states were found. The first one  $\Psi(3686)$  was found only ten days after the discovery of  $J/\Psi$ . However, the mass of this state was just below the threshold for open charm production. Instead the  $\Psi(3686)$  could decay into a  $J/\Psi(3096)$  by the  $c$ - or  $(\bar{c})$ -quark emitting a gluon, which create a quark-antiquark pair and together with a quark-antiquark pair from the vacuum form a meson anti-meson pair, as shown in Figure 4.17

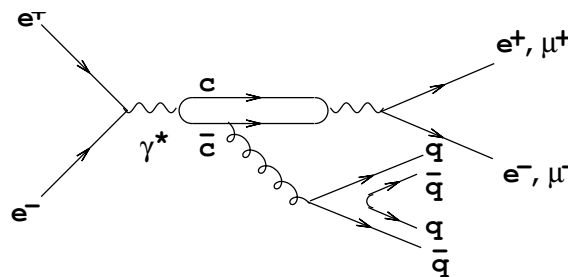


Figure 4.17: Feynman diagram showing the production of a  $\Psi(3686)$ -meson from  $e^+e^-$  collisions and its decay into a  $J/\Psi$  and a meson anti-meson pair. The  $J/\Psi$  subsequently decays into an  $e^+e^-$ - or a  $\mu^+\mu^-$ -pair.

The second-lightest quark compared to the  $c$ -quark would be the  $s(\bar{s})$ -quark, which together with a  $\bar{u}(u)$  quark creates a  $K$ -meson. However, the  $K$ -meson has a mass of around  $500 \text{ MeV}$ , so that the masses of the final state particles add up to around  $3.2 \text{ GeV}$ . Thus, the process  $e^+e^- \rightarrow \Psi(3686) \rightarrow J/\Psi(3096)K^+K^-$ , at the threshold, i.e. where the  $\Psi(3686)$  is produced at rest, can not happen. The remaining possibility for  $\Psi(3686)$  to decay would be for the emitted

gluon to create a  $d\bar{d}$  pair and then  $K$ -mesons in the final state would be replaced by  $\pi$ -mesons. The mass of the  $\pi$ -meson is around  $140 \text{ MeV}$ , which means that the required mass for this decay would be around  $3.4 \text{ GeV}$  and thus the  $\Psi(3686)$  is allowed to decay into  $J/\Psi\pi^+\pi^-$ .

The next higher  $\Psi$ -state is  $\Psi(3770)$  and this would thus allow for a decay into  $D$ -mesons. As already mentioned in the previous section, particles which contain combinations of charm (anticharm) quark(s) with lighter quark(s) (antiquark(s)) are called *charmed particles*, since they have a net charm quantum number. The charmed mesons and baryons can be seen in the multiplets shown in Figure 3.51.

An example of a possible decay of a  $D$ -meson is:

$$D^- \rightarrow K^+ + \pi^- + \pi^- ,$$

and the corresponding Feynman diagram is shown in Figure 4.18.

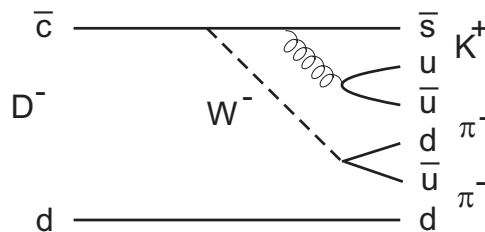


Figure 4.18: Feynman diagram showing the decay of a  $D^-$ -meson into a  $K^+\pi^-\pi^-$  final state.

The  $c$ -quark decays predominately into an  $s$ -quark in weak decays, whereas the decay into a  $d$ -quark is suppressed. Thus, the  $D$ -mesons predominantly decay into final states with  $K$ -mesons since  $c \rightarrow s$  is a Cabibbo favoured transition.

With the discovery of the  $c$ -quark we had two complete families of quarks and leptons as shown in Figure 4.1.

flavour	charge	spin
$\nu_e \quad \nu_\mu$	0	1/2
$e \quad \mu$	-1	1/2
$u \quad c$	2/3	1/2
$d \quad s$	-1/3	1/2

Table 4.1: The situation of known quarks and leptons after the discovery of the  $c$ -quark.

## 4.2.12 The Discovery of the Tau-lepton

Shortly after the discovery of charm the experiment at SLAC reported the observation of anomalous events with a muon and an electron in the final state and nothing else, i.e.  $e^+ + e^- \rightarrow e^\pm + \mu^\mp + \text{missing energy}$ . Since such processes violate lepton number conservation they



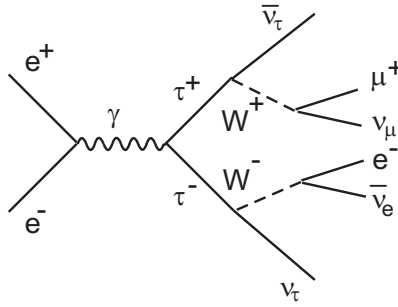


Figure 4.19: Feynman diagram describing the production of a pair of  $\tau$ -mesons from an  $e^+e^-$ -collision, and their subsequent decay into a lepton final state.

should not be able to happen. On the other hand, if a new heavy lepton, the  $\tau$ -lepton, was introduced, the lepton number conservation could be restored and the decay would be as shown by the Feynman diagram of Figure 4.19,

The four neutrinos in these decays are responsible for the missing energy.

The energy threshold needed to produce a  $\tau^+\tau^-$ -pair was 3.6 GeV, implying a mass of the  $\tau$ -lepton of about 1.8 GeV. Due to its large mass it can, in contrast to electrons and muons, also decay into hadrons, i.e. the emitted  $W$  decays into a quark-antiquark pair.

Since the electron and muon have their own neutrino particles,  $\nu_e$  and  $\nu_\mu$ , respectively, it was assumed that also the  $\tau$ -lepton should have its own neutrino,  $\nu_\tau$ . The evidence for its existence would, however, take until 2002 (see Section 4.2.13).

With this assumption we would have three families of leptons but only two families of quarks. This is summarized in Table 4.2.

flavour	charge	spin
$\nu_e \quad \nu_\mu \quad \nu_\tau$	0	1/2
$e \quad \mu \quad \tau$	-1	1/2
$u \quad c$	2/3	1/2
$d \quad s$	-1/3	1/2

Table 4.2: The situation of known quarks and leptons after the discovery of the  $\tau$ -lepton.

### 4.2.13 The Experimental Observation of the Tau Neutrino

In 2002 the Donut-experiment (Direct Observation of the NU Tau) at Fermi-lab reported the direct observation of the  $\tau$ -neutrino. The experiment used an 800 GeV proton beam to create a beam of neutrinos. This was obtained by directing the high-energy proton beam onto a block of high-density material, like tungsten. When protons collide with atoms in the target, many different kinds of particles emerge, including neutrinos. Very strong magnets were used to deflect the charged particles from the beam. The remaining particles, except the neutrinos,

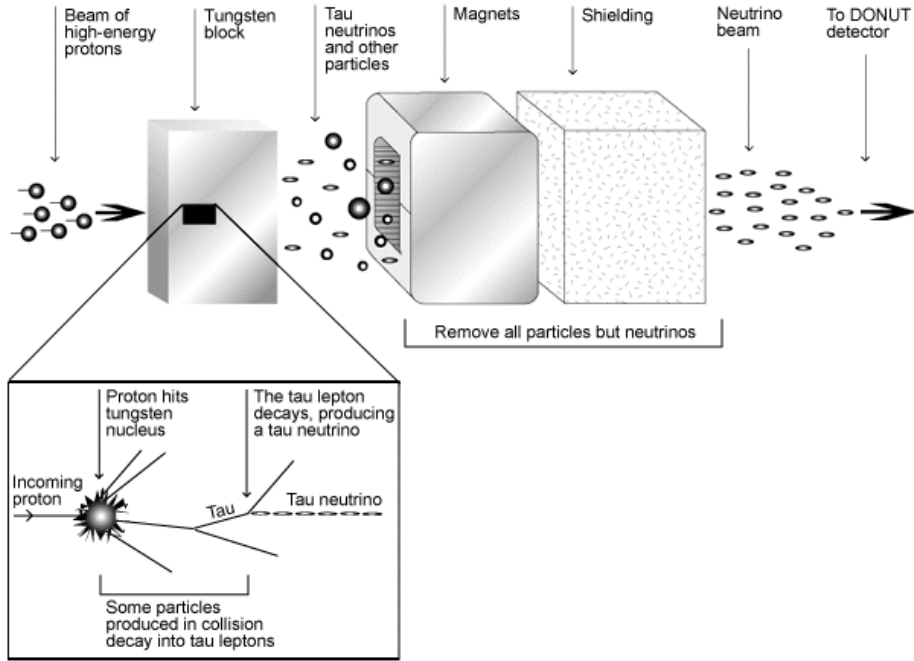


Figure 4.20: The production of a neutrino beam at Fermi-lab used for a direct observation of the tau-neutrino

were absorbed in a fifteen meter deep shielding wall. The production of the neutrino beam is illustrated in 4.20.

The occasional interaction of the  $\nu_\tau$ :s in the detector produce  $\tau$ -leptons, according to:

$$\nu_\tau + n \rightarrow \tau^- + p$$

The produced  $\tau$ -lepton only has a range of a few millimeter before it decays and give a very clear signature in form of a short track with a kink.

#### 4.2.14 The Discovery of the $b$ -quark

The discovery of the  $\tau$ -lepton indicated that there should be another family of quarks and a search for a third quark family was initiated. In an experiment at Fermi-lab, led by Leon Lederman, similar to that of the Brookhaven experiment, at which  $J/\Psi$  was observed, 400 GeV protons were directed towards a fixed target of copper and platinum, respectively.

$$p + N \rightarrow \mu^+ + \mu^- + X \quad ,$$

where N represents a nucleon and X the additional particles produced in the reaction.

Final states containing a  $\mu^+ \mu^-$ -pair were selected. The produced muons were detected in a double arm magnetic spectrometer. Each of the two spectrometer arms contained a long Beryllium filter, which absorbed the strongly interacting particles, whereas the muons were penetrating

with a minimum of scattering. The muon trajectories were measured in Multi Wire Proportional Chambers (see Section 7.5.2) and their momenta were determined through their deviations in the two spectrometer magnets. A search for peaks in the  $\mu^+\mu^-$ -spectrum, with invariant masses greater than  $5 \text{ GeV}$ , was performed. The challenge was to identify a few interesting muon-pairs on top of a huge background. The invariant mass spectrum of  $\mu^+\mu^-$ -pairs is shown in Figure 4.21. This is the original plot that was shown in the announcement of the discovery. As can be seen there is a peak at around  $10 \text{ GeV}$ , which after a more detailed analysis turned out to give a better agreement with a fit of two peaks as shown in Figure 4.22, where the background has been subtracted. The second peak is an excited resonance state.

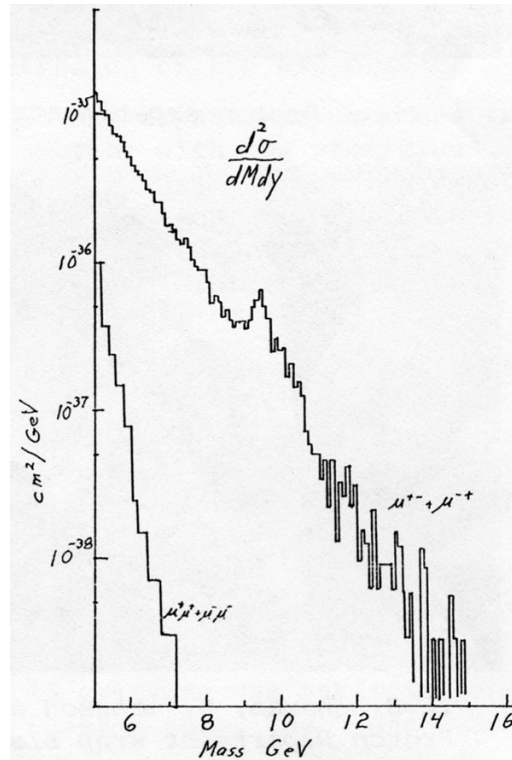


Figure 4.21: *The differential cross section as a function of the invariant mass of a two-muon (four-muon) final state. In the invariant mass spectrum of the two-muon final state a peak at around  $9.5 \text{ GeV}$  can be observed, which indicates a new resonance particle (the  $\Upsilon$  particle).*

The resonance was assumed to be a bound state of a new quark and its antiquark and was called the  $\Upsilon$ -particle (upsilon-particle). In the following year several  $\Upsilon$  resonance states were found from measurements with much higher precisions in  $e^+e^-$  collisions at DESY. By accurately measuring the widths of the resonance peaks for the ground state ( $\Upsilon$ ) and the first excited state ( $\Upsilon'$ ), it could be concluded that these resonances must contain a new quark of charge  $-1/3$ . This was called the bottom quark or the  $b$ -quark with a mass around  $4.5 \text{ GeV}$ . Figure 4.22 shows the resonance peaks as measured at Fermilab, compared to those measured at the  $e^+e^-$ -collider DORIS at DESY. The difference in mass resolution is striking.

The  $\Upsilon$ -particle has the  $b$  quantum number equal to zero since it is a bound  $b\bar{b}$  state. The  $b$ -quark adds another dimension in the quantum number space, extending the multiplets of mesons and

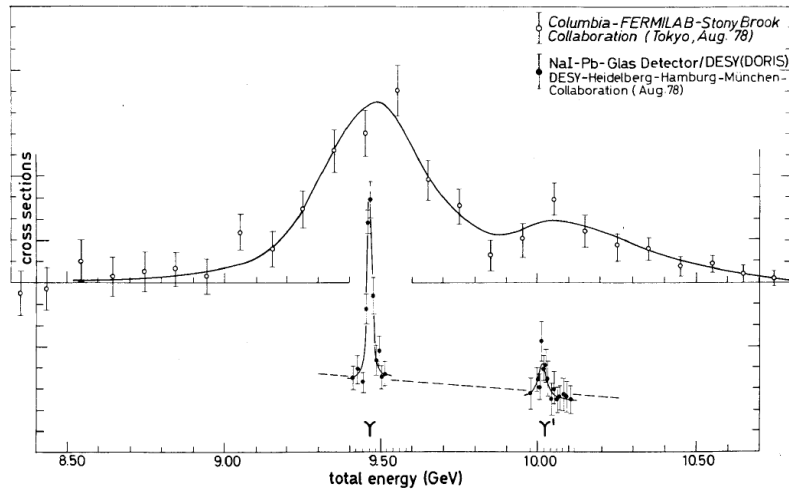


Figure 4.22: The  $\Upsilon$  resonance peaks as measured in hadron collisions and in electron-positron collisions.

baryons. Thus, B-mesons are  $\bar{b}q(b\bar{q})$  states, where  $q(\bar{q})$  represents a lighter quark (anti-quark). Thus, the combination  $\bar{b}u$  forms a  $B^+$ -meson, whereas a  $b\bar{u}$  pair gives rise to a  $B^-$ -meson. A  $\bar{b}d$ -pair corresponds to a  $B^0$ -meson and a  $b\bar{d}$ -pair gives a  $(\bar{B}^0)$ -meson. If the  $\bar{b}(b)$ -quark is combined with an  $s(\bar{s})$ - or  $c(\bar{c})$ -quark the notation is  $B_s$  and  $B_c$ , respectively. B-baryons are three-quark states with one or more  $b(\bar{b})$  quark(s) and to indicate this, the notation is for example  $\Lambda_b^0$ , which has the quark content  $udb$ .

Particles containing a  $b$ -quark tend to decay into particles which contain a  $c$ -quark, since the decay  $b \rightarrow c$  is Cabibbo favoured compared to  $b \rightarrow u$ . However, as seen from the full mixing matrix, shown in Figure 4.26, it is still suppressed compared to the decay  $c \rightarrow s$ . Therefore the lifetimes of B-hadrons are normally higher than those of charmed particles.

#### 4.2.15 The Discovery of the $t$ -quark

Already in 1973 the Japanese physicists Makoto Kobayashi and Toshihide Maskawa considered an extension of the Cabibbo mixing matrix (see Section 3.3.6) by adding another generation of quarks. Their proposal was based on the idea which led to the prediction of the charm quark several years before it was discovered. The prediction of another generation of quarks was supported by the discovery of the  $\tau$ -lepton in 1974, in order to restore the symmetry between lepton- and quark-generations.

The discovery of the  $b$ -quark led to intense searches for its  $+\frac{2}{3}$  charge partner, called the top quark or the  $t$ -quark. The most clear evidence for new bound quark-antiquark states is obtained from their production in  $e^+e^-$  collisions. The procedure is very simple. The production rate of hadronic final states (or/and  $e^+e^-/\mu^+\mu^-$ ) is measured at points of continuously increasing energies of the colliding beams. As the threshold for production of a new state is reached the

counting rate increases drastically and the beam energy is a measure of the mass of the new quark. The collision energy needed for producing such a resonance state is thus twice the mass of the new quark. After having pushed the energies of existing  $e^+e^-$  colliders as far as was possible it was clear that the  $t$ -quark had to be heavier than the first naive predictions.

The first indication that the top-quark is very heavy came already in 1987 from the study of  $B$ -mesons. It was shown from  $e^+e^-$  collisions at DESY that  $B^0$ - $\bar{B}^0$  oscillations might occur. The normal process would be  $e^+ + e^- \rightarrow b + \bar{b}$ , which would result in a  $B^0$ -meson and a  $\bar{B}^0$ -meson in the final state. However, in some cases the  $B^0$ -meson can oscillate into a  $\bar{B}^0$ -meson or vice versa giving final states of  $B^0B^0$  or  $\bar{B}^0\bar{B}^0$ . Oscillations are produced according to the process given in Figure 4.23.

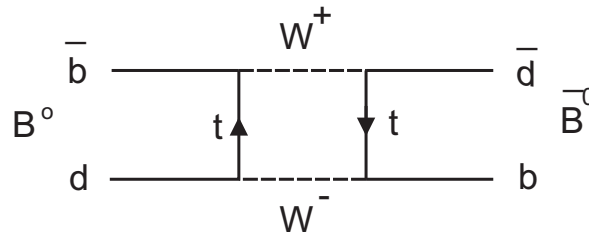


Figure 4.23: Feynman diagram showing the oscillation of a  $B$ -meson into a  $\bar{B}$ -meson via the exchange of virtual  $t$ -quarks in a box diagram.

These oscillations provide basic information on the parameters of the Standard Model, and any deviation from the SM predictions would be an indication for contributions from new physics. The probability for such oscillations can be expressed as the ratio,  $r$ , between final states with equal type  $B$ -mesons and opposite type  $B$ -mesons, given by:

$$r = \frac{N(B^0B^0) + N(\bar{B}^0\bar{B}^0)}{N(B^0\bar{B}^0)} = \frac{\chi^2}{\chi^2 + 2}$$

where: 
$$\chi = \frac{\tau_B G_F^2 m_b}{6\pi^2} B_B f_B^2 |V_{td} V_{tb}^*|^2 m_t^2 F\left(\frac{m_t^2}{M_W^2}\right) \eta_{QCD}$$

It is seen that the oscillation strength depends on a number of parameter but especially it should be noted that it depends on the top quark mass squared. Using the measured value of  $r$  and inserting the most accurate determinations of the other parameters, it was found that the mass of the top quark should be larger than 50 GeV.

The fact that electrons lose energy via synchrotron radiation if they are bent makes it difficult to reach very high energies in circular  $e^+e^-$  colliders. Protons, which are much heavier, do not suffer from this problem and can therefore be brought to much higher energies than electrons. On the other hand high energy collisions between two protons (or a proton and an antiproton) are essentially collisions between two of the quarks inside the protons. The quarks which do not participate in the collision will, however, also be converted into hadrons and will therefore contribute a very severe background which makes the observation of a resonance state much more difficult than in the background free events from  $e^+e^-$  collisions. Anyhow, since the energy range of  $e^+e^-$  colliders was not sufficient, the search had to be performed at hadron colliders. The main production mechanisms from such collisions are presented in Figure 4.24.

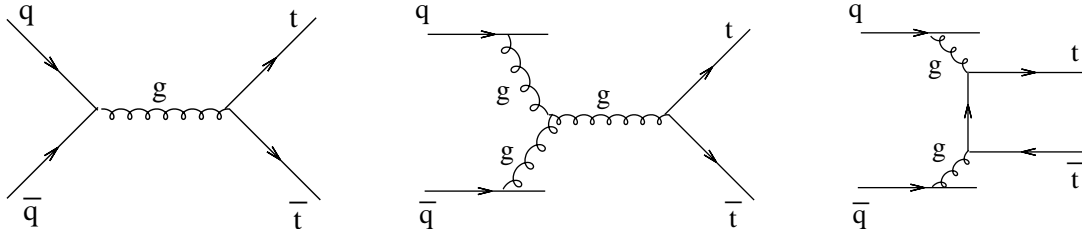


Figure 4.24: Feynman diagram showing the main production mechanisms of a top-quark pair from hadron collisions.

The lifetime of the  $t$ -quark is as short as  $10^{-25}$  seconds, which makes it decay almost instantly before a bound state of a  $t\bar{t}$ -pair can be formed. Therefore the  $t$ -quark has to be identified through its decay, which makes the observation much more difficult. Since only  $u$  and  $d$  quarks are stable the  $t$  quark will go through a cascade decay, which in Figure 4.25 is illustrated by the Cabibbo favoured decay modes.

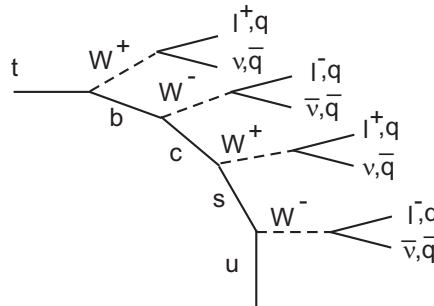


Figure 4.25: Cascade decay of a top quark.

Thus, the  $t$ -quark decays in the first step mainly into a  $b$ -quark and a  $W$ -boson, of which the  $b$ -quark produces a high energy jet of hadrons and the  $W$ -boson produces either two lower energy jets or a lepton-neutrino pair. The main decay modes of a  $t\bar{t}$ -pair are:

$$\begin{aligned}
 t\bar{t} &\rightarrow b\bar{b}q\bar{q}q\bar{q} \\
 t\bar{t} &\rightarrow b\bar{b}q\bar{q}e\nu \\
 t\bar{t} &\rightarrow b\bar{b}q\bar{q}\mu\nu \\
 t\bar{t} &\rightarrow b\bar{b}q\bar{q}\tau\nu ,
 \end{aligned}$$

whereas those where both  $W$ -bosons decay leptonically are strongly suppressed.

In the 1980:ies the top search started at the SPS (Super Proton Synchrotron) at CERN, where collisions between protons and anti-protons, up to energies of  $540 \text{ GeV}$ , could be achieved. However, the actual collisions is between the constituents inside the protons, which only carry a fraction of the proton energy. Eventually the CERN-experiments in 1988 were just able to set a lower mass limit of  $77 \text{ GeV}$ . After that it didn't make sense to continue due to the competition from the Tevatron collider at Fermilab, which was taken into operation in 1986. In 1988 it

reached its designed performance at a collision energy of 1800  $GeV$ . Early 1995 the two experiments had collected enough top-quark events to rule out that they were due to background and they could announce the observation of the top-quark. Further measurements fixed its mass to 173  $GeV$ .

The complete picture of quarks and leptons is shown in Figure 4.3.

flavour	charge	spin
$\nu_e \quad \nu_\mu \quad \nu_\tau$	0	1/2
$e^- \quad \mu^- \quad \tau^-$	-1	1/2
$u \quad c \quad t$	+2/3	1/2
$d \quad s \quad b$	-1/3	1/2
$\bar{\nu}_e \quad \bar{\nu}_\mu \quad \bar{\nu}_\tau$	0	1/2
$e^+ \quad \mu^+ \quad \tau^+$	+1	1/2
$\bar{u} \quad \bar{c} \quad \bar{t}$	-2/3	1/2
$\bar{d} \quad \bar{s} \quad \bar{b}$	+1/3	1/2

Table 4.3: *The situation of known quarks and leptons after the discovery of the top quark.*

The possible transitions of the quarks and leptons between the families, through absorption and emission of W-bosons are listed in Table 4.4. Note that transitions between charged leptons and neutrinos are only allowed within the same family, whereas transitions between  $up - type$  and  $down - type$  quarks can also occur between different families.

	absorption	emission
$l^- \rightarrow \nu_l$	$W^+$	$W^-$
$\nu_l \rightarrow l^-$	$W^-$	$W^+$
$l^+ \rightarrow \bar{\nu}_l$	$W^-$	$W^+$
$\bar{\nu}_l \rightarrow l^+$	$W^+$	$W^-$
$u - type \rightarrow d - type$	$W^-$	$W^+$
$d - type \rightarrow u - type$	$W^+$	$W^-$
$\bar{u} - type \rightarrow \bar{d} - type$	$W^+$	$W^-$
$\bar{d} - type \rightarrow \bar{u} - type$	$W^-$	$W^+$

Table 4.4: *The possible transitions of quark and leptons in the first family, through absorption and emission of W-bosons*

#### 4.2.16 The Cabibbo-Kobayashi-Maskawa Matrix and CP-violation

Already before the discovery of the b- and t-quark (and even the c-quark) Kobayashi and Maskawa in 1973 suggested an extension of the quark mixing matrix of Cabibbo (see section 3.3.6) by introducing a third family of quarks. This provided an explanation to the observed CP-violation in kaon decays. In their picture CP-violation occurs as a consequence of the fact that in quark

mixing the mass eigenstates are being different from the weak interaction eigenstates. As we have discussed earlier the mass- and weak interaction eigenstates are by convention set to be the same for up-type quarks (u, c, t) whereas the relation between the mass- and weak interaction eigenstates for the down-type quarks are given by the Cabibbo-Kobayashi-Maskawa (CKM)-matrix V according to Figure 4.26.

$$\begin{pmatrix} d' \\ s' \\ b' \end{pmatrix} = \begin{pmatrix} V_{ud} & V_{us} & V_{ub} \\ V_{cd} & V_{cs} & V_{cb} \\ V_{td} & V_{ts} & V_{tb} \end{pmatrix} \begin{pmatrix} d \\ s \\ b \end{pmatrix}$$

Weak eigenstates

CKM Matrix

Mass Eigenstates

Figure 4.26: The weak (mixed) quark states, for three generations, are related to the mass (flavour) eigenstates through the Cabibbo, Kobayashi, Maskawa matrix.

The CP-operation changes particles into antiparticles and coupling constants into their complex conjugate such that a transition from a down-type to an up-type quark is described by  $V_{ud}$ , whereas a transition from an up-type to a down-type quark is given by  $V_{ud}^*$ . The corresponding Feynman diagrams are presented in Figure 4.27.



Figure 4.27: Feynman diagrams describing weak decays of a d-quark into a u-quark (left) and a u-quark into a d-quark (right), respectively.

Kobayasi and Maskawa parametrized the matrix as in Figure 4.28.

$$\begin{pmatrix} d' \\ s' \\ b' \end{pmatrix} = \begin{pmatrix} c_1 & -s_1 c_3 & -s_1 s_3 \\ s_1 c_2 & c_1 c_2 c_3 - s_2 s_3 e^{i\delta} & c_1 c_2 s_3 + s_2 c_3 e^{i\delta} \\ s_1 s_2 & c_1 s_2 c_3 + c_2 s_3 e^{i\delta} & c_1 s_2 s_3 - c_2 c_3 e^{i\delta} \end{pmatrix} \begin{pmatrix} d \\ s \\ b \end{pmatrix}$$

Figure 4.28: The original parametrization of the CKM-matrix.

where  $c_i = \cos\theta_i$  and  $s_i = \sin\theta_i$  with the three real mixing angles  $\theta_1, \theta_2$  and  $\theta_3$ , and a complex phase  $\delta$  that is responsible for the CP-breaking. The magnitude of the matrix elements can be determined from measurements of processes that are related to the transitions represented by the matrix elements. The results are shown in Figure 4.29.



$$V = \begin{pmatrix} V_{ud}=0.975 & V_{us}=0.221 & V_{ub}=0.005 \\ V_{cd}=0.221 & V_{cs}=0.974 & V_{cb}=0.04 \\ V_{td}=0.01 & V_{ts}=0.041 & V_{tb}=0.999 \end{pmatrix}$$

Figure 4.29: The values of the CKM-matrix elements as experimentally measured.

Although CP-violation was discovered in weak decays of K-mesons it can also occur in the decays of B-mesons where the CP-breaking effect is even larger. However, the CP-violation of the Standard Model seems not to be large enough to completely explain the conversion of antimatter into matter in the early stage of Universe. This suggests that there are other sources of CP-violation in addition to those provided by the CKM matrix.

The coupling strengths which we derived earlier are thus modified by the value of the relevant matrix element. One example is shown in Figure 4.30.

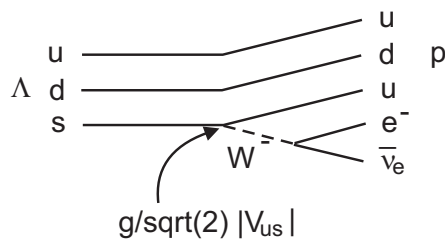


Figure 4.30: Feynman diagram showing the decay of a  $\Lambda$ -particle and the coupling strength of the decay.

## 4.2.17 The Discovery of Higgs

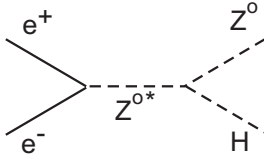
In the same way as *photons* couple to particles with electric charge, *weak vector bosons* to particles carrying 'weak charge' ( $g, g'$ ) and gluons to particles carrying colour charge, the Higgs particle couples to particles with mass. The coupling of Higgs to fermions and bosons is, thus, essentially proportional to the masses of the particles.

No Higgs particle was found at low energies, and it was necessary to go to energies of several  $TeV$  at LHC in order to find evidence for the existence of the Higgs particle.

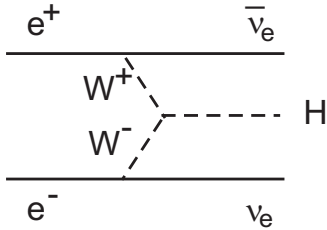
### Higgs Production in Electron-Positron Collisions

In  $e^+e^-$  there are two main production mechanisms:

- 1) The *Higgs strahlung*:  $e^+ + e^- \rightarrow Z^{0*} \rightarrow H + Z^0$



2) *W-fusion*:  $e^+ + e^- \rightarrow W^+ + W^- + \nu_e + \bar{\nu}_e \rightarrow H + \nu_e + \bar{\nu}_e$



The experimental signature of the Higgs particle is not always very outstanding. It decays primarily to heavy particles, which decays to lighter particles in a decay chain.

*Some possible final states from the Higgs strahlung process:*

	$Z^0$	$H$
4 jets	$q\bar{q}$	$b\bar{b}$
2 jets	$\nu\bar{\nu}$	$b\bar{b}$
	$l^+l^-$	$b\bar{b}$
	$q\bar{q}$	$\tau^+\tau^-$

where a *jet* is a collimated flow of particles. The Higgs particle produced in the *W*-fusion process differs from one produced through the Higgs strahlung process in so far that there is no contribution from the  $Z^0$ -decay, and thus the final state is less complex.

*Background processes:*

$$e^+ + e^- \rightarrow Z^0 + Z^0$$

$$e^+ + e^- \rightarrow W^+ + W^-$$

In addition to these backgrounds there is a large background from strong interaction processes.

In the LEP collider (Large Electron-Positron collider) at CERN electrons and positrons were collided up to energies of  $\sqrt{s} = 209 \text{ GeV}$ . The dominant process at this energy is the Higgs strahlung process. The Higgs particle was not discovered at LEP, but we can use the absence of a signature to estimate the lower limit of the Higgs mass.

$$s = (p_{e^+} + p_{e^-})^2 = (p_{Z^0} + p_H)^2 = m_{Z^0}^2 + m_H^2 + 2p_{Z^0}p_H$$

Production of the Higgs particle at rest corresponds to the mass limit:

$$p_{Z^0} = (m_{Z^0}, 0)$$

$$p_H = (m_H, 0)$$

$$\Rightarrow s = m_{Z^0}^2 + m_H^2 + 2m_{Z^0}m_H$$

$$\Rightarrow m_H^2 + 2m_{Z^0}m_H + m_{Z^0}^2 - s = 0$$

$$\Rightarrow m_H = -m_{Z^0} \pm \sqrt{m_{Z^0}^2 - (m_{Z^0}^2 - s)} = -m_{Z^0} \pm \sqrt{s}$$

The negative solution is unphysical  $\Rightarrow m_H = \sqrt{s} - m_{Z^0} = 209 - 92 = 117 \text{ GeV}$

which was the low limit of the Higgs mass, set by the LEP-experiments.

## Higgs Production in Proton-Proton Collisions

The search for the Higgs particle has been continued at higher energies using collisions between protons at the LHC (Large Hadron Collider) at CERN. The major production mechanisms in proton-proton collisions are through:

- gluon fusion from which the Higgs particle is produced through a quark loop, predominantly a top-quark loop, since the top-quark has the heaviest mass.
- Higgs strahlung from a process, in which a produced virtual vector boson ( $Z$  or  $W$ ) emits a Higgs particle and becomes real.
- $W$  or  $Z$ -fusion.

These processes are shown in Figure 4.31.

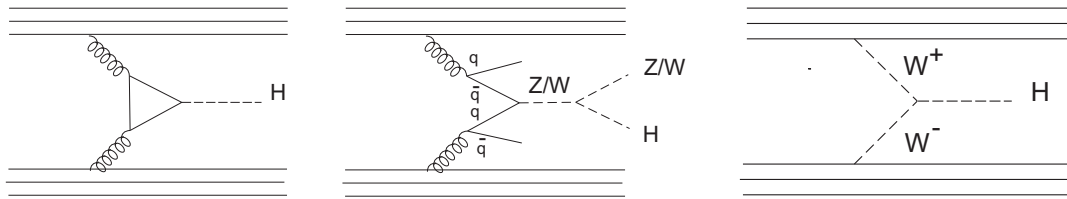


Figure 4.31: Feynman diagrams showing some production mechanisms for producing Higgs bosons.

Since the Higgs particle is extremely short lived it decays almost immediately through various decay channels, some of which are listed below.

- $H \rightarrow b\bar{b}$ . The b-quarks then hadronize into jets of particles.
- $H \rightarrow WW^*$ , where  $W^*$  is virtual. This decay mode is the reverse of the Higgs strahlung process. Each  $W$ -boson will then decay into a quark-antiquark pair or into a lepton and a neutrino.
- $H \rightarrow \tau^+\tau^-$ . The  $\tau$ -lepton is the lepton that couples the strongest to Higgs due to the fact that it is the heaviest lepton. Each  $\tau$  then can decay to either a quark-antiquark pair or a lepton-neutrino pair.
- $H \rightarrow ZZ^*$ , where one of  $Z^*$  is virtual. Each  $Z$  can then decay either into a quark-antiquark pair, a lepton pair or a neutrino-antineutrino pair.

- $H \rightarrow c\bar{c}$ , where the c-quarks hadronize into particle jets.
- $H \rightarrow \gamma\gamma$ . This decay proceeds via a quark loop and is essentially the reverse of production mechanism a) with the difference that the gluons are exchange by photons.
- $H \rightarrow \gamma Z$ . This decay is similar to the previous one with one of the photons replaced by a Z-boson.

Already the large number of possible decay channels gives a clear indication that the observation of the Higgs particle is extremely difficult and thus requires a tremendous analysis effort. Due to its extremely short lifetime the direct measurement of the Higgs particle is prevented but it can only be observed through the reconstruction of its decay products. The individual decay channels must be investigated separately and sorted out from a, in some cases, huge background.

On the 4th of July 2012 two of the LHC-experiments, ATLAS and CMS, announced that they both, in collisions between protons at 7 (8) TeV collision energy, had observed an excess of events at a mass around 125 GeV in their data samples from 2011 (2012). The signal has a statistical significance of about five standard deviations ( $\sigma$ ) above background expectations for both experiments. The search for the Higgs particle by the two LHC experiments was, so far, performed by investigating the following final states:

- $\gamma\gamma$
- $ZZ^* \rightarrow l^+l^-l^+l^-$ , where  $l = e$  or  $\mu$
- $ZZ^* \rightarrow l^+l^-q\bar{q}$
- $bb$ , from the Higgs strahlung process where the accompanying  $W \rightarrow l\nu$  alternatively  $Z \rightarrow l^+l^-$  or  $\nu\bar{\nu}$ .
- $WW^* \rightarrow 2l\nu$ .
- $\tau\tau \rightarrow 2l\nu$ .

The  $\gamma\gamma$  and  $ZZ^*$  channels are especially important as they allow a precise determination of the Higgs mass. Although the decay probabilities are not the highest, the Higgs peak is quite narrow, whereas the other decay channels lead to fairly broad distributions. In the case of the  $\gamma\gamma$  final state, the Higgs mass is measured through the direction and energies of the  $\gamma$ 's, whereas in the  $ZZ$  decay the Higgs mass is extracted from the invariant mass of the lepton pairs produced in the two Z-decays. These two decay modes are the ones that provide the main contributions to the measured significance whereas the other either contribute very little or not at all. In Figure 4.32 the invariant mass spectrum of two gammas are shown and in Figure 4.33 that of four leptons.

The excess of events observed, lies in a mass range consistent with the expectations for a Standard Model Higgs, and so far all of the measured properties of the particle state have confirmed that this is the case. However, further investigations of the properties of the new particle have to be performed in order to finally settle this. Such properties are for example the spin, which should be zero, the parity, and the coupling strength to all particles, which should be proportional to their mass. Of special interest is the measurement of the Higgs self coupling i.e. how strongly the Higgs particle couples to itself, since this provides information about the Higgs potential itself. This can be measured through a process in which a virtual Higgs boson emits a real Higgs particle. However, for this the linear  $e^+e^-$ -collider is needed.

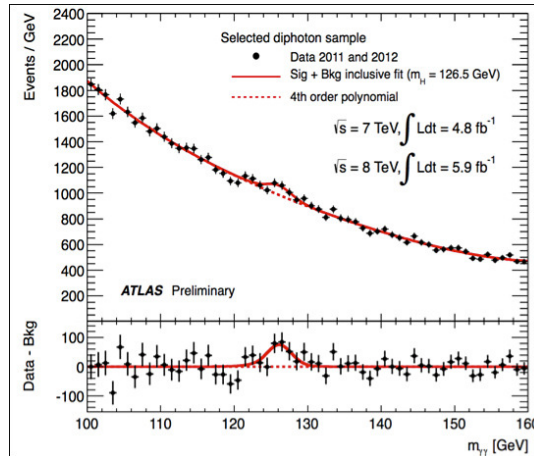


Figure 4.32: The invariant mass spectrum of two gammas from proton-proton collisions. In the spectrum below the background has been subtracted. A small peak is observed at around 125 GeV.

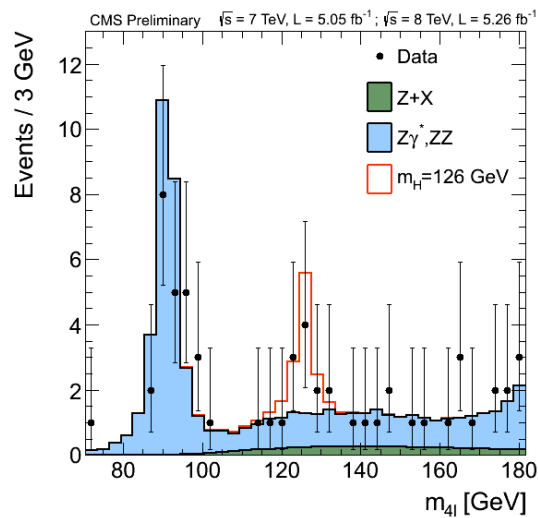


Figure 4.33: The invariant mass of four leptons produced in proton collisions. The backgrounds are presented as the grey histograms and the contribution of a Higgs with mass 125 GeV as the open histogram.

Some of the shortcomings of the SM are that it is not able to describe dark matter and why there are more baryons than antibaryons in our universe. Models that have been developed to solve these problems often have additional Higgs bosons (see Section 6.2).

### 4.3 Are There More Families?

The question whether there are still more families of quarks and leptons is of fundamental interest. It might be hard to build accelerators that produce quarks that are significantly heavier than the top quark so we need to concentrate on the lepton family. Even if we in  $e^+e^-$  collisions do not observe any new heavier charged leptons we can not for that reason exclude the possibility that the next generation would have a lepton with a mass that lies beyond the reach of our accelerator. The way out of this problem is to study the properties of the  $Z^0$  boson which can be copiously produced at  $e^+e^-$  colliders with a collision energy higher than the  $Z^0$  mass. The width of the  $Z^0$  resonance peak is due to Heisenberg's uncertainty principle inversely proportional to the lifetime of  $Z^0$  (see Section 4.1.2). On the other hand, the lifetime depends on how many decay modes the particle has. The more decay possibilities the shorter is the lifetime.  $Z^0$  decays into either a quark-antiquark pair or a lepton pair. Since the mass of the  $Z^0$  particle is 92 GeV it is kinematically allowed to decay into  $d\bar{d}$ -,  $u\bar{u}$ -,  $s\bar{s}$ -,  $c\bar{c}$  and  $b\bar{b}$ -pairs but it can not decay into a  $t\bar{t}$ -pair since twice the  $t$  mass is as high as 350 GeV.  $Z^0$  can also decay into  $e^+e^-$ ,  $\mu^+\mu^-$ ,  $\tau^+\tau^-$  and possibly into heavier lepton pairs if they exist and twice their mass is lower than 92 GeV. Now, if we assume that the neutrino particles have zero mass or at least that their mass is very small then  $Z^0$  can decay into all possible neutrino-antineutrino pairs, even those belonging to possible new generations. Every additional decay mode would have an impact on the width of the  $Z^0$ -peak. Precision measurements at CERN have shown that the width is consistent with that calculated for three families of quarks and leptons, as shown in Figure 4.34. This result excludes further generations of quarks and leptons beyond the three we have already observed.

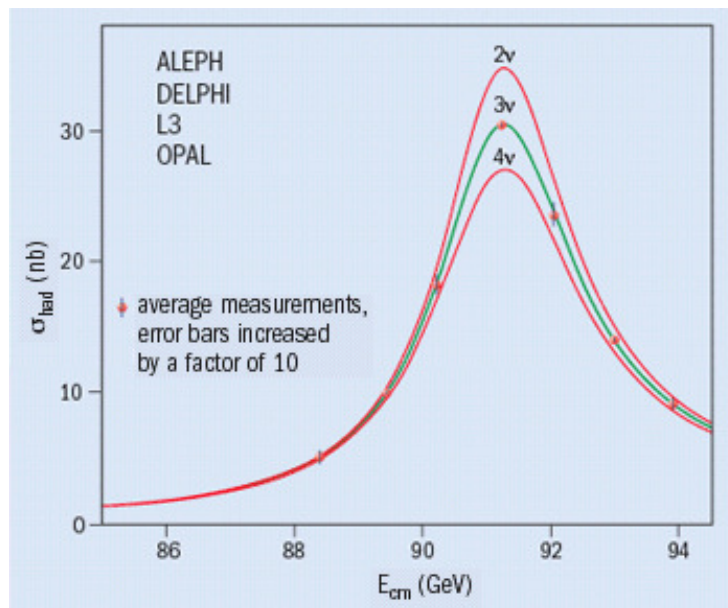


Figure 4.34: *The hadronic cross section as a function of the centre-of-mass energy in the range of the  $Z^0$  peak, from which the measured width of the peak can be compared to the theoretical prediction for 2, 3 and 4 generations of quarks and leptons. The results are clearly consistent with 3 generations of quarks and leptons.*

# Chapter 5

## Nucleon shape and structure

The most important experiments to determine the shape of the nuclei and nucleon as well as to provide information on the nucleon structure, are lepton (electron, muon, neutrino) scattering experiments. The basic principle is the same as Rutherford used in 1911 as he scattered  $\alpha$ -particles against a gold foil to investigate the structure of the atom. There are two big advantages in using leptons as probes. One is that they are so called *point-like particles* i.e. they don't have any internal structure. The second advantage is that the scattering between charged leptons and hadrons proceeds via electromagnetic and weak interactions which can be calculated to a very high degree of accuracy from the theory. Although the principle of scattering experiments is the same whether you want to investigate the structure of the atoms, the nuclei or the nucleons, the energy needed is different.

The relation between wave length and momentum,  $\lambda = \hbar/p$ , where  $\hbar$  is the Planck constant, means that:

small  $p \Rightarrow$  large  $\lambda \Rightarrow$  low resolution power.

large  $p \Rightarrow$  small  $\lambda \Rightarrow$  high resolution power.

To the lowest order in the electromagnetic coupling constant the scattering of charged leptons (electrons and muons) off charged particles can be described by an exchange of a virtual photon. One can distinguish between the following four energy areas in the scattering against nucleons:

- Very low momentum lepton scattering, where the wave length of the exchanged photon is much longer than the size of the nucleon. In this case the nucleon can be regarded as a point-like spin-less object.
- Low momentum lepton scattering, where the wave length of the exchanged photon is comparable to the size of the nucleon. In this case the size of the nucleon has to be taken into account, such that the scattering occurs against an extended object.
- High momentum lepton scattering, where the wave length of the exchanged photon is shorter than the size of the nucleon. In this case the wave length of the exchanged photon is sufficiently short to resolve the inner structure of the nucleon.



- Very high momentum lepton scattering, where the wave length of the exchanged photon is much shorter than the size of the nucleon. In this case the wave length of the exchanged photon is so short that it can resolve the gluons and sea-quarks in the nucleon.

The description of lepton-nucleon scattering as an exchange of a virtual photon is valid as long as the momentum transfer is small compared to the mass of the weak vector bosons. As the momentum transfer approaches such energies the influence of the weak interaction gets increasingly important and has to be taken into account.

## 5.1 Elastic scattering of electrons

Consider an electron, which is elastically scattered against a proton sitting at rest, i.e. the proton stays intact. As discussed above the scattering can be described to lowest order in  $\alpha_S$ , as an exchange of a virtual photon between the electron and the proton. The kinematics of electron scattering at low energies is illustrated in Figure 5.1.

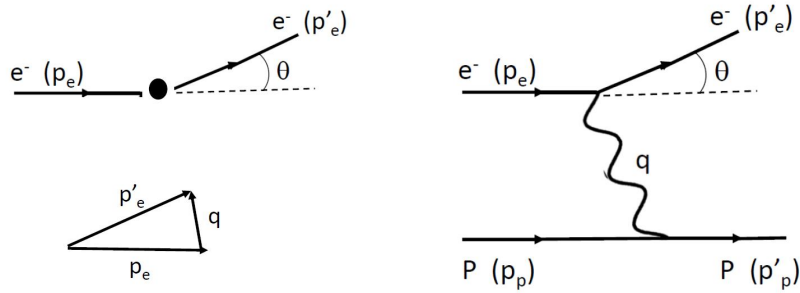


Figure 5.1: Kinematics of elastic scattering of an electron off a nucleus.

In this Figure  $\vec{p}_e$  and  $\vec{p}'_e$  represent the three-momenta of the incoming and scattered electron, respectively, and  $\vec{q} = \vec{p}_e - \vec{p}'_e$  is the momentum transfer, i.e. the momentum carried by the exchanged photon. The electron is scattered through an angle  $\theta$  in the laboratory frame. At low energies the proton does almost not recoil, due to the fact that the electron is so much lighter than the proton. In case that the proton is sitting at rest we have:

$$p_e \approx p'_e \approx E_e \approx E'_e$$

$$p_e^2 = p_e'^2 = E_e^2 - \vec{p}_e^2 = m_e^2$$

$$p_p^2 = m_p^2 = E_p^2 \quad \text{and} \quad \vec{p}_p = 0$$

where  $p_e, p'_e, E_e, E'_e, p_p, p'_p, E_p$  and  $E'_p$  are the four-momenta and energies, respectively, of the incoming and final state electron and proton. The square of the center-of mass energy is given by:

$s = (p_e + p_p)^2 = p_e^2 + p_p^2 + 2p_e \cdot p_p \approx m_p^2 + 2p_e p_p$  , since  $m_e$  can be neglected.

$$\Rightarrow \boxed{2p_e \cdot p_p = s - m_p^2} \quad (5.1)$$

The momentum transfer squared is:

$$q^2 = (p_e - p'_e)^2 = p_e^2 + p'^2_e - 2p_e \cdot p'_e = p_e^2 + p'^2_e - 2(E_e E'_e - |\vec{p}_e| |\vec{p}'_e| \cos\theta)$$

$$\Rightarrow \boxed{q^2 \approx -2E_e E'_e (1 - \cos\theta) = -4E_e E'_e \sin^2 \frac{\theta}{2}}, \quad (5.2)$$

where  $m_e$  has been neglected. Usually one defines  $Q^2 = -q^2$ .

In deriving further kinematic variables the following products of four-momenta are useful.

$$p_e \cdot p_p = E_e E_p - \vec{p}_e \vec{p}_p \approx E_e m_p \quad (5.3)$$

since  $p_p = m_p$  and  $\vec{p}_p = 0$  for a proton at rest.

$$p_e \cdot p'_e = E_e E'_e - \vec{p}_e \vec{p}'_e \approx E_e E'_e - E_e E'_e \cos\theta = E_e E'_e (1 - \cos\theta) \quad (5.4)$$

$$p_p \cdot p'_e = m_p E'_e - \vec{p}_p \vec{p}'_e = m_p E'_e \quad (5.5)$$

$$q \cdot p_p = (p_e - p'_e) \cdot p_p = p_e \cdot p_p - p'_e \cdot p_p = E_e E_p - \vec{p}_e \vec{p}_p - (E'_e E_p - \vec{p}'_e \vec{p}_p)$$

But  $E_p = m_p$  and  $\vec{p}_p = 0$

$$\Rightarrow q \cdot p_p = E_e m_p - E'_e m_p$$

$$\Rightarrow q \cdot p_p = m_p (E_e - E'_e) \quad (5.6)$$

However, we have:  $(q + p_p)^2 = p'^2_p$

$$\Rightarrow q^2 + p_p^2 + 2q \cdot p_p = p'^2_p$$

$$\Rightarrow q^2 + m_p^2 + 2q \cdot p_p = m_p^2$$

$$\Rightarrow q \cdot p_p = -\frac{q^2}{2} \quad (5.7)$$

Now, equations 5.6 and 5.7 give:  $m_p (E_e - E'_e) = -\frac{q^2}{2}$

$$\Rightarrow (E_e - E'_e) = -\frac{q^2}{2m_p} \quad (5.8)$$

The energy transfer or energy loss of the exchanged photon is denoted  $\nu$  and is defined as:

$$\Rightarrow \nu = (E_e - E'_e) = \frac{p_p \cdot q}{m_p}, \quad (5.9)$$

using equation 5.6. The fractional energy loss of the incoming electron or the *inelasticity* is denoted  $y$  and is given by:

$$y = \frac{E_e - E'_e}{E_e} = \frac{\nu}{E_e} = \frac{m_p \nu}{m_p E_e}$$

But according to equation 5.9, we have  $m_p(E_e - E'_e) = m_p \nu = p_p \cdot q$ , and according to equation 5.3, we have  $E_e m_p = p_e \cdot p_p$ .

$$\Rightarrow y = \frac{q \cdot p_p}{p_e \cdot p_p} = \frac{2m_p \cdot \nu}{s - m_p^2} \quad (5.10)$$

since from equation 5.1 we have  $p_e \cdot p_p = \frac{s - m_p^2}{2}$ .

Equations 5.2 and 5.8 give:  $-2E_e E'_e (1 - \cos\theta) = -2m_p (E_e - E'_e)$

$$\Rightarrow E'_e = \frac{m_p (E_e - E'_e)}{E_e (1 - \cos\theta)}$$

$$\Rightarrow E'_e = \frac{m_p E_e}{E_e (1 - \cos\theta)} - \frac{m_p E'_e}{E_e (1 - \cos\theta)}$$

$$\Rightarrow E'_e + \frac{m_p E'_e}{E_e (1 - \cos\theta)} = \frac{m_p}{(1 - \cos\theta)}$$

$$\Rightarrow E'_e \left( \frac{E_e (1 - \cos\theta) + m_p}{E_e (1 - \cos\theta)} \right) = \frac{E_e m_p}{E_e (1 - \cos\theta)}$$

$$\Rightarrow \frac{E'_e}{E_e} = \frac{m_p}{m_p + E_e (1 - \cos\theta)}$$

$$\Rightarrow E'_e = \frac{m_p E_e}{m_p + E_e (1 - \cos\theta)} \quad (5.11)$$

Inserting the expression for  $E'_e$  given by equation 5.2 gives:

$$q^2 = - \frac{2m_p E_e^2 (1 - \cos\theta)}{m_p + E_e (1 - \cos\theta)} \quad (5.12)$$

and the energy transfer becomes:

$$\nu = \frac{m_p E_e}{m_p + E_e (1 - \cos\theta)} \quad (5.13)$$

and the fractional energy transfer can be written:

$$y = 1 - \frac{m_p E_e}{m_p + E_e(1 - \cos\theta)} \quad (5.14)$$

For elastic scattering there is only one independent parameter such that the full kinematics of the event is determined by e.g. measuring the scattering angle of the electron, as shown in equations 5.11 - 5.14.

The differential cross section for scattering of particles against a target is defined as:

$$\frac{d\sigma}{d\Omega} = \frac{\text{number of particles scattered per unit time into a solid angle } \Delta\Omega(\theta)}{(\text{number of scattering objects}) \times (\text{flux of impinging particles})}$$

In case the incoming charged particle is spinless and is scattered against a static point charge, Rutherford showed that the differential cross section is (see section 3.2.4):

$$\frac{d\sigma}{d\Omega} \sim \frac{\alpha^2}{E^2 \cdot \sin^4 \frac{\theta}{2}},$$

where  $\alpha$  is the electromagnetic coupling constant,  $E$  is the energy of the incident particle and  $\theta$  the scattering angle in the laboratory frame. Thus, Rutherford scattering is in an energy range where the recoil of the proton can be neglected. From the Rutherford formula one can conclude that in this energy region, only interactions between the electric charges of the particles matter. Interactions through the intrinsic magnetic moments are not considered. As the spin of the electron is taken into account a further term has to be added to the Rutherford formula, which then becomes:

$$\frac{d\sigma}{d\Omega} \sim \frac{\alpha^2}{E^2 \cdot \sin^4 \frac{\theta}{2}} \cos^2 \frac{\theta}{2},$$

This is called the Mott cross section. In case the recoil and spin of the nucleon is considered the Mott cross section has to be modified, and becomes:

$$\frac{d\sigma}{d\Omega} \sim \frac{\alpha^2}{E^2 \cdot \sin^4 \frac{\theta}{2}} \frac{E'_e}{E_e} \left( \cos^2 \frac{\theta}{2} - \frac{q^2}{2m_p^2} \sin^2 \frac{\theta}{2} \right)$$

where  $E'_e/E_e$  describes the recoil of the proton and the second term inside the brackets comes from the spin-spin interaction.

Finally the size of the particle has to be taken into account. The size of an extended charged object, like an atom, nucleus or nucleon, is given by the spatial distribution of its charge and magnetism. The charge distribution can be described through a charge density function

$$\rho(\vec{r}) = \rho_0 \cdot f(\vec{r})$$

where  $\rho_0$  is the central charge density and  $f(\vec{r})$  is a function that describes how the charge density varies with the distance  $r$  from the centre. For a point-like particle  $f(0) = 1$  and the charge distribution is a  $\delta$ -function at  $r = 0$ .

$$\int \rho(\vec{r}) d^3r = 1$$

The magnetism of a particle is characterized by the nuclear magnetic momentum, which for a nucleus arises from the spins of the protons and neutrons. For a single nucleon with spin 1/2 the intrinsic magnetic dipole moment is expressed in units of the nuclear magneton, which in the SI-system is defined as  $\mu_N = \frac{e\hbar}{2m}$ , where  $e$  is the elementary charge,  $\hbar$  the Planck constant and  $m$  is the mass of the nucleon. The magnetic moment of a nucleon is parallel to its spin. For a particle to have intrinsic magnetic moment it must have both charge and spin. Since the proton has charge  $+1e$ , it should have a magnetic moment  $\mu_p = 1\mu_N$ , in case of it being a point-like particle, whereas a point-like neutron, since it has no charge, consequently should have a magnetic moment  $\mu_n = 0\mu_N$ .

### 5.1.1 Determination of the nucleon size

Already in 1933 the German physicist Otto Stern measured the magnetic moment of the proton and found that it was about 2.8 times larger than expected for a point-like particle. The magnetic moment of the proton was re-measured by Stern and independently by others in the following year and eventually its value was determined to  $\mu_p = 2.79\mu_N$ . Also the magnetic moment of the deuteron was measured and since the deuteron is composed of a proton and a neutron with aligned spins, the neutron's magnetic moment could be inferred by subtracting the deuteron and proton magnetic moments. The resulting value was not zero as expected for a point-like neutron, but had a negative non-zero value. The first direct measurement of the neutron magnetic moment was performed in 1940 by the American physicists Luis Alvarez and Felix Bloch who found a value of  $\mu_n = -1.91\mu_N$ . The fact that the measured values deviated from those expected for point-like spin 1/2 nucleons, indicated that the nucleons had a finite extension. Today we know that a nucleon (proton or neutron) contains charged quarks, which all have magnetic moments such that to first approximation the magnetic moments of the constituent quarks add up to that of the nucleon.

Assume that we want to use a beam of electrons to probe ('photograph') an extended object. In case of scattering against an extended atom, nucleus or nucleon, its shape alternative structure is probed by the exchanged virtual photon, and the higher the momentum transfer,  $q$ , the higher the resolving power. At low energies the resolution is not sufficient to resolve the inner structure of the object but the size can be measured. The scattering cross section can be written in the general form:

$$\frac{d\sigma}{d\Omega} = \frac{d\sigma}{d\Omega_{point}} \cdot |G(q^2)|^2 \quad (5.15)$$

where  $\frac{d\sigma}{d\Omega_{point}}$  is the cross section for scattering against the point charge, as given by the Mott cross section, and  $q$  is the momentum transferred by the virtual photon exchanged between the incident electron and the target.  $G(q^2)$  is called the *form factor*, and it contains information about the shape of the object as probed by a virtual photon of momentum  $q$ . Thus, in order to obtain the differential cross section, for scattering against an extended particle, the point-like cross section has to be multiplied by  $|G(q^2)|^2$ . The description of elastic electron scattering against a spin 1/2 nucleon, in the lowest order  $\alpha$ , however, requires two form factors. One is

the *electromagnetic form factor*,  $G_E(q^2)$ , describing the charge distribution of the particle. The charge related form factor can be expressed in terms of the charge density,  $\rho(\vec{x})$ .

$$G_E(q^2) = \int e^{i\vec{q}\vec{r}} \cdot \rho(\vec{r}) d^3r \quad (5.16)$$

The integral is performed over the volume of the target object. The other form factor is the *magnetic form factor*,  $G_M(q^2)$ , which is related to the distribution of the magnetic moment in the nucleon. Including these form factors the cross section for scattering a spin 1/2 electron against a finite size spin 1/2 nucleon is given by the so called Rosenbluth formula:

$$\frac{d\sigma}{d\Omega} \sim \frac{\alpha^2}{4E^2} \frac{E'_e}{E_e} \left( \frac{G_E^2 + \tau G_M^2}{(1 + \tau)} \cos^2 \frac{\theta}{2} + 2\tau G_M^2 \sin^2 \frac{\theta}{2} \right),$$

where  $\tau = \frac{Q^2}{4m_p^2}$ . The form factors have to be determined experimentally. As realized from equation 5.15 a measurement of the differential scattering cross section,  $d\sigma/d\Omega_{exp}$ , can be used to determine the form factors.

$$\Rightarrow |G_{E,M}(q^2)|^2 = \frac{d\sigma}{d\Omega_{exp}} / \frac{d\sigma}{d\Omega_{point}}$$

Then, for example, the charge distribution,  $\rho(r)$ , is obtained by taking the inverse Fourier transformation of the electromagnetic form factor  $G_E(q^2)$ , as given in equation 5.16.

$$\rho(\vec{r}) = \int G_E(q^2) e^{-i\vec{q}\vec{r}} d^3q$$

This would in principle require that  $G_E(q^2)$  is measured over the full  $q$ -range, which in practice is not possible. Instead a model is built, which fits the measured values of  $G_E(q^2)$ . Note, that already the information that an object has a finite size implies an inner structure.

An experiment where 188 MeV electrons were elastically scattered against protons, contained in a gaseous hydrogen target, was performed by the American physicists R.W. McAllister and R. Hofstadter in 1956, at the Stanford Linear Accelerator (SLAC). They used a magnetic spectrometer, which could be rotated around the scattering target, to measure the scattered electron at different angles. By comparing their results with theoretical calculations for a point-like proton, they found deviations at large scattering angles, which showed that the proton has a finite size and indicated the possibility of an inner structure. The form factors  $G_E$  and  $G_M$  should be 1 and 0, respectively in the case of a point-like proton. For a point-like neutron  $G_E$  and  $G_M$  should both be zero. McAllister and Hofstadter were able to determine the mean square radius of the proton's charge distribution by measuring the charge form factor at low momentum transfer. Figure 5.2 shows the square of the charge form factor as a function of the momentum transfer squared,  $q^2$ . The data points are fitted to an exponential curve and from this they found  $\langle r^2 \rangle^{1/2} = 0.80 \cdot 10^{-15}$  meter.

However, it should be kept in mind that the size of a nucleon can not be unambiguously defined since it is not a rigid body. Instead it is defined by the distribution of quarks, which are not sitting at fixed positions but are moving around.

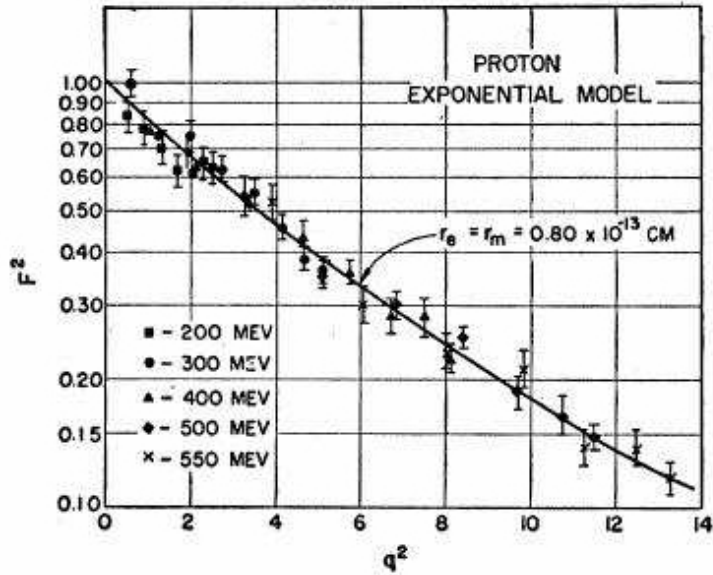


Figure 5.2: The form factor squared versus the momentum transfer squared,  $q^2$ . An exponential curve is fitted to the data.

## 5.2 Deep inelastic scattering

Although the results of McAllister and Hofstadter indicated an inner structure of the nucleon, the beam energy was not sufficiently high to resolve the nucleon structure. The general opinion at the time was based on results from soft scattering measurements between hadrons, which suggested that the nucleon was an extended object with a diffuse inner structure. Such experiments also found that the scattering cross section decreased with increasing momentum transfer between the scattered hadrons. The final evidence and more detailed information about the inner structure of the nucleon was obtained from the study of inelastic scattering of leptons against nucleons.

### 5.2.1 Measurement of the nucleon structure

In 1967 SLAC had been upgraded to produce electron beams up to an energy of 21 GeV, which provided a very powerful probe of the nucleon structure. An experiment led by J.I. Freedman, H.W. Kendall and R.E. Taylor, used a big magnetic spectrometer, which could be rotated around the target position, to detect and measure the scattering of the incoming electrons against protons and neutrons. The spectrometer covered a momentum interval of  $\delta p/p = 3.5\%$ , and the momentum of the scattered electron was measured to an accuracy of 0.1%. At these energies the scattering is unlikely to be elastic but is merely inelastic, in which a fraction of the electron energy is used to excite or break up the proton.

$$e + p \rightarrow e + X ,$$

where X can be an excited proton state (resonance states with higher internal energy) or represents hadrons which have been produced in the scattering process. The Feynman diagram describing this process is shown in Figure 5.3.

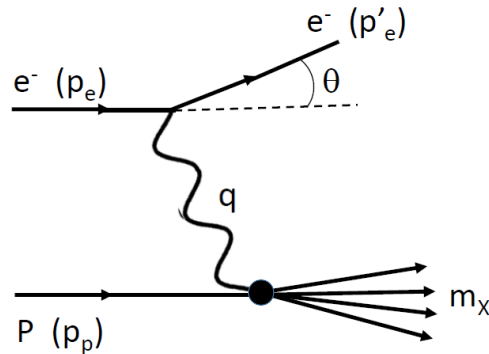


Figure 5.3: Kinematics of inelastic scattering of an electron off a proton.

The final state has to contain at least one baryon (due to baryon number conservation), which means that the final state invariant mass  $m_X > m_p$ .  $m_X$  is also frequently referred to as  $W$ , and can be expressed as:

$$m_X^2 = W^2 = (p_p + q)^2 = m_p^2 + 2p_p q + q^2 \approx 2p_p q + q^2 ,$$

if we neglect the mass of the proton. According to equation 5.2

$$Q^2 = -q^2 = 2E_e^2(1 - \cos\theta) .$$

The results of the SLAC experiment showed that the excited states appeared at specific values of energy and momentum transfer, given by certain combinations of scattering angle and energy, corresponding to the invariant masses of the resonance states. The data exhibited a number of properties, which depended on the initial and final electron energies, and on the scattering angle, as can be seen from Figure 5.4. Up to a missing mass of the hadronic system of about  $1.8 \text{ GeV}$  the elastic scattering peak and resonance excitations were observed, whereas above  $1.8 \text{ GeV}$  the non-resonant region of deep inelastic scattering is reached. For small momentum transfer the peak structures were very prominent, whereas the contribution from non-resonant scattering was very small. As the momentum transfer increased the elastic and resonance cross sections rapidly decreased, as expected from the results of previous soft scattering between hadrons. The surprising observation was that the non-resonant cross section showed very little dependence on the momentum transfer and for deep inelastic scattering it was almost independent on  $q^2$ . In Figure 5.5 the ratio  $(d\sigma/d\Omega)/\sigma_{Mott}$ , where  $\sigma_{Mott}$  is the pointlike cross section, is shown as a function of the momentum transfer squared  $q^2$  compared to what is expected for elastic scattering. The weak dependence on  $q^2$  is consistent with a point-like inner structure of the nucleon.

At the time these experiments started there were no detailed models describing the internal structure of the hadrons. Quarks had been introduced to successfully explain the family structure of hadron but the general opinion was that quarks should not be taken seriously as real particles.



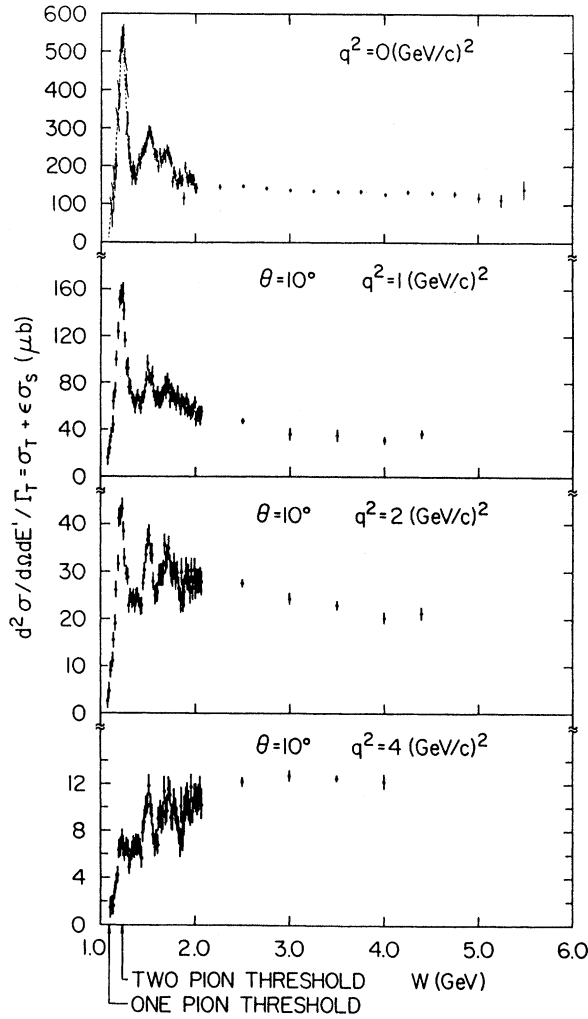


Figure 5.4: Spectra from electron scattering against protons in hydrogen, shown as differential cross section versus the missing mass,  $W$ , of the hadronic system in the final state for different momentum transfer squared,  $q^2$ .

Richard Feynman was the first to propose a model, the so called *parton model*, which explained the results from the SLAC experiment. According to his model hadrons contain a collection of charged point-like constituents, which he called *partons*. For an object probed in an electron scattering experiment, the resolving power of the exchanged photon is  $\lambda \sim 1/\sqrt{q^2}$ . Thus, at high momentum transfers short distances are probed. This means that deep inelastic scattering against nucleons probes partons that are being close to each other. By assuming that the partons interact very weakly at these short distances, so that they can be regarded as essentially freely moving particles inside the nucleon, Feynman was able to describe the SLAC data. This property of the strong force could at the time not be theoretically explained but the explanation had to await the development of QCD, in which this phenomenon was named *asymptotic freedom*. This property was discussed in Section 3.4.2. In the simplest version of the parton model, the partons are assumed to move in a direction parallel to the nucleon direction so that

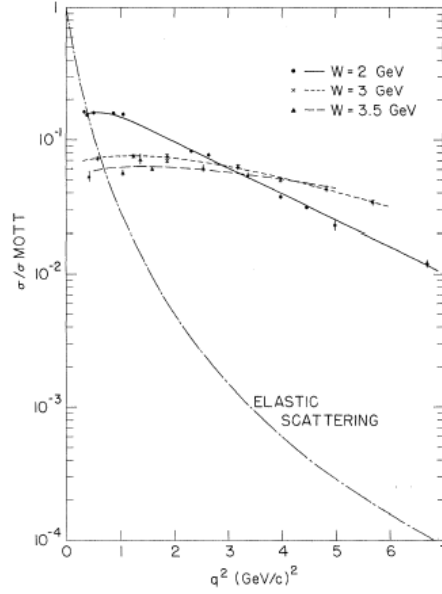


Figure 5.5: The cross section dependence on the momentum transfer squared  $q^2$ .

all parton momenta are collinear, each parton carrying a fraction  $x$  of the proton momentum, in a frame where the proton carries a very high momentum (the so called *infinite momentum frame*). In fact the partons can move in all directions inside the nucleon but with transverse momenta that are typically small compared to the momenta involved in the center-of-mass system of the virtual photon and the proton, for deep inelastic scattering processes. These so called *primordial momenta*, which are the parton momenta inside a nucleon at rest, can thus to first order be neglected such that the transverse momenta of the partons can be set to zero.

As compelling evidence was presented that the partons were spin 1/2 fermions it became clear that the partons could be identified as the quarks, introduced by Gell-Mann in 1963 to explain the hadron family structure.

Deep inelastic electron scattering off a nucleon can thus be treated as elastic scattering of an electron against a 'free' quark inside the nucleon,  $e^- + q \rightarrow e^- + q$ , which is illustrated in Figure 5.6.

Four-momentum conservation gives:

$$(p_e + p_q) = (p'_e + p'_q)$$

$$p'_q = p_e + p_q - p'_e$$

$$p_q'^2 = (p_e + p_q - p'_e)^2 = p_e^2 + p_q^2 + p_e'^2 - 2p_e \cdot p'_e + 2p_q \cdot (p_e - p'_e)$$

$$\text{but } p_e^2 = p_e'^2 = m_e^2 \quad \text{and} \quad p_q^2 = p_q'^2 = m_q^2$$

At high energies we can neglect the mass of the electron since:  $m_e^2 \ll E_e^2 \Rightarrow m_e \approx 0$

$$m_q^2 = m_q^2 - 2p_e \cdot p'_e + 2p_q \cdot (p_e - p'_e)$$

$$\Rightarrow 2p_q \cdot (p_e - p'_e) = 2p_e \cdot p'_e$$

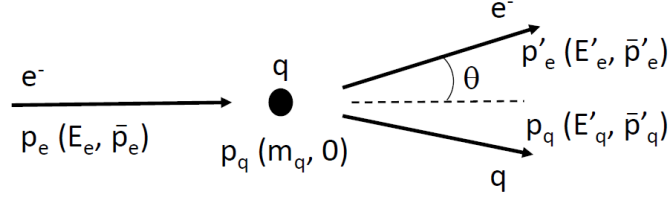


Figure 5.6: Illustration of the elastic scattering of an electron off a quark in the laboratory system, showing the four-momenta of the particles in the initial and final states.

But  $p^2 = E^2 - \bar{p}^2$

$$\Rightarrow E_q(E_e - E'_e) - \bar{p}_q(\bar{p}_e - \bar{p}'_e) = E_e E'_e - \bar{p}_e \bar{p}'_e \quad (5.17)$$

However,  $m_e \approx 0 \Rightarrow E_e \approx |\bar{p}_e|$  and  $E'_e \approx |\bar{p}'_e|$

$\Rightarrow \bar{p}_e \bar{p}'_e = |\bar{p}_e| |\bar{p}'_e| \cos \theta \sim E_e E'_e \cos \theta$  since the masses are neglected

Now, the quark is at rest  $\Rightarrow \bar{p}_q = 0 \Rightarrow E_q = m_q$ . Inserting in equation 5.17:

$$\Rightarrow m_q(E_e - E'_e) = E_e E'_e - E_e E'_e \cos \theta = E_e E'_e (1 - \cos \theta)$$

$$\Rightarrow m_q = \frac{E_e E'_e (1 - \cos \theta)}{(E_e - E'_e)}$$

This is the mass on which the electron is scattering

Define the fraction of the proton four-momentum that is carried by the quark as  $x$ . Since  $p_q^2 = m_q^2$  and  $p_p^2 = m_p^2$  we have:

$$x = \frac{m_q}{m_p} = \frac{E_e E'_e (1 - \cos \theta)}{m_p (E_e - E'_e)}; \quad 0 < x < 1$$

Since we know the energy of the incoming electron beam,  $E_e$ , and measure the energy,  $E'_e$ , and scattering angle,  $\theta$ , of the outgoing electron, we can extract  $x$ .

But we have shown in equation 5.2 that  $q^2 = -2E_e E'_e (1 - \cos \theta)$  and  $(E_e - E'_e)$  is the energy transfer  $\nu$  by the exchanged photon, and according to equation 5.9  $m_p \nu = p_p q$ .

$$\Rightarrow \boxed{x = -\frac{q^2}{2m_p \nu} = -\frac{q^2}{2p_p q}} \quad (5.18)$$

which is a dimensionless parameter called the Bjorken scaling parameter. From equation 5.10 we have  $y = \frac{2m_p \nu}{(s - m_p^2)}$  and from equation 5.18 we have  $x = -\frac{q^2}{2m_p \nu} = \frac{Q^2}{2m_p \nu}$ . By multiplying these expressions we get:

$$x \cdot y = \frac{Q^2}{s - m_p^2}$$

$$\Rightarrow Q^2 = (s - m_p^2)x \cdot y$$

But in deep inelastic scattering the mass of the proton can be neglected.

$$\Rightarrow \boxed{Q^2 = s \cdot x \cdot y}$$

In deep inelastic scattering we have two independent variables, which have to be measured in order to fully reconstruct the kinematics of the event. Since the energy of the incoming electron is known to high degree of accuracy, the kinematics of the scattering process can be completely determined by measuring the energy of the final state electron and the scattering angle. Thus, the produced hadrons doesn't have to be measured, but constitute the missing mass of the process. The two independent variables are normally chosen to be  $x$  and  $Q^2$ .

$$\boxed{x = \frac{m_q}{m_p} = \frac{E_e E_e' (1 - \cos \theta)}{m_p (E_e - E_e')}$$

$$\boxed{Q^2 = 2E_e^2 (1 - \cos \theta)}$$

and the cross section is then given by:

$$\frac{d^2 \sigma}{dx dQ^2} = \frac{4\pi \alpha^2}{Q^4} \left[ \left(1 - y - \frac{m_p^2 y^2}{Q^2}\right) \frac{F_2(x, Q^2)}{x} + y^2 F_1(x, Q^2) \right]$$

For deep inelastic scattering the form factors are replaced by *structure functions* since we are here probing the constituents of the nucleon.

Note that although the same notation for form factors and structure functions are often used, they do not describe the same thing. Form factors describe the shape of a nucleon, whereas structure functions contain information about the inner structure of a nucleon i.e. the partonic content of a nucleon.

In the table below a comparison between the kinematic variables for the proton and parton, respectively, are shown.

	<i>Proton</i>	<i>Parton</i>
<i>Energy</i>	$E$	$xE$
<i>Momentum</i>	$p_L$	$xp_L$
	$p_T = 0$	$p_T = 0$ <i>if we neglect the primordial motions of the partons</i>
<i>Mass</i>	$m_p = \sqrt{E^2 - p_L^2}$	$m_q = \sqrt{(x^2 E^2 - x^2 p_L^2)} = x \sqrt{(E^2 - p^2)} = x m_p$

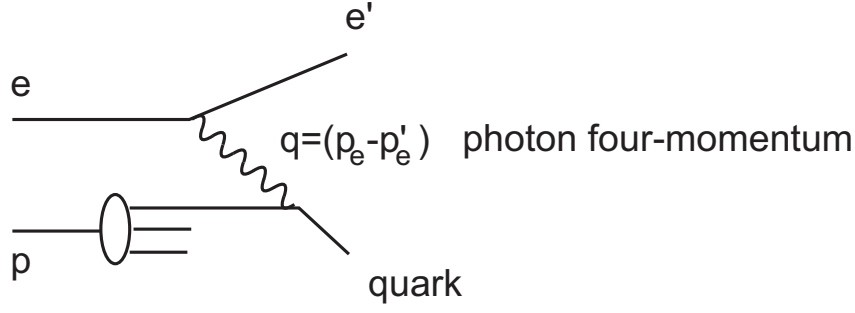


Figure 5.7: Feynman diagram describing a deep inelastic electron-proton scattering via the exchange of a photon (neutral current process).

The dominant  $ep$ -scattering at low energies proceeds via virtual photon exchange (*neutral current process*), the Feynman diagram of which is shown in Figure 5.7.

Since the photon couples to both  $u$ - and  $d$ -quarks only the total  $x$ -distribution for the quarks are measured in this process and not for the  $u$ - and  $d$ -quarks individually.

We found in Section 3.2.4:  $\frac{d\sigma^{ee}}{d\Omega} \sim \frac{e^4}{q^4}$  for electron-electron scattering, where  $q^2$  is the momentum transfer squared.

For electron-quark scattering we consequently have:  $\frac{d\sigma^{eq}}{d\Omega} \sim \frac{e^2 e_q^2}{q^4}$

where  $e^2$  comes from the  $e\gamma e$  vertex and  $e_q^2$  from the  $q\gamma q$  vertex and  $e_q = +2/3$  or  $-1/3$ .

The cross section for  $ep$  scattering can be factorized according to:

$$\frac{d\sigma^{ep}}{d\Omega} = \sum_{quarks} \int_0^1 F(x) \frac{d\sigma^{eq}}{d\Omega} dx \sim \sum_{quarks} e_q^2 \int_0^1 F(x) \sim \frac{4}{9} \int_0^1 F_u(x) + \frac{1}{9} \int_0^1 F_d(x), \quad (5.19)$$

measured at a specific  $q^2$ .

where  $F_u$  and  $F_d$  are called *parton distribution functions*, or abbreviated *pdf:s*, and they represent the probabilities for the electron to scatter against a  $u$ - or  $d$ -quark in the proton carrying a fraction  $x$  of the proton momentum, if it is probed at a momentum transfer squared of  $q^2$ .

Both the photon and the  $Z^0$ -boson, which are exchanged in neutral current processes, couple to  $u$ - and  $d$ -quarks. In charged current processes a  $W$ -particle is exchanged and we have the following reactions:

$$e^- + p \rightarrow \nu_e + X,$$

and

$$e^+ + p \rightarrow \bar{\nu}_e + X,$$

of which the Feynman diagrams are shown in Figures 5.8 and 5.9.

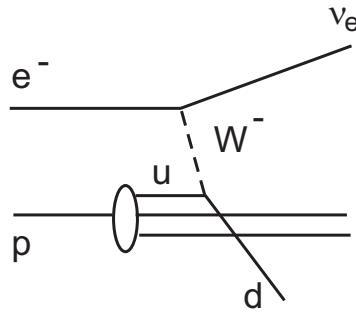


Figure 5.8: Feynman diagram describing a deep inelastic electron-proton scattering via the exchange of a  $W^-$ -boson (charged current process).

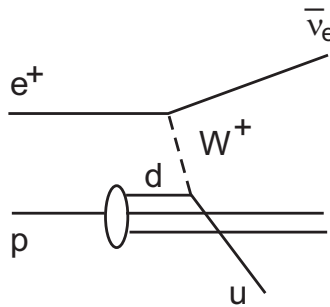


Figure 5.9: Feynman diagram describing a deep inelastic electron-proton scattering via the exchange of a  $W^+$ -boson (charged current process).

Thus, by choosing either an incoming electron beam or a positron beam we can measure the structure functions of the  $u$ - and  $d$ -quarks separately.

Note that parton distribution functions can not be calculated from QCD but have to be determined through measurements. By measuring the differential cross section  $\frac{d\sigma}{dx dQ^2}$ , the *structure functions* can be extracted and fits to the data point of QCD-based models, provide information on the parton distribution functions. The measurement of the parton distribution functions at SLAC is shown in Figure 5.10. Integrating the parton distribution functions from SLAC over the entire  $x$ -range, resulted in a momentum contribution from  $u$ - and  $d$ -quarks of approximately 50% of the total proton momentum. The remaining momentum is carried by the gluons.

### 5.3 Experimental evidence for confinement and asymptotic freedom

After the quarks had been introduced in the beginning of the 1960:ies, an extensive experimental effort started in order to find free quarks. As this failed, it became clear that the quarks, if they existed as real particles, couldn't escape the nucleon and that the strong force had to accommodate such a property. This feature was called *confinement* and has been discussed in Section 3.4.2. On the other hand the parton model was able to explain the results from the

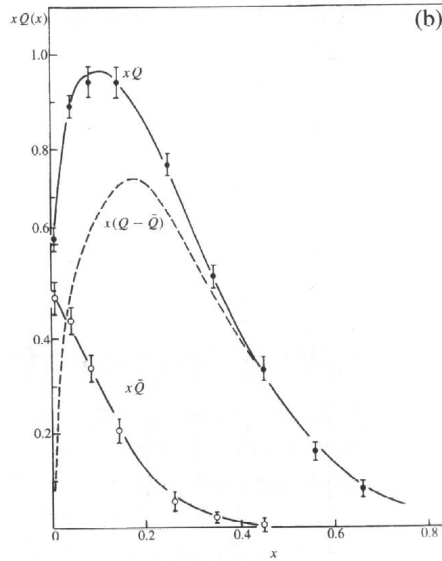


Figure 5.10: Measured parton distribution functions of quarks and antiquarks.

SLAC-experiment, by assuming that the partons are moving as free particles within the nucleon if they are close together. Thus, the strong force also has to incorporate *asymptotic freedom*. Thus, any theory that claims to correctly describe the dynamics of partons (parton has been accepted as a common name for quarks and gluons) inside the nucleon has to include these two extreme properties. These two properties of the strong force is reflected in the behaviour of the strong coupling constant,  $\alpha_S$ . As the nucleon is probed at short distances i.e. at high momentum transfers (energies), the strong interaction is weak, meaning that the value of  $\alpha_S$  is small. On the other hand if the nucleon is probed at lower momentum transfers i.e. at larger distances between the partons, of the order of  $1 \text{ fm}$ , the strength of the strong force increases i.e. the value of  $\alpha_S$  gets bigger. This so called *running coupling constant* had to be tested, quantified and proven by experiments in order to verify the asymptotic freedom.

The most obvious evidence for confinement is the failure to produce isolated quarks, even though the energies entering into the process was far beyond the pair production energy for a quark-antiquark pair. Confinement is also supported by the production of jets from the hadronization process, as discussed in Sections 3.4.4 and 3.4.5.

In deep inelastic scattering experiments the momentum transfer changes from event to event depending on how hard the scattering is. At HERA the  $Q^2$ -range was sufficiently wide to measure the running of  $\alpha_S$  in one and the same experiment, which minimized the systematic errors of the measurement. Figure 5.11 shows the results on  $\alpha_S$  as a function of the transverse energies of the jets produced, from the two HERA experiments H1 and ZEUS, together with a QCD fit.

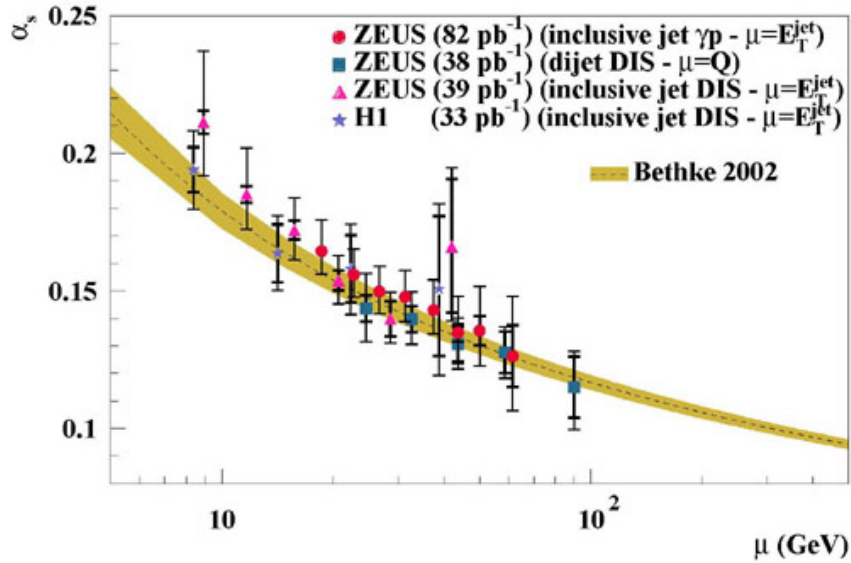


Figure 5.11: Measurements of  $\alpha_S$  as a function of the jet energy measured perpendicular to the direction of the incoming proton (the transverse jet energy),  $\mu = E_T^{jet}$ .

## 5.4 The Behaviour of the Structure Function

What can we expect the structure function to look like? Let us start by assuming that the proton contains just one quark. Then this quark will carry the total momentum of the proton i.e.  $x = 1$ . But we know that the proton has three *valence quarks*, two  $u$ -quarks and one  $d$ -quark, and provided they don't interact they have to share the momentum of the proton such that  $x = 1/3$  for each quark. Due to the fact that the quarks continuously exchange gluons and thereby momentum is transferred from one quark to another, each quark does not necessarily carry exactly  $1/3$  of the proton momentum at each instant. This results in a momentum distribution around  $x = 1/3$ . This is, however, again not the full story since a gluon which is emitted by a quark can fluctuate into a quark-antiquark pair (*sea quarks*), which at that moment also takes a share of the proton momentum. Since the sea quarks predominantly will take a smaller fraction of the proton momentum they will give contributions in the lower region of the  $x$ -distribution. This behaviour is illustrated in Figure 5.12.

Early results from deep inelastic scattering experiments showed little dependence of the structure function on  $Q^2$ . However, as the ep-collider HERA came into operation in 1992 a much wider kinematic range could be investigated. Figure 5.13 shows the structure function as a function of  $x$ , in different bins of the photon virtuality,  $Q^2$ . The most prominent feature is the unexpectedly strong rise of the structure function at low  $x$ -values, which according to the discussion above is dominated by sea-quarks and gluons.

Since LHC is mainly a gluon-collider (see Figure 4.2.17) the precise knowledge of the gluons structure function at low  $x$  is essential for e.g. Higgs production and W/Z production. For example the cross section for Higgs production can be written:

$$\sigma(pp \rightarrow HX) \sim \int_0^1 \int_0^1 g(x_1)g(x_2)\sigma(gg \rightarrow H)dx_1dx_2 ,$$



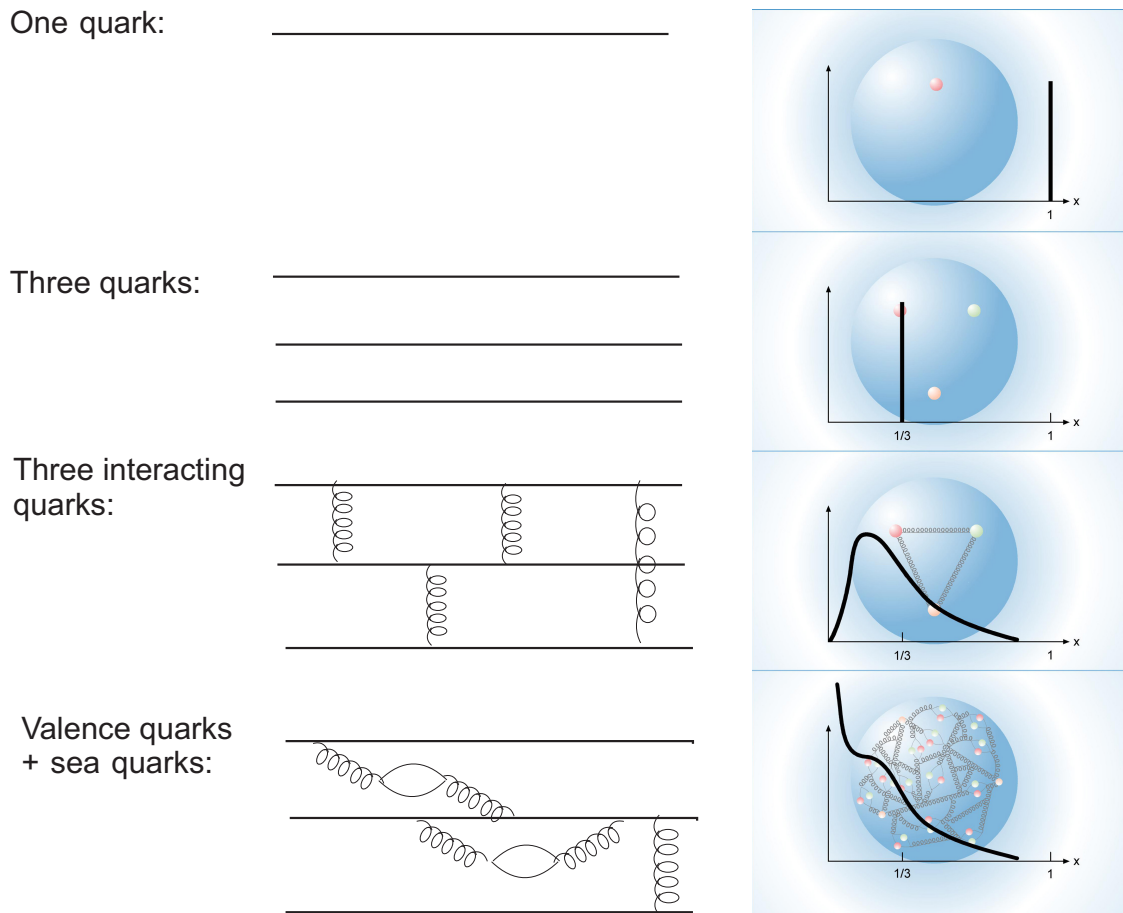


Figure 5.12: *Expected spectra of the fractional momenta (structure function) for different assumptions of the parton content in the proton.*

where  $x_1$  and  $x_2$  are the fractional gluon momenta. The precision measurements of the structure functions at HERA decreased the error of the Higgs measurement from 25%, prior to HERA, to 5%.

## 5.5 Scaling

As already discussed in Section 5.1 the scattering of the photon against a composite nucleon has a cross section, which depends on the momentum transferred by the exchanged photon  $\bar{q}$ , through form factors which reflects the shape of the object (see equation 5.16). However, as the momentum of the photon becomes very large it will penetrate deeply into the nucleon and assuming that the nucleon is composed of point-like constituents the electrons should scatter elastically against a point-like quark in the proton. Since quarks have no extension there is no shape to be measured and therefore the cross section should not depend on the momentum of

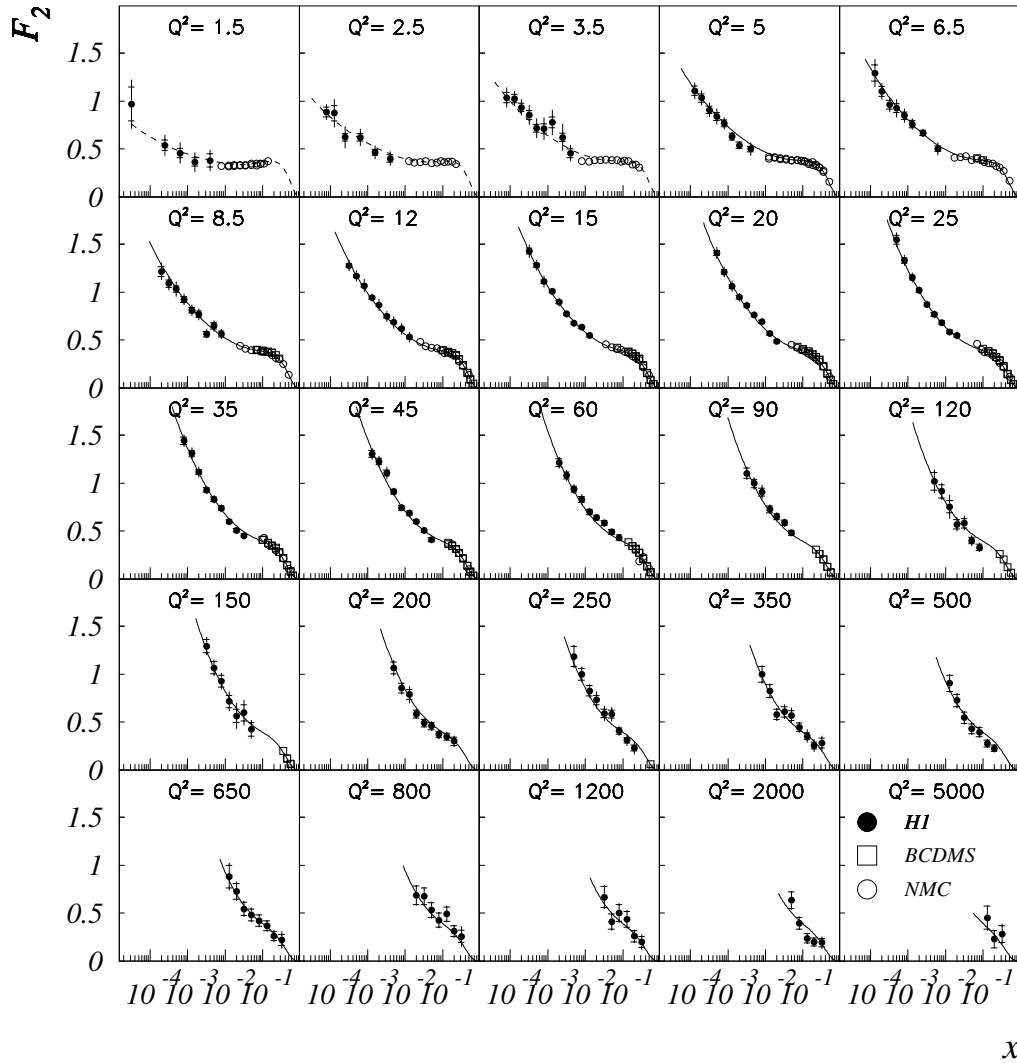


Figure 5.13: Measurements of the structure function  $F_2$ , as a function of the fraction of the proton momentum carried by the parton,  $x$ , for different virtualities (resolution power),  $Q^2$ , of the exchanged photon.

the virtual photon i.e. the momentum transfer. Influenced by the results from SLAC the American physicist J. Bjorken performed calculations based on the assumption that the nucleon is composed of point-like constituents and came to the conclusion that that the structure functions should exhibit a scaling property in the limit of  $Q^2$  approaching infinity, which implies that the structure function should not depend on the momentum transfer but only on a dimensionless quantity. This quantity is the so called Bjorken scaling variable  $x$ , which is given in equation 5.18 and the scaling property was consequently called *Bjorken scaling*.

The SLAC results and subsequent early experimental measurements of the structure function, which covered an  $x$ -range around 0.3, did not exhibit any dependence on  $Q^2$ , consistent with scaling. However, as deep inelastic scattering could be investigated in a wider kinematic range, through the advent of HERA, clear deviations from scaling were observed, which can be seen from the Figure 5.14.

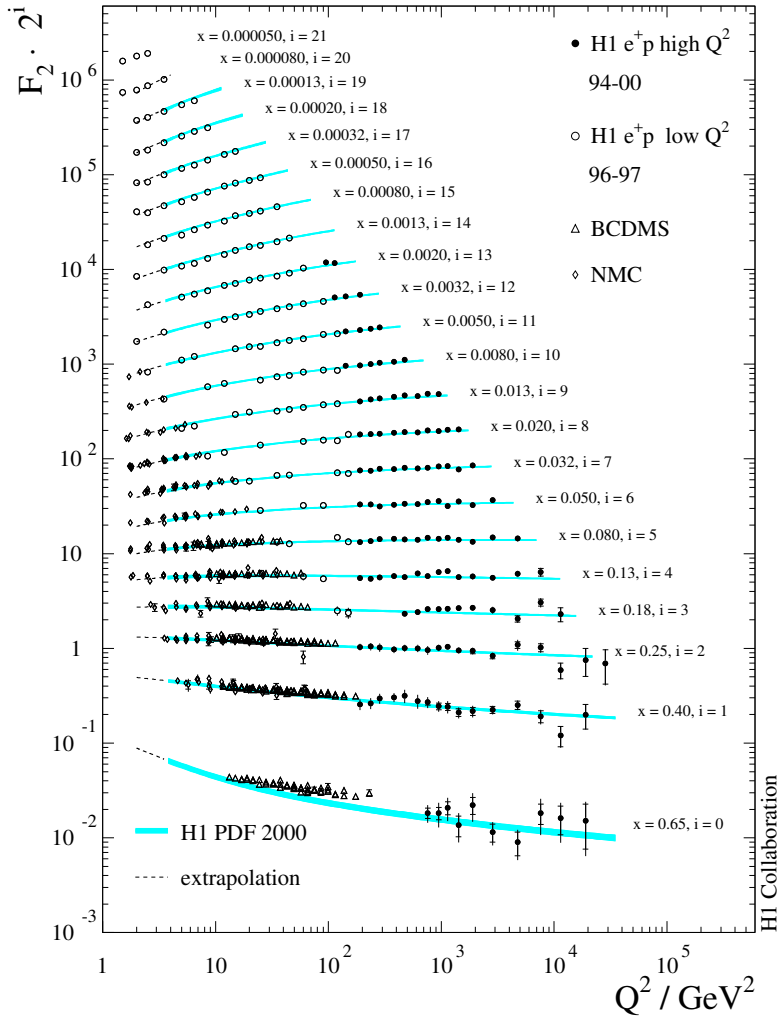


Figure 5.14: Measurements of the structure function  $F_2$ , as a function of the virtuality (resolution power),  $Q^2$ , of the exchanged photon, for different fractions of the proton momentum carried by the parton,  $x$ .

## 5.6 Scaling Violation

We have now realized that the proton is a particle with a very complex structure of quarks and gluons. It means that when we probe the inner of the proton the probe does not necessarily scatter against a valence quark but could with a certain probability instead scatter against a sea quark.

Extended measurements of the structure function into a wider range of  $x$  and  $q^2$  revealed violation of the scaling behaviour, such that the structure function decreases with  $q^2$  at higher  $x$ -values and increases with  $q^2$  for lower  $x$ -values as can be observed in Figure 5.14.

This can be understood in the following way. If the momentum of the photon is relatively low it will scatter against one of the valence quarks in a way that is described by the lowest

order diagram as shown in Figure 5.15. This diagram is of zeroth order in the strong coupling constant,  $\alpha_S$ , since the scattering is a pure electromagnetic process. (At higher energies also  $Z^0$  exchange will contribute). In this case the process is very similar to the lowest order electron-electron scattering.

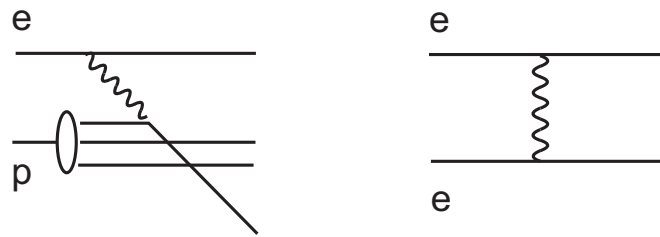


Figure 5.15: *Feynman diagrams showing the similarity between a neutral current electron-proton scattering of zeroth order in the strong coupling constant (effectively electron-quark scattering) and electron-electron scattering.*

If the photon momentum is increased it may resolve details in the quantum-mechanical substructure of the proton such that what to a lower momentum photon appeared as a single quark, will be revealed by a higher momentum photon to be a quark accompanied by a gluon, as illustrated in Figure 5.16. This process is called QCD-Compton scattering (QCDC) and resembles the Compton scattering process in QED.

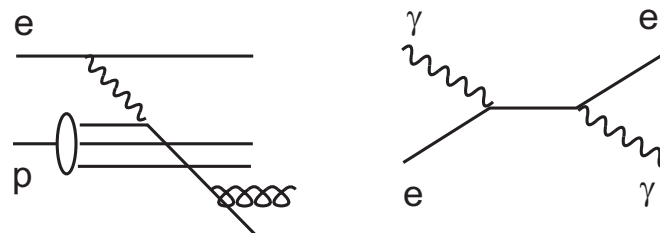


Figure 5.16: *Feynman diagrams showing the similarity between a neutral current electron-proton scattering of first order in the strong coupling constant (QCD Compton scattering) and QED Compton scattering.*

An even higher momentum photon may resolve a gluon, radiated by a valence quark and subsequently fluctuating into a sea-quark pair. This process, depicted in Figure 5.17, is called boson-gluon fusion (BGF) and is similar to photon-photon fusion in QED.

So, the momentum, which was originally assigned to a single quark as the proton was probed at low momenta must be divided between the quark and the gluon as the proton is probed at higher momenta. In case a sea-quark pair is resolved the fraction of the valence quark momentum taken by the gluon is split between the quark-antiquark pair and the more quarks we resolve in the proton the less momentum each of them will carry. Thus the higher the momentum of the probe is the more low  $x$  quarks will be probed. This makes the structure function look different if it is measured at low  $q^2$  than at high  $q^2$ , as illustrated in Figure 5.18.

If we choose a specific  $x$ -value in the diagram of Figure 5.14, we notice that if  $x$  is small,  $F(x)$  is higher at large values of  $q^2$  than at small values of  $q^2$ . On the other hand if we choose a large

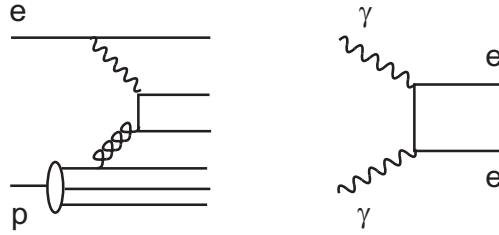


Figure 5.17: Feynman diagrams showing the similarity between a neutral current electron-proton scattering of first order in the strong coupling constant (Boson-Gluon-fusions) and gamma-gamma fusion.

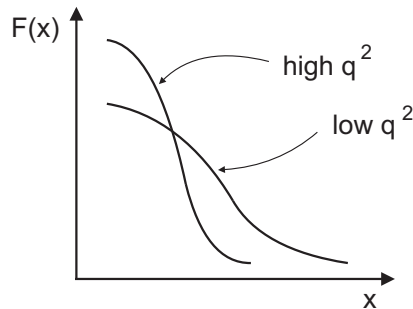


Figure 5.18: Behaviour of the structure function,  $F_2$ , as a function of the fractional momentum,  $x$ , for low and high power resolution,  $q^2$ , respectively.

value of  $x$ ,  $F(x)$  will be large for low values of  $q^2$  and small for high values of  $q^2$ . Thus, the scaling violations are driven by gluon emission.

## 5.7 Comparison of Neutral and Charged Current Processes

For electron-electron scattering we have previously found:

$$\frac{d\sigma}{d\Omega} \sim \frac{e^4}{(m_\gamma^2 - Q^2)^2}$$

and for electron-proton (electron-quark) scattering the corresponding expression is:

$$\frac{d\sigma}{d\Omega} \sim \frac{e^2 e_q^2}{(m_\gamma^2 - Q^2)^2}$$

If we now have a  $Z^0$  or  $W$ -exchange instead of a photon exchange we get:

$$\frac{d\sigma}{d\Omega} \sim \frac{\text{coupling}^4}{(m_Z^2 - Q^2)^2}$$

$$\frac{d\sigma}{d\Omega} \sim \frac{\text{coupling}^4}{(m_W^2 - Q^2)^2}$$

Note that the four-momentum of the exchanged virtual particle is not the same as the rest mass of the corresponding real particle (see section 3.1).

As long as  $m_{Z^0}$  and  $m_W$  are large compared to  $Q^2$  the weak interaction is suppressed relative to the electromagnetic interaction. Only if  $Q^2$  becomes comparable to  $m_{Z^0}$  and  $m_W$ , the weak interaction makes a significant contribution.

Processes where a photon (or a  $Z^0$ -boson) has been exchanged are called *neutral current* processes, whereas processes where a charged  $W$ -boson has been exchanged are called *charged current* processes.

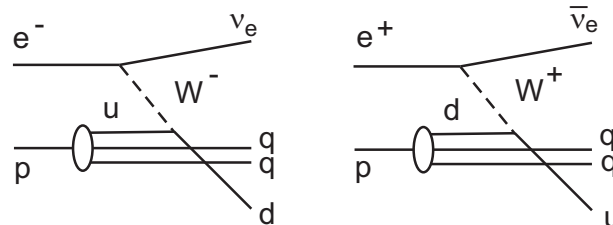


Figure 5.19: Feynman diagram showing charged current electron-proton process of zeroth order in the strong coupling constant, corresponding to electron scattering against a  $u$ - (left) and  $d$ -quark (right), respectively.

The cross section for  $e^-p$  scattering ( $W^-$ -exchange) is in first approximation expected to be twice as big as that of  $e^+p$  scattering ( $W^+$ -exchange), since the proton contains two valence quarks of  $u$ -type but only one of  $d$ -type.

At small  $Q^2$  values  $\gamma$ -exchange will dominate, due to the suppression of the cross section by the high masses of the weak bosons. Since the mass of the photon is zero the cross section will vary as  $1/Q^4$ . The charged current cross section is essentially flat in this region since  $Q^2$  is small compared to  $m_W^2$ . As  $Q^2$  gets of the same order as the mass squared of the weak bosons, the neutral- and charged-current cross sections become essentially equal because the processes then are dominated by  $Z$  and  $W$  exchange and their masses are almost the same. At even higher  $Q^2$ -values, the charge current cross sections start falling off again as  $Q^2$  starts to dominate over the square of the  $W$ -masses. These results from HERA provided a manifestation of the electroweak unification, as seen in Figure 5.20.

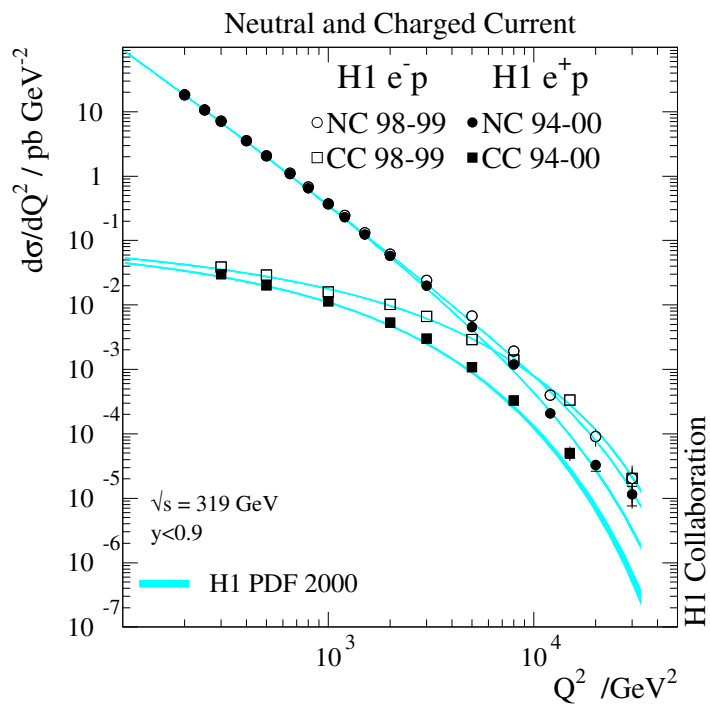


Figure 5.20: Measurements comparing the cross sections of charged and neutral current electron-proton scattering processes as a function of the momentum transferred by the virtual boson exchanged in the process.

# Chapter 6

## Extensions of the Standard Model

It is clear that the standard model is not the final theory since there are several fundamental questions that this theory does not provide answers to, like:

- Why are there six flavours of leptons and quarks?
  - Why are there three families?
  - Why do we have a mass hierarchy of leptons and quarks?
  - What determines the couplings of the particles?
  - Will the forces unify?
  - Why are the electric charges quantized?
  - What is the field theory of gravitation?
  - What is dark matter made of?
- etc.

### 6.1 Grand Unified Theories (GUT)

A natural next step following the successful unification of the weak and electromagnetic forces, was an attempt to include also the strong force into an extended symmetry group, which means that the known fermions, the leptons and the quarks, are incorporated into the same multiplet, such that leptons and quarks may transform into each other. There are several ways to do this and below we will only discuss the simplest one. Consider the basic family structure for the first generation of quarks and leptons, as shown in Figure 6.1.

Here all known fermions i.e. both leptons and quarks, are included into multiplets, which provide a natural charge quantization, giving  $d = -1/3$  and  $u = +2/3$ . The first multiplet contains left handed particles and anti particles. Note that there is no left handed  $\bar{\nu}_e$ . The second multiplet contains right handed particles and anti particles. Note that there is no right handed  $\nu_e$ . Similar multiplets exist for the heavier quarks and leptons. The possible transitions within such a multiplet are illustrated by the matrix shown in Figure 6.2.



$$\begin{array}{cc}
\left( \begin{array}{c} \nu_e \\ e^- \end{array} \left| \begin{array}{c} \bar{d}^r \bar{d}^g \bar{d}^b \end{array} \right. \right) & \left( \begin{array}{c} \bar{u}^r \bar{u}^g \bar{u}^b \\ d^r d^g d^b \end{array} \left| \begin{array}{c} u^r u^g u^b e^+ \end{array} \right. \right) \\
\text{Charge } -1 \quad +1 & -2-1 \quad 2+1 \\
\left( \begin{array}{c} \bar{\nu}_e \\ e^+ \end{array} \left| \begin{array}{c} d^r d^g d^b \end{array} \right. \right) & \left( \begin{array}{c} u^r u^g u^b \\ \bar{d}^r \bar{d}^g \bar{d}^b \end{array} \left| \begin{array}{c} \bar{u}^r \bar{u}^g \bar{u}^b e^- \end{array} \right. \right) \\
\text{Charge } +1 \quad -1 & 2+1 \quad -2-1
\end{array}$$

Figure 6.1: The family structure for the first family of quarks and leptons according to GUT.

	$d^{\text{red}}$	$d^{\text{green}}$	$d^{\text{blue}}$	$e^+$	$\bar{\nu}_e$
$d^{\text{red}}$	$g^o, \gamma, Z^o$	$g^{r \rightarrow g}$	$g^{r \rightarrow b}$	$X_{-4/3}^r$	$X_{-1/3}^r$
$d^{\text{green}}$	$g^{g \rightarrow r}$	$g^o, \gamma, Z^o$	$g^{g \rightarrow b}$	$X_{-4/3}^g$	$X_{-1/3}^g$
$d^{\text{blue}}$	$g^{b \rightarrow r}$	$g^{b \rightarrow g}$	$g^o, \gamma, Z^o$	$X_{-4/3}^b$	$X_{-1/3}^b$
$e^+$	$X_{+4/3}^r$	$X_{+4/3}^g$	$X_{+4/3}^b$	$\gamma, Z^o$	$W^+$
$\bar{\nu}_e$	$X_{+1/3}^r$	$X_{+1/3}^g$	$X_{+1/3}^b$	$W^-$	$Z^o$

Figure 6.2: The possible quark-quark, lepton-lepton and quark-lepton transitions for the first family according to GUT.

The frame in the upper left corner includes transition between quark states, whereas the frame in the lower right corner contains leptonic transitions as we know them from our previous discussion. The  $X$ -particles provide transitions between quarks and leptons and vice versa. These particles are therefore called *leptoquarks* and they have to have masses in the range  $10^{15}$  GeV in order to give the right  $W$  and  $Z$  masses. Consequently they have not yet been observed. However, if GUT is valid it should be possible to observe the transitions given in Figure 6.3.

$$\begin{array}{cc}
e^+ \xrightarrow{X_{+4/3}} d & e^- \xrightarrow{X_{-4/3}} \bar{d} \\
\bar{\nu}_e \xrightarrow{X_{+1/3}} d & \nu_e \xrightarrow{X_{-1/3}} \bar{d}
\end{array}$$

Figure 6.3: The possible transitions between quarks and leptons according to GUT.

A consequence of this is that the proton may decay according to the Feynman diagram in Figure

6.4.

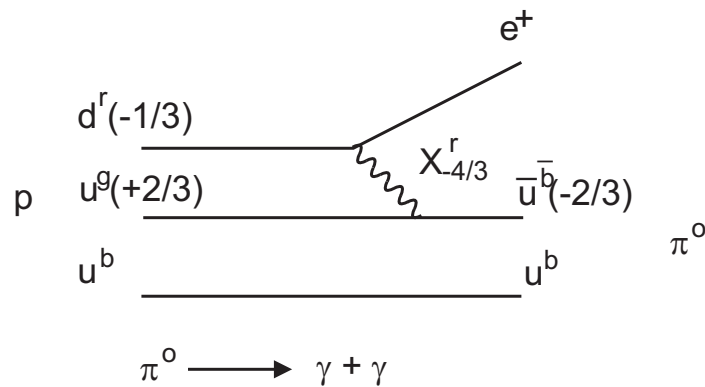


Figure 6.4: A proton decay where the  $d$ -quark is converted into an  $e^+$  via the exchange of a leptoquark.

Thus, the final state of a proton decay contains a positron and two photons. A calculation of the proton life time within this teoretical framework gives a value of  $\tau_p \approx 10^{30 \pm 1}$  years. The Superkamiokande experiment, which looks for proton decays in a water volume containing  $3 \cdot 10^{32}$  protons, has been able to set a lower limit of the proton lifetime of  $5 \cdot 10^{32}$  years. This causes some problems to the model discussed above.

## 6.2 Supersymmetry (SUSY)

We believe that all particles gain their masses through coupling to the Higgs field and from the mass spectrum of the known particles we can estimate that the Higgs particle has to have a mass in the range 100-200 GeV. One problem of the Standard Model is that, due to quantum fluctuations of the Higgs field, the Higgs mass gets large corrections from vacuum polarization diagrams, as illustrated in Figure 6.5, where  $f$  stands for fermion.

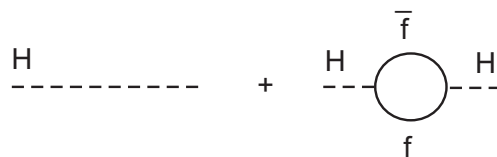


Figure 6.5: Higgs and its fluctuation, through a loop diagram, into a sfermion-anti-sfermion pair.

In an experimental measurement the 'physical mass' is always measured, whereas in a calculation the 'physical mass' is obtained as a sum of the 'bare mass' and corrections from 'loop diagrams' such that the mass may be written as:

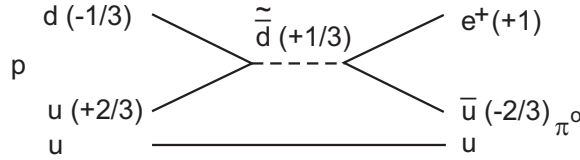


Figure 6.6: *The proton decay via an anti-d-squark.*

$$m_H^2 = m_o^2 + \delta m^2,$$

where  $\delta m^2$  is the correction to the 'bare mass'.

It turns out that  $\delta m^2 \sim \Lambda^2$ , where  $\Lambda$  is some scale which defines the energy range over which the theory is valid i.e. perturbation theory is valid. Although it is not obvious what the scale should be, it is frequently chosen to be the Planck scale i.e.  $10^{19}$  GeV. The Planck scale is obtained from the Newton gravitational constant, which in contradiction to the other coupling constants in the standard model, has the dimension of  $1/(mass)^2$ . The consequence of this is that the theoretical mass of the Higgs is pushed up to the energy scale of Grand Unification,  $m_H \sim 10^{16}$  GeV. This is called the *hierarchy problem*.

If there are more massive particles in the unexplored mass range, these would inevitably appear in virtual processes at lower energies and give large corrections. Although bosons and fermions seem to have different behaviours, it might be that they are related on a more fundamental level. In the theory of *Supersymmetry*, or short *SUSY*, it is assumed that every particle in the Standard Model has its supersymmetric partner, in the sense that the laws of physics are symmetric under the exchange of bosons and fermions. The SM particles and their SUSY partners differ in their spin by half a unit such that:

Standard Model	SUSY partner
fermion (spin 1/2)	boson (spin 0) = SUSY-fermion
boson (spin 1)	fermion (spin 1/2) = SUSY-boson

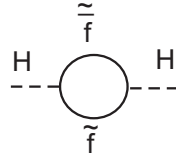
Note that the SM-bosons have spin 1 and are thus *vector bosons* whereas the SUSY-bosons have spin 0 and are *scalar bosons*.

The supersymmetric particles are generally called *sparticles*, and their names are more specifically given in the table below:

Standard Model	SUSY
quarks	squarks
leptons	sleptons
photon	photino
gluon	gluino
W	wino
Z	zino
Higgs	higgsino
Gauge bosons	gauginos

Standard Model					SUSY				
$u$	$c$	$t$	$\gamma$	$H$	$\tilde{u}$	$\tilde{c}$	$\tilde{t}$	$\tilde{\gamma}$	$\tilde{H}$
$d$	$s$	$b$	$g$		$\tilde{d}$	$\tilde{s}$	$\tilde{b}$	$\tilde{g}$	
$\nu_e$	$\nu_\mu$	$\nu_\tau$	$Z$		$\tilde{\nu}_e$	$\tilde{\nu}_\mu$	$\tilde{\nu}_\tau$	$\tilde{Z}$	
$e$	$\mu$	$\tau$	$W$		$\tilde{e}$	$\tilde{\mu}$	$\tilde{\tau}$	$\tilde{W}$	

It is assumed that Higgs couple to supersymmetric particles in the same as to normal particles. Including the contribution from loop diagrams containing supersymmetric particles



the mass of the Higgs is modified such that:

$$m_H^2 = m_o^2 + \delta m^2 + \delta \tilde{m}^2,$$

where  $\delta \tilde{m}^2$  denotes the corrections from loop diagrams with sfermions. The correction  $\delta \tilde{m}^2$  is also proportional to  $\Lambda^2$  but since the radiative corrections from virtual boson and fermion loops are of opposite signs, there will be a cancelation of the large corrections.

This cancellation would be complete if the masses of a particle and its corresponding sparticle would be exactly the same,  $m_{SM} = m_{SUSY}$ , which we know it is not since we haven't seen any sparticles yet. In order for the cancellation to occur at the right accuracy, giving a Higgs mass of about 100 GeV, the supersymmetric particles should have masses around the TeV scale or below. Thus, if they exist they should be found at a future accelerator which provides enough energy to produce such high mass particles. For a specific point in the parameter space of SUSY the mass spectrum looks like in Figure 6.7.

It should be noticed that the heaviest sparticle is the gluino and the lightest squark is the stop particle. In SUSY models a minimum of two Higgs doublets are required. The gauginos  $\tilde{\gamma}$ ,  $\tilde{W}^\pm$  and  $\tilde{Z}$  will mix with the Higgsinos to form mass eigenstates called *charginos* and *neutralinos* according to:

$$\chi^o = N_1 \tilde{\gamma} + N_2 \tilde{Z}^o + N_3 H^o + N_4 h^o$$

where the N-coefficients are normalised such that  $\sum_{i=1}^4 N_i = 1$ . There are four chargino and four neutralino states as seen from Figure 6.7. The lightest supersymmetric particle (LSP) is the lightest neutralino,  $\chi_1^o$ , which has to be stable. Some production mechanisms in proton-proton collisions are shown in Figure 6.8.

Each SUSY particle will decay in a cascade process into  $\chi_1^o$ . The decay of a gluino is shown in Figure 6.9 as an example.

By observing the rotational velocity of galaxies it is possible to estimate the total mass inside a radius at which the velocity is measured. It turns out that the mass required for the observed velocity is much higher than the mass that can be observed by astronomical instruments. Actually as much as around 90 % of the galactic mass is carried by these unobservable objects,

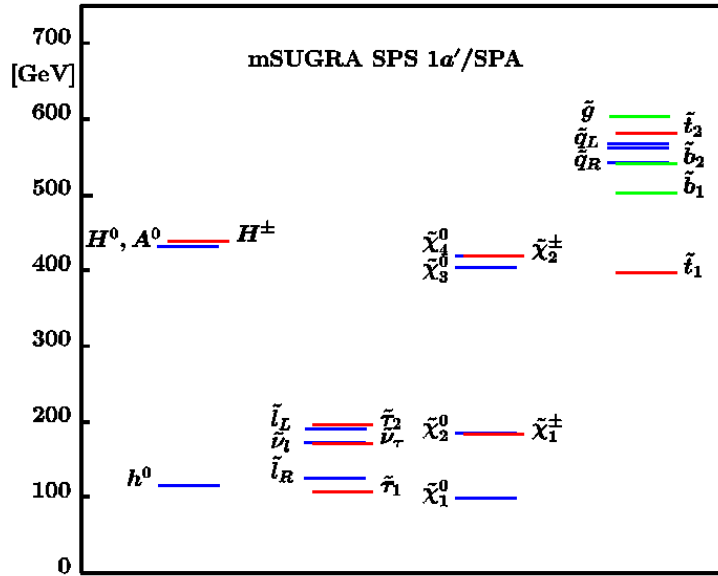


Figure 6.7: The mass spectrum of supersymmetric particles for a specific point in the parameter space of SUSY.

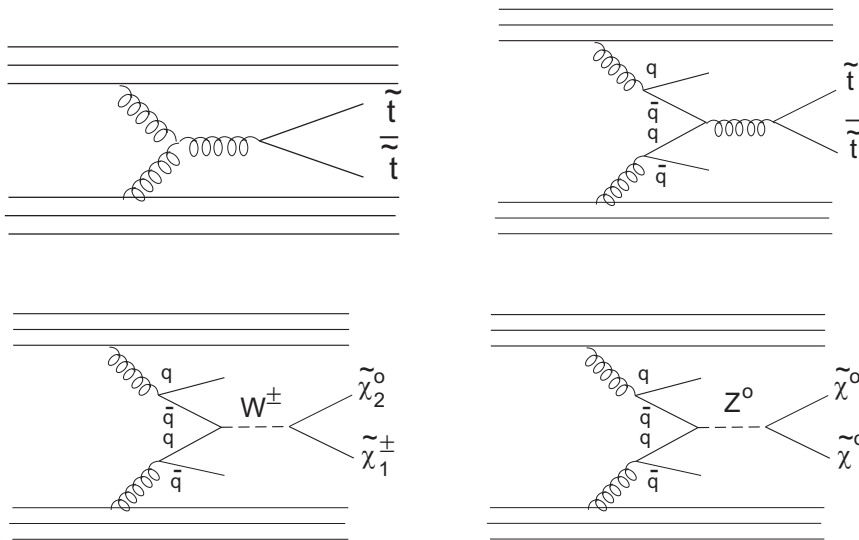


Figure 6.8: Examples of Higgs production mechanisms from proton-proton collisions with subsequent decays.

which for that reason is called *dark matter*. A possible candidate for dark matter is the lightest neutralino, which is stable and doesn't interact with matter.

A problem with the SUSY theory is that the proton decay time comes out very short, whereas we know that most protons were created in the first fractions of a second after Big Bang and thus must have a lifetime comparable to the lifetime of Universe.

From the Feynman diagram shown in Figure 6.10 it is clear that the baryon and lepton numbers

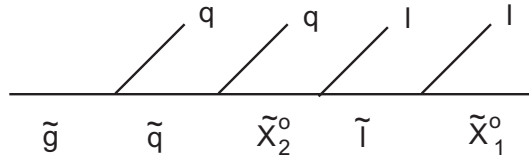


Figure 6.9: *The decay chain of a gluino.*

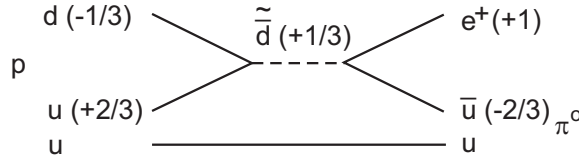


Figure 6.10: *The proton decay via an anti-d-squark.*

are not conserved in this decay. Instead the theorists have introduced a new quantum number, called *R-parity*, which, if required to be conserved, would increase the lifetime of the proton such that it will be consistent with experimental limits. The definition of R-parity is  $R = (-1)^{3(B-L)+2J}$ , where  $B$  is the baryon number,  $L$  is the lepton number and  $J$  the spin.

### 6.3 String Theories

Since field theories have been very successful in describing the electromagnetic, weak and strong forces, it seems very attractive to try to also formulate a field theory for gravitation. This would provide a quantum mechanical description of the objects in Universe and would therefore need a combination of quantum mechanics and general relativity. General relativity states that space and time are bent through the influence of the gravitational force in a way which allows the motion of heavy macroscopic objects to be described and understood. On the other hand microscopic objects needs quantum mechanics for their description. In some extreme situations like black holes we have very massive objects which are at the same time microscopic and for their description we need both quantum mechanics and general relativity. It turns out that when we try to combine the two we get predictions which are unphysical in the sense that probabilities become infinite (i.e. so called *singularities* appear), if we assume that the fundamental particles are pointlike, as in the Standard Model.

The reason for this is related to the Heisenberg uncertainty principle according to which energy can be created out of vacuum provided that it disappears again within a time that is given by Heisenberg's relation. As we have already mentioned this is called *quantum fluctuations*. In normal situations space and time are varying smoothly but if we look on a microscopic scale the quantum fluctuations will appear and distort the smooth space-time geometry. This is the situation that normal field theories, in which the fundamental particles are treated as pointlike objects, can not handle.

The string theory modifies the picture of the standard field theories by assuming that the fundamental constituents are not pointlike particles but small loops of one-dimensional vibrating strings. The smallest length of a string is given by the Planck length ( $10^{-35}$  m), which makes the strings appear pointlike unless they are observed with a resolution better than the Planck length. The Planck length is given by:

$$l_{Planck} = (G \cdot \hbar / c^3)^{1/2}$$

where  $G$  is Newton's constant and  $\hbar$  is the Planck constant. The conflict between the general relativity and quantum mechanics has its origin in the behaviour of the space-time geometry at scales below the Planck length. Due to its length a string can not resolve structures smaller than the Planck length and is therefore not sensitive to the catastrophic consequences of the quantum fluctuations, which lead to infinities in normal field theories

Only vibrational patterns (the number of waves) which fit into the length of the string are possible and lead to resonance patterns, where the properties of each elementary particle corresponds to a certain resonance pattern. This is similar to the vibrational modes by strings of musical instruments, which correspond to distinct tones. The mass of a particle is equivalent to the energy contained in the string, which is given by the wavelength and amplitude of the string together with the string tension. Consequently, if we were able to calculate the allowed vibration patterns for the strings it should be possible to explain the properties of the elementary particles, which is not possible in the standard model, where these properties have to be introduced by hand. The energy of a string is a multiple of the Planck energy ( $10^{19}$  GeV). How is it possible that a string with an energy that is several orders of magnitude higher than the masses of the particles that build up our world, can reproduce these? According to Heisenberg uncertainty principle, strings are also subject to quantum fluctuations which, however, contribute negative energy and thus compensate for the energy content in the original string. This will lead to essentially a cancellation of the energy in the string vibration patterns with the lowest energy (equal to about the Planck energy) by the negative energy of the quantum fluctuations such that the net energy will be low and the corresponding masses will be equal to the masses of the known matter- and force mediating particles. Each of the infinite number of vibration patterns should correspond to a particle state but due to the high string tension, all but a few states will have very high masses. These particles are, however, unstable and have decayed into lighter particles.

The equations of the string theory provide vibrational pattern which have properties similar to those of electrons, muons, neutrinos and quarks but also to those of the photon, W and Z bosons and gluons. Especially one vibration pattern corresponds to the properties of the graviton, which means that gravity is a natural ingredient in the string theory.

Consider the Feynman diagrams shown in Figure 6.11

The left hand diagram describes the interaction of two pointlike particles e.g. an electron and a positron, which annihilate and give rise to a virtual photon, that in turn can create a new particle-antiparticle pair. The right hand diagram illustrates how two string loops, representing the electron and positron, respectively, evolve with time (the direction of time is to the right as always). At some point they combine into a third loop, representing the virtual photon, which later on splits up into two new string loops.

In Feynman diagrams describing the interaction between pointlike particles, the point where the particles meet is exactly defined and this is where the interaction takes place. Thus, all



Figure 6.11: A normal Feynman diagram describing the electron positron annihilation process via a virtual photon (left), and how the corresponding diagram looks using string loops (right).

the energy that is available for the interaction is concentrated in one single point. This leads to singularities for gravitational interactions as already mentioned above. On the other hand the point of interaction between strings is not well defined but depends on the position of the observer as indicated in Figure 6.12. This smears out the interaction in such a way that the calculations give finite answers.

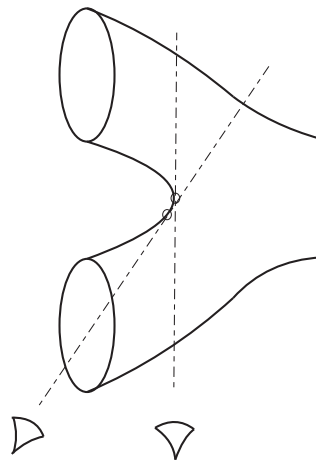


Figure 6.12: A detailed view of a string vertex.

Our Universe has three space dimensions but it can not be excluded that there are additional dimensions if they are tightly curled up so that they are confined within such a small space that they are difficult (or impossible) to observe. This can be compared to a thin water hose, which seen from far just appears to have one dimension, but at a closer look also has a small circular dimension. Why do we need extra dimensions? If a string is limited to vibrate in three dimensions, it turns out that some calculations in string theory give negative probabilities, which of course is unphysical. If, however, the string is allowed to vibrate in 9 dimensions, out of which 6 are curled-up dimensions, all the negative probabilities disappear. Thus, string theory requires that Universe has 10 dimensions in total, one time dimension and nine space dimensions.

As we already discussed, the vibrational modes of a string give the properties of the particles, and the string are vibrating in 9 space dimensions, which means that the geometry of the extra dimensions is decisive for the masses and charges of the fundamental particles that we can observe in our 3-dimensional world. However, these extra dimensions can not be curled up



in any way but has to fulfill the requirements of a special class of 6-dimensional geometrical shapes, called Calabi-Yau shapes. The present problem is that the exact equations needed to calculate the vibrational states of different Calabi-Yau shapes are so complicated that they have not yet been derived. Therefore, approximations have to be introduced, which leads to results that are not accurate enough to determine which Calabi-Yau shape is the one, that reproduces the properties of the known fundamental particles.

At present there are several different versions of the string theory but the belief is that they are just different formulations of a common 'theory of everything' (TOE). In the search for for a unifying theory (the so called M-theory), it has been realized that the string theory requires 11 dimensions (one time dimension and 10 space dimensions) instead of totally 10 dimensions as discussed above. The extra dimension becomes visible when the coupling constant of the strings becomes bigger than unity (where perturbation calculations are longer applicable) and causes one dimensional string loops to look like 'tyres' i.e. they become 2-dimensional with one dimension along the string and one circular (2-dimensional membrane). The question we may ask at this point is whether the fundamental constituent can be extended objects in even more dimensions (p-branes). In principle it could be possible but nobody knows and to find the answer the complete and exact equations of the string theory has to be found.

# Chapter 7

## Experimental Methods

### 7.1 Accelerators

Particle accelerators use electric fields to accelerate stable charged particles. The most commonly used particles to accelerate are electrons, positrons, protons and antiprotons. The principle is to let the particle pass a pair of electrodes over which an electric field is applied at the moment when it passes. This is illustrated in Figure 7.1.

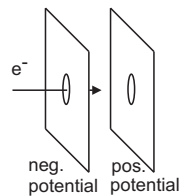


Figure 7.1: *The principle of acceleration via an electric field.*

However, a static field will only enable acceleration within a limited energy range ( typically up to 20 MeV) and in order to reach higher energies it is necessary to use an alternating electric (a.c.) field, which provides a repeated energy transfer to the particles each time they are traversing an acceleration gap. Acceleration using varying electromagnetic fields is called RF (Radio Frequency) acceleration, since the accelerator is operated at frequencies that are usually in the range of radio frequencies (MHz - GHz).

#### 7.1.1 Linear Accelerators

Since only a limited amount of energy can be transferred in each step it is favourable to let the particles travel through a succession of accelerating elements or *cavities*. Such an arrangement

makes up a *linear accelerator*, which is normally used as *injector* to all kinds of more complicated accelerator complexes. Normally, the acceleration cavities are arranged in such a way that the acceleration is performed in a standing wave mode. Typically, the electric field is driven by a voltage varying as a sinus wave, which means that the polarity of the field will have the right direction during half the period and the wrong direction during the other half of the period, as shown in Figure 7.2.

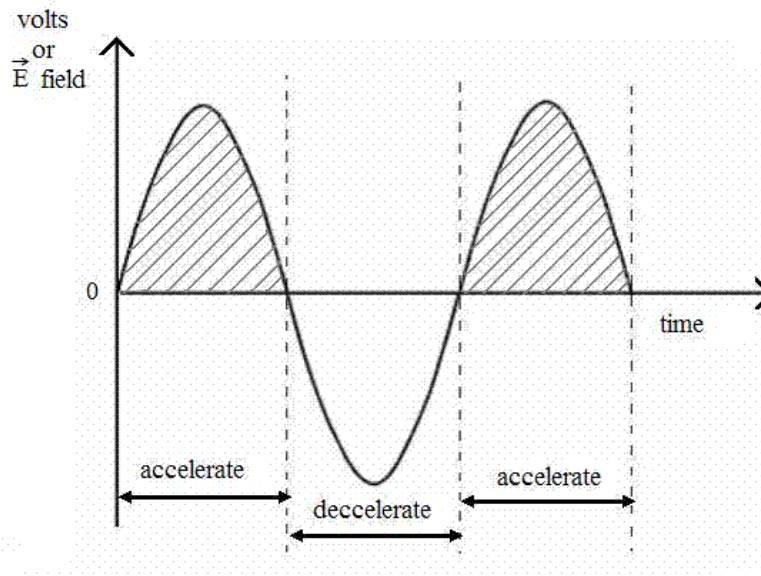


Figure 7.2: Acceleration in a standing wave mode.

This means that the beam can not be continuous since then half of the particles would be decelerated instead of accelerated so therefore the particles must come in intervals which are matched to the sinus wave. During the time of the decelerating cycle the particles must be shielded from the field, which can be made by using shielding tubes (drift tubes), acting like a Faraday's cage, through which an outside field can not penetrate. Figure 7.3 illustrates how a sequence of accelerating gaps (cavities) and drift tubes are arranged with respect to the sinus wave.

If the velocity of the particles is increased by every step of the acceleration, the particles will travel longer and longer distances during the acceleration time, which means that the lengths of the acceleration gaps and the drift tubes must be increased or alternatively that the frequency of the a.c. field is tuned to cavities of constant length.

The probability for one particle to interact and produce a reaction of interest is limited and to increase this as much as possible a large number of particles are collected into a *bunch* of particles which are accelerated together. In modern accelerators typical numbers of particles in a bunch vary between  $10^{10} - 10^{14}$  depending on what kind of particle is used. The beam of particles are kept inside a *vacuum tube* to prevent it to interact with the air. The maximum frequency of bunches would in the case of a linear accelerator be given by the distance between the cavities. In conventional cavities, based on e.g. normal conducting copper material, fields of a few MV per meter can be obtained. Thus an accelerator providing particles with a final energy of 50 MeV has to be  $\sim 50/5 = 10$  meters long if we assume 5 MV per meter. It is clear

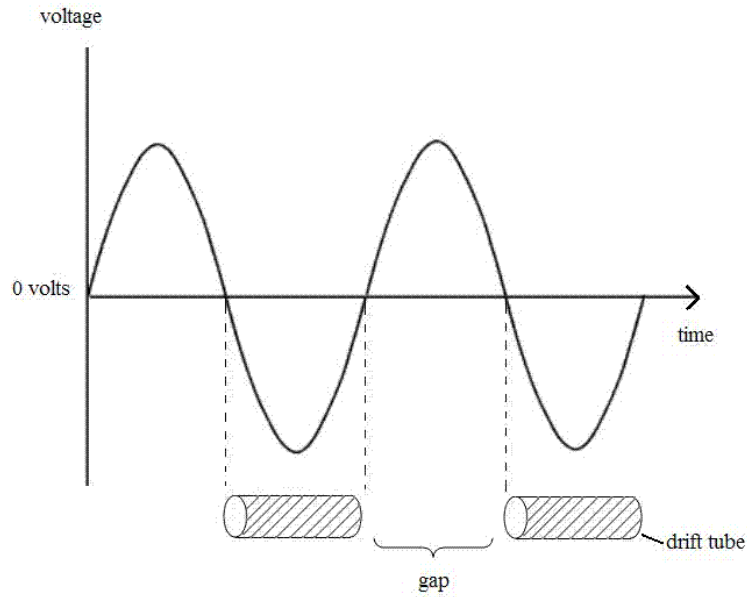


Figure 7.3: Acceleration in a standing wave mode with drift tubes to shield from the deceleration phases.

that if we want to build accelerators for energies in the range of GeV or more, then they have to be several kilometers long. For example if we want to reach a maximum energy of 5 GeV the accelerator has to have a length of 10 km.

### 7.1.2 Circular Accelerators

The way to circumvent this problem is to let the particles pass the same cavities several times, which means that they have to be directed into a loop to come back to the same position over and over again. Such a machine is called a *synchrotron*. Thus, the vacuum tube is bent in a closed loop (frequently a circle) and a magnetic field is applied perpendicular to the bending plane. The strength of the field has to be increased as the momentum of the particles increases, according to the relation:

$$p = Be\rho$$

where  $p$  is the momentum,  $B$  the magnetic field strength,  $e$  the electric charge of the particle and  $\rho$  the bending radius. The charge and radius are fixed by the particle chosen to be accelerated and the size of the accelerator, respectively. The obvious limitation of such a machine is the strength of the magnetic field that can be provided. Typical fields of normal conducting magnets are 1 Tesla and the largest accelerator of this kind provides 400 GeV protons. If instead magnets based on superconducting technology are used, a field strength of up to 10 Tesla has been reached for the LHC accelerator, giving beam energies of 7 TeV for the circulating protons.

What is said above is true for proton machines but not for electron machines, which suffer from other limitations. An electron (positron) which is forced to change its direction of motion will lose energy by sending out *synchrotron radiation*. The energy lost,  $\Delta E$ , is given by:

$$\Delta E \sim \frac{E^4}{\rho m^4}$$

where  $\rho$  is the bending radius (in meter),  $E$  the beam energy (in GeV) and  $m$  is the mass of the particle. Thus, for relativistic protons and electrons of the same momentum the ratio of the energy loss is  $(m_e/m_p)^4 \sim (1/2000)^4 \sim 10^{-13}$ . This is the reason why synchrotron radiation causes no problems in circular proton accelerators whereas it sets a limit to what energy can be reached in electron synchrotrons. At a certain point the energy which is provided by the cavity at each turn is just enough to compensate for the energy loss and no further acceleration is possible. Since the electron mass is very small compared to the proton mass, only very weak magnetic fields are needed to bend the electrons and therefore this is not a limiting factor.

## 7.2 Colliders

### 7.2.1 Circular Colliders

In conventional accelerator experiments the accelerated beam is extracted and directed towards a fixed target of some material. This gives a high interaction probability since Avogadro's number tells us that we have as many as  $6 \cdot 10^{23}$  atoms per mol. (One mol is the weight in grams given by the atomic number). On the other hand we have seen in previous kinematic considerations that only a fraction of the energy carried by the beam particles is available for producing new physical states and the rest is needed to move the centre-of-mass of the system. In order to make the interactions more energy-efficient, colliders were built in which two counter-rotating beams are brought to collide in certain points around the ring. In the case of electron-positron colliders where the particles are circulating in the same beam tube but in opposite directions, the centre-of-mass energy will be twice the beam energy. In a proton-proton (antiproton) collider the collisions take place between the quarks inside the protons, which carry only a fraction of the beam energy.

The disadvantage with colliding beams is that the density of particles is much lower than in a fixed target. Typically one has  $10^{10}$  to  $10^{14}$  particles per bunch circulating in the beam tube. For this reason it is very important to focus the beams as much as possible in the collision point. Transverse beam sizes down to a few nanometers have been achieved at modern colliders.

The number of bunches which can be circulating in the beam tubes depends on the structure of the collider. If the beams are stored in one common vacuum tube, as one can do when colliding particles and antiparticles like electrons and positrons or protons and antiprotons, the number of bunches in each direction is limited to the number of experiments divided by two. Thus, if we have two experiments only one bunch in each direction is stored, which means that they are colliding in two opposite points along the ring, where the detectors are positioned.

If we would store more bunches we would also have collisions at points where there are no detectors and this is not what we want. If, on the other hand, the beams are stored in separate beam tubes, as must be the case for collisions between particles of the same charge or between different particle types, a large number of bunches can be stored and the limitation is given by the length of the vacuum tube where the beams have to be brought together in order to collide. This is because we only want to have one collision point in the piece of vacuum tube that is common to both beams and which is surrounded by the detector. In the HERA electron-proton collider one can store as many as 210 bunches of each particle type, which gives a collision rate of 10 MHz. In the LHC proton-proton machine there is only 25 ns between the bunches, which gives a collision rate of 40 MHz.

As mentioned above circular  $e^+e^-$ -colliders suffer from energy losses due to synchrotron radiation. The energy losses increase as the fourth power of the beam energy whereas they only decrease inversely proportional to the radius of the collider. This means that at some stage it is no longer financially defensible to build larger circular  $e^+e^-$ -colliders. This point was reached by the LEP collider at CERN which had a circumference of 27 km and reached a maximum collision energy of about 200 GeV. In order to make a significant step in energy, which is motivated by the new physics that is needed to explain the mass generation of particles, the unification of the electroweak and strong forces etc., one has to get into the TeV range. This is obtained at the proton-proton collider LHC by using superconducting magnets which provide a magnetic field strength of up to around 10 Tesla, allowing a maximum beam energy of 7 TeV i.e. the collision energy will be 14 TeV at most. Although protons at these energies do not suffer from synchrotron radiation, proton-proton collisions have the disadvantage, compared to  $e^+e^-$ -collisions, that the initial state is not well-defined in the sense that we don't know the momenta and flavours of the colliding quarks. Further the final state contains a large background produced by the hadronization of the quarks, which do not participate in the collision (*spectator quarks*). Obviously the precision of the measurements is suffering from these disadvantages, which complicates the extraction of tiny signals of new phenomena. In an electron-positron collider the energies of the colliding particles are known to a precision which is given by the requirements for having them circulating several hours in the collider. The final state is completely background free and provides the cleanest possible environment. However, the energy limitations of such a collider due to synchrotron radiation constitutes a major problem and makes a ring collider in this energy range unaffordably large.

One possibility to circumvent the problem with synchrotron radiation and still have collisions between pointlike particles would be to use muons instead of electrons. Since the muon is about 200 times heavier than the electron the effect of energy losses due to synchrotron radiation is about a factor  $10^{-8}$  smaller in an accelerator of the same size. However, there is one obvious problem with muons and that is that they decay with a decay time of  $2.2 \mu\text{s}$  if at rest. As we have seen from the example in Section 1.3.6 the lifetime of the muon increases significantly as it becomes relativistic. So, in principle it should be possible to accelerate a beam of muons if it can be made relativistic fast enough. On the other hand there are other complications in the production of muons (see Section 7.4) and collection of the muons into a monoenergetic beam of high flux. Although there is ongoing research in this area we may not expect a technological breakthrough for many years yet.

## 7.2.2 Linear Colliders

Another way to avoid the problem caused by synchrotron radiation is to use linear electron-positron colliders as foreseen for the next generation facilities. In a linear collider the particle bunches are not reused, in the sense that they are brought to collide over and over again, as they are in a circular machine, but are lost once they have reached the collision point. Thus, the about  $10^{10}$  particles per bunch have to be created instantly and the particle beams have to gain their final energy in passing through the acceleration structure only once. These are the major technological challenges. In order to fulfil the latter requirement much larger acceleration fields are needed than has been used for circular machines, in order to keep the length of the machine within limits. Intense work has been invested over the past decade to develop technologies which allow a significant increase of the field strength per unit length. Typical fields for cavities used in circular machines are around 5 MV/m. There are essentially two ways to achieve higher acceleration fields.

The first one is based on cavities with normal conducting materials like copper or aluminium. If the cavities are made smaller i.e. the cavity gap is shorter but with preserved field strength, then obviously the field per unit length will increase. The distance between bunches is given by the length of the cavities and as a consequence the radio frequency has to increase with shorter cavities. The advantage of this technology is that there is no physical limit to what fields can be obtained. The shorter the cavities, the higher radiofrequencies and the higher field per unit length. For example at 30 GHz one can obtain 150 MV/m. The disadvantage is the short distance between the bunches, which leads to a very high collision frequency. A further disadvantage is the smallness of the cavities; the hole through which the beam has to pass is of the order of millimeters, which requires a very good control of the beam position. So far one has not managed to keep such facilities operating for longer periods of time.

The second possibility is to use superconducting materials (pure Niobium) in the cavities and keep the present size of cavities (several centimeters long). Due to the size of the cavities such a machine can be operated at low frequencies (around 1 GHz) and thus the distance between the bunches are significantly longer which has several advantages. With superconducting technology fields up to 40 MV/m has been achieved, which is close to the physical limit.

A linear electron-positron collider called the International Linear Collider (ILC) with collision energies up to 1 TeV is planned as a world wide project. It will use the superconducting technology for acceleration with the aim to achieve a field strength of more than 30 MeV/m. For a collision energy of 1 TeV it results in a total length of around 32 km, comparable to the circumference of LEP.

## 7.3 Collision Rate and Luminosity

The collision rate,  $R$ , in a collider is given by:

$$R = \sigma L$$

where  $\sigma$  is the cross section of the process studied and  $L$  is the *luminosity*, which is measured in  $cm^{-2}s^{-1}$ . Luminosity is a measure of the quality of the colliding beams and can thus vary with time. Thus, the luminosity has to be measured continuously. This can be achieved by collecting the rate of a process which is frequently produced and has a well determined cross section. In  $e^+e^-$ -colliders normally Bhabha scattering ( $e^+e^- \rightarrow e^+e^-$ ) is measured and in  $ep$  collisions the Bethe Heitler process ( $ep \rightarrow e\gamma p$ ) is used. By determining the luminosity and simultaneously measuring the rate of any other process that we are interested in, we can calculate the cross section of that process. For two colliding beams of relativistic particles the luminosity can be written in the following way:

$$L = fB \frac{n_1 n_2}{A}$$

where  $n_1$  and  $n_2$  are the number of particles in each bunch,  $B$  is the number of bunches,  $f$  is the frequency with which the bunches cross each other and  $A$  is the transverse area of the beams in the collision point. The transverse particle distribution of a bunch follows a gaussian shape and the area is then given by:

$$A = 4\pi\sigma_x\sigma_y$$

where  $\sigma_x$  and  $\sigma_y$  are the widths of the horizontal and vertical distributions. Normally the number of particles per bunch is not well known but instead there are methods of measuring the electric current of the beam, which is related to number of particles through:

$$i = nefB$$

where  $n$  is the number of particles in the bunch. The collision rate can then be expressed as:

$$R = \frac{i_1 i_2}{4\pi e^2} \cdot \frac{1}{\sigma_x \sigma_y f B} \cdot \sigma$$

If we for a circular electron-positron collider assume the following values:

$B = 1$ ,  $f = 10^6$ ,  $i_1 = i_2 = 50 \text{ mA}$ ,  $\sigma_x = 0.1 \text{ cm}$  and  $\sigma_y = 0.01 \text{ cm}$  we get:

$$R \approx 10^{31} \sigma \text{ sec}^{-1}$$

i.e.  $L = 10^{31} \text{ cm}^{-2} \text{ sec}^{-1}$

This is a typical value for previous circular  $e^+e^-$ -colliders, whereas typical luminosities for  $p\bar{p}$ -colliders are  $10^{30} \text{ cm}^{-2} \text{ sec}^{-1}$  and for  $pp$  colliders  $10^{33} \text{ cm}^{-2} \text{ sec}^{-1}$ . The future linear  $e^+e^-$ -collider will have a luminosity of  $10^{34} \text{ cm}^{-2} \text{ sec}^{-1}$ . The luminosities are mainly increased by better focusing of the beams in the collision point and at the linear  $e^+e^-$ -collider the vertical beam dimension at the interaction point is as small as  $5 \text{ nm}$ .

Cross sections typically decrease as  $1/s$  (where  $s$  is the collision energy squared). This means that our searches for new phenomena at increasingly higher energies automatically requires higher luminosities in order to collect a sufficient number of events over a reasonable time period.



## 7.4 Secondary Beams

Particles which are used for acceleration and for storage in colliders are stable and carry electric charge. However, it is also interesting to study interactions which involve other types of particles like photons and neutrinos as well as muons, pions and kaons. Such particles can be produced by directing a primary beam of particles from an accelerator towards a metal target. From the interaction with the target nuclei, several new types of particles are produced in a mixture. By using a system of focusing magnets and bending magnets, particles of a specific momentum and charge can be selected, since the deflection in a magnetic field is

$$p = B \cdot e \cdot \rho$$

This relation can be fulfilled by particles of different masses as long as they have the same momenta and therefore the secondary beam will remain a mixture of several particle types e.g.  $\pi^-$ ,  $K^-$ ,  $\bar{p}$ . In order to separate these one can use electric and magnetic fields in a combination. It can be shown that the difference in angular deflection of two relativistic particles with masses  $m_1$  and  $m_2$ , and momentum  $p$ , passing a transverse electric field of strength  $E$  and length  $L$  is:

$$\Delta\theta = E \cdot e \cdot L(m_1^2 - m_2^2)/2p^3$$

Since the deflection of particles in an electric field has a different momentum dependence compared to that in a magnetic field, a combination of electric field and magnetic fields will allow us to pick out a specific particle type of a specific momentum.

This method can only be used up to a few GeV since the deflection angle in a given electric field is inversely proportional to  $p^3$ . At higher energies so called radiofrequency (RF) separators are used, the principle of which is illustrated in Figure 7.4. RF-cavities are normally used to accelerate particles. The RF-cavities are placed one after the other such that the particles enter them perpendicular to their electric fields. The radiofrequency is chosen such that the electric field changes direction as a relativistic particle passes from one cavity to the next. If the directions of two subsequent cavities are in opposite phase, the particle traversing these cavities will always see an electric field, which has the same direction and the particle will get accelerated transversely to its original motion. With a constant frequency the field has a certain direction over a constant time.

Consider a particle with originally no transverse motion entering the first cavity. From the transverse acceleration in this cavity it will gain some momentum. As it enters the second cavity it already has some transverse velocity and the electric field will cause it to travel a longer transverse distance in the time it takes for the particle to traverse this cavity. This means that the second cavity has to be somewhat longer than the first one. Consequently, the third cavity has to be longer than the second and so on. Since particles of different masses will travel different distances under the influence of a given field during a given time, only a particle with a specific mass will be in phase with the chosen radiofrequency, and since particles with other masses will get out of phase with the frequency they will be decelerated. This provides an efficient method to separate particle types at high momenta.

An alternative method is to keep the length of the cavities constant and change the RF-frequency of consecutive cavities.

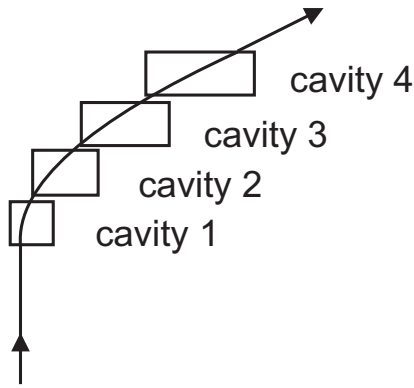


Figure 7.4: *The principle of particle separation using cavities.*

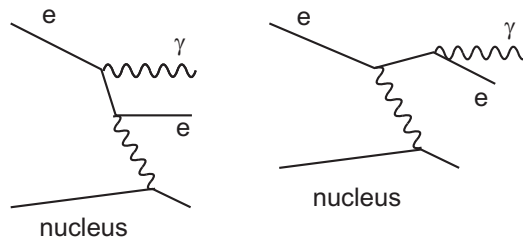


Figure 7.5: *Feynman diagrams of Bremsstrahlung processes.*

*Photons* are produced by slowly steering an electron beam circulating in an accelerator towards an internal thin metal wire, where the photons are produced via the bremsstrahlung process. The corresponding Feynman diagrams are shown in Figure 7.5.

The photons will leave the accelerator, tangential to the beam orbit, through a thin window. The photons will not be monoenergetic but follow a specific momentum spectrum (bremsstrahlung spectrum).

*Muon* and *neutrino* beams are produced from a secondary beam of pions or kaons. When these are travelling down a long vacuum pipe they will decay in flight according:

$$\pi \rightarrow \mu + \nu_{\mu} \quad \text{or} \quad K \rightarrow \mu + \nu_{\mu}$$

A pure beam of neutrinos can be produced by letting the secondary beam pass through a thick absorber in which the hadrons and muons will be absorbed. A muon beam of fixed momentum can be obtained using a system of bending and focusing magnets as described above for hadrons.

## 7.5 Detectors

### 7.5.1 Scintillation Counters

Scintillation counters have been used for a long time to detect charged particles in particle physics experiments. The detector consists of a chemical compound (organic or inorganic) that emits short light pulses after the molecules of the material have been excited by the passage of a charged particle. The light produced is collected via a so called light guide onto a photomultiplier tube (PMT) or a photosensitive silicon detector, as illustrated in Figure 7.6. The PMT has a photocathode from which electrons are emitted through the photoelectric effect. The electrons are accelerated in the electric field between several subsequent electrodes, *dynodes*, inside the PMT. Due to the increased energies of the electrons, each electron will kick out a number of secondary electrons as they hit the surface of the dynodes. This sequence is illustrated in Figure 7.6. With a suitable number of dynodes an amplification factor of between  $10^6 - 10^8$  is obtained before an electric signal is read out at the anode of the PMT.

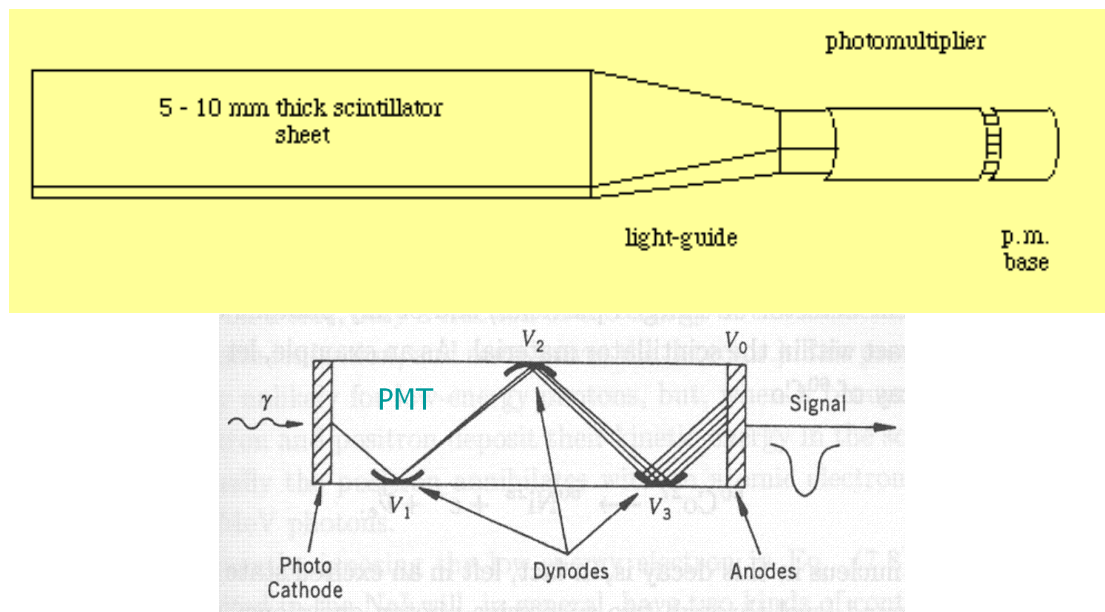


Figure 7.6: A drawing of a typical scintillation counter (upper figure) and a Photo Multiplier Tube (PMT) (lower figure).

Scintillation counter are continuously sensitive and provide very fast signals, which make them suitable for *trigger* purposes. A trigger is a signal delivered by one or several detectors, which announces the passage of a particle that fullfils predefined requirements concerning direction, momentum etc. The time resolution of scintillators is very good and a pair of them at some distance can be used to measure the flight time of a particle (time of flight), which together with a momentum measurement can be used to identify the particle (see Section 7.6). On the other

hand the space resolution is given by the size of the counter and is thus not competitive with that of modern tracking detectors. Scintillators can also be used as active material in sampling calorimeters (see Section 7.5.2).

## 7.5.2 Tracking Chambers

### Ionization Chambers

This type of detectors are based on the property that charged particles create ionization when they traverse a gas volume. A simple example of an ionization chamber is the *Geiger counter*, illustrated in Figure 7.7. The Geiger counter consists of a tube filled with gas, where the outer wall is put on ground (*cathode*) and a central *sense wire* (*anode wire*) is given a positive voltage of several hundred volts. A radial electric field is created with a strength that is inversely proportional to the distance from the wire:

$$E = \frac{1}{r} \frac{V_0}{\ln(b/a)}$$

where  $r$  is the radial distance of the track from the sense wire,  $b$  is the radius of the cylinder,  $a$  is the radius of the central wire and  $V_0$  the applied voltage.

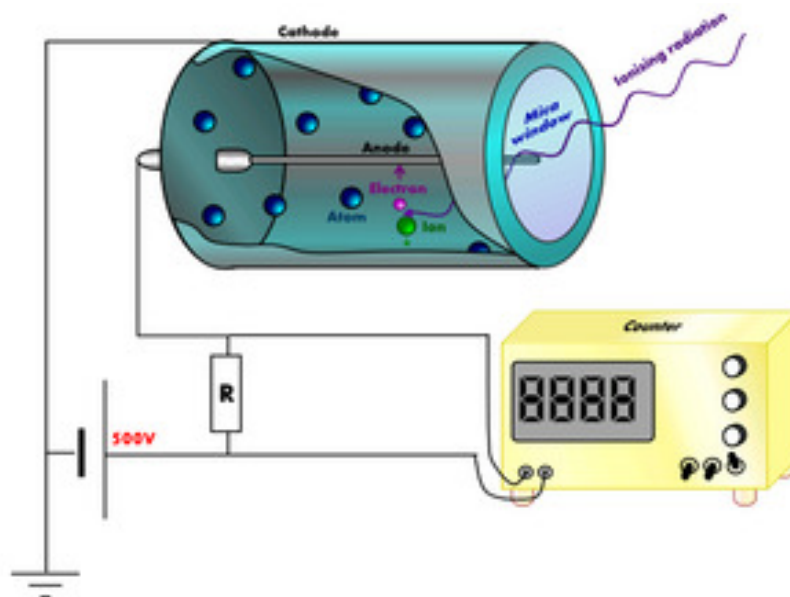


Figure 7.7: Drawing of a Geiger counter.

When a particle passes through the tube it ionizes the gas molecules along its trajectory, creating electrons and positively charged ions. The strong electric field accelerates the ions towards the cathode (wall) and the electrons towards the wire where they are all collected. As the electrons gain enough energy approaching the strong field around the sense wire they will create

secondary ion pairs through the collisions with the gas molecules, such that an *avalanche* of charged particles develops. As the ion cloud moves away from the sense wire it induces a short pulse of current on the wire, which can be registered. The avalanche procedure is shown in Figure 7.8. If the voltage is chosen in a certain range the number of electron-ion pairs in the avalanche is directly proportional to the primary electrons created by the particle (*proportional chambers*).

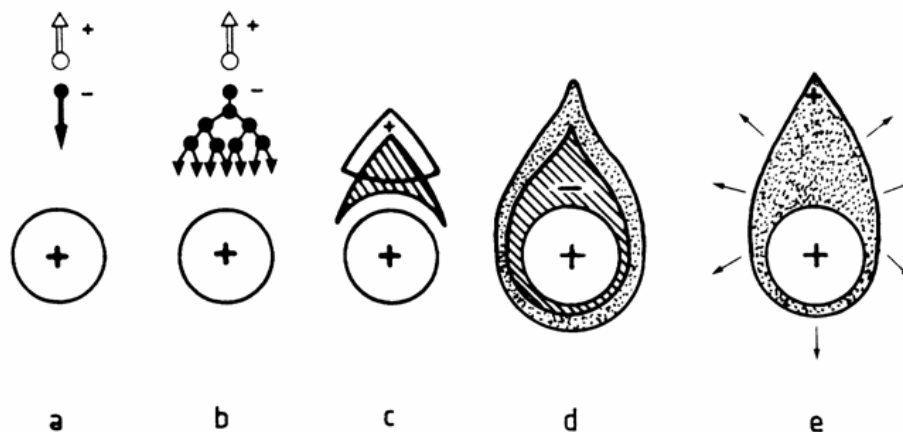


Figure 7.8: Illustration of the development of an avalanche.

### Multiwire Proportional Chambers

In order to construct a detector for the reconstruction of particle trajectories one would need to build a large array of proportional chambers. This, however, has the disadvantage that the chamber walls introduce a lot of 'dead' material in the detector which will cause scattering of the particle and thereby influence the trajectory. This problem can be circumvented by constructing an array of many closely spaced anod (sense) wires in a common chamber. Each wire will act as an independent proportional chamber provided that they are equipped with individual readout electronics. Such a chamber is called Multi Wire Proportional Chamber (MWPC) and the build-up is illustrated in Figure 7.9. The position resolution will then be of the order of the wire spacing.

A typical separation between adjacent anod wires,  $s$ , is 2 mm, and between the anod wires and the cathod,  $l$ , about 1 cm. The radius of the wire is typically  $10 \mu\text{m}$ . Many Multiwire Proportional Chambers (MWPC) can be positioned after each other so as to get many position measurements along a particle track. If every second chamber is rotated by  $90^\circ$  with respect to the previous one the wires will be perpendicular to each other and the system will provide space coordinates. Each wire can stand a counting rate of several hundred thousand per second, which allows for a data taking rate much beyond what was previously possible.

A charged particle traversing the chamber will thus produce electrons and positive ions along its path in the gas. These will drift along the electric field lines such that the electrons are approaching the anod wire and the ions the cathode planes. As seen from Figure 7.9 the density of the

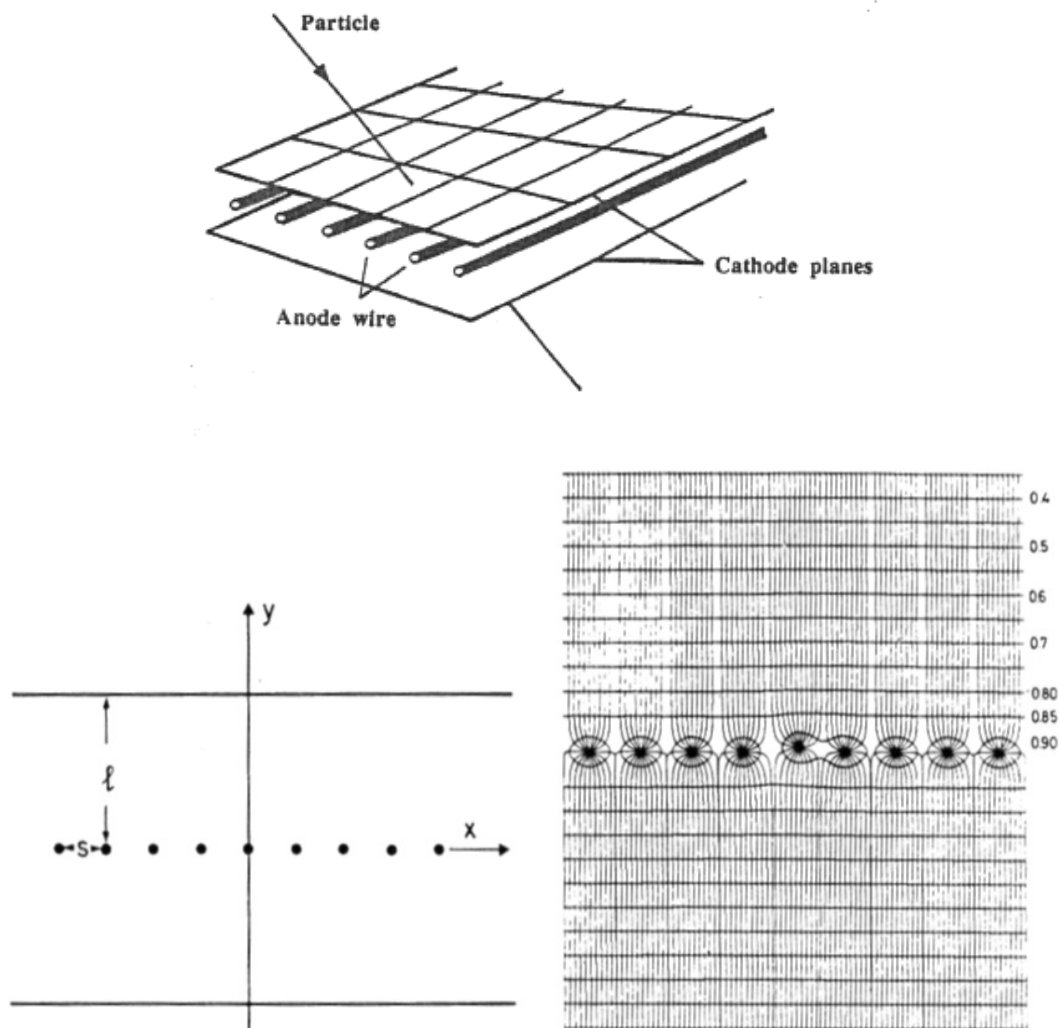


Figure 7.9: *The Multi Wire Proportional Chamber (MWPC).*

field lines increases drastically close to the wire which is the region where the primary electrons will gain enough energy to create new electron-ion pairs. Each primary electron will create an avalanche which contains  $10^3 - 10^6$  electron-ion pairs. This is called the *gas amplification*.

A particle which enters the chamber at  $90^\circ$  will only fire one wire. However, in a realistic situation most tracks will have some inclination angle and consequently the primary electrons created along the track will leave signals in several adjacent wires, as illustrated in Figure 7.10. Since the primary ionization happens at different distances from the wires, the signal recorded from the wires are spread over a time interval that corresponds to the differences in drift time of the primary electrons. The desired signals are those arriving first.

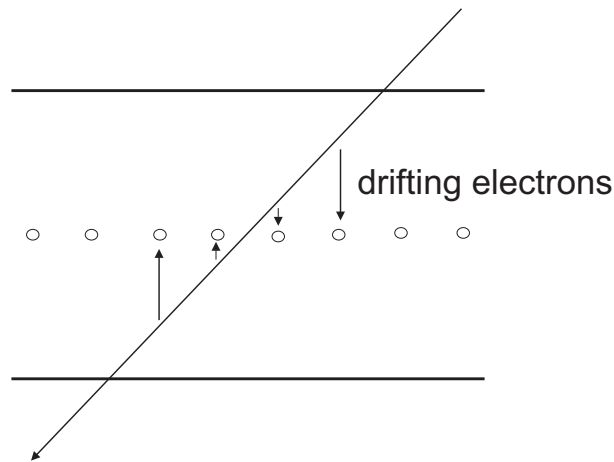


Figure 7.10: A particle traversing a Multi Wire Proportional Chamber at an angle.

### The Drift Chamber

In the drift chamber the distance between the anode wires are larger (5-10 cm) than in the MWPC but the loss in resolution due to this is compensated for by measuring the time it takes for the primary electrons to drift from the track to the wire. In order to get a useful measurement a constant electric field is needed within a drift cell so as to get a constant drift velocity. Such a field is obtained by introducing a series of *field shaping wires*, which define the borders of the drift cell. The construction of a planar drift chamber is shown in Figure 7.11. Since the drift time can be measured quite accurately the spatial resolution was improved from typically 2 mm in the MWPC to typically 100  $\mu\text{m}$  in the drift chamber. One disadvantage is that drift chambers are 'slower' than MWPC:s due to the longer time it takes for the electrons to drift to the sense wire.

The method to determine the drift time is to start a high frequency clock when the particle enters the detector and stop it when a pulse is registered at the wire. Since the drift velocities are well known for the various types of gases (gas mixtures) used in drift chambers, the corresponding distance can be calculated. Typically the drift velocities are around 4  $\text{cm}/\mu\text{sec}$ , which would correspond to 1.25  $\mu\text{sec}$  for a drift cell of 10 cm. The counting rate would then be limited to  $8 \cdot 10^5$ .

Drift chambers have been built in many different shapes and sizes, and essentially every modern experiment in high energy physics uses drift chambers for reconstruction of the trajectories of charged particles. One example of a cylindrical drift chamber is shown in Figure 7.12.

If the drift chamber is placed in a homogenous magnetic field the momentum,  $p$ , of the particle can be determined from the measured curvature of the trajectory according to the relation:

$$p = B \cdot e \cdot \rho$$

where  $B$  is the magnetic field strength,  $e$  the electric charge of the particle and  $\rho$  is the radius of the measured curvature.

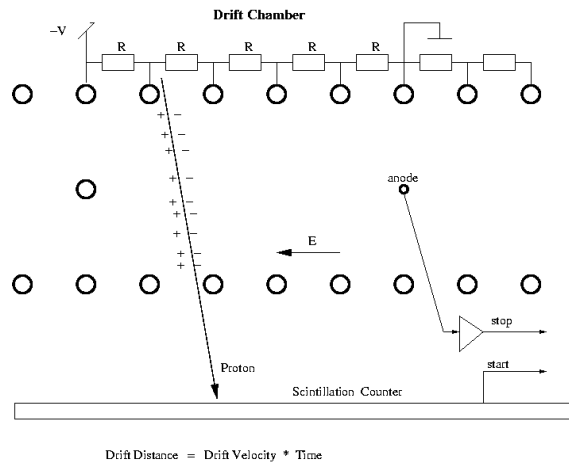


Figure 7.11: *The construction of a planar drift chamber.*



Figure 7.12: *The cylindrical drift chamber used in the ARGUS experiment at DESY.*

### The Time Projection Chamber

The most advanced ionization detector is the *time projection chamber* (TPC), which provides a large number of three-dimensional coordinates along a particle track. In that sense the TPC could be called an 'electronic bubble chamber'. It combines the principles of the MWPC and the drift chamber. The detector consists of a large gas-filled cylinder with a thin voltage electrode in the middle. Typical dimensions in a large collider experiment are up to 2 meters in diameter and a length of similar size. In a collider experiment the beam tube follows the axis of the cylinder such that the collision point is at the centre of the cylinder. The electric field responsible for the drift of the electrons is parallel to the axis of the cylinder and the end plates of the cylinder are covered with detectors. The basic structure of a TPC is shown in Figure 7.13.

A closer look at the end plate is given in Figure 7.14 and shows a *wire grid* plane followed by a plane of *sense-* and *field* wires and below these a *pad* plane.

Electrons drifting along the electric field lines will be collected on the sense wires and produce



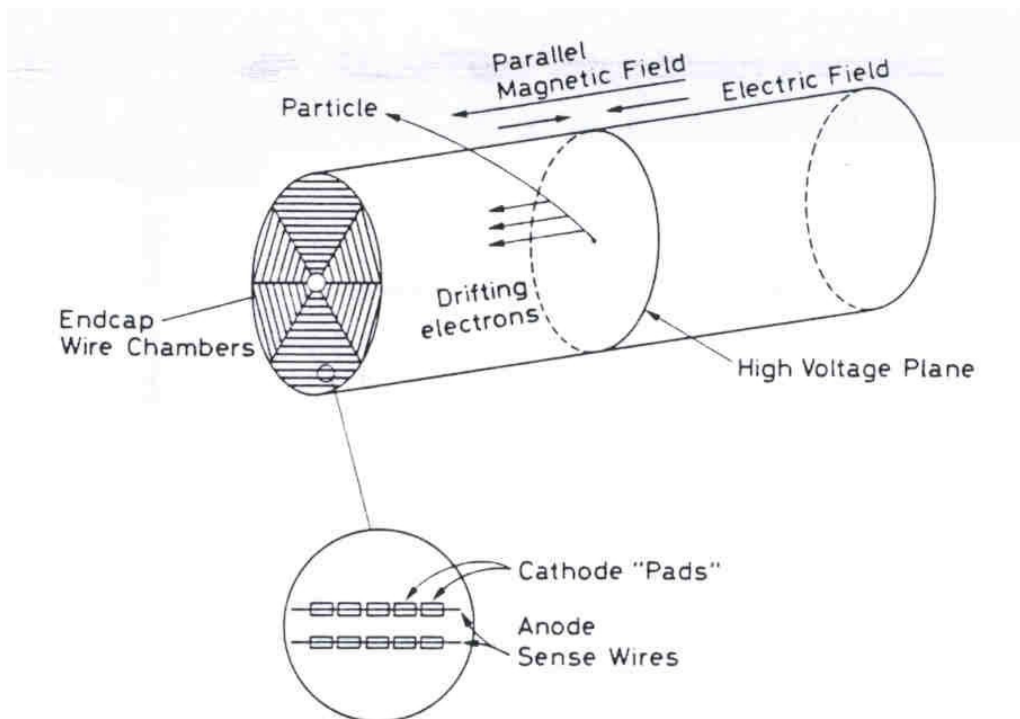
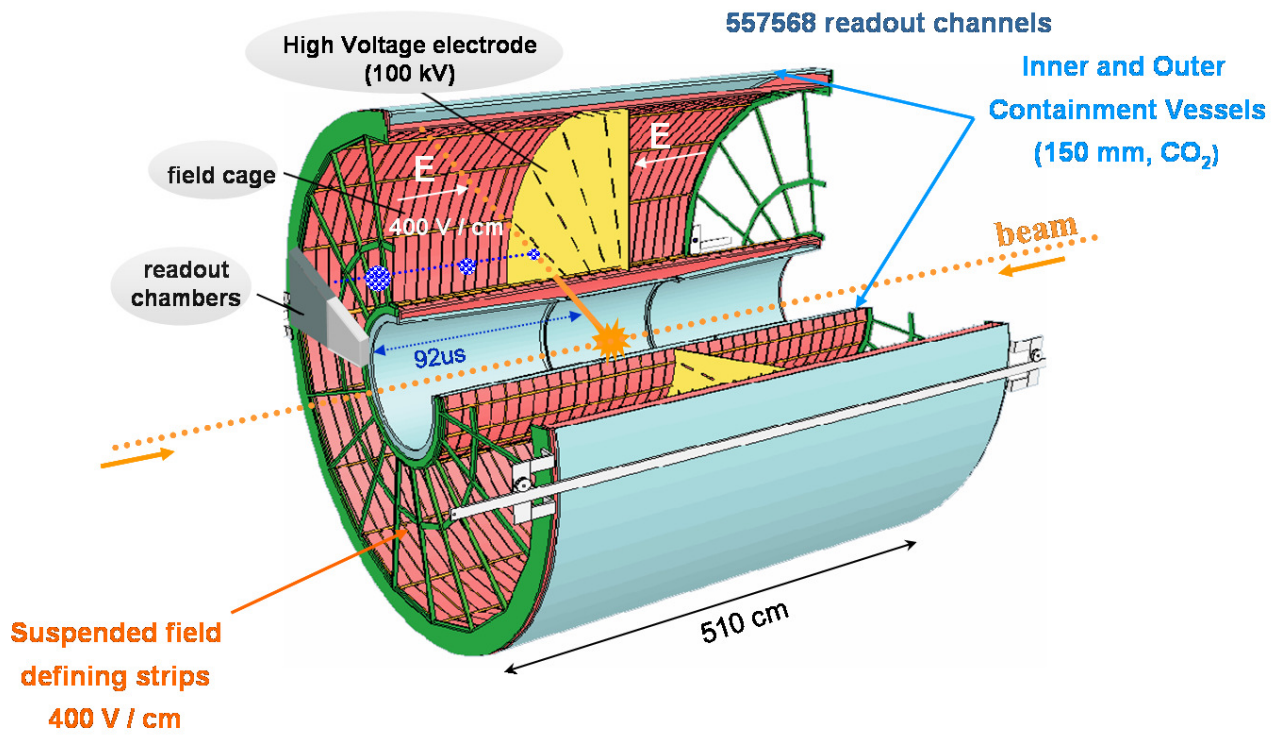


Figure 7.13: A drawing of a typical cylindrical TPC and the measuring principle.

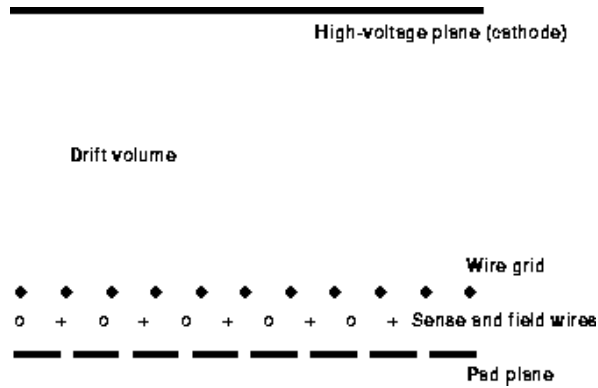


Figure 7.14: *The wire and pad structure of the end plate in a TPC.*

a signal according to the same principle as for the MWPC. The charge cloud at the sense wire will induce a signal in the cathode pads below the wires. In order to prevent the positive ions created in the avalanche to enter into the drift volume the wire grid is switched on at negative potential for a short period of time to collect the positive ions.

The drift time is measured by starting a clock at the time of the collision and stopping it as a signal is registered on a wire. Each wire is connected to a clock such that there will be a common starting time given by the collision time and individual stopping times for each wire. A track produced in the collision point and travelling the full radial distance through the chamber will thus produce signals in a large number of wires along its track. By measuring the drift times from the arrival of the ionization electrons at each wire we can extract the coordinates along the drift direction ( $z$  coordinate). For each point a measurement of the charge deposition on the pads below a wire can be used to determine the coordinates in the plane transverse to the drift ( $x$ - $y$  coordinates). In this way a large number of space coordinates are obtained for each track, where the precision in the  $z$  coordinate is related to the drift velocity and in the  $x$ - $y$  coordinates is related to the pad size.

## Semiconductor Detectors

The basic operating principle of semiconductor detectors is analogous to gas ionization devices. Instead of gas the medium is a solid semiconductor material. The passage of a charged particle creates electron-hole pairs along its track (instead of electron-ion pairs), the number being proportional to the energy loss. An externally applied field separate the pairs before they recombine such that the electrons drift towards the anode and the holes towards the cathode. The charge is collected on the electrodes where they produce a pulse whose integral equals the total charge generated by the incident particle. A schematic view of a strip detector is shown in Figure 7.15.

High resistivity  $n$ -type silicon is used as the starting material (wafer), i.e. the silicon has been doped with atoms containing an extra electron compared to the pure silicon and thus electrons are the majority charge carriers. Diode strips of  $p$ -type are implanted, where the doping atoms have one less valence electron compared to the base material and therefore they will provide

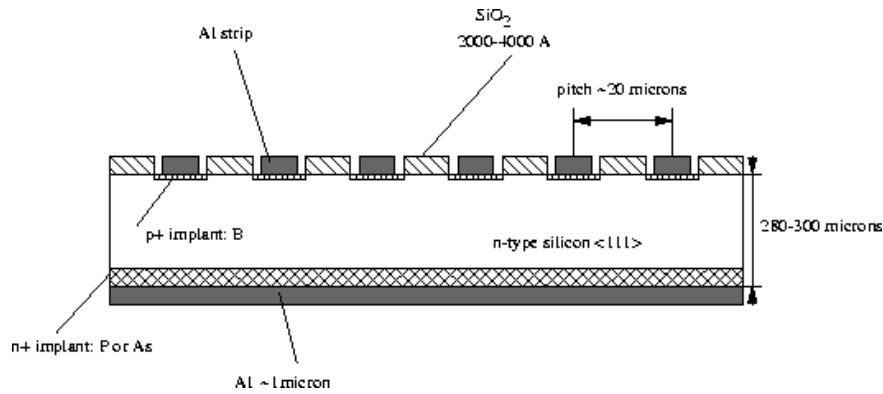


Figure 7.15: A typical construction of a silicon strip detector.

an excess of holes, which thus are the majority charge carriers in this case. The '+' sign is used to indicate heavily doped materials. Onto the strips aluminium contacts are used for read-out. An  $n^+$  electrode is similarly implanted on the opposite face. The electrons produced by the traversing particle will thus drift towards the  $p^+$ -strips whereas the holes will drift in the direction of the  $n^+$  electrode. The collected charge will be distributed over several strips according to a Gaussian distribution and by determining the centre-of-gravity for this distribution a position resolution of  $5 \mu\text{m}$  can be achieved.

Another advantage of the semiconductor is that the average energy required to create an electron-hole pair is of the order 10 times smaller than that required for gas ionization. Thus, the amount of ionization produced for a given energy is an order of magnitude greater resulting in increased energy resolution. They can be built very compact and have very fast response times. Semiconductor detectors have been used in high-energy physics in the form of *pixel detectors* and *microstrip detectors*.

### 7.5.3 Calorimeters

Calorimeters are detectors, which are constructed with the purpose to totally absorb the energy of the particles they are intended to measure. Total absorption means that a material has to be chosen for which the interaction cross section is large, in order to keep the depth of the detector within reasonable limits. The most favourable case is if the same material which is used as 'absorber' can also be used to measure the deposited energy. This is, however, not always possible and instead one has to use a 'sandwich' structure in which absorbing plates are interleaved with energy sensitive materials. The materials which might be used in calorimeters varies depending on whether electrons and photons or hadrons are going to be detected. Typical energy sensitive materials are scintillators and liquid Argon.

## Electromagnetic Calorimeters

For the identification of electrons (positrons) and photons calorimeters play an important role. High energy electrons and photons mainly interact via *bremsstrahlung* processes and *pair production*, respectively.

*Bremsstrahlung* occurs when a charged particle is forced to change its direction of motion. It will then be accelerated toward the center of the bending curvature and thereby lose energy by emitting a photon. An electron traversing the material of a calorimeter will feel the strong electric field of the atomic nuclei it passes, each causing a deflection of the electron (*multiple scattering*), and thereby the emission of a photon. *Pair production* happens when a photon experiences the intense electric field close to an atomic nucleus and create an electron-positron pair.

Consider a high energy electron entering a calorimeter. The incoming electron will emit a photon through the bremsstrahlung process. The photon will create an electron-positron pair through the pair production mechanism. The produced electron and positron will both emit new photons via bremsstrahlung and so on. In this way an avalanche of electrons, positrons and photons will develop. This is called an *electromagnetic shower*. The shower development will cease at a point where the energy of the photons fall below what is needed to create a pair. Bremsstrahlung dominates the energy loss of electrons above a *critical energy*,  $E_c$ , below which ionization gets important. The critical energy is different for different materials.

The probability for electromagnetic interactions can be expressed in terms of *radiation length*. The radiation length  $X_0$  is defined as the distance in the material at which the electron retains a fraction  $1/e$  of its initial energy, where  $e$  is Euler's number ( $e \approx 2.718$ ). The development of an electromagnetic shower is illustrated in Figure 7.16.

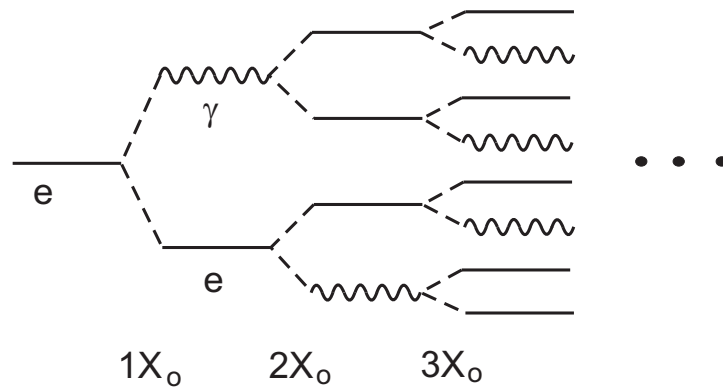


Figure 7.16: *The development of an electromagnetic shower.*

As can be seen from the figure the shower contains two particles after about 1 radiation length, four particles after 2 radiation lengths and consequently  $2^t$  particles after  $t$  radiation lengths. The energy is divided roughly equally between the electrons and the photons such that each particle carries an energy of:

$$E(t) = E_0/2^t \quad \text{where } E_0 \text{ is the initial energy.}$$

The amount of ionization which is produced by the shower electrons is proportional to the total energy of the incoming particles and has to be measured. The response of a given calorimeter to two identical incident particles is different due to statistical fluctuations of the shower development. Also the thickness of the absorber plates in a sandwich calorimeter will affect the energy resolution of the measurement. Different materials can be used for the absorber plates but the most common ones are lead (Pb) and tungsten (W). A typical energy resolution for an electromagnetic sandwich calorimeter is  $\Delta E/E = 10\% / \sqrt{E}$ .

Examples of electromagnetic calorimeters with homogenous materials, combining efficient absorption and light emission, are lead glass and various types of scintillating monocrystals, like Sodium Iodide (NaI(Tl)), Cesium Iodide (CsI(Tl)), Bismuth Germanate (BGO), Lead Tungstate (PbWO<sub>4</sub>) etc. In lead glass detectors the Cherenkov light (see Section 7.6.3) is detected, whereas in scintillating crystals, light is produced via a scintillation process. The best energy resolution is obtained with scintillating crystals, for which it is of the order of  $\Delta E/E = 2 - 3\% / \sqrt{E}$ .

The transverse size of an electromagnetic shower is given by multiple scattering of low momentum electrons and is quantified through the so called Molière radius,  $R_M = 21 \text{ MeV} \cdot X_o / E_c$ , where  $X_o$  is the radiation length of the material and  $E_c$  the critical energy. The shower profile is different for electromagnetic showers and hadronic showers.

A shower produced by electrons (positrons) and photons of the same energy look the same and can not be used to identify the particles. However, an electron leaves a track in the tracking chamber pointing at the position of the shower, whereas the signature of a photon is a shower without any track pointing to it. Muons interact in the same way as electrons but since they are about 210 times heavier, the influence of the atomic nuclei on the muons is so small that they doesn't cause the muons to change direction significantly. They go right through the calorimeter without radiating photons.

## Hadronic Calorimeters

Since hadrons are much more massive than electrons they will not be significantly deflected by the atomic nuclei of the calorimeter and consequently they will not develop an electromagnetic shower. However, hadrons interact strongly and will undergo various nuclear processes as they traverse the material of the calorimeter. The final state products of these interactions will subsequently create further nuclear interactions and so on until the total energy of the original particle has been shared among so many secondary particles that they stop in the calorimeter and their ionization can be measured. The secondary particles are mostly pions and nucleons. A fraction of the pions are  $\pi^0$ 's, which decay into two photons, which develop an electromagnetic shower. Thus, the hadronic shower also has an electromagnetic component. The hadronic multiplication process is measured at the scale of *nuclear interactions length*,  $\lambda$ , which is defined as the *mean free path* between two inelastic collision processes in a specific material.

The intrinsic limitations in the energy resolution of a hadronic calorimeter are due to the following:

- A sizable amount of the available energy is used to break up nuclei. Only a small fraction of this energy will eventually appear as a detectable signal.
- A certain fraction of the energy is spent on reactions which do not result in an observable signal, such as:
  - production of muons and neutrinos, which escape detection or slow neutrons, which are absorbed by the absorber plates.
  - nuclear excitation or nuclear breakup producing low energetic photons or heavy fragments, which can not traverse the absorber plate.

All this influences the energy resolution of the hadronic calorimeter.

Hadronic calorimeters are normally of sandwich type and in order to fully absorb the energy of the shower, the absorber plates have to be significantly thicker than for electromagnetic calorimeters. The material of the plates might be stainless steel or Uranium. Uranium has the advantage that thermal neutrons, produced in the showering process, give rise to spallation processes, where the products contribute to the signal. Therefore the energy resolution of Uranium calorimeters is around  $\Delta E/E = 35\% \sqrt{E}$ , compared to  $\Delta E/E = 50\% \sqrt{E}$  in the case of steel absorbers.

## 7.6 Particle Identification

So far we have discussed tracking detectors, which can, if placed inside a magnetic field, be used to measure the momentum and charge of particles. Calorimeters are used to measure the total energy of particles and together with the tracking information, electrons and photons can be distinguished. Figure 7.17 shows how various particles leave signals in different detectors.

For the investigation of certain processes it may be important to identify the particles involved. Particle identification relies on special properties of the different particles. For example *muons* do not produce showers in electromagnetic calorimeters and do not interact strongly. Thus they will penetrate large distances of matter, a property which can be used for their identification. Characteristic for electrons and photons is that they create showers in electromagnetic calorimeters, which is used to distinguish them from other particles. Electrons and photons can be separated from the fact that the electrons leave trajectories in a tracking device which is not true for the photons. Separation of hadrons is based on either time-of-flight measurements, the energy loss per unit path length of the particle (specific ionization) or the emission of Cherenkov light.

### 7.6.1 Time of Flight

From the knowledge of the particle momentum, the length of the particle trajectory and the time it takes for the particle to go from one point to another, i.e. the time-of-flight (TOF), the mass of the particle can be calculated through:

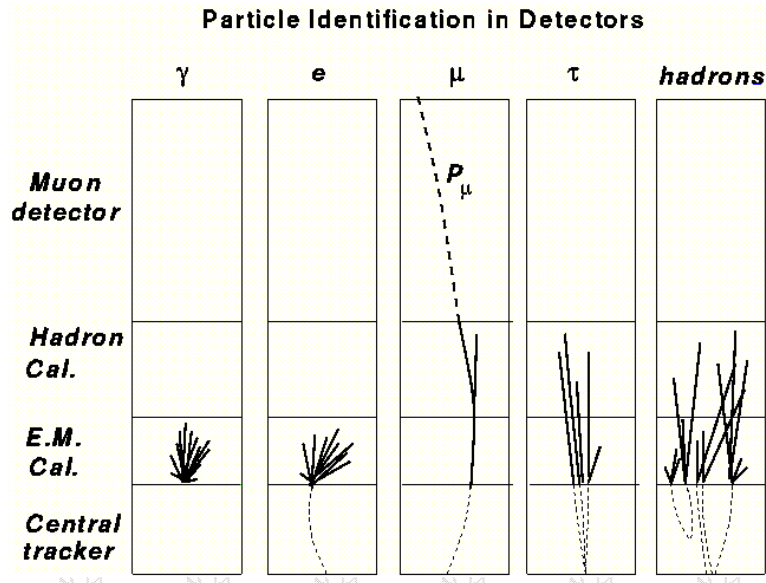


Figure 7.17: Particle identification using the information from various detectors.

$$m = \frac{m_o}{\sqrt{1-v^2/c^2}}$$

$$m_o = m\sqrt{1 - \beta^2} \quad \text{but} \quad \bar{p} = mv$$

$$m_o = \frac{\bar{p}}{v}\sqrt{1 - \beta^2}$$

where  $\beta = \frac{v}{c}$ ;

with  $v$  = velocity of the particle,  $c$  = velocity of light

Good particle identification through time of flight measurement requires sufficient flight path and good timing resolution in the detectors used for the TOF measurement. For a flight path of 10 meters and a timing resolution of 300 ps one may separate pions from kaons up to 2.4 GeV, whereas pions and protons are separated up to 4.6 GeV.

## 7.6.2 Ionization Measurement

Hadrons traversing a gas will loose energy through ionization and atomic excitation. The energy loss per unit track length is given by the Bethe-Block formula:

$$-\frac{dE}{dx} = \frac{4\pi}{m_e c^2} \cdot \frac{nz^2}{\beta^2} \cdot \left(\frac{e^2}{4\pi\epsilon_0}\right) \cdot \left[\ln\left(\frac{2m_e c^2 \beta^2}{I \cdot (1-\beta^2)}\right) - \beta^2\right]$$

where  $z$  = the charge of the incoming particle,  $n$  = density of atomic electrons,  $m_e$  = rest mass of the electron, and  $I$  = average atomic excitation potential.

As can be seen from the formula the energy loss is to a good approximation proportional to the electron density in the medium and to the square of the projectile electric charge. It decreases as  $1/\beta^2$  for increasing velocity of the particle until it reaches a minimum, which corresponds

to *minimum ionization*. We talk about *minimum ionization particles*. The energy loss then rises logarithmically, which is called the *relativistic rise*, due to the fact that the particles are relativistic. Finally, the energy loss starts levelling off to a constant value, the so called *Fermi plateau*.

The measurement of the energy loss,  $dE/dx$ , of a charged particle over many points along its trajectory, combined with a momentum measurement, can be used to determine the mass of the particle. The  $dE/dx$  measurement is usually done in the tracking chamber, like a drift chamber or a Time Projection Chamber, such that for each position measurement also the charge is sampled. Due to the statistical fluctuations in the energy loss over small distances it is important to record a large number of samples along the track.

Figure 7.18 shows two examples of  $dE/dx$  measurement as a function of momentum obtained from two different Time Projection Chambers. They illustrate the capability to separate pions, kaons and protons, depending on the precision in the measurements. In the second case a separation is possible even in the region of relativistic rise.

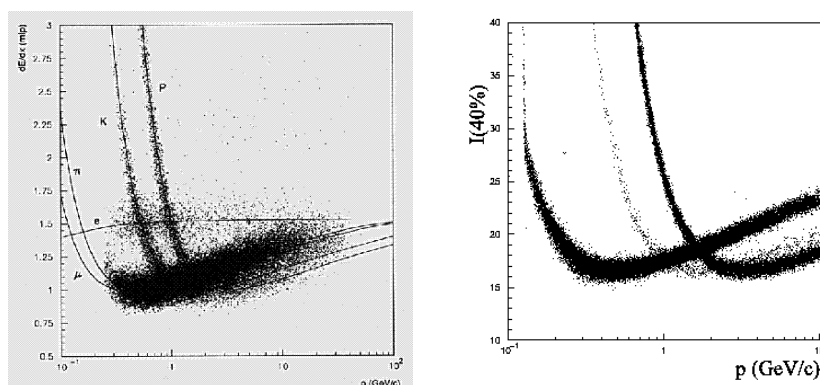


Figure 7.18: the  $dE/dx$  measurements from two different detectors.

### 7.6.3 Cherenkov Radiation

In vacuum the speed of light is a universal constant ( $c$ ), although it can be significantly lower than  $c$  when light travels through some material. For example, the speed of light in water is only  $0.75c$ . Elementary particles, which have been accelerated to high velocities may exceed the speed of light in that material. Cherenkov radiation is produced when a charged particle travels through a dielectric medium with a speed higher than the speed of light in that medium. In such a case the particle will cause the electrons of the atoms in the medium to be displaced with respect to the nuclei along its trajectory such that a polarization of the atoms occurs. Photons will be emitted as the electrons returns to their equilibrium state as soon as the charged particle has passed. In the normal case these photons interfere destructively and no radiation is detected but if the particle travels faster than the photons they will interfere constructively and create an electromagnetic shock wave. This is equivalent to a a sound wave generated by a supersonic aircraft or a bow shock, which is generated by a boat travelling faster than the waves themselves.



This phenomenon is illustrated in Figure 7.19, where  $v = c/n$  is the velocity of light in a medium with refractive index  $n$ . The velocity of the particle in this medium is  $v_{particle}$ , such that  $\beta = v_{particle}/c$ . A particle emitting Cherenkov radiation must therefore fulfill  $v_{particle} > c/n$ . The angle between the direction of the wave front and the traversing particle  $\theta$  is given by:

$$\cos \theta = \frac{(c/n) \cdot t}{\beta ct} = \frac{1}{n\beta}$$

Since the refractive index  $n$  is known and  $\theta$  is measured,  $\beta$  can be determined. If now the momentum of the particle is measured the mass can be calculated from  $m_0 = \frac{p}{v} \sqrt{1 - \beta^2}$

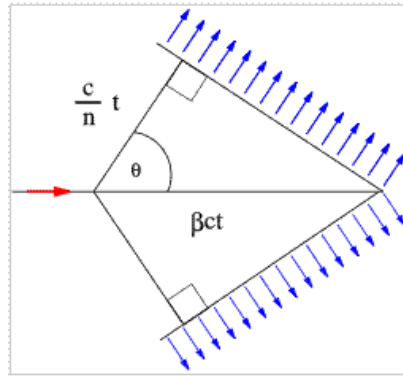


Figure 7.19: Illustration of a Cherenkov wave front.

Cherenkov detectors are in most cases containers filled with some suitable gas. By choosing the gas and adjusting the pressure one can achieve that particles with masses below some value generate Cherenkov light but particles with masses higher than that value do not. This is, however, only true over a certain momentum range, which means that it is important to measure also the momentum of the particle for a correct identification of the particle. In this case the detector is used as a threshold device. Using several subsequent detectors with different gas pressures one may identify different particle types over a limited momentum range. The Cherenkov light is usually detected by photomultipliers.

In modern detectors it is more common to use Ring Imaging Cherenkov detectors (RICH detectors), the principle of which is shown in Figure 7.20. In such a detector the traversing particle produces a cone of Cherenkov light in passing a relatively thin (several centimeters) radiator. This light cone is detected as a ring on a position sensitive planar photon detector at some distance from the radiator. From the radius of the reconstructed ring and the distance between the radiator and the photon detector, the Cherenkov emission angle can be calculated. Since this angle is different for particles with different masses at a certain momentum, this detector can be used to identify particles over the full momentum range over which the particle momenta can be measured with sufficient accuracy.

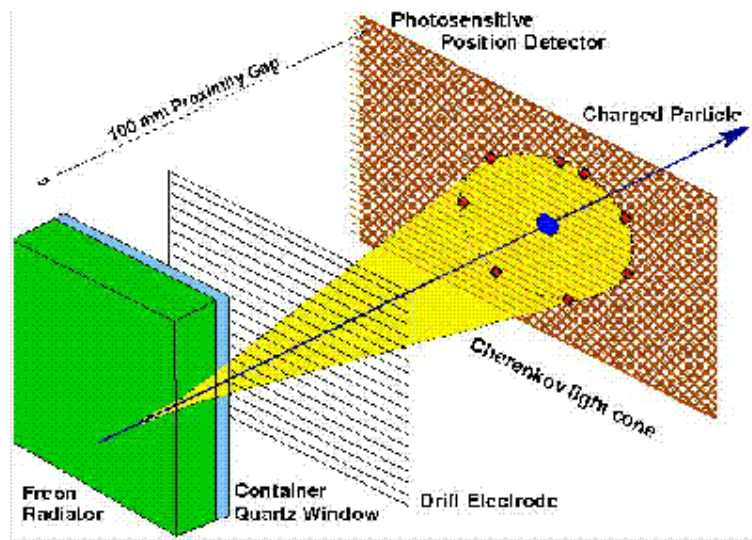


Figure 7.20: *The principle of a Ring Imaging Cherenkov counter.*

# Chapter 8

## Cosmology

How could the universe be created out of nothing in the Big Bang? The key to this apparent miracle might be hidden in the concept of Quantum Mechanics. We have seen that in quantum processes matter can be created out of nothing during a time which is given by the Heisenberg uncertainty principle. Thus, the idea that the universe arose from nothing is not completely absurd. Quantum Cosmology is a field attempting to study the effects of Quantum Mechanics on the formation of the universe, or its early evolution, especially just after Big Bang. The field, however, still remains a rather speculative branch of Quantum Gravity.

The table below summarizes the various phases in the evolution of Universe.

Time (s)	Temp (K)	Energy GeV	
$10^{-43}$	$10^{32}$	$10^{19}$	Planck scale; needs a quantum field theory for gravitation to be described.
$10^{-36}$ $10^{-10}$	$10^{28}$ $10^{15}$	$10^{15}$ 100	The electroweak and strong forces split up <u>Radiation dominated Universe</u> ; soup of leptons, antileptons, neutrinos, antineutrinos, photons, W, Z, quarks, antiquarks and gluons in thermal equilibrium
$10^{-5}$	$10^{12}$	0.3 (300) MeV	<u>The quark era</u> ; quarks combine into hadrons. The Universe consists of leptons, antileptons, neutrinos, antineutrinos, photons, protons and neutrons
1	$10^{10}$	0.001 (1 MeV)	<u>The lepton era</u> ; $\gamma \rightarrow e^+e^-$ stopped. Leptons and antileptons have annihilated ( $l^+l^- \rightarrow \gamma\gamma$ ). We are left with neutrinos, antineutrinos, electrons, muons, photons, protons and neutrons.
$10^{13}$ $= 5 \cdot 10^5$ yrs	4000		<u>Start of the nucleosynthesis</u> . Formation of H and $^4\text{He}$ , neutral atoms through electron capture. Universe gets transparent to optical photons $\Rightarrow$ <u>Matter dominated Universe</u> .

As the quarks and antiquarks had formed nucleons at the end of the quark era at  $t \approx 10^{-5}$  seconds, there was a small surplus of quarks over antiquarks. Since there are 3 quarks in a nucleon we have in the case that the number of nucleons existing today is  $N_o$ :

$$N_o = 1/3(N_q - N_{\bar{q}})$$

where  $N_q$  and  $N_{\bar{q}}$  are the original number of quarks and antiquarks.

On the other hand, the number of quarks and antiquarks at the start of the nucleon synthesis must have been about the same as the number of photons, since the energy was high enough that all particles were in thermal equilibrium. As the number of photons has essentially not changed we get:

$$N_{o,\gamma} \approx N_q \approx N_{\bar{q}}$$

$$\Rightarrow \frac{N_q - N_{\bar{q}}}{N_q + N_{\bar{q}}} = \frac{3N_o}{2N_{o,\gamma}} \approx 10^{-8}$$

which thus gives a small surplus of matter over antimatter.

At the end of the quark era, protons and neutrons are produced, but all antiquarks are annihilated:  $q + \bar{q} \rightarrow e^+ + e^-, \dots$

In the early phase  $N_{protons} = N_{neutrons}$  since:

$$n \rightarrow p + e^- + \bar{\nu}_e \text{ and } p \rightarrow n + e^+ + \nu_e$$

both occurred at the same rate. This means that  $e^-, e^+, \nu, p$  and  $n$  were all in thermal equilibrium. However, the small difference in mass between protons and neutrons played an essential role as the universe cooled off since it then became more difficult to produce neutrons than protons.

The ratio can be estimated from the Boltzmann factor  $N \sim e^{-E/kT}$ , giving the probability of having a state with energy  $E$  relative to having a state of zero energy.

$$r = \frac{N_n}{N_p} = \frac{e^{-m_n c^2/kT}}{e^{-m_p c^2/kT}} = e^{-(m_n - m_p)c^2/kT}$$

For  $kT = 1 \text{ MeV}$ , which was the average energy of universe at that point (and having  $m_n - m_p \approx 1 \text{ MeV}$ ), we get  $r = e^{-1} \approx 0.27$ . A more careful analysis gives  $r = 0.14$ .

As the energy decreased further we got:  $n + p \rightarrow d$  with a binding energy of 2.2 MeV.

Now the nucleosynthesis started.

$$p + n \rightarrow d + \gamma + 2.2 \text{ MeV}$$

$$d + n \rightarrow t(\text{tritium}) + \gamma + 6.26 \text{ MeV}$$

$$t + p \rightarrow {}^4\text{He} + \gamma + 19.81 \text{ MeV}$$

$$t + d \rightarrow {}^4\text{He} + n + 17.59 \text{ MeV}$$

$$d + p \rightarrow {}^3\text{He} + \gamma + 5.49 \text{ MeV}$$

$$d + d \rightarrow {}^3\text{He} + n$$

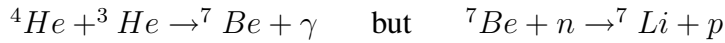
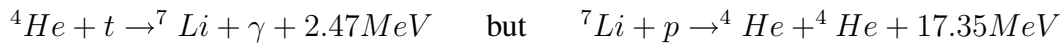
$$d + d \rightarrow {}^4\text{He} + \gamma + 23.85 \text{ MeV}$$

$${}^3\text{He} + n \rightarrow {}^4\text{He} + \gamma + 20.58 \text{ MeV}$$

After  ${}^4\text{He}$  had been produced the nucleosynthesis was essentially finished since there are no long lived isotopes with  $A = 5$  (which is obtained if a proton or neutron is added to  ${}^4\text{He}$ ) or

$A = 8$  (which is obtained if two  ${}^4\text{He}$  fuse). Thus there are no stable nuclei with  $A$  between 4 and 7.

A small amount of  ${}^7\text{Li}$  is created according to:



However, the bulk of the heavier elements was created later in the formation of stars.

After 200 seconds all neutrons are used up in the production of  ${}^4\text{He}$ .

$$N_n = 2N_{\text{He}} \quad N_p = 2N_{\text{He}} + N_H$$

$$\Rightarrow N_{\text{He}} = \frac{N_n}{2} = \frac{0.14N_p}{2} = 0.07N_p \quad \text{and} \quad N_H = N_p - 2N_{\text{He}} = N_p - 2 \cdot 0.07N_p = 0.86N_p$$

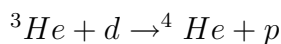
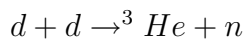
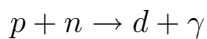
where 0.14 comes from the Boltzman ratio for  $N_n/N_p$ .

The ratio between the number of nucleons bound in helium and the total number of nucleons will be:

$$\frac{4N_{\text{He}}}{N_n + N_p} = \frac{4 \cdot 0.07 \cdot N_p}{(0.14 + 1)N_p} = 25\%$$

which is consistent with measurements.

Since the neutron has a life time of about 15 minutes before it decays, the universe must have cooled off to a temperature where the neutrons could be bound to protons to form deuterons within this time.



The binding energy of the deuteron is as low as 2.2 MeV.

If the temperature would not have decreased to the critical value within the decay time of the neutron, there would have been less neutrons left to produce  ${}^4\text{He}$ . If on the other hand the universe would have cooled off faster a larger number of neutrons would have been available for being bound into  ${}^4\text{He}$ .

## 8.1 Formation of Galaxies

Entering into the matter dominated universe after 500000 years leads to the formation of clusters of matter, which are getting increasingly denser due to gravitation and thereby attracting additional matter from the surroundings. In order for a gas volume to reach equilibrium the gravitational force must become balanced by the gas pressure. During the radiation dominated universe the pressure is dominated by the radiation pressure given by the energy density of the radiation.

As universe entered into the matter dominated universe, the photon radiation did no longer provide a pressure and the galaxies could more easily contract.

Most galaxies seem to be disc-like, which can be understood if the density clusters are rotating.

Observation of rotation velocity  $\Rightarrow$  need for dark matter.

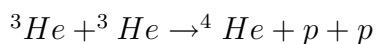
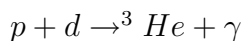
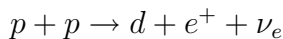
## 8.2 The Creation of a Star

Around half a million years after the Big Bang the universe consists of a gas of Helium and Hydrogen (as  $H_2$  molecules). Local clusters of gas will contract due to gravitation, which will develop into galaxies. These will in turn subdivide into gas clouds, creating stars.

The development of stars is governed by the balance between the gravitational attraction of the gas molecules and the gas pressure. Normally the temperature of a gas volume, which is compressed increases. However, as long as the hydrogen exists as  $H_2$  molecules, the produced heat is used to produce a rotation of the  $H_2$  molecules, which is then radiated as infrared radiation. This means that the temperature will remain at around 10K. Some of the radiation will split up the  $H_2$  molecules into some ionized plasma, which becomes non-transparent to the radiation.

$\Rightarrow$  protostar

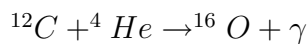
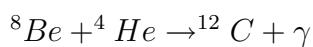
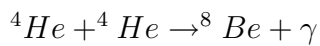
With increasing temperature, fusion processes will occur:



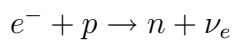
The protostar starts shining and becomes a star. An equilibrium is reached where the produced energy increases the temperature and consequently the pressure such that the compression stops. This is a self adjusting system in the sense that if the fusion increases the temperature, the increased pressure will blow up the star, which is then cooled off and the fusion processes are slowed down. This leads to contraction and an increase of the fusion reactions.

## 8.3 The Death of a Star

As the hydrogen fuel in the centre of the star is used up the fusion continues in the outer regions of the star, which blow up to a *red giant*. This is due to the fact that the energy is not only transported outwards by radiation but also by matter. The red giant will continue to grow until the fuel in the inner of the star is used up. Mass is during the combustion process converted to energy but as the fuel is consumed the radiation pressure decreases and the star will start to contract. The contraction increases the temperature and it eventually reaches a point where the next heavier element start burning. The contraction is temporarily halted until the fuel of this heavier element is consumed. This is repeated as the next phase is started according to the following sequence.

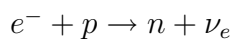


After around  $60 \cdot 10^6$  years the inner of the star is mainly carbon and oxygen. The outer parts have drifted away and form planetic *nebulosae*. When the helium is used up the star starts contracting and turns into a *white dwarf*. At high enough temperatures the electron gas behaves like any other ideal gas but when the temperature decreases the Pauli principle has to be fulfilled. When all the lower energy states have been occupied the gas can not get any colder and it is said that the electron gas is *degenerate*. If the electron gas collapses, the electrons will react with the protons according to:



The neutrinos will leave the star, which develops into a *neutron star*.

If the mass is big enough carbon and neon will produce magnesium in about 100 years, neon and oxygen will produce silicon in about 1 year, and silicon and neon will produce  ${}^{56}\text{Fe}$ ,  ${}^{56}\text{Co}$  and  ${}^{56}\text{Ni}$ . After that the fusion processes will not be able to create more energy and the core of the star collapses in about 0.1 seconds. The outer parts fall inwards and bounce out again, in a gigantic collision, and the star dies as a *supernova*. A large number of neutrinos are emitted due to the reaction:



in the centre of the star. The neutron star remaining at the centre of the supernova frequently will rotate with a large frequency and is therefore called *pulsar*. If the shock wave created from the supernova explosion is not able to turn the implosion of the star into an explosion, the star will collapse into a *black hole*. This happens if the mass of the star is bigger than 30 sun masses.

# Chapter 9

## Appendix A

### Why is the speed of light in vacuum the ultimate speed limit?

It is generally not so well-known that the reason why nothing can go faster than the speed of light in vacuum is a consequence of the laws of electricity and magnetism i.e. that light is an electromagnetic wave motion. As a matter of fact Einstein's original paper on relativity was called 'On the Electrodynamics of Moving Bodies'. Einstein himself didn't like the concept 'relativity' but preferred 'invariance'.

A simple 'Gedanken' experiment might help to demonstrate how the interaction of electric and magnetic fields causes all velocities to be less than the speed of light. If you place a small positively charged object, with charge  $q$ , next to a thin positively charge rod with a total charge  $Q$ , distributed evenly over its length  $L$ , both objects sitting at rest, the two are repelled by the electric force  $F_E$ . We can choose to place the rod along the  $y$ -axis, in a cartesian coordinate system, as shown in Figure 9.1.

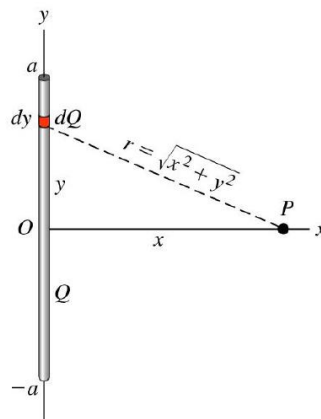


Figure 9.1: A small charged object placed next to a thin charged rod.

If we subdivide the rod into sufficiently small pieces, each piece having a charge of  $dQ = Q/L \cdot dy$ , the force can be written:



$$F_E = \frac{1}{4\pi\epsilon_0} \cdot \frac{q \cdot Q/L dy}{r^2}$$

where  $r$  is the distance between the small object and the length element of the rod and  $\epsilon_0$  is the vacuum permittivity

Since  $r^2 = x^2 + y^2$  and  $x$  is constant we have  $r dr = y dy$ . Then, the force between the small object and the rod can be written:

$$F_E = \frac{q}{4\pi\epsilon_0} \int \frac{Q/L dr}{r^2}$$

$$\Rightarrow F_E = q \cdot \frac{(Q/L)}{2\pi\epsilon_0 r}$$

However, a property of electricity and magnetism is that moving charges create magnetic fields and thus if our rod moves it will be surrounded by a magnetic field. In case our charged object is moving alongside the rod it will feel the force of the magnetic field,  $F_B$ . The strength of the magnetic field can be calculated from Faraday's law.

$$F_B = -\mu_o \cdot q \cdot \frac{(Q/L) \cdot v^2}{2\pi r}, \quad \text{where}$$

$\mu_o$  = the vacuum permeability

The negative sign indicates that the magnetic force is attractive i.e. the electric and magnetic forces work in opposite directions.

This leads to kind of a paradox insofar that if the rod and object both are at rest they are repelled by the electric force but if they both are moving alongside each other they will feel two competing forces; the repulsive electric force and the attractive magnetic force.

This paradox becomes even more apparent if we consider two observers  $A$  and  $B$ . The observer  $A$  sits at rest watching the rod and the charged object fly by at a speed of  $v$ . The observer  $B$ , on the other hand, is moving together with the rod and the charged object, so from his point of view nothing is moving. Observer  $A$  would see the competing electric and magnetic forces,  $F_E$  and  $F_B$ , while observer  $B$  would only be aware of the electric force,  $F_E$ . In case  $F_B > F_E$  observer  $A$  would see the charged object approach the rod, whereas  $B$  would perceive that the charged object moves away from the rod. A correct description of nature cannot accommodate both these outcomes.

This consequently would mean that the magnetic force is always weaker than the electric force, regardless of velocity. Thus,

$$F_B < F_E \quad \rightarrow \quad |-\mu_o \cdot v^2| < |1/\epsilon_o| \quad \rightarrow \quad v < \frac{1}{\sqrt{\epsilon_o \mu_o}}$$

But the numerical value of the quantity  $1/\sqrt{\epsilon_o \mu_o} = 3 \cdot 10^8$  meter per second, which is exactly the speed of light. So, by setting this as a velocity limit we avoid that a person at rest would experience one reality which is different from that experienced by a person moving.

The attentive reader would notice that even if  $v$  is always less than the speed of light, observer  $B$  would see the object move faster than observer  $A$ . The solution to this problem is given by *time dilatation* described in Section 1.3.1.

# Chapter 10

## Appendix B

### How Einstein's formula $E = m \cdot c^2$ has to be understood

In order to get a correct interpretation of Einstein's simple formula  $E = m \cdot c^2$ , we start by recollecting the outcome of a well-known experiment. If you walk from the rear end to the front of a boat, floating frictionless on the water, you may notice that the boat moves backwards. The distance the boat moves depends on your weight and that of the boat. If you would be able to measure it, you would also find that the center-of-mass of the system, consisting of you and the boat, does not move. Let us define the mass of the boat as  $M$  and assume that it is symmetrically distributed over its length,  $L$ . We set your weight (or rather mass) to  $m$ . In order to calculate the position of the center-of-mass, we choose the front end of the boat as reference point (you may choose any point as reference and you get the same result).

In the initial state we have:

$$x_{c.m.} = \frac{M \cdot L/2 + m \cdot L}{M+m}$$

After you have moved to the front of the boat we have:

$$x_{c.m.} = \frac{M \cdot (L/2 + \Delta x) + m \cdot (L + \Delta x - L)}{(M+m)}$$

where  $\Delta x$  is the distance the boat moved.

Due to the fact that the center-of-mass doesn't move the expression for the initial and final states can be set equal and we get after some rearrangements:

$$\frac{M \cdot L/2 + m \cdot L}{M+m} = \frac{(M+m) \cdot \Delta x + M \cdot (L/2)}{M+m}$$

$$\rightarrow \Delta x = \frac{m \cdot L}{M+m}$$

So, in the case the boat is a light canoe, and you manage to walk from one end to the other without falling into the water, it will move a considerable distance. However, if the boat is much heavier than you, your weight can be ignored, and the boat would essentially not move at all.

Now, let us consider the following 'Gedanken' experiment where we use a long tube, of length  $L$ , which can move frictionless. The tube has light absorbing end-caps and we place a light source inside the tube next to one of the ends. When we switch on the light it will instantly hit the nearby end-cap, whereas the distant end-cap will only be hit after some time  $L/c$ . Light is an electromagnetic wave and, although it has no mass, it according to Maxwell's theory carries momentum. The momentum is transferred to a surface hit by the light wave, which gives rise to a pressure (force) on the surface. This is called *radiation pressure*,  $P$ , and its strength is related to the energy intensity,  $I$ , of the light, such that  $P = I/c$ , and the total force exerted on the end-cap is  $P \cdot A$ , where  $A$  is the area of the end-cap.

In a time course the following takes place; when the light hits the closest end-cap the radiation pressure exerts a force on this end-cap, whereas there is no such force on the distant end-cap until the light has reached it after a time  $L/c$ . This gives the tube some momentum in the direction of the close end-cap, which will remain until the light is switched off. Right after the light is switched off there is a radiation pressure on the distant end-cap for a time interval  $L/c$ , but none on the close end-cap. Consequently, the tube will stop moving. The net effect is that the tube has moved although no outside force has been involved. If the mass of the tube is  $M$ , the shift of the tube is:

$$\Delta x = \frac{P \cdot A}{M} \cdot \frac{L}{c}.$$

Remember that light is massless.

But  $P = I/c$  and  $I = E/A$

$$\rightarrow P = \frac{E}{A \cdot c}$$

$$\rightarrow \Delta x = \frac{E}{A \cdot c} \cdot \frac{A}{M} \cdot \frac{L}{c}$$

$$\rightarrow \Delta x = \frac{E \cdot L}{M \cdot c^2}$$

This result tells us that the centre of mass has moved without any external force has been involved, apparently violating a fundamental rule in physics. The explanation is that although we didn't move any mass around by switching on the light source, we did move energy. When light hit the end-cap it transferred momentum and caused the tube to start moving. This can be compared to you start walking in the boat, which means moving mass. To extract the relation between energy and mass we can compare our result from the light experiment with that from the boat exercise, where we can ignore your mass relative to the mass of the boat.

$$\Delta x = \frac{m \cdot L}{M} = \frac{E \cdot L}{M \cdot c^2}$$

$$\rightarrow E = m \cdot c^2$$

Thus, energy and mass are related through the square of the light velocity,  $c^2$ , where  $c^2$  is just a conversion factor to go from energy to mass and vice versa. Since  $c^2$  is an enormously big number it means that when you walk in a boat you move a considerable amount of energy. The most spectacular and frightening example of converting mass to energy is occurring in the atomic bomb.

As a final consequence of these considerations. we can state that the conservation of center-of-mass is just an, in most cases, very good approximation to the conservation of the centre-of energy.

# Chapter 11

## Appendix C

### The Double Slit Experiment

In an attempt to understand the results of the double slit experiment we will investigate what happens when we use bullets, water waves and electrons, respectively.

1) **Bullets:** If we fire a machine gun randomly toward a wall with a slit and look how the pattern caused by the bullets on a wall behind looks like, we find that it is essentially an image of the slit. However, since some of the bullets are scattered against the edges of the slit the image is not sharp but somewhat diffuse. The distribution of the bullets follows a Gaussian shape.

If we now open up another slit in the first wall and again fire the machine gun randomly against it we will find that after some while approximately the same number of bullets have passed the two slits. We have got two Gaussian distributions, which if the slits are sufficiently apart can be seen as separate distributions. However if they are close enough only one distribution appear but the number of bullets contained in this distribution is the same as the sum of the bullets going through the two slits.

2) **Water waves:** If we let a wave front approach the wall, a narrow slit will act as a point like source and the water which passes the slit will propagate in circular patterns from the slit. The distribution of the energy carried by the waves and hitting the second wall will show a similar shape (a Gaussian shape) as for the bullets.

With two slits we will have two point sources but the result we obtain is completely different from what we got with the bullets. The reason is that a wave is either on its crest or trough depending on the different distances the waves have to travel from slit 1 and 2, respectively, to a point on the second wall. The waves from the two slits overlap and for every point on the second wall the amplitudes of the two waves will both contribute and give an interference pattern (see Figure 2.3). If both are in their crest or trough, the amplitudes will add up but if one is in its crest and the other in its trough, they will cancel partly or completely, giving an interference pattern with minima and maxima. However, the pattern we find with both slits open is not the sum of patterns we find with one slit open at a time.

So we have seen that the results from this experiment are completely different if we treat the source as particles or waves.

3) **Electrons:** If we now redo the experiment with electrons using a phosphorous screen to detect the flashes from electrons hitting the screen, after having passed the wall with the slits. The electrons are obviously particles with a mass and electric charge that can be experimentally determined. Thus, we would expect to get the same result from the two slit experiment as for the bullets. To our great surprise we however see an interference pattern. How does this come about? In order to understand this we have to understand how Quantum Mechanics works.

In the macroscopic world, described by Newtonian mechanics, a particle, where the starting conditions are known, will follow a well-defined path such that its position at any later time can be calculated exactly. In micro cosmos, described by Quantum Mechanics, the situation is completely different. Heisenberg tells us that the position and velocity of an object can not be measured with infinite accuracy simultaneously. The precision is limited by Plancks constant,  $\hbar$ , due to the relation:

$$\Delta v \cdot \Delta x \geq \hbar/m,$$

where  $m$  is the mass of the object. If we rewrite this expression we become:

$$m\Delta v \cdot \Delta x \geq \hbar.$$

$m \cdot v$  is however the momentum,  $p$ , of the object and thus:

$$\Delta p \cdot \Delta x \geq \hbar$$

i.e. if we know the momentum with infinite accuracy the position is completely undetermined and vice versa.

Normally light is described as a wave motion. However, when Einstein looked for an explanation to the photoelectric effect he realized that this required that light had to be regarded as quanta of energy, photons, which knocked out electrons when hitting an atom. In a similar way electrons may be considered to perform a wave pattern in some situations. This is called the particle-wave duality.

The energy of light (photons) can be written as  $E = \hbar \cdot \nu$ , where  $\nu$  is the frequency of the wave motion. This is equivalent to  $E = \hbar/\lambda$ , where  $\lambda$  is the wave length, and thus we have  $E \cdot \lambda = \hbar$ . But for massless particles  $E = p$  and consequently  $\Delta E = \Delta p$ . The length of the wave,  $\lambda$  can equally well be written as  $\Delta x$  (it is only a matter of which notation you are using). Thus, we have the product  $\Delta p \cdot \Delta x$ , which according to Heisenberg must be  $\geq \hbar$ . From this follows that a photon or an electron travelling through space without being disturbed (i.e.  $\Delta p = 0$ ), corresponds to a wave extending infinitely through space and therefore the uncertainty in wavelength i.e. position is infinitely big.

If we apply this to the double slit experiment, we would expect to observe similar interference patterns for electrons as for light waves, which is exactly what we do.

Can we investigate what the origin of the interference is experimentally? We may fire off electrons one by one to find out whether the interference pattern occur due to the interaction of one electron passing through the slit number 1 with one that passes through the slit number 2. Only after having measured where one electron ends up we fire off the next electron and repeat the observation, and so on. After having fired off enough electrons we will discover that

the distribution of electrons still exhibits an interference pattern. This result thus disproves the hypothesis we made in the beginning of this paragraph.

Could it be that an electron somehow is going through both slits simultaneously? If we try to observe this we necessarily have to interact with the electron by for example shining light on it. A macroscopic object would not be much affected by the light but for a tiny quantum particle it may have a big effect as we will see. We thus place a small light bulb behind the wall with the slits to see which path the electron is following. What we will observe is that every electron is acting normal in the sense that approximately half of the electrons are going through slit 1 and half of them are going through slit 2. And to our surprise the interference pattern has disappeared. This is really weird!!! Could the reason for this be the disturbance that we have introduced by shooting light against the electrons?

In order to minimize the disturbance caused by the light we are using to shine on the electron we may turn down its intensity. First no interference pattern is observed but as the intensity of the light has been decreased to the point where it is so faint that we miss some of the electrons the interference pattern starts coming back. Thus, this investigation was of no help in understanding what is going on.

The second way of minimizing the disturbance is to decrease the energy of the light by increasing its wavelength. In the beginning everything seems to work as we expect, half of the electrons are going through slit number 1 and the other half going through slit number 2. However, the ability to resolve two positions in space depends on the wavelength of the light we are using for our observation as we have shown above. Although we will still be able to observe the electrons, at some point the wavelength of the light is getting too long for us to tell through which slit the electron went and we will get the interference pattern back.

Thus, the conclusion is that there is no way of performing an experiment that can explain what is happening to the electrons when they pass the slits. Feynman's interpretation of the phenomenon was that, in contrast to Newton mechanics, it is not possible to predict what path a particle will take from its starting point to its final destination even if we know the starting conditions. In fact it will take every possible path simultaneously, which means that the paths of one and the same electron through slit number 1 will interfere with the paths through slit number 2. Although this sounds completely crazy Feynman was able to show mathematically, by taking all possible paths into account, that a probability for a particle, starting at a position A to arrive at a position B, can be calculated. Since the number of paths is infinite the calculations are somewhat complicated but the result agrees with the observation. This description was generalized to apply to all systems such that the probability of a system to evolve from an initial state to a final one is the sum of all possible evolutions (Compare with the discussion on summation of Feynman diagrams in Sections 3.2.5 and 3.2.6). Feynman once made the following statement: 'I think I can safely say that nobody understands quantum mechanics'. So in case you are confused you are at least in very good company.